

Self-Assembled Graphene oxide Nanoparticles for Damaging DNA in Cancer Cells

**A THESIS
SUBMITTED TO PARTIAL FULFILMENT OF THE DEGREE
OF
DOCTOR OF PHILOSOPHY
IN CHEMISTRY**

**BY
ADITI NANDI**

ID: 20122030

UNDER THE GUIDANCE OF DR. SUDIPTA BASU

AT



**INDIAN INSTITUTE OF SCIENCE EDUCATION AND RESEARCH,
PUNE**

CERTIFICATE

Certified that the work incorporated in the thesis entitled “*Self-Assembled Graphene oxide Nanoparticles for Damaging DNA in Cancer Cells*” submitted by **Ms. Aditi Nandi** was carried out by the candidate, under my supervision. The work presented here or any part of it has not been included in any other thesis submitted previously for the award of any degree or diploma from any other University or institution.

Date: 6/8/2019

Sudipta Basu

Dr. Sudipta Basu

(Research Supervisor)

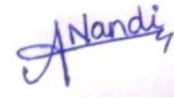
Nirmalya B
Dr. Nirmalya Ballav 7/8/2019
(Co-Supervisor)

निर्मल्या बल्लव / Nirmalya Ballav
सहाय्यी प्राध्यापक, रसायनशास्त्र / Associate Professor, Chemistry
भारतीय विज्ञान शिक्षा एवं अनुसंधान संस्थान
Indian Institute of Science Education & Research
Pune - 411 008, India

DECLARATION

I declare that this written submission represents my ideas in my own words and where others' ideas have been included, I have adequately cited and referenced the original sources. I also declare that I have adhered to all principles of academic honesty and integrity and have not misrepresented or fabricated or falsified any idea/data/fact/source in my submission. I understand that violation of the above will be cause for disciplinary action by the Institute and can also evoke penal action from the sources which have thus not been properly cited or from whom proper permission has not been taken when needed.

Date: 22-10-2019



Aditi Nandi
ID-20122030

ACKNOWLEDGMENT

Foremost, I would like to express my sincere gratitude to my supervisor **Dr. Sudipta Basu** for giving me the opportunity to work in his lab. His constant guidance and support was valuable. I also want to thank **Dr. Nirmalya Ballav** for being my administrative advisor.

Besides my advisor, I would like to thank the Research Advisory Committee (RAC): **Dr. B.L.V Prasad** and **Dr. Nirmalya. Ballav** for their encouragement and insightful comments which helped me improve my work. A special thanks to all the faculty members who taught me during my masters at IISER-Pune. I'm grateful to the former director **Prof. K.N. Ganesh** and current director **Prof. Jayant B. Udgaonkar** of IISER-Pune, for providing the facilities to carry out my research work. I want to thank all instrument technicians **Anil, Megha, Sandeep, Mahesh, Yatish, Ganesh Dimber**, and IISER Pune Microscopy facility (**Santosh, Rahul and Vijay**) for their assistance. I also want to thank **Tushar sir** and other people from the administrative department of IISER Pune for always tending to our academic related issues.

I really want to thank all my labmates **Dr. Abhik, Dr. Chandramouli, Dr. Sandeep, Sohan, Shalini, Aman, Meenu, Kamil, Ankur, Sainath, Piyush**, for their help valuable suggestions and for all the time we have spent in lab together. A special thanks to **Abhik and Meenu** for teaching me biological experiments and stimulating discussions. I am grateful to **Abhik and Chandra, Aman and Shalini** for giving me some really useful suggestions apart from all the worthless, but fun discussions we have had in and out of lab. I also want to thank **Dr. Poulomi Sengupta** for her help in chapter 2, **Mukul** for teaching me western blot experiment and **Maduskar** for solving my biology related doubts.

I am grateful to my 2012 Int. Ph.D. friends: **Meghna, Hridya, Jerrin, Mukul, Amogh, Ankitha** (my one and only room-mate), **Anjusha, Chetan** for all the good times we have spent. My partner in crime **Sneha**, without her these 7 years would have been extremely boring. My fellow BTS crazy friends: **Maduskar and Harshini** for introducing me to BTS (my stress buster) and K-dramas. **Sunil (Grumpy/Buddha Aadmi)** for supporting, advising and motivating me. I would like take the opportunity to thank my friends **Pooja, Mriga, Anjali, Kunal, Tripathi, Sanku, Jyoti, Bag, Reja, Babar, and Aman** for providing a fun-filled environment. Last but not the least; I want to thank **Aditya** for always being there for me unconditionally.

My acknowledgment would be incomplete without sincerely thanking my parents, grandparents and my entire family for their blessings, love and support. I specially want to thank my father for being my first and best chemistry teacher, without him I don't think I would have liked chemistry.

**Dedicated to
My Beloved Family**

ABSTRACT

Cancer is a multifactorial mutagenic disease, which is one of the leading causes of death globally. The complexity and heterogeneity associated with cancer presents a challenging problem with respect to its treatment. In recent times, the incorporation of nanotechnology in the treatment regimen has revolutionized the field of cancer therapy. Various nanoplateforms have been used for anticancer drugs to specifically target cancer cells, but all have their own associated drawbacks, thus limiting their application. In addition, the combined packaging of multiple drugs into a single nanoplateform still remains a considerable challenge. Graphene oxide-based biocompatible nanoscale materials, by virtue of their unique physicochemical properties and the large surface have the potential to tackle this complication. To address this issue, we have developed novel cisplatin-mediated self-assembled 3D graphene oxide spherical nanoparticles (GO-NP's) of size less than 200nm from 2D graphene oxide sheets. The nanoparticles can also be loaded with additional DNA damaging drugs along with cisplatin- which is a widely used drug in cancer treatment. These dual drug-containing graphene oxide spherical nanoparticles successfully displayed their anticancer activity by damaging the DNA- which is the most important target to cease essential cellular functions and hence induce apoptosis in cancerous cells. Further, to improve the dispersibility and biocompatibility of 3D GO-NP's for safer biomedical applications, we employed surface functionalization of the graphene oxide sheets with biocompatible polymers like polyethyleneglycol (PEG) and poly-maleic acid (PMA) and self-assembled them into spherical nanoparticles via cisplatin. Subsequently, we loaded the nanoparticles with an inhibitor of an important DNA-associated enzyme, Topoisomerase I. The modified nanoparticles induced DNA damage along with enzyme inhibition, activating programmed cell death in HeLa cervical cancer cells. Lastly, we engineered a lipid-coated self-assembled spherical 3D-GO nanoparticle (GO-Nanocell), which can concomitantly load and release multiple drugs: topoisomerase I and II inhibitors along with cisplatin. The GO-Nanocells simultaneously induced DNA damage along with Topoisomerase (TOP 1 and TOP 2) poisoning, triggering apoptosis in HeLa cells. The graphene oxide based approaches presented here can serve as a tool to impair multiple targets inside the cancer cells in a synchronized manner for better therapeutic effect in future cancer therapy.

CONTENTS

List of Figures and Table.....	iv
Synopsis.....	,xi
List of Publications.....	xiii
Abbreviations.....	xiv
Chapter 1 : Introduction	1
1.1 Cancer.....	2
1.1.1 DNA damage and Replication stress	4
1.1.2 Proteotoxic stress	4
1.1.3 Mitotic stress.....	4
1.1.4 Metabolic stress	4
1.1.5 Oxidative stress.....	5
1.2 DNA as a Target for Cancer Therapy	5
1.3 Selective Targeting of Tumor Cells	8
1.4 Nanomaterials in Tumor Targeting	11
1.5 Aim of the Thesis	15
1.6 References	17
Chapter 2: Cisplatin-Induced Self-Assembly of Graphene Oxide Sheets into Spherical Nanoparticles for Damaging Sub-cellular DNA.....	25
2.1 Abstract	26
2.2 Introduction	26
2.3 Result and Discussion	29
2.4 Materials and Methods.....	49
2.4.1 Materials:	49
2.4.2 Synthesis of aquated cisplatin (3).....	49
2.4.3 Synthesis of GO-Prof conjugate (2).....	49
2.4.4 Synthesis of GO-Prof-CDDP conjugate (4) and GPC-NPs	49
2.4.5 Synthesis of GO-Dox conjugate (5).....	49
2.4.6 Synthesis of GO-Dox-CDDP conjugate (6) and GDC-NPs	50
2.4.7 Field-Emission Scanning Electron Microscopy (FESEM) of GPC and GDC-NPs.....	50
2.4.8 Atomic Force Microscopy (AFM) of GPC-NPs and GDC-NPs.....	51

2.4.9	Transmission Electron Microscopy (TEM) of GPC-NPs and GDC-NPs.....	51
2.4.10	Resonance Raman Spectroscopy	51
2.4.11	Powder X-ray diffraction (PXRD).....	51
2.4.12	X-ray photoelectron spectroscopy (XPS)	51
2.4.13	<i>In vitro</i> assays	51
2.4.14	Quantification of drug release from GPC-NPs and GDC-NPs.....	52
2.5	Conclusion.....	52
2.6	Salient Features	52
2.7	References	53
Chapter 3: Polymer Modified GO-Nanoparticles for TOP1 Inhibition and DNA Damage in Cancer Cells.....		
		57
3.1	Abstract	58
3.2	Introduction	58
3.3	Result and Discussion	61
3.3.1	Synthesis and characterization of GO-PEG-SN-38-CDDP and GO-PIMA_Ed-SN-38-CDDP nanoparticles.....	61
3.3.2	Cellular internalisation.....	68
3.3.3	Drug release	72
3.3.4	DNA damage and Topoisomerase I inhibition	73
3.3.5	Apoptosis and cell death	78
3.4	Experimental Section	80
3.4.1	Materials	80
3.4.2	Synthesis of poly(isobutylene-alt-maleic anhydride) conjugated ethylenediamine ..	81
3.4.3	Synthesis of GO-Peg-SN38-CDDP and GO-PIMA_Ed-SN38-CDDP nanoparticles .	81
3.4.4	Characterization	82
3.4.5	Estimation of size, shape and morphology by FESEM and AFM.....	82
3.4.6	Raman Spectroscopy.....	82
3.4.7	Quantification of drug loading in nanoparticles	82
3.4.8	Fluorescence spectroscopy.....	82
3.4.9	Cellular internalisation by confocal laser scanning microscopy (CLSM).....	82
3.4.10	Study of endocytosis pathway	83
3.4.11	Detection of γ H2AX by immunostaining	83
3.4.12	Western blot analysis	83

3.4.13 Apoptosis detection by FACS.....	83
3.4.14 Cell viability assay.....	83
3.5 Conclusion.....	84
3.6 Salient Features	84
3.7 Appendix	85
3.8 References	86
Chapter 4: Graphene oxide Nanocells for Impairing Topoisomerase and DNA in Cancer Cells.	93
4.1 Abstract	94
4.2 Introduction	94
4.3 Result and Discussion	96
4.3.1 Engineering GO Nanocell.....	96
4.3.2 Cellular internalization.....	103
4.3.3 DNA damage and Topoisomerase Inhibition	106
4.3.4 Cell cycle arrest, apoptosis induction and cell death	109
4.4 Materials and Methods	111
4.4.1 Reagents.....	111
4.4.2 Synthesis of Graphene oxide-Topotecan-Cisplatin nanoparticles (GTC NPs).....	111
4.4.3 Synthesis of Cholesterol-Doxorubicin Conjugate	112
4.4.4 Synthesis of GO-Nanocell	113
4.4.5 Determination of size, shape, and morphology	113
4.4.6 Resonance Raman Spectroscopy	113
4.4.7 Quantification of drug loading in GO-Nanocell	113
4.4.8 Fluorescence spectroscopy.....	114
4.4.9 Cellular internalization by confocal laser scanning microscopy (CLSM).....	114
4.4.10 Detection of γ H2AX by immunostaining	114
4.4.11 Western blot, flow cytometry, cell viability	114
4.5 Conclusion.....	114
4.6 Salient Features	115
4.7 Appendix	116
4.8 References	119
Chapter 5: Conclusion and Future Directions.....	125

LIST OF FIGURES AND TABLE

Figure 1.1: Development of cancer (adapted from Iacobuzio-Donahue et al. <i>Clin. Cancer Res.</i> 2012, 18, 4257-4265.).....	2
Figure 1.2: Hallmarks of Cancer (adapted from Hanahan et al. <i>Cell</i> , 2011, 144, 646-674.).....	3
Figure 1.3: Stress phenotypes associated with the tumorigenic state of cells (adapted from Luo et al. <i>Cell</i> 2009, 136, 823-837.)	3
Figure 1.4: Consequences of DNA damage.....	6
Figure 1.5: Biophysical features of nanoparticles for cancer therapy (adapted from Xia et al. <i>Angew. Chem. Int. Ed.</i> 2014, 53, 12320-12364.).....	9
Figure 1.6: Accumulation of nanoparticles in normal and tumor tissues (adapted from Xia et al. <i>Angew. Chem. Int. Ed.</i> 2014, 53, 12320-12364.).....	10
Figure 1.7: Representation for delivery of nanoparticles by passive and active targeting by exploiting EPR effect (adapted from Riley et al <i>Nat. Rev. Drug Discov.</i> 2019, 18, 175-196.)....	11
Figure 1.8: Synthesis of graphene oxide (GO) from graphene by modified Hummers method (adapted from Xu et al. <i>ACS Appl. Mater. Interfaces</i> 2014, 6, 17265-17276).	12
Figure 1.9: Applications of GO (adapted from Chung <i>Acc. Chem. Res.</i> 2013, 46, 2211-2224.) .	13
Figure 1.10: GO as multifunctional nano-carrier (adapted from Liu et al. <i>Acta Biomaterialia</i> 2013, 9, 9243-9257.).....	14
Figure 2.1: Stacking of proflavine and doxorubicin on GO-sheets that self-assembled into spherical nanoparticle after reaction with cisplatin.	29
Figure 2.2: (a-c) FESEM images of GO, GO-Prof and GO-Dox complex respectively. (d,e) FESEM images of GPC-NPs and GDC-NPs respectively. (f,g) AFM images of GPC-NPs and GDC-NPs. (h,i) Mean diameter of GPC and GDC NP's.....	30
Figure 2.3: TEM images of (a) GPC and (b) GDC-NPs.....	30
Figure 2.4: Fluorescence emission spectra of (a) GO-Prof and (b) GO-Dox showing fluorescence quenching of proflavine and doxorubicin upon stacking on GO surface.	31
Figure 2.5: (a) On particle Resonance Raman spectra of GO, GPC-NP and GDC-NP. (b) PXRD spectra of GO, GO-Prof and GPC-NPs.....	32
Figure 2.6: Fluorescence emission spectra of GPC-NPs and GDC-NPs showing fluorescence quenching of proflavine and doxorubicin upon stacking on GO surface.	33
Figure 2.7: EDXS of GPC-NPs from FESEM images showing the presence of cisplatin.	34

Figure 2.8: EDXS of GDC-NPs from FESEM images showing the presence of cisplatin.	34
Figure 2.9: (a-b) XPS of GPC-NPs showing the presence of nitrogen from proflavine moiety and Pt(II) from cisplatin.....	35
Figure 2.10: (a-e) FESEM images of GO-CDDP composites in different weight ratios to evaluate cisplatin mediated self-assembly.	35
Figure 2.11: EDX of GO-CDDP-NPs at different weight ratios to show the presence of cisplatin.	36
Figure 2.12: PXRD of GO-CDDP composites in different weight ratios.....	37
Figure 2.13: CLSM images of HeLa cells after incubating with GPC-NPs at 1h, 3h and 6h time points. Lysosomes and nucleus were stained with LysoTracker Red and DAPI (blue). Merged images show the colocalization of GPC-NPs in lysosomes in a time dependent manner. Scale bar = 10 μ m.	38
Figure 2.14: CLSM images of HeLa cells after incubating with GDC-NPs at 1h, 3h and 6h time points. Lysosomes and nucleus were stained with LysoTracker Green and DAPI (blue). Merged images show the colocalization of GDC-NPs in lysosomes in a time dependent manner. Scale bar = 10 μ m.	39
Figure 2.15: CLSM images of HeLa cells after incubating with GO-Prof composite at 1h, 3h and 6h time points. Lysosomes and nucleus were stained with LysoTracker Red and DAPI (blue). Merged images show the colocalization of GO-Prof in lysosomes in a time dependent manner. Scale bar = 10 μ m.	40
Figure 2.16: CLSM images of HeLa cells after incubating with GO-Dox composite at 1h, 3h and 6h time points. Lysosomes and nucleus were stained with LysoTracker Red and DAPI (blue). Merged images show the colocalization of GO-Dox in lysosomes in a time dependent manner. Scale bar = 10 μ m.	41
Figure 2.17: FACS analysis of HeLa cells pre-treated with different endocytosis inhibitors followed by (a) GPC-NPs and (b) GDC-NPs treatment.....	42
Figure 2.18: (a-b) Time dependent release of proflavine/cisplatin and doxorubicin/cisplatin from GPC-NPs and GDC-NPs respectively at pH = 5.5 mimicking lysosome environment. (c) Plausible mechanism of dual drug release at pH = 5.5 leading to the dis-assembly of spherical nanoparticles into sheet like structures.	43
Figure 2.19: FESEM images of GPC-NPs at different time points at pH = 5.5 mimicking lysosome environment.	44

Figure 2.20: FESEM images of GDC-NPs at different time points at pH = 5.5 mimicking lysosome environment.	44
Figure 2.21: Time dependent release of proflavine/cisplatin and doxorubicin/cisplatin from (a)GPC-NPs and (b) GDC-NPs respectively at pH = 7.4	45
Figure 2.22: FESEM images of GPC-NPs (a-b) and GDC (c-d) after 24h and 54h time points at pH = 7.4.	45
Figure 2.23: (a) Western blot analysis of γ H2AX and PARP after treatment of HeLa cells with GPC-NPs and GDC-NPs. (b-c) Quantification of γ H2AX and PARP after treating HeLa cells with GPC-NPs and GDC-NPs from western blot analysis.	46
Figure 2.24: FACS analysis of HeLa cells after treatment of HeLa cells with GPC-NPs and GDC-NPs. Apoptotic cells were stained with Annexin V-FITC and necrotic cells were stained with PI.....	47
Figure 2.25: Cell viability of GPC-NPs and GDC-NPs in HeLa cells at 48h post-incubation measured by MTT assay.	48
Figure 2.26 (a-b) Concentration dependent cell viability assay of GPC-NPs and GDC-NPs in L929 mouse fibroblast cells respectively at 24h post-incubation. (c) Concentration dependent cell viability assay of GO in L929 mouse fibroblast cells at 24h post-incubation.	48
Figure 2.27: Synthesis of: GO-Prof conjugate (2), aquated cisplatin (3), GO-Prof-CDDP (GPC-NPs) conjugate (4), GO-Dox conjugate (5), GO-Dox-CDDP conjugate (GDC-NPs) (6).....	50
Figure 3.1: Synthesis of GO-PEG-SN38-CDDP and GO-PIMA_Ed-SN38-CDDP NPs.....	63
Figure 3.2: IR characterization of (a) GO-PEG, (b) PIMA_Ed and GO-PIMA_ED. Representative AFM images with height profiles (c) GO, (d) GO-PEG, (e) GO-PIMA_Ed.....	64
Figure 3.3: (a-b) FESEM images of GO-PEG-SN38 and GO-PIMA_Ed-SN38 (c-d) FESEM images of GO-PEG-SN38-CDDP NPs and GO-PIMA_Ed-SN38-CDDP NPs (e-f) AFM images of GO-PEG-SN38-CDDP and GO-PIMA_Ed-SN38-CDDP NPs.....	65
Figure 3.4: Fluorescence quenching of SN38 in (a) GO-PEG-SN38-CDDP and (b) GO-PIMA_Ed-SN38-CDDP NPs vs. Free SN38 (λ_{max} -560 nm), (c) Single particle resonance Raman spectra of GO-PEG-SN38-CDDP, GO-PIMA_Ed-SN38-CDDP NPs and GO, (d) Energy dispersive X-ray analysis (EDAX) of GO-PEG-SN38-CDDP.....	66
Figure 3.5: Standard curve of (a)SN38, (b) Cisplatin, (c) Loading of SN38 and CDDP in GO-PEG-SN38-CDDP (c) and GO-PIMA_Ed-SN38-CDDP(d).....	67

Figure 3.6: Time dependent colloidal stability of GO-PEG-SN38-CDDP and GO-PIMA_Ed-SN38-CDDP NPs vs. unmodified GO-SN38-CDDP NPs..... 68

Figure 3.7: Representative confocal scanning laser microscope images of HeLa cells post incubation with green fluorescent GO-PEG-SN38-CDDP NPs for 1h, 3h, and 6h. The lysosomes were stained with LysoTracker DND-99 (red fluorescence). The yellow merged areas depict the colocalization of GO-PEG-SN38-CDDP NPs into the lysosomes. [Inset is the % colocaliation volume]. Scale bar =10 μ m. 69

Figure 3.8 Representative confocal scanning laser microscope images of HeLa cells post incubation with green fluorescent GO-PIMA_Ed-SN38-CDDP NPs for 1h, 3h, and 6h. The lysosomes were stained with LysoTracker DND-99 (red fluorescence). The yellow merged areas depict the colocalization of GO-PEG-SN38-CDDP NPs into the lysosomes. [Inset is the % colocaliation volume]. Scale bar =10 μ m. 70

Figure 3.9: Confocal scanning laser microscope images of HeLa cells pre-treated with endocytosis inhibitors (chlorpromazine, genistein and amiloeide) followed by GO-PEG-SN38-CDDP NPs (green). Lysosomes of HeLa cells were stained with LysoTracker Red DND-99 dye. Scale bar = 10 μ m. 71

Figure 3.10: Confocal scanning laser microscope images of HeLa cells pre-treated with endocytosis inhibitors (chlorpromazine, genistein and amiloeide) followed by GO-PIMA_Ed-SN38-CDDP NPs (green). Lysosomes of HeLa cells were stained with LysoTracker Red DND-99 dye. Scale bar = 10 μ m. 72

Figure 3.11: Drug release profiles of SN38 and Cisplatin at pH 5.5 and pH 7.4 from (a) GO-PEG-SN38-CDDP NPs, and (b) GO-PIMA_Ed-SN38-CDDP NPs..... 73

Figure 3.12: (a) Western blot image for Topoisomerase I (TOP1) after treatment with GO-PEG-SN38-CDDP NPs and GO-PIMA_Ed-SN38-CDDP NPs, (b) Quantification for expression of TOP1 from western blot..... 74

Figure 3.13: (a) Confocal microscope images of HeLa cells to visualize γ -H2AX as DNA damage biomarker post 24h treatment with GO-PEG-SN38-CDDP and GO-PIMA_Ed-SN38-CDDP NPs. γ -H2AX was stained with the Alexa Fluor 594-labeled secondary antibody (red fluorescent), the nuclei of HeLa cells were stained with DAPI (blue). (b) Quantification for expression of γ -H2AX from fluorescence images. (c) Western blot image for the expression of γ -H2AX in HeLa cells. (d) Quantification of γ -H2AX from western blot. 75

Figure 3.14: (a) Confocal microscope images of HeLa cells to visualize p53 as DNA damage and apoptosis biomarker post 24h treatment with GO-PEG-SN38-CDDP and GO-PIMA_Ed-SN38-CDDP NPs. p53 was stained with the Alexa Fluor 594-labeled secondary antibody (red fluorescent) and the nuclei of cells were stained with DAPI (blue). (b) Quantification for expression of p53 from fluorescence images. (c) Western blot image for the expression of p53 in HeLa cells. (d) Quantification of p53 from western blot..... 76

Figure 3.15: Western blot images and corresponding quantification for the expression of (a-b) PARP and (c-d) Cleaved PARP in HeLa cells after treatment with GO-PEG-SN38-CDDP and GO-PIMA_Ed-SN38-CDDP NPs for 24h. 77

Figure 3.16: FACS analysis of HeLa cells for induction of apoptosis after 24h treatment with GO-PEG-SN38-CDDP and GO-PIMA_Ed-SN38-CDDP NPs..... 78

Figure 3.17: (a) Western blot analysis for expression of caspase 3 and cleaved caspase 3 in HeLa cells as markers for apoptosis. (b-c) Quantification of caspase 3 and cleaved caspase 3. post treatment with GO-PEG-SN38-CDDP NPs and GO-PIMA_Ed-SN38-CDDP NPs. 79

Figure 3.18: Cell viability of HeLa cells at 48 h post-incubation with concentration dependent (a) GO-PEG-SN38-CDDP NPs and (b) GO-PIMA_Ed-SN38-CDDP NPs quantified by MTT assay. 80

Figure 4.1: Synthetic scheme of GO-Nanocell. 98

Figure 4.2: (a-c) FESEM images of GO, GT and GTC-NPs respectively. (d) Elemental mapping of Pt from FESEM, (e,f) 2-D and 3D AFM images of GTC-NPs respectively 98

Figure 4.3: (a, b) Resonance Raman spectra of GT and GTC-NPs confirming the presence of GO moiety. 99

Figure 4.4: (a, b) Fluorescence emission spectra of GT and GTC-NPs confirming the stacking of topotecan on GO. 100

Figure 4.5: Characterization of GO-Nanocells by (a) dynamic light scattering (DLS), (b) FESEM and (c) AFM. (d) Single particle resonance Raman spectra of GO-Nanocells and GO. 100

Figure 4.6: (a) UV-Vis spectra of GO-Nanocells confirming the presence of topotecan and doxorubicin. (b) Fluorescence emission spectra of GO-Nanocell exhibiting the stacking of topotecan on GO surface..... 101

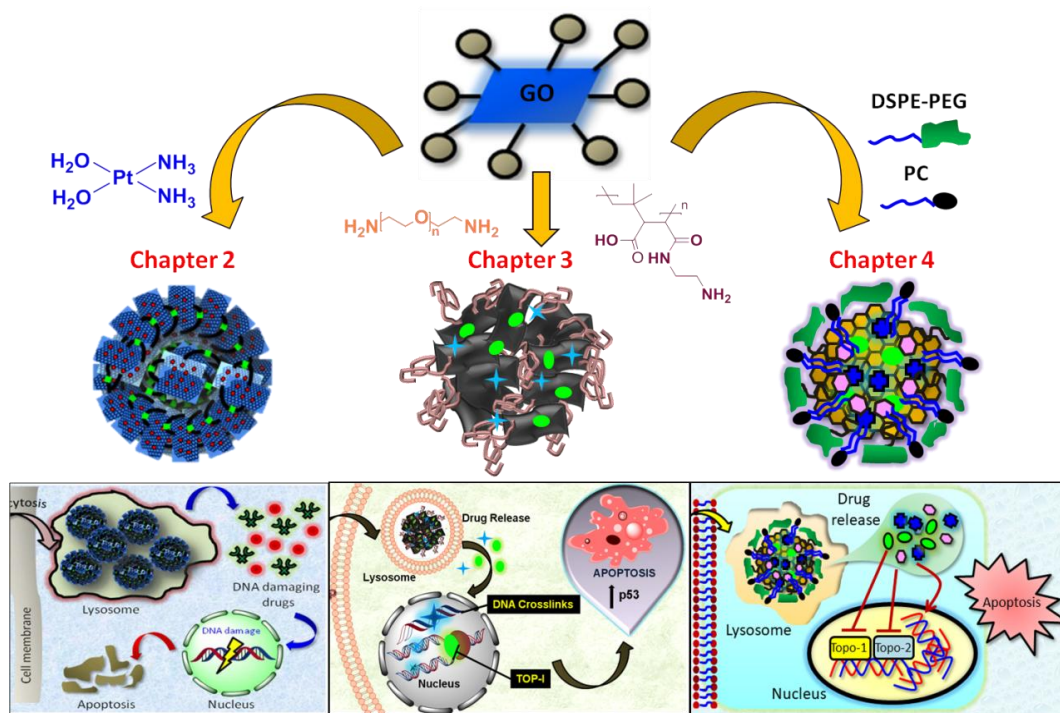
Figure 4.7:EDAX of GO-Nanocell from FESEM confirming the presence of cisplatin..... 102

Figure 4.8: (a-c) Absorbance versus concentration graph of cisplatin, topotecan and doxorubicin respectively determined by UV-Vis spectra. (d) Loading of topotecan, cisplatin and doxorubicin in GO-Nanocell.....	102
Figure 4.9: Confocal laser scanning microscopy (CLSM) images of HeLa cells treated with GO-Nanocells (red fluorescence) at 1 h, 3 h and 6 h time points. The cells were co-stained with LysoTracker DND-26 (green fluorescence). The yellow regions show the co-localization of GO-Nanocells into the lysosomes. Scale bar = 10 mm.....	104
Figure 4.10: CLSM images of HeLa cells at 12 h and 24 h post incubation with GO-Nanocells (red fluorescence). Lysosomes were stained with green fluorescently labeled LysoTracker Green DND-26. Scale bar = 10 μ m.	104
Figure 4.11: (a, b) Release profile of different drugs from GO-Nanocells at pH = 5.5 and 7.4 respectively over 72 h.	106
Figure 4.12: CLSM images of HeLa cells treated with GO-Nanocells for 24h followed by incubation with the γ H2AX antibody labeled with Alexa Fluor 594 dye (red fluorescence). The nuclei were stained with blue fluorescent DAPI. Scale bar = 10 mm.	107
Figure 4.13: Western blot analysis of (a) γ H2AX, (b) p53, (c) PARP and (d) TOPO-1 in HeLa cells after treatment with GO-Nanocells for 24 h.....	108
Figure 4.14: HeLa cells were treated with GO-Nanocells for 24 h and (a, b) γ H2AX expression was quantified from confocal microscopy and Western blot analysis respectively and (c-f) quantification of p53, PARP, Topo-1 and Cas-3 from Western blot analysis respectively.....	108
Figure 4.15: Cell cycle analysis of HeLa cells via flow cytometry after treatment with GO-Nanocells for 24 h and 48 h. The cellular DNA was stained by red fluorescent propidium iodide (PI).	109
Figure 4.16: Induction of apoptosis in HeLa cells at 24 h and 48 h postincubation with GO-Nanocells determined by flow cytometry analysis.	110
Figure 4.17: (a) Western blot analysis of caspase-3 in HeLa cells as a marker for apoptosis after treatment with GO-Nanocells for 24 h. (b) Viability of HeLa cells at 24 h and (c) 48 h post-incubation with GO-Nanocells quantified by MTT assays.....	111
Table 1: DNA damaging chemotherapeutics and their clinical status.....	7
Table 2: Self-assembly of GO sheets at different interfaces.....	27

Table 3: Quantification of % volume colocalization of GO-Nanocells into lysosomes of HeLa cells in different time points (1h, 3h, 6h, 12h and 24h) from confocal microscopy.....105

SYNOPSIS

Till date cancer remains as one of the most dreaded diseases and is the second leading cause of mortality worldwide. Even though our understanding of cancer biology has shown outstanding progress over the years, its translation into clinics is distantly comparable. Cancer treatment mainly relies on chemotherapy and radiation therapy which use agents that exploit the sensitivity of cancer cells towards DNA damage, to induce apoptosis, and necrosis in them. The poor selectivity of the therapeutic drugs, which leads to reduced amounts reaching the desired target, along with their associated off-target collateral damage accounts for the impediments in cancer therapy. To overcome the hurdles of traditional cancer treatments, nanotechnology based platforms were incorporated which revolutionized the field of cancer therapy. Various nanoplateforms have been used for anticancer drugs to specifically target cancer cells, but all have their own associated drawbacks limiting their application. The combined use of multiple drugs in a single nanoplateform still remains a considerable challenge. Thus, graphene oxide-based biocompatible nanoscale materials, by virtue of their unique physicochemical properties and the large surface have the potential to tackle this complication (**Chapter 1**). In this thesis, we have tried to address these challenges by integrating nanomaterials, organic synthesis, and chemical biology.



Scheme 1: Novel graphene oxide based nanoparticles for damaging nuclear DNA in cancer cells

In **Chapter 2**, we have reported the hitherto unobserved cisplatin induced self-assembly of 2D-graphene oxide sheets into 3D-spherical nano-scale particles (GO-NPs). These nanoparticles can encompass dual DNA damaging drugs simultaneously. A combination of confocal microscopy, gel electrophoresis and flow cytometry studies clearly demonstrated that these novel nanoparticles can internalize into cancer cells by endocytosis, localize into lysosomes, followed by DNA damage leading to apoptosis. Cell viability assays indicated that these nanoparticles were more cytotoxic towards cancer cells compared to healthy cells.

Chapter 3 deals with enhancing the dispersibility and biocompatibility of the previously synthesised graphene oxide nanoparticles (GO-NPs), along with inhibiting multiple targets in cervical cancer HeLa cells. To achieve this, we have engineered hydrophilic polymer (PEG and PIMA) grafted self-assembled GO nanoparticles containing a hydrophobic topoisomerase inhibitor: SN38 and cisplatin concurrently. A combination of confocal microscopy, gel electrophoresis, and flow cytometry studies revealed that the GO-PEG-SN38-CDDP-NPs and GO-PIMA_Ed-SN38-CDDP NPs were ingested into the acidic lysosomes of HeLa cells within 6h leading to topoisomerase I inhibition, DNA damage and finally inducing apoptosis. They also demonstrated remarkably greater cytotoxicity towards HeLa cells.

Lastly, in **Chapter 4** we have developed a self-assembled spherical 3D-graphene oxide nanoparticle coated with lipid (GO-Nanocell) which can concomitantly load and release multiple Topoisomerase inhibitors (topotecan and doxorubicin) and DNA damaging drug (cisplatin) in a controlled manner. Fluorescence confocal microscopy confirmed that these GO-Nanocells were taken up by the HeLa cervical cancer cells and homed into lysosomes temporally over 6h. A combination of confocal microscopy, gel electrophoresis, and flow cytometry study revealed that these GO-Nanocells damaged nuclear DNA along with Topoisomerase inhibition leading to induction of apoptosis through cell cycle arrest in G2-M phase. These GO-Nanocells killed HeLa cancer cells with remarkably greater efficacy compared to free drug cocktail at 48 h post-incubation. These self-assembled GO-Nanocells can serve as a nanoscale tool to perturb multiple therapeutically important sub-cellular targets simultaneously for improved efficacy in future cancer chemotherapy.

We envision that the presented novel graphene oxide based approaches can serve as a tool for strategic impairment of multiple cellular targets within cancer cells in a synchronized manner, increase the therapeutic efficacy and reduce off-target toxicity of the drugs. Hence, harbours the potential to be translated to clinics for future combination chemotherapy.

LIST OF PUBLICATIONS

1. Cisplatin-Induced Self-Assembly of Graphene Oxide Sheets into Spherical Nanoparticles for Damaging Sub-cellular DNA.

Aditi Nandi, Abhik Mallick, Piyush More, Poulomi Sengupta, Nirmalya Ballav, and Sudipta Basu; *Chem. Commun.* **2017**, 53, 1409-1412.

2. Polyethylenimine Coated Graphene Oxide Nanoparticles for Targeting Mitochondria in Cancer Cells.

Abhik Mallick, Aditi Nandi, and Sudipta Basu ; *ACS Appl. Bio Mater.* **2018**, 2, 14–19.

3. Graphene oxide Nanocells for Impairing Topoisomerase and DNA in Cancer Cells.

Aditi Nandi, Chandramouli Ghosh, Aman Bajpai and Sudipta Basu; *J. Mater. Chem. B*, **2019**, 7, 4191-4197.

4. Polymer Conjugated Graphene-oxide Nanoparticles Impair Nuclear DNA and Topoisomerase I in Cancer.

Aditi Nandi, Chandramouli Ghosh and Sudipta Basu; *Nanoscale Adv.*, **2019**, 1, 4965-4971.

5. Supramolecular Self-Assembly of Triazine-Based Small Molecule: Targeting Endoplasmic Reticulum in Cancer Cells.

Chandramouli Ghosh, Aditi Nandi, and Sudipta Basu; *Nanoscale* **2019**, 11, 3326–3335.

6. Lipid Nanoparticle-Mediated Induction of Endoplasmic Reticulum Stress in Cancer Cells.

Chandramouli Ghosh, Aditi Nandi, and Sudipta Basu; *ACS Appl. Bio. Mater.* **2019**, 2, 3992-4001.

ABBREVIATIONS

AFM	Atomic Force Microscopy
Boc	Di- <i>tert</i> -butyl dicarbonate
CDDP	Cisplatin
CIN	Chromosome instability
CPT	Camptothecin
DNA	Deoxyribonucleic acid
DMEM	Dulbecco's Modified Eagle Media
DOX	Doxorubicin
DSB	Double strand break
DSPE-PEG	1,2-distearoyl-sn-glycero-3-phosphoethanolamine-N-[amino(polyethylene glycol)-2000] (ammonium salt)
DLS	Dynamic light scattering
DMSO	Dimethyl sulfoxide
DCM	Dichloromethane
EPR	Enhanced permeability and retention
FACS	Fluorescence-activated cell sorting
FDA	Food and Drug Administration
FESEM	Field Mission Scanning Electron Microscope
FITC	Fluorescein Isothiocyanate
GO	Graphene oxide
HeLa	Henrietta Lacks
H2AX	H2A histone family member X

HRP	Horseradish peroxidase
IR	Infrared radiation
Prof	Proflavine
PARP	Poly (ADP-ribose) polymerase
PC	Phosphatidylcholine
PEG	Polyethylene glycol
PIMA	Poly(isobutylene-alt-maleic anhydride)
ROS	Reactive oxygen species
SSB	Single strand break
TOP1	Topoisomerase I
TOP2	Topoisomerase II

Chapter 1 : Introduction

1.1 Cancer

In a generation which has witnessed tremendous advancement in all fields including medicine, cancer still remains as one of the most lethal diseases accounting for 9.6 million deaths worldwide.¹ Cancer is a multistep process involving genetic mutations which alters the developmental pathways.² This endows cells with adaptive and unlimited multiplicative power under circumstances that would normally be dangerous to the cells.³ The uncontrolled proliferation of cells leads to the formation of a primary tumor mass, from where cancer cells can diverge and colonise distant organs through metastasis (**Figure 1.1**).⁴ Cancer can originate in any tissue giving rise to various types of cancers like lung, breast, colon, and blood cancer and more.⁵

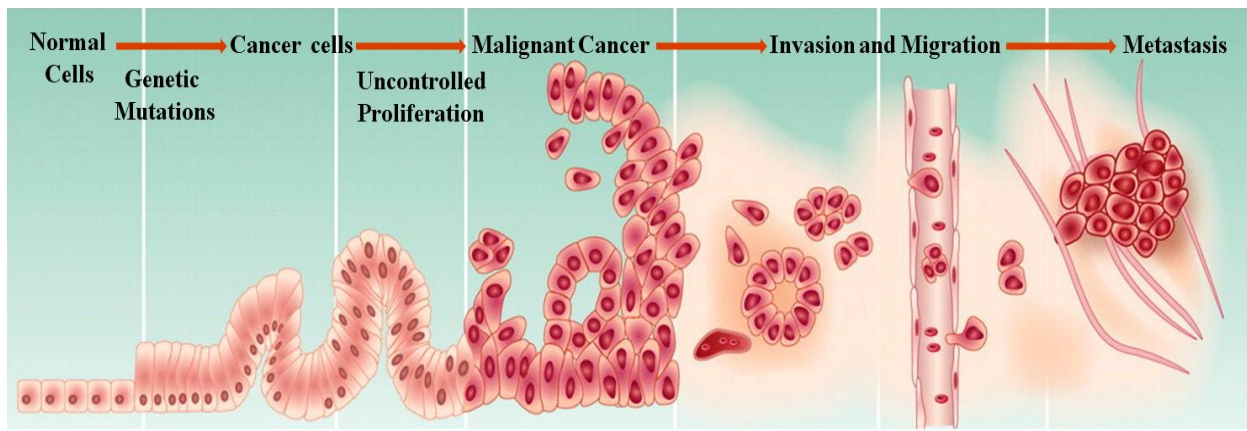


Figure 1.1: Development of cancer (adapted from Iacobuzio-Donahue et al. Clin. Cancer Res. 2012, 18, 4257-4265.)

Though cancer is remarkably complex and diverse, the cancer cells acquire a common set of biochemical and biological properties like: self-sufficiency in growth signalling, unlimited replication potential, resisting apoptosis, elude growth suppressors, sustained angiogenesis, and activating tissue invasion by metastasis. These characteristics along with additional features like reprogramming of energy metabolism, evading immune scrutiny, genomic instability and inflammation promoting tumor growth are termed as the “Hallmarks of Cancer” by Hanahan and Weinberg (in 2000 and modified in 2011), and are the necessary attributes to achieve the malignant phenotype (**Figure 1.2**).^{6,7}

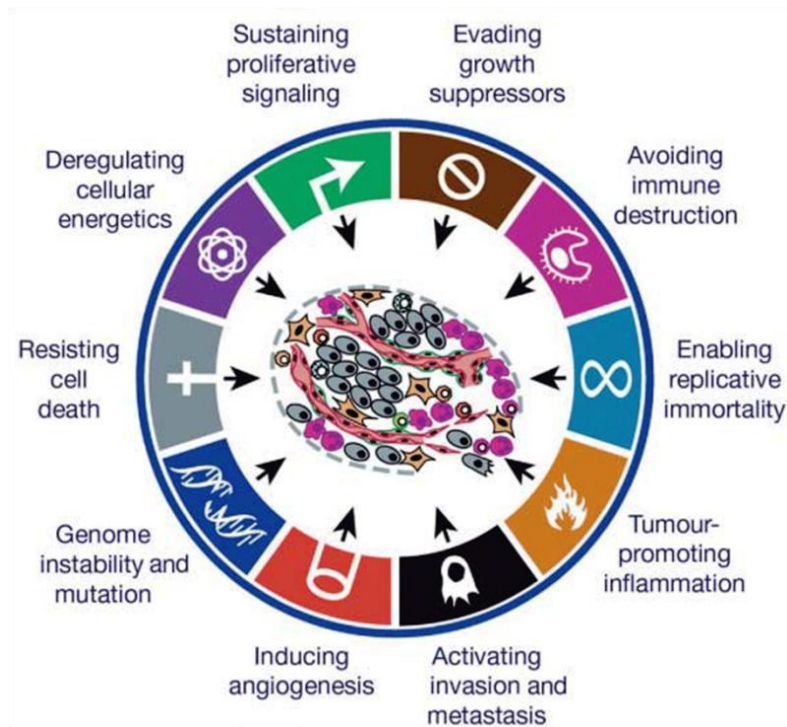


Figure 1.2: Hallmarks of Cancer (adapted from Hanahan et al. *Cell*, 2011, 144, 646-674.)

Apart from the hallmarks of cancer, Elledge and colleagues proposed additional traits of tumor cells which they termed as the stress phenotypes of cancer (**Figure 1.3**). These stresses are not responsible for initiating tumorigenesis but are an aftermath of it and include⁸:

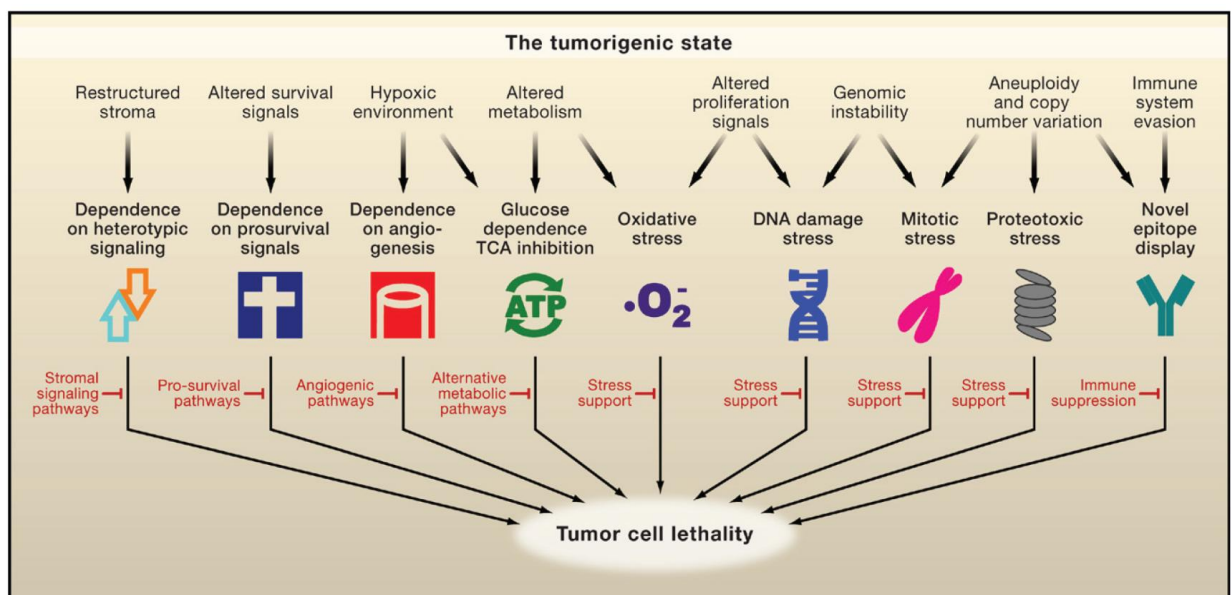


Figure 1.3: Stress phenotypes associated with the tumorigenic state of cells (adapted from Luo et al. *Cell* 2009, 136, 823-837.)

1.1.1 DNA damage and Replication stress:

Tumors are often associated with severe genomic instability due to endogenous and exogenous DNA damages such as: point mutations (addition or deletion), aneuploidy, chromosomal rearrangement⁹ and DNA strand lesions. These mutations activate the DNA damage response pathways which are deregulated in many types of cancers, due to alteration in the genes involved in the specific pathway. The inability to repair the abrasion leads to the persistence of the DNA damage and adds to genomic instability¹⁰. Further, the cancer cells adapt to such damage and continue to proliferate at a fast pace in the presence the DNA lesion leading to stress conditions.

1.1.2 Proteotoxic stress:

Altered chromosome number (aneuploidy) is a characteristic of tumor cells which results in the development of proteotoxic stress.¹¹⁻¹³ The high degree of aneuploidy can change the balance between the growth and survival signals promoting cancer progression. This imbalance also leads to the enhancement in aggregation of unfolded proteins in the cell, which adds to the burden on the protein degradation machinery to discard the misfolded or unfolded proteins.¹⁴ The activation of the heat shock protein pathway as a response to counteract the proteotoxic stress helps proper folding and or degradation of the proteins by proteolysis.¹⁵

1.1.3 Mitotic stress:

Genomic instability in tumors leads to increased chromosome mis-segregation which is termed as chromosome instability (CIN).¹⁶ The instability arises due to defects in the pathways and proteins involved in mitosis, such as defect in spindle assembly checkpoint, which maintains the arrangement of chromosomes along the mitotic spindle during anaphase, and existence of extra chromosomes in malignant cells¹⁷. Further, double strand lesions and alterations in genes like RAS, p53 also contribute to the chromosome instability¹⁸. This chromosomal distribution imbalance enables tumor cells to quickly evolve and replicate in the presence of the defects.

1.1.4 Metabolic stress:

Mitochondrial oxidative phosphorylation is the common metabolic pathway for ATP synthesis in normal cells. In contrast, cancer cells exhibit altered behaviour and predominantly depend on the glycolysis pathway for energy generation. The dependence of tumor cells on glycolysis helps it adapt to the varying oxygen environment as well as the acidic conditions, which promotes tumor metastasis and evasion of immune surveillance.¹⁹

1.1.5 Oxidative stress:

Oxidative stress is produced as a result of the generation of reactive oxygen species (ROS). ROS are highly reactive and leads to oxidative damage of the DNA proteins lipids and other cellular components contributing to endogenous DNA damage. Generally, tumor cells generate higher concentration of ROS as compared to normal cells, and are thus are subjected to greater oxidative stress.²⁰

These cellular stresses are intricately associated with the hallmarks and if left unchecked can be lethal for tumor cells. Thus, they pose as promising targets for cancer therapeutics. Exploiting the cellular stresses to selectively kill tumor cells can be accomplished by either hampering the stress support pathways, so that the cells cannot overcome the stress and cease to proliferate inducing apoptosis, or stress overload by which the already existing oncogenic stress are amplified leading to cell growth arrest or death. These approaches if applied tactfully in cancer treatment can be deleterious for tumor cells.⁸

Cancer treatment modality mainly involves chemotherapy, radiation therapy and surgery. Chemotherapy is based on the use of therapeutic drugs or particular kinase inhibitors to target receptor tyrosine kinases and signalling pathways of rapidly replicating cells.²¹⁻²² Whereas, radiation therapy employs high energy X-rays , gamma rays to eradicate tumor cells.²³ All these therapies have certain drawbacks: (i) off target cytotoxicity to normal tissues (killing the normal healthy cells of the body along with the cancerous cells), (ii) dose limiting cytotoxicity, (iii) multidrug resistance and relapse.²⁴ The heterogeneity and complexity associated with cancer also presents a challenging task with respect to the treatment. To tackle this, identification of critical aspects of the oncogenic network is important whose inhibition will result in systemic failure.⁸

1.2 DNA as a Target for Cancer Therapy

Over the years, the DNA has been established as an important target for many anticancer drugs used in clinic for chemotherapy.²⁵ The DNA is a highly coiled structure present inside the nucleus which is the control centre of every cell present in the body. It contains all the genetic information and helps govern essential functions of the cell like replication, transcription and translation. The DNA is frequently subjected to various endogenous and exogenous damaging factors, leading to the formation of DNA lesions (base mismatch, inter and intra strand crosslinks, single strand break (SSB) and double strand break (DSB) (**Figure 1.4**).²⁶ The lesions

trigger repair pathways which rehabilitate the effects of the damage, and thus maintain proper functioning of the DNA. One of the most common types of damage is single strand break (SSB) which causes a lesion in a single strand of the DNA duplex.²⁶⁻²⁷ Failure of cancer cells to timely revoke such damage due to faulty repair proteins and pathways, and their sustained proliferating signals, can lead to stalled replication fork and blocked transcription. This leads to the generation of replication stress and double strand breaks (DSB). Double strand break is a type of DNA lesion which is the most lethal of all the abrasions encountered by the DNA and leads to cell death.²⁸⁻²⁹ The generated replication stress if left unaltered can lead to genomic changes like mutations and chromosomal rearrangement and can promote the entrance of the tumour cells into phases of the cell cycle, where unresolved stresses can be catastrophic for the cells. Various anticancer drugs (Table 1) are employed in chemotherapy which orchestrates their activity by directly damaging the DNA, thereby increasing DNA replication stress, inducing lethal DNA lesions or depleting cellular resources.²⁹ Thus, exploiting the enhanced sensitivity of cancer cells towards DNA damage can be an effective tool for cancer treatment.

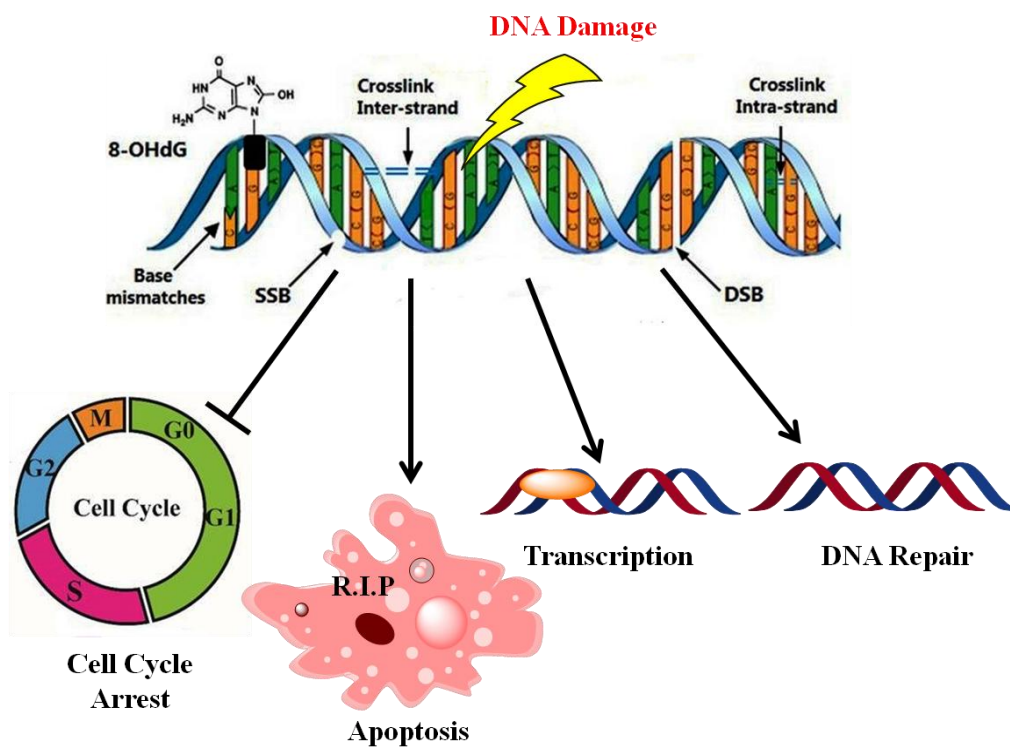


Figure 1.4: Consequences of DNA damage

Class of agents or targets	Function	Compounds	Clinical stage
Nucleoside analogues	Inhibition of DNA replication	Azacitidine Cytarabine Decitabine 5-Fluorouracil	All approved for use
Alkylating compounds and Platinum compounds	Direct modification of the DNA and DNA adducts	Carboplatin Cisplatin Cyclophosphamide Dacarbazine Methotrexate Mitomycin C Oxaliplatin Procarbazine Temozolomide	All approved for use
Topoisomerase I and II	Relax DNA supercoiling that occurs during DNA replication and Transcription	Belotecan Doxorubicin Epirubicin Etoposide Idarubicin Irinotecan Mitoxantrone Teniposide Topotecan	All approved for use
		CRLX101	Phase II
		LMP400	Phase I
		LMP 776	Phase I
		NKTR-102	Phase III
PARP	Single strand DNA Repair	Olaprib Niraparib	Approved

		Rucaparib Talazoparib	
		Veliparib	Phase III
ATR	Central replication stress response kinase	AZD6738 BAY1895344 M6620	Phase I/II Phase I/II Phase II
CHK1	Main effector kinase of ATR in replication stress response	GDC-0575 SCH900776 SRA737 Prexasertib	Phase I Phase I Phase I Phase I/II
WEE1	G ₂ -M Checkpoint kinase	AZD1775	Phase I/II

Table 1: DNA damaging chemotherapeutics and their clinical status

1.3 Selective Targeting of Tumor Cells

Cancer treatment has improved dramatically over the last decade; however certain barriers still exist in the pursuit of effective cancer cure.³⁰ One of the main hurdles pertaining to the use of chemotherapy in clinics is the incompetency to safely deliver the therapeutic agents specifically to tumor cells without severely affecting the healthy tissues and organs. The amalgamation of nanotechnology into medicine (nano-medicine) has led to unparalleled growth in the treatment of cancer. Nanotechnology is a multidisciplinary field that deals with the engineering of systems (therapeutic agents and diagnostic tools) through the control of matter on the nanometer scale. It has steered a lot of interest owing to its potential to resolve obstacles associated with traditional chemotherapy, such as- poor water solubility of drugs, inadequate targeting capability and erratic drug bio-distribution inside the body, systemic toxicity and low therapeutic index of drugs.^{24, 31-32}

The physiochemical properties of the nanotechnology-based therapeutics/nanoparticles can be tuned by tailoring the chemical composition, size, and surface morphology; to overcome biological barriers, differentiate between cancerous and non-cancerous tissues and smartly (stimuli responsive) release the drug payload inside the heterogeneous tumor microenvironment (**Figure 1.5**). Another critical property of the drug loaded nanoparticles is that, they should be

stable at physiological pH (pH=7.4) The shape, size, surface charge and functionalities play an important role in determining the cellular uptake of nanoparticles into tumor cells and further, their blood circulation half-life inside the body.^{24,33-34} The accumulation of the internalized nanoscale particles carrying various therapeutic agents into cancer tissues occurs either by passive targeting or active targeting via enhanced permeability and retention (EPR) effect.

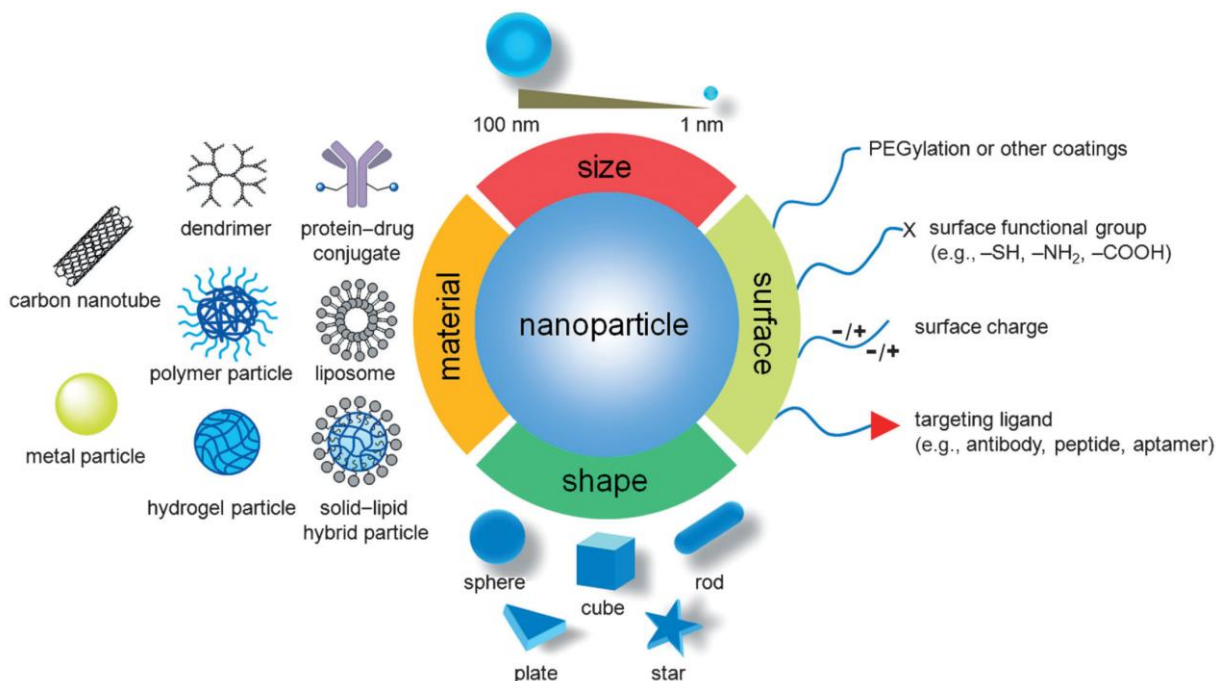


Figure 1.5: Biophysical features of nanoparticles for cancer therapy (adapted from Xia et al. *Angew. Chem. Int. Ed.* 2014, 53, 12320-12364.)

In passive targeting, the nanoparticles in the size range of 30-200nm, having long blood circulation time and stealth behaviour can extravasate into the tumor tissues. Unlike small molecules which diffuse non-specifically into normal as well as cancer tissues, nanoparticles cannot pass through the tight junctions of endothelial cells on the vascular lining of healthy cells. Solid tumors, on the contrary, are characterized by leaky vasculature and dysfunctional lymphatic drainage allowing nanoparticles/nanovectors to accumulate in and release their drug payload in the vicinity of the tumor tissues. **(Figure 1.6)** This effect is commonly known as enhanced permeability and retention effect (EPR effect) and is the basis of the bio-distribution of nano-therapeutics through passive targeting-which is an attractive approach for drug delivery.³⁵⁻

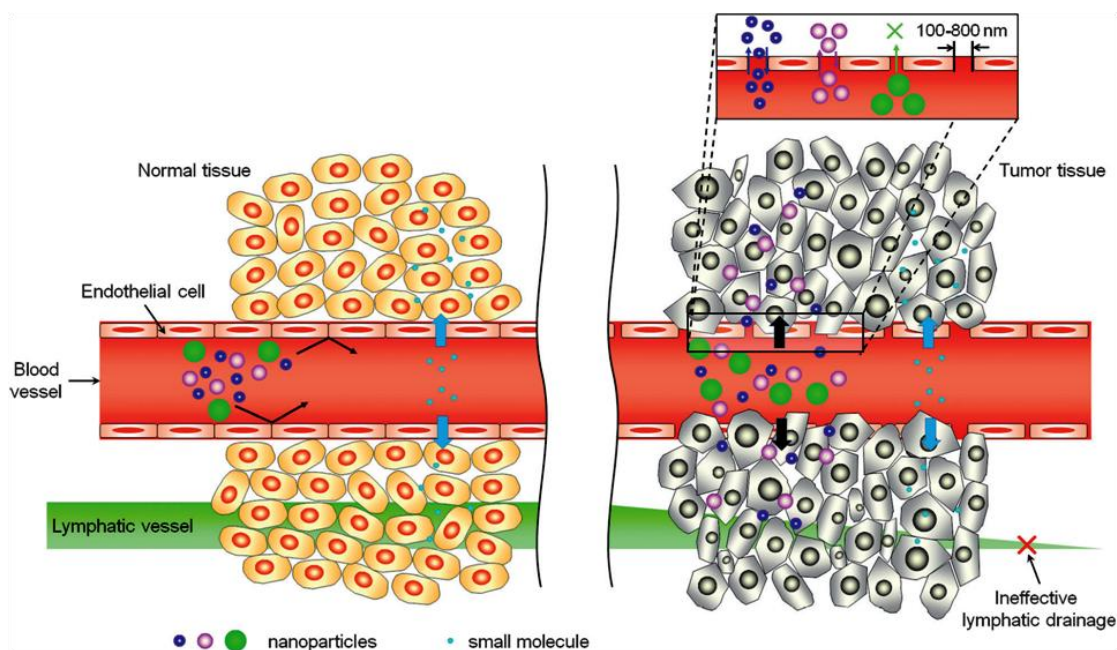


Figure 1.6: Accumulation of nanoparticles in normal and tumor tissues (adapted from Xia et al. *Angew. Chem. Int. Ed.* 2014, 53, 12320-12364.)

Another strategy that is widely being investigated for spatial and temporal localization of nanoscale systems into tumors is active targeting. This new targeting approach is based on molecular recognition of specific receptors expressed on the surface of cancer cells, by nanomaterials modified with targeting ligands, peptides, nucleic acids and antibody fragments. This enables enhanced nanoparticle internalization due to better binding to the surface of specific types of cancer cells. Active targeting of nanomaterials to solid tumors also depends on EPR effect to pass through the fenestrae in the vascular walls, which fosters cellular toxicity and ameliorates the therapeutic efficacy of the genotoxic drugs delivered to the specific tumor cells.⁴⁰⁻⁴² (**Figure 1.7**).

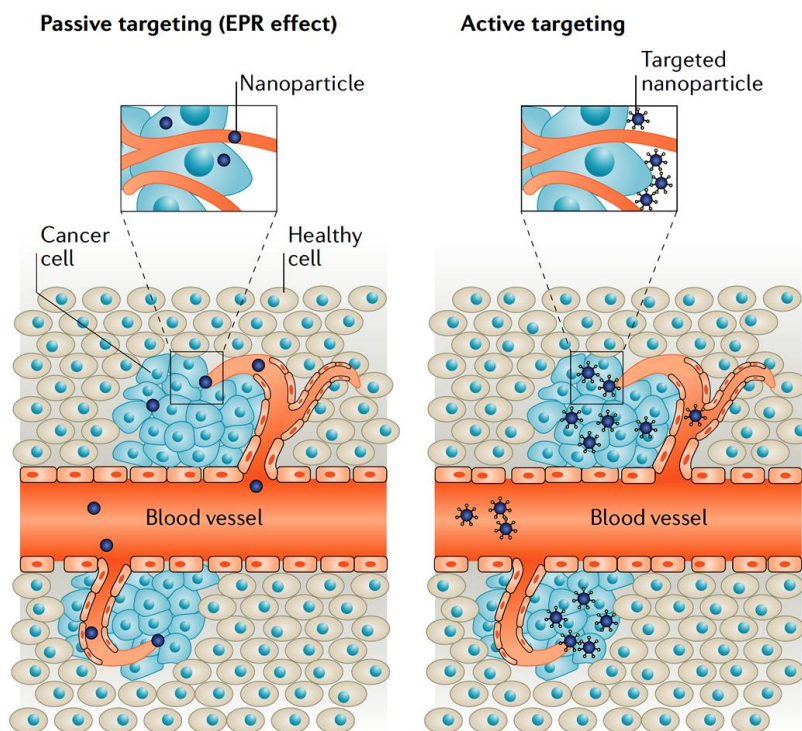


Figure 1.7: Representation for delivery of nanoparticles by passive and active targeting by exploiting EPR effect (adapted from Riley et al *Nat. Rev. Drug Discov.* 2019, 18, 175-196.)

1.4 Nanomaterials in Tumor Targeting

The paradigm changing impact of nanotechnology in cancer therapy has led to the development of various types of nanomaterials (NPs) for diagnosis, drug delivery and treatment.⁴³ Nanomaterials such as liposomes, polymeric nanoparticles, dendrimers, iron oxide, gold NPs, mesoporous silica nanoparticles have been engineered using materials ranging from proteins, lipids, polysaccharides, synthetic polymers, metals and other organic and inorganic materials.⁴⁴⁻⁴⁶ Another material that has attracted great interest in the last decade, for its biomedical application is graphene and its derivative graphene oxide (GO), which are regarded as 2D wonder materials.⁴⁷ Graphene oxide is an oxidized off-shoot of graphene (**Figure 1.8**) with atomic layer of sp^2 hybridised carbon atoms along with sp^3 carbon atoms decorated with oxygen functional groups like epoxy, hydroxyl and carboxylic acid.



Figure 1.8: Synthesis of graphene oxide (GO) from graphene by modified Hummers method (adapted from Xu et al. *ACS Appl. Mater. Interfaces* 2014, 6, 17265-17276).

The unique morphology of GO imparts intriguing physico-chemical characteristics such as amphiphilicity, negative surface charge, high conductivity and photoluminescence property. The large surface area and versatile surface chemistry of GO enables various covalent modifications as well as non-covalent stacking of aromatic small molecule drugs, proteins, nucleic acid and genes by hydrophobic or Π - Π interactions.⁴⁸⁻⁵⁴ One of the main concerns relating to the different ingredients used to develop nanomaterials is their toxicity and biokinetics.⁵⁵ As a nanomaterial, GO exhibits cytocompatible properties and is generally considered negligibly harmful at lower concentrations. Hence it is biocompatible to mammalian cells *in vitro* as well as *in vivo*.⁵⁶ Some reports in literature mention that GO does not show any apparent toxicity over 50 $\mu\text{g/ml}$ dose *in vitro*, but higher concentration leads to loss of cell viability due to dose dependent oxidative stress by ROS.⁵⁷ Though the *in vivo* toxicity of GO is poorly understood, studies on zebra fish suggests that it is easily cleared from the system and has no long lasting effects.⁵⁸ Further, intravenous administration of upto 0.2 mg dose of GO also didn't promote any obvious toxicity in mice model.⁵⁹ The compatibility can be improved by tuning parameters such as the lateral dimensions, by reducing the oxidation state and surface modification with biologically safe molecules which lowers the inflammatory response of GO post administration.^{58,60} However, ascertaining the *in vivo* toxicity of GO still requires further investigation.

The biocompatibility coupled with myriad of features of GO makes it desirable for biomedical applications, especially in cancer treatment: for the development of multifunctional nanoplatfoms⁶¹ (**Figure 1.9**). It has been investigated for its use as a biosensor for detection of nucleic acids, telomeres, proteins (like Cyclin) that are over expressed in various types of cancers, and detection of ATP in live cells using fluorescently labelled aptamers.⁶²⁻⁶⁴ In addition graphene oxide strongly absorbs in the NIR region, where the radiations are non-invasive and

harmless when penetrating the skin. Thus, owing to the high light to heat conversion, GO can be employed for ablation of tumor cells by photothermal therapy.⁶⁵

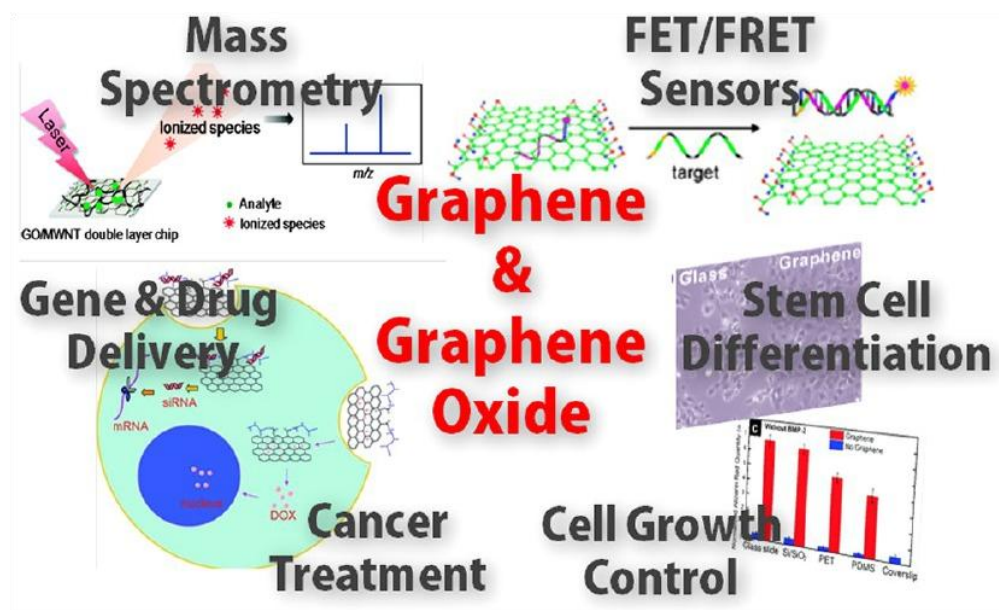


Figure 1.9: Applications of GO (adapted from Chung *Acc. Chem. Res.* 2013, 46, 2211-2224.)

Moreover, GO can be effectively used for stimuli responsive drug delivery because of the large surface area which allows stacking of hydrophobic as well as hydrophilic anticancer drugs.⁶⁶ Various research groups have also explored GO based nanoplatfoms for bio-imaging by stacking fluorescent molecules, modifying the basal $-COOH$ groups with fluorescently labelled polyethyleneglycol (PEG) polymers, or incorporating radio-labelled I^{125} , ^{64}Cu on its structural defects, which can be used for PET imaging of tumors.⁶⁷⁻⁶⁸ GO can also be used as a multimodal platform to achieve combinatorial therapy (**Figure 1.10**). Combination chemotherapy involves the use of two or more synergistic drugs which helps enhance the efficacy of each drug, or combining different treatment approaches like chemotherapy-photothermal therapy or chemotherapy-photodynamic therapy, which can prove to be a better strategy for cancer treatment.⁶⁹

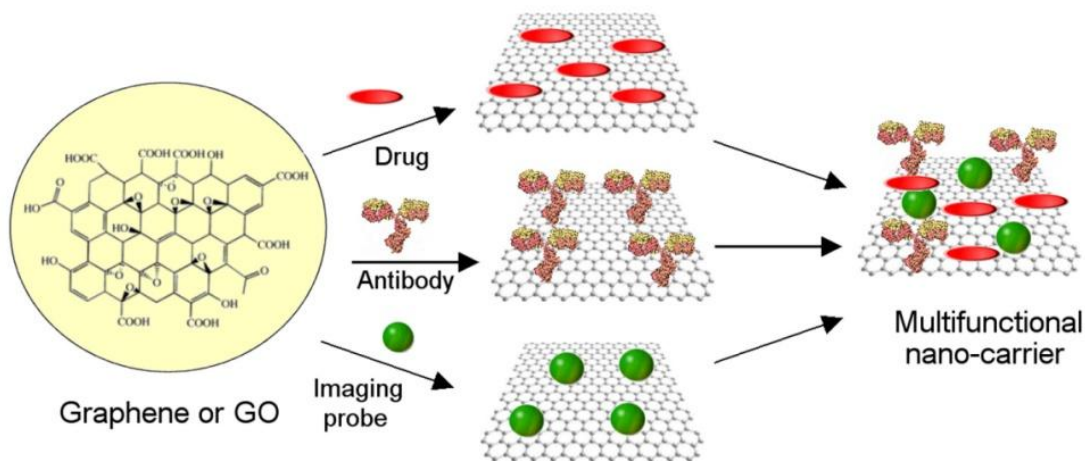


Figure 1.10: GO as multifunctional nano-carrier (adapted from Liu et al. *Acta Biomaterialia* 2013, 9, 9243-9257.)

In this context, Zhang et al. developed a folic acid (FA) modified GO nanoplatform which was loaded with drugs: doxorubicin (DOX) and camptothecin (CPT). This platform was specific for active targeting to MCF-7 human breast cancer cells which have FA receptors over-expressed on its cell surface and thus it displayed better cell killing ability.⁷⁰ Shen et al. used pegylated nano graphene oxide (PEG-NGO) modified with Gd^{3+} and stacked with DOX, to achieve superior imaging efficiency along with tumor cytotoxicity because of DOX release.⁷¹ Researchers have also investigated the delivery of dual drugs like Doxorubicin and Irinotecan using GO decorated with polaxmer 188; which can absorb NIR radiation and hence be lethal to cancer cells by combined effect of chemo- and photothermal therapy.⁷² Another interesting feature of GO which stems from its amphiphilic property, is the ability to form morphologically different nanostructures due to interfacial self-assembly.⁷³ GO forms sack cargo based structures by addition of a second component into the GO hydrosol droplets at the liquid-air interface, followed by evaporation. The GO- nanosacks demonstrate a biological response similar to GO sheets and have low acute cytotoxicity. Thus, they show promising potential for biomedical applications; for controlled drug delivery and release. Cellular uptake experiments of GO based nano-sacks with human lung epithelial cells also demonstrated its potential use in biomedicine.⁷⁴ A drawback related to GO nano-sacks is the leakage of drugs, which is not favourable for its use as a drug delivery carrier. Zhao *et. al* engineered a drug delivery platform for cancer treatment based on graphene oxide nanoparticles (GON) of suitable size and morphology. They developed DOX loaded biocompatible reduction responsive nanocarriers, by surface modification of GON with

biocompatible pegylated-alignate brushes. The pegylated-alignate brushes were grafted onto GON through GSH responsive disulphide linkage. The GON-Cy-ALG-PEG nanocarriers prevented leakage to DOX at physiological conditions, but higher GSH concentration and acidic conditions (which a characteristic of tumor cells) triggered increased release of DOX due to detachment of Cy-ALG-PEG brushes from GON. The GON-Cy-ALG-PEG nanoparticles showed good stability and greater cytotoxicity towards cancer cells.⁷⁵ Graphene oxide based quantum dots are nanostructures that are also being investigated for their potential as anti-cancer drug delivery carriers. Owing to their ultra small lateral dimensions they display lower *in vitro* and *in vivo* toxicity as compared to micrometer sized GO-nanosheets. Ding *et al* developed a GQD based theranostic platform by loading DOX on the surface, and further conjugating Cy5.5 dye to the GQD surface using a cathepsin D responsive peptide. The modified GQDs presented improved tissue penetration and cellular uptake which enhanced the *in vitro* and *in vivo* therapeutic performance. Using the same system as a probe they could further track the delivery and release of DOX.⁷⁴ Researchers have also developed GQD capped magnetic mesoporous silica nanoparticles as a multifunctional scaffold to achieve combinatorial magnetic hyperthermia and chemo-photothermal therapy. The synergistic effect resulted in greater breast cancer killing efficacy.⁷⁶ Thus, GO presents great opportunities for cancer therapy, which can be translated to clinics.

1.5 Aim of the Thesis

Inspired by the properties of GO we hypothesized to develop novel GO-drug nanoplatforms to damage the nuclear DNA in cancer cells. In literature, most of the dual drug delivery achieved using GO employs π - π stacking interaction as the approach to load the drugs onto GO. Our strategy in **chapter 2** involved direct covalent linking of a DNA damaging drug molecule to the –COOH groups present on the basal plane of GO, along with stacking of another aromatic DNA binding drug on the surface. The release of the two drugs inside the tumor cells could bring about DNA damage and initiate cell death by apoptosis. Using a similar strategy in **chapter 3** and **chapter 4** we hypothesized to simultaneously inhibit different accessory enzymes associated with the DNA (Topoisomerase 1 and Topoisomerase 2, which play an instrumental role in maintaining the topology and functioning of the DNA), in addition to bringing about DNA damage. We envision that by damaging the nuclear DNA using GO as a nanoplatform to safely deliver the anticancer drugs, we can capitalize upon the sensitivity of cancer cells towards

nuclear DNA damage stress and trigger programmed cell death i.e. apoptosis in them. Thus, the GO based approaches could provide a plausible outcome which can be applied for next generation cancer therapy.

1.6 References

1. Bray, F.; Ferlay, J.; Soerjomataram, I.; Siegel, R. L.; Torre, L. A.; Jemal, A. Global Cancer Statistics 2018: GLOBOCAN Estimates of Incidence and Mortality Worldwide for 36 Cancers in 185 Countries. *CA. Cancer J. Clin.* **2018**, *68*, 394–424.
2. Vogel, B.; Kinzler, T. W. The Multistep Nature of Cancer. *Trends Genet.* **1993**, *9*, 138-141.
3. Anajwala, C. C.; Jani, G. K.; Vijayendra Swamy, S. M. Current Trends in Nanotechnology for Cancer Therapy. *Int. J. Pharm. Sci. Nanotech.* **2010**, *3*, 1043-1056.
4. Seyfried, T. N.; Huysentruyt, L. C. On the Origin of Cancer Metastasis. *Crit Rev Oncog.* **2013**, *18*, 43-73.
5. Hassanpour, S. H.; Dehghani, M. Review of Cancer from Perspective of Molecular. *J. Cancer Res. Pract.* **2017**, *4*, 127–129.
6. Hanahan, D.; Weinberg, R. A. The Hallmarks of Cancer. *Cell* **2000**, *100*, 57–70.
7. Hanahan, D.; Weinberg, R. A. Review Hallmarks of Cancer: The Next Generation. *Cell* **2011**, *144*, 646–674.
8. Luo, J.; Solimini, N. L.; Elledge, S. J. Principles of Cancer Therapy: Oncogene and Non-Oncogene Addiction. *Cell* **2009**, *136*, 823–837.
9. Hartwell, L. H.; Kastan, M. B. Cell Cycle Control and Cancer. *Science* **1994**, *266*, 1821–1828.
10. Harper, J. W.; Elledge, S. J. The DNA Damage Response: Ten Years After. *Mol. Cell* **2007**, *28*, 739–745.
11. Ganem, N. J.; Storchova, Z.; Pellman, D. Tetraploidy, Aneuploidy and Cancer. *Curr. Opin. Genet. Dev.* **2007**, *17*, 157–162.
12. Torres, E. M.; Williams, B. R.; Amon, A. Aneuploidy: Cells Losing Their Balance. *Genetics* **2008**, *179*, 737–746.

13. Williams, B. R.; Prabhu, V. R.; Hunter, K. E.; Glazier, C. M.; Whittaker, C. a; Housman, D. E.; Amon, A. Aneuploidy Affects Proliferation and Spontaneous Immortalization in Mammalian Cells. *Science* **2008**, *322*, 703–710.
14. Denoyelle, C.; Abou-Rjaily, G.; Bezrookove, V.; Verhaegen, M.; Johnson, T. M.; Fullen, D. R.; Pointer, J. N.; Gruber, S. B.; Su, L. D.; Nikiforov, M. A.; et al. Anti-Oncogenic Role of the Endoplasmic Reticulum Differentially Activated by Mutations in the MAPK Pathway. *Nat. Cell Biol.* **2006**, *8*, 1053–1063.
15. Whitesell, L.; Lindquist, S. L. HSP90 and the Chaperoning of Cancer. *Nat. Rev. Cancer* **2005**, *5*, 761–772.
16. Komarova, N.L.; Lengauer, C.; Vogelstein, B.; Nowak, M.A. Dynamics of genetic instability in sporadic and familial colorectal cancer. *Cancer Biol. Ther.* **2002**, *1*, 685–692.
17. Cahill, D. P.; Lengauer, J. Y.; Riggins, G. J.; Willson, J. K.; Markowitz, S. D.; Kinzler, K. W.; Vogelstein, B. Mutations of Mitotic Checkpoint Genes in Human Cancers. *Nature* **1988**, *392*, 300–303.
18. Denko, N. C.; Giacciat, A. J.; Stringer, J. R.; Stambrooku, P. J. The Human Ha-Ras Oncogene Induces Genomic Instability in Murine Fibroblasts within One Cell Cycle. *Proc. Nad. Acad. Sci. USA* **1994**, *91*, 5124–5128.
19. Warburg, O. On the Origin of Cancer Cells. *Science* **1956**, *123*, 309-314.
20. Szatrowski, T. P.; Nathan, C. F. Production of Large Amounts of Hydrogen Peroxide by Human Tumor Cells. *Cancer Res.* **1991**, *51*, 794–798.
21. Urruticoechea, A.; Alemany, R.; Balart, J.; Villanueva, A.; Vinals, F.; Capella, G. Recent Advances in Cancer Therapy: An Overview. *Curr. Pharm. Des.* **2010**, *16*, 3-10.
22. DeVita, V. T.; Chu, E. A History of Cancer Chemotherapy. *Cancer Res.* **2008**, *68*, 8643–8653

23. Song, G.; Cheng, L.; Chao, Y.; Yang, K.; Liu, Z. Emerging Nanotechnology and Advanced Material for Cancer Radiation Therapy. *Adv. Mater.* **2017**, *29*, 1700996.
24. Sun, T.; Zhang, Y. S.; Pang, B.; Hyun, D. C.; Yang, M.; Xia, Y. Engineered Nanoparticles for Drug Delivery in Cancer Therapy. *Angew. Chem. Int. Ed.* **2014**, *53*, 12320–12364.
25. Pan, L.; Liu, J.; Shi, J. Cancer Cell Nucleus-Targeting Nanocomposites for Advanced Tumor Therapeutics. *Chem. Soc. Rev.* **2018**, *47*, 6930–6946.
26. Khanna, A. DNA Damage in Cancer Therapy, A Boon or a Curse?. *Cancer Rev.* **2015**, *75*, 2133-2138.
27. Zhou, B. –B. S.; Elledge, S. The DNA Damage Response: Putting Checkpoints in Perspective. *Nature* **2000**, *408*, 433-439.
28. Cannan, W.; Pederson, D. S. Mechanism and Consequences of Double-strand DNA Break Formation in Chromatin. *J Cell Physiol.* **2016**, *231*, 3-14.
29. Ubhi, T.; Brown, G. W. Exploiting DNA Replication Stress for Cancer Treatment. *Cancer Res.* **2019**, *79*, 1730–1739.
30. Xu, X.; Ho, W.; Zhang, X.; Bertrand, N.; Farokhzad, O. Cancer Nanomedicine: From Targeted Delivery to Combination Therapy. *Trends Mol Med.* **2015**, *21*, 223-232.
31. Wang, X.; Yang, L.; Chen, Z.; Shin, D. M. Application of Nanotechnology in Cancer Therapy and Imaging. *CA. Cancer J. Clin.* **2008**, *58*, 97–110.
32. Peer, D.; Karp, J. M.; Hong, S.; Farokhzad, O. C.; Margalit, R.; Langer, R. Nanocarriers as an Emerging Platform for Cancer Therapy. *Nat. Nanotechnol.* **2007**, *2*, 751–760.
33. Blanco, E.; Shen, H.; Ferrari, M. Principles of Nanoparticle Design for Overcoming Biological Barriers to Drug Delivery. *Nature Biotechnol.* **2015**, *33*, 941-951.
34. Yu, M. K.; Park, J.; Jon, S. Targeting Strategies for Multifunctional Nanoparticles in Cancer Imaging and Therapy. *Theranostics* **2012**, *2*, 3-44.

35. Bazak, R.; Hourri, M.; Achy, S. E.; Hussein, W.; Refaat, T. Passive Targeting of Nanoparticles to Cancer: A Comprehensive Review of the Literature. *Mol. Clin. Oncol.* **2014**, *2*, 904–908.
36. Jiang, W.; Huang, Y.; An, Y.; Kim, B. Y. S. Remodeling Tumor Vasculature to Enhance Delivery of Intermediate-Sized Nanoparticles. *ACS Nano* **2015**, *9*, 8689–8696.
37. Hashizume, H.; Baluk, P.; Morikawa, S.; McLean, J. W.; Thurston, G.; Roberge, S.; Jain, R. K.; McDonald, D. M. Openings between Defective Endothelial Cells Explain Tumor Vessel Leakiness. *Am. J. Pathol.* **2000**, *156*, 1363–1380.
38. Maeda, H.; Nakamura, H.; Fang, J. The EPR Effect for Macromolecular Drug Delivery to Solid Tumors: Improvement of Tumor Uptake, Lowering of Systemic Toxicity, and Distinct Tumor Imaging in Vivo. *Adv. Drug Deliv. Rev.* **2013**, *65*, 71–79.
39. Rajora, A.; Ravishankar, D.; Osborn, H.; Greco, F. Impact of the Enhanced Permeability and Retention (EPR) Effect and Cathepsins Levels on the Activity of Polymer-Drug Conjugates. *Polymers* **2014**, *6*, 2186–2220.
40. Wang, M.; Thanou, M. Targeting Nanoparticles to Cancer. *Pharmacol. Res.* **2010**, *62*, 90–99.
41. Bazak, R.; Hourri, M.; El Achy, S.; Kamel, S.; Refaat, T. Cancer Active Targeting by Nanoparticles: A Comprehensive Review of Literature. *J. Cancer Res. Clin. Oncol.* **2015**, *141*, 769–784.
42. Byrne, J. D.; Betancourt, T.; Brannon-Peppas, L. Active Targeting Schemes for Nanoparticle Systems in Cancer Therapeutics. *Adv. Drug Deliv. Rev.* **2008**, *60*, 1615–1626.
43. Wang, A. Z.; Langer, R.; Farokhzad, O. C. Nanoparticle Delivery of Cancer Drugs. *Annu. Rev. Med.* **2012**, *63*, 185–198.
44. Ferrari, M. Cancer Nanotechnology: Opportunities and Challenges. *Nat. Rev. Cancer* **2005**, *5*, 161–171.

45. Shi, J.; Votruba, A. R.; Farokhzad, O.; Langer, R. Nanotechnology in Drug Delivery and Tissue Engineering: From Discovery to Applications. *Nano Lett.* **2010**, *10*, 3223-3230.
46. Qin, W.; Huang, G.; Chen, Z.; Zhang, Y. Nanomaterials in Targeting Cancer Stem Cells for Cancer Therapy. *Front. Pharmacol.* **2017**, *8*, 1-15.
47. Goenka, S.; Sant, V.; Sant, S. Graphene-Based Nanomaterials for Drug Delivery and Tissue Engineering. *J. Control. Release* **2014**, *173*, 75–88.
48. Liu, J.; Cui, L.; Losic, D. Graphene and Graphene Oxide as New Nanocarriers for Drug Delivery Applications. *Acta Biomater.* **2013**, *9*, 9243–9257.
49. Chung, C.; Kim, Y. K.; Shin, D.; Ryoo, S. R.; Hong, B. H.; Min, D. H. Biomedical Applications of Graphene and Graphene Oxide. *Acc. Chem. Res.* **2013**, *46*, 2211–2224.
50. Gonçalves, G.; Vila, M.; Portolés, M. T.; Vallet-Regi, M.; Gracio, J.; Marques, P. A. A. P. Nano-Graphene Oxide: A Potential Multifunctional Platform for Cancer Therapy. *Adv. Healthcare Mater.* **2013**, *2*, 1072–1090.
51. Kostarelos, K.; Novoselov, K. S. Exploring the Interface of Graphene and Biology. *Science* **2014**, *344*, 261–263.
52. Dreyer, D. R.; Park, S.; Bielawski, C. W.; Ruoff, R. S. The Chemistry of Graphene Oxide. *Chem. Soc. Rev.* **2010**, *39*, 228-240.
53. Eigler, S.; Hirsch. Chemistry with Graphene and Graphene Oxide-Challenges for Synthetic Chemists. *Angew. Chem. Int. Ed.* **2014**, *53*, 7720-7738.
54. Georgakilas, V.; Tiwari, J. N.; Kemp, K. C.; Perman, J. A.; Bourlinos, A. B.; Kim, K. S.; Zboril, R. Noncovalent Functionalization of Graphene and Graphene Oxide for Energy Materials, Biosensing, Catalytic, and Biomedical Applications. *Chem. Rev.* **2016**, *116*, 5464–5519.
55. Guo, X.; Mei, N. Assessment of the Toxic Potential of Graphene Family Nanomaterials. *J. Food Drug Anal.* **2014**, *22*, 105–115.

56. Sun, C.; Wakefield, D. L.; Han, Y.; Muller, D. A.; Holowka, D. A.; Baird, B. A.; Ditchel, W. R. Graphene Oxide Nanosheets Stimulate Ruffling and Shedding of Mammalian Cell Plasma Membranes. *Chem.* **2016**, *1*, 273-286.
57. Chang, Y.; Yang, S. T.; Liu, J. H.; Dong, E.; Wang, Y.; Cao, A.; Liu, Y.; Wang, H. In Vitro Toxicity Evaluation of Graphene Oxide on A549 Cells. *Toxicol. Lett.* **2011**, *200*, 201–210.
58. Sydlik, S. A.; Jhunjhunwala, S.; Webber, M. J.; Anderson, D. G.; Langer, R. In Vivo Compatibility of Graphene Oxide with Differing Oxidation States. *ACS Nano* **2015**, *9*, 3866–3874.
59. Zhang, X.; Yin, J.; Peng, C.; Hu, W.; Zhu, Z.; Li, W.; Fan, C.; Huang, Q. Distribution and Biocompatibility Studies of Graphene Oxide in Mice after Intravenous Administration. *Carbon.* **2011**, *49*, 986–995.
60. Xu, M.; Zhu, J.; Wang, F.; Xiong, Y.; Wu, Y.; Wang, Q.; Weng, J.; Zhang, Z. Chen, W.; Liu, S. Improved In Vitro and In Vivo Biocompatibility of Graphene Oxide through Surface Modification: Poly(Acrylic Acid)-Functionalization is Superior to PEGylation. *ACS Nano* **2016**, *10*, 3267–328.
61. Feng, L.; Wu, L.; Qu, X. New Horizons for Diagnostics and Therapeutic Applications of Graphene and Graphene Oxide. *Adv. Mater.* **2013**, *25*, 168–186.
62. Feng, L.; Wu, L.; Wang, J.; Ren, J.; Miyoshi, D.; Sugimoto, N.; Qu, X. Detection of a Prognostic Indicator in Early-Stage Cancer Using Functionalized Graphene-Based Peptide Sensors. *Adv. Mater.* **2012**, *24*, 125–131.
63. Wu, L.; Qu, X. Cancer Biomarker Detection: Recent Achievements and Challenges. *Chem. Soc. Rev.* **2015**, *44*, 2963–2997.
64. Hu, D.; Li, Z.; Lin, Y.; Li, J.; Lin, C.-T.; Wang, Y. Aptamer/Graphene Oxide Nanocomplex for in Situ Molecular Probing in Living Cells. *J. Am. Chem. Soc.* **2010**, *132*, 9274–9276.
65. Tian, B.; Wang, C.; Zhang, S.; Feng, L.; Liu, Z. Photothermally Enhanced Photodynamic Therapy Delivered by Nano-Graphene Oxide. *ACS Nano* **2011**, *5*, 7000-7009.

66. Liu, Z.; Robinson, J. T.; Sun, X.; Dai, H. PEGylated Nanographene Oxide for Delivery of Water-Insoluble Cancer Drugs. *J. Am. Chem. Soc.* **2008**, *130*, 10876–10877.
67. Yang, K.; Wan, J.; Zhang, S.; Zhang, Y.; Lee S. T.; Liu, Z. *In Vivo* Pharmacokinetics, Long-Term Biodistribution, and Toxicology of PEGylate Graphene in Mice. *ACS Nano* **2011**, *5*, 516-522.
68. Zhang, Y.; Yang, K.; Hong, H.; Engle, J.; Feng, L.; Theuer, C.; Barnhart, T.; Liu, Z.; Cai, W. *In Vivo* Targeting and Imaging of Tumor Vasculature with Radiolabeled, Antibody-Conjugated Nano-Graphene. *Med. Phys.* **2012**, *39*, 3950.
69. Mokhtari, R. B.; Homayouni, T. S.; Baluch, N.; Morgatskaya, E.; Kumar, S.; Das, B.; Yeger, H. Combination Therapy in Combating Cancer. *Oncotarget* **2017**, *8*, 38022–38043.
70. Zhang, L.; Xia, J.; Zhao, Q.; Liu, L.; Zhang, Z. Functional Graphene Oxide as a Nanocarrier for Controlled Loading and Targeted Delivery of Mixed Anticancer Drugs. *Small* **2010**, *6*, 537–544.
71. Shen, A. J.; Li, D. L.; Cai, X. J.; Dong, C. Y.; Dong, H. Q.; Wen, H. Y.; Dai, G. H.; Wang, P. J.; Li, Y. Y. Multifunctional Nanocomposite Based on Graphene Oxide for *in Vitro* Hepatocarcinoma Diagnosis and Treatment. *J. Biomed. Mater. Res. Part A* **2012**, 2499–2506.
72. Tran, T. H.; Nguyen, H. T.; Pham, T. T.; Choi, J. Y.; Choi, H. G.; Yong, C. S.; Kim, J. O. Development of a Graphene Oxide Nanocarrier for Dual-Drug Chemo-Phototherapy to Overcome Drug Resistance in Cancer. *ACS Appl. Mater. Interfaces* **2015**, *7*, 28647–28655.
73. Shao, J. J.; Lv, W.; Yang, Q. H. Self-Assembly of Graphene oxide at Interfaces. *Adv. Mater.* **2014**, *26*, 5586-5612.
74. Chen, Y.; Guo, F; Jachak, A.; Kim, S. P.; Datta, D.; Liu, J.; Kulaots, I.; Vaslet, C.; Jang, H. D.; Huang, J.; Kans, A.; Shenoy, V. B.; Hurt, R. B. Aerosol Synthesis of Cargo-Filled Graphene Nanosacks. *Nano Lett.* **2012**, *12*, 1996-2002.

75. Zhao, X.; Lei, L.; Li, X.; Zeng, J., Jia, X.; Liu, P. Biocompatible Graphene Oxide Nanoparticle-Based Drug Delivery Platform for Tumor Microenvironment-Responsive Triggered Release of Doxorubicin. *Langmuir* **2014**, *30*, 10419-10429.

76. Yao, X.; Niu, X.; Ma, K.; Huang, P.; Grothe, J.; Kaskel, S.; Zhu, Y. Graphene Quantum Dots-Capped Magnetic Mesoporous Silica Nanoparticles as a Multifunctional Platform for Controlled Drug Delivery, Magnetic Hyperthermia, and Photothermal Therapy. *Small* **2017**, *13*, 1602225.

Chapter 2: Cisplatin-Induced Self-Assembly of Graphene Oxide Sheets into Spherical Nanoparticles for Damaging Sub-cellular DNA.

This chapter has been published as:

Aditi Nandi, Abhik Mallick, Piyush More, Poulomi Sengupta, Nirmalya Ballav, and Sudipta Basu. Cisplatin-Induced Self-Assembly of Graphene Oxide Sheets into Spherical Nanoparticles for Damaging Sub-cellular DNA. *Chem. Commun.* **2017**, 53, 1409-1412.

(Reproduced by the permission from The Royal Society of Chemistry)

2.1 Abstract

In last couple of decades, graphene oxide (GO) has evolved as one of the most interesting carbon materials for myriads of biomedical applications. GO can self-assemble into interesting functional 3D structures in different interfaces. However, the interaction of these 3D-GO-based macro/micro structures with the biological milieu is largely untapped. In this chapter, for the first time, we demonstrate the hitherto unobserved morphological transformation of 2D-GO sheets into 3D-spherical nano-scale particles upon reaction with a DNA damaging drug cisplatin viz. a hierarchical self-assembly. These novel GO-based nanoparticles can comprise dual DNA-damaging drugs and compartmentalize into cancer cells in a significantly different manner than their 2D-precursors. Remarkably, these GO-NPs demonstrated much augmented efficacy in cancer cells keeping healthy cells unscathed. We envisage our new observation has the potential to be translated into clinics in future.

2.2 Introduction

In recent years, graphene oxide (GO) has emerged as one of the most interesting carbon materials for biomedical applications for its unique two dimensional structure and biocompatibility.¹⁻⁶ The amphiphilic nature enabled GO to self-assemble into myriad of three dimensional macro and micro structures including membranes,⁷ hydrogels,⁸ crumpled particles,⁹ hollow spheres¹⁰ and so on. The self assembly of GO can be easily exploited in different solvents like water, DMF and DMSO and at various interfaces to produce variety of GO based structures. The self concentration of GO sheets followed by non-covalent intersheet interactions lead to the interfacial self assembly of GO. The self assembly of GO sheets can occur at 3 different interfaces; liquid-air, liquid-liquid, liquid-solid and self assembly method employed, gives rise to varied morphologies. The table below (**Table 2**) summarises the typical GO self assemblies at interfaces.¹¹ However, all these 3D-structures are largely incompatible for modulating the functions of intracellular bio-molecules in diseased states (like cancer) as size, shape and morphology play crucial role to interact with the biological milieu¹²⁻¹⁵ and are mostly unexplored.



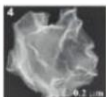
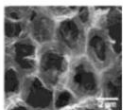
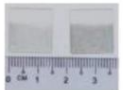
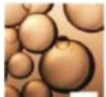




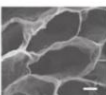
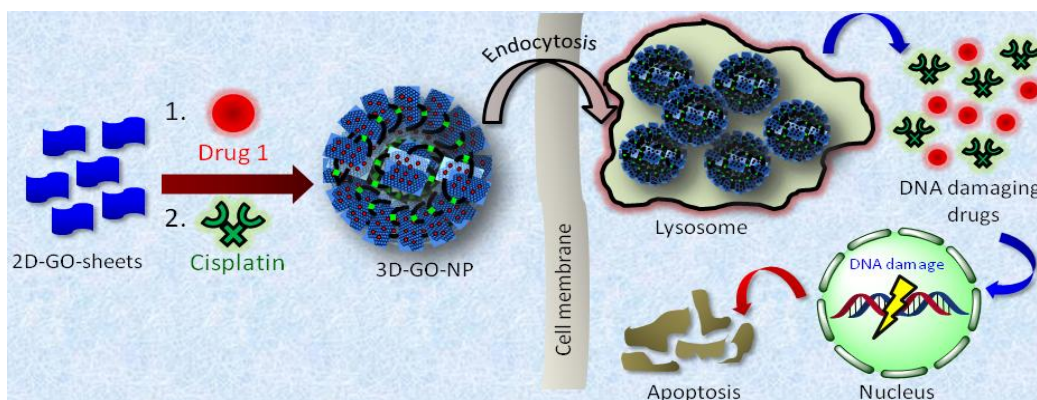
Types of interfaces	Self-assembly methods	Assembled structures	Typical images
Liquid-air interface	Langmuir-Blodgett assembly	Single-layer film; thin film	
	Evaporation-induced assembly at 2D interface	Free-standing membrane	
	Evaporation-induced assembly at 3D interface	Crumpled particles	
Liquid-liquid interface	Breath Figure (BF) assembly	Polymer/GO hybrid with honeycomb microstructure	
	Assembly at 2D interface	Thin film	
	Assembly at 3D interface in Pickering Emulsions	Hollow or spherical structures	
Liquid-solid interface	Promoted by chemical interaction	Hydrogel	
	Promoted by electrostatic interaction	Hydrogel; Hybrid materials	
	Assembly at surface of nanoparticles	All-carbon hybrid materials	
	Flow-directed assembly at solid substrate	Freestanding membranes	
	Assembly at dynamic ice-water interface	Porous materials	

Table 2: Self-assembly of GO sheets at different interfaces (adapted from Shao et al. *Adv. Mater.* 2014, 26, 5586-5612.)

Herein, for the first time, we describe an easy and robust synthesis of spherical graphene oxide-based nanoparticles (GO-NPs) which was successfully used to damage sub-cellular DNA in cancer cells. 2D-sheets of GO can host aromatic DNA damaging drugs (proflavine or doxorubicin) by π - π interaction.^{4,6} However, upon addition of cisplatin (CDDP) (DNA damaging, FDA approved anti-cancer drug), a remarkable morphological transformation from 2D-sheet into 3D-spherical nanoparticles was observed which can be ascribed to a hierarchical self-assembly. Compartmentalization of these composite GO-NPs inside the cancer cells was noted to be significantly different from the 2D-sheet like precursors, followed by DNA damage to induce improved efficacy through programmed cell death (apoptosis). In this study, we have chosen proflavine and doxorubicin for stacking on the surface of GO-sheets due to their (i) π - π interaction ability with the surface of GO-sheets (ii) intrinsic fluorescent nature allowing sub-cellular tracking and (iii) DNA binding capability leading to potential augmented DNA damage along with cisplatin in cancer cells. (**Scheme 1**)



Scheme 1: Self-assembly of GO sheets and their cellular fate.

2.3 Result and Discussion

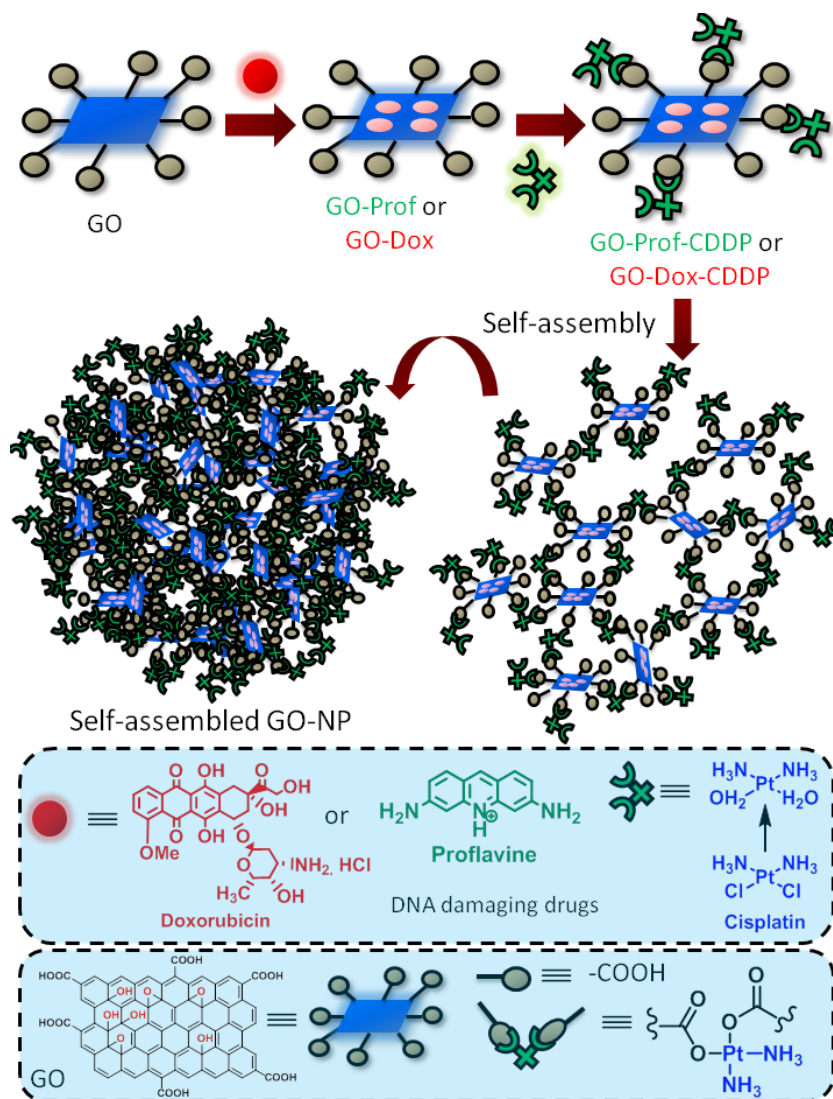


Figure 2.1: Stacking of proflavine and doxorubicin on GO-sheets that self-assembled into spherical nanoparticle after reaction with cisplatin.

The cisplatin mediated hierarchical self-assembly of graphene oxide sheets into spherical nanoparticles is proposed in **Figure 2.1**. A detailed description of the reaction scheme is shown in **Figure 2.27**. Briefly, aromatic DNA damaging drugs were first stacked on GO and preserved the 2D-sheet like structures as shown by field-emission microscopy (FESEM) and atomic force microscopy (AFM) studies (**Figure 2.2a-c**).

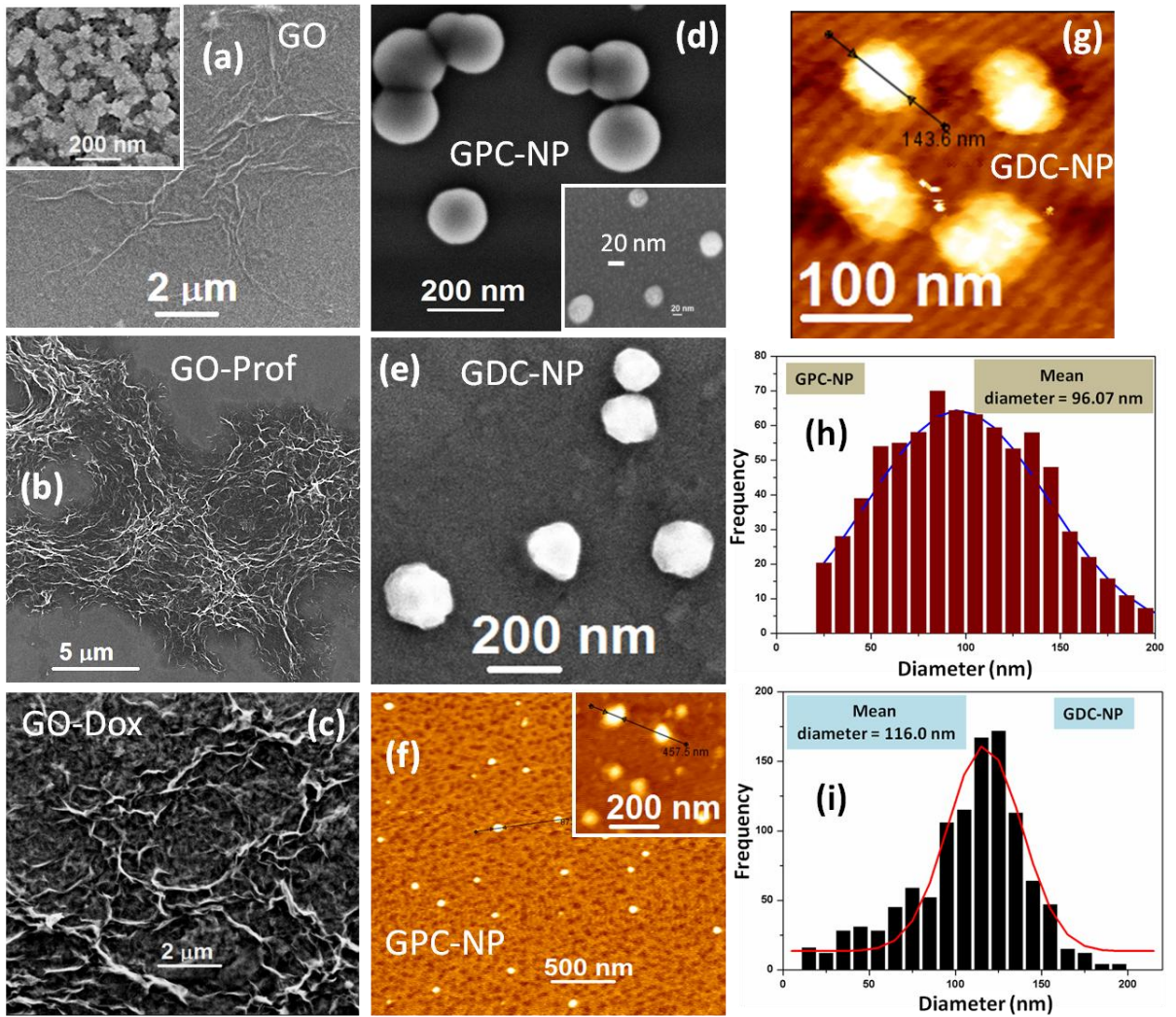


Figure 2.2: (a-c) FESEM images of GO, GO-Prof and GO-Dox complex respectively. (d,e) FESEM images of GPC-NPs and GDC-NPs respectively. (f,g) AFM images of GPC-NPs and GDC-NPs. (h,i) Mean diameter of GPC and GDC NP's.

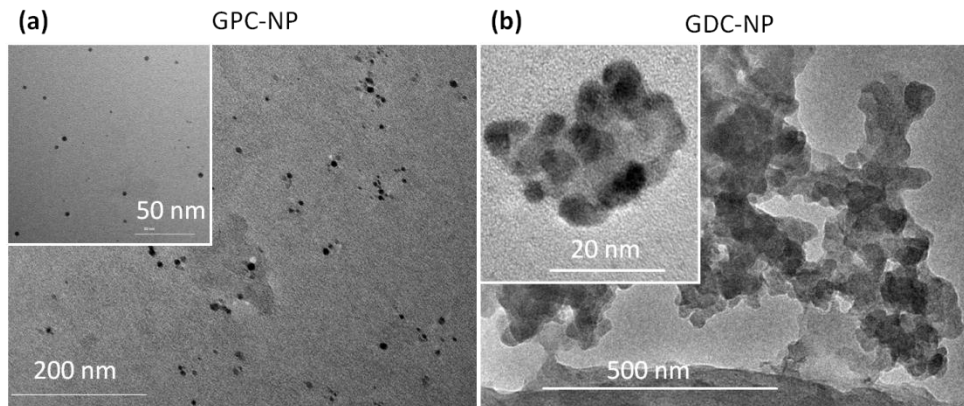


Figure 2.3: TEM images of (a) GPC and (b) GDC-NPs

Encapsulation of proflavine and doxorubicin by π - π interaction on GO surface were confirmed by the dramatic quenching of fluorescence emission spectrum of free proflavine ($\lambda_{\text{max}} = 510 \text{ nm}$) and free doxorubicin ($\lambda_{\text{max}} = 590 \text{ nm}$ respectively (**Figure 2.4 a-b**). Graphene oxide is regarded a good quencher and it strongly quenches the emission of fluorescent molecules through energy transfer. The quenching efficiency depends upon the distance between the fluorophore and GO surface.¹⁶

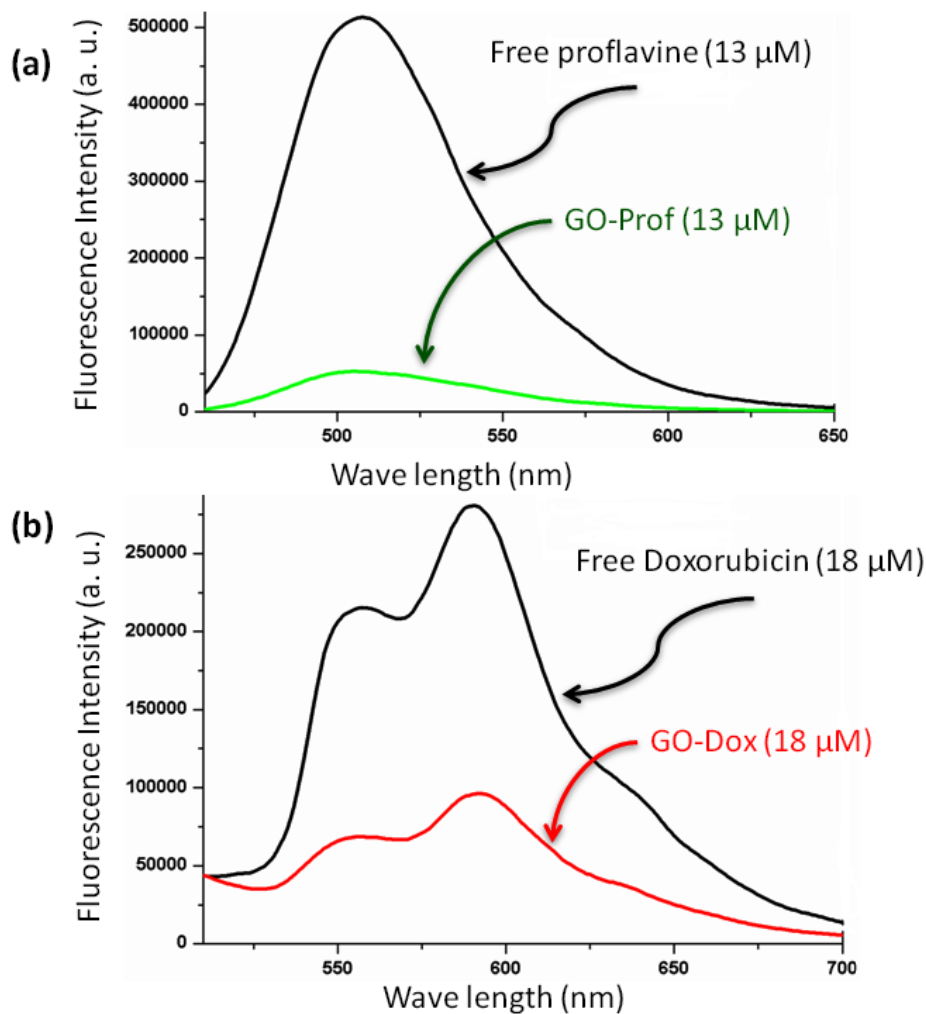


Figure 2.4: Fluorescence emission spectra of (a) GO-Prof and (b) GO-Dox showing fluorescence quenching of proflavine and doxorubicin upon stacking on GO surface.

Electron microscopy (FESEM, AFM and TEM) images clearly revealed that upon addition of cisplatin to GO-Prof and GO-Dox (**Figure 2.2d-g**) and (**Figure 2.3**) systems altered their shapes into spherical nanoparticles with size range of 80-200nm in diameter (**Figure 2.2h-i**). Raman spectroscopy is one of the best techniques to validate the

presence of GO. The on particle resonance raman spectra of the GPC and GDC nanoparticles revealed- characteristic D and G bands of GO at 1350 cm^{-1} and 1590 cm^{-1} , which confirmed the presence of GO in the respective nanoparticles. The G band arises because of the in-plane vibrational mode of the sp^2 hybridized carbon atoms. The characteristic D band originates due to the ring breathing modes of sp^2 carbon atoms and requires a defect for its activation¹⁶ (**Figure 2.5a**). Powder x-ray diffraction (PXRD) pattern of GPC-NPs showed the appearance of a new broad peak at much reduced d spacing of $\sim 6.2\text{ \AA}$ thereby indicating the stapling of GO-sheets into more closer and compact structures. Whereas, GO-Prof conjugate showed much elongated d spacing at 14.5 \AA , characteristic for intercalation of proflavine into GO sheets.¹⁷(**Figure 2.5b**)

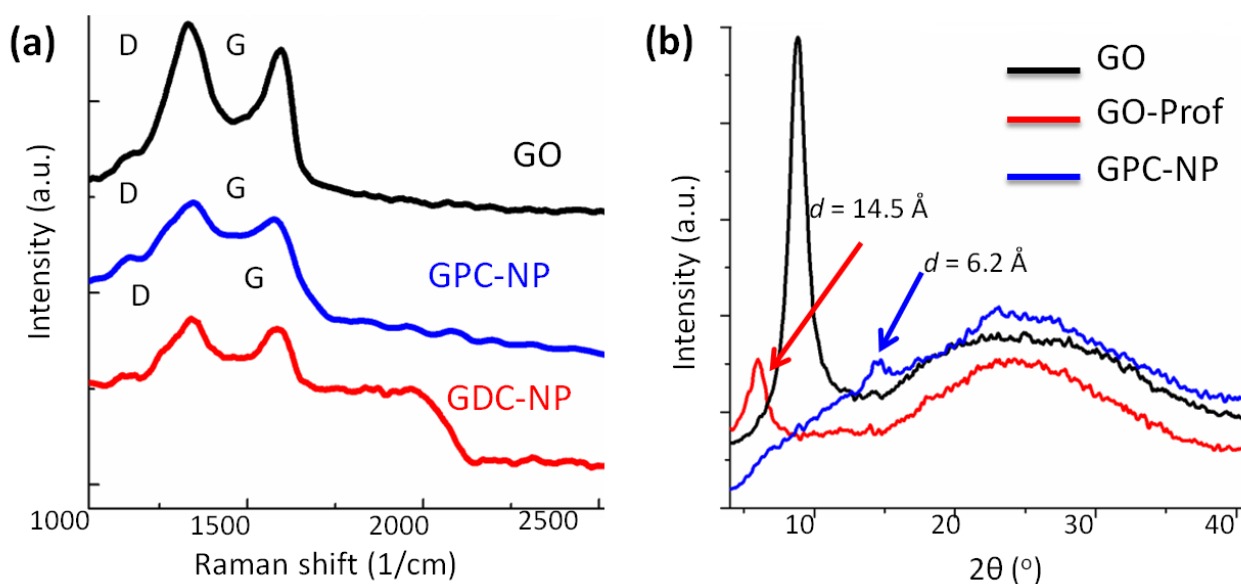


Figure 2.5: (a) On particle Resonance Raman spectra of GO, GPC-NP and GDC-NP. (b) PXRD spectra of GO, GO-Prof and GPC-NPs.

Presence of proflavine and doxorubicin stacked on GO surface in the nanoparticle was again confirmed by the dramatic fluorescence quenching of free proflavine and free doxorubicin (**Figure 2.6a-b**).

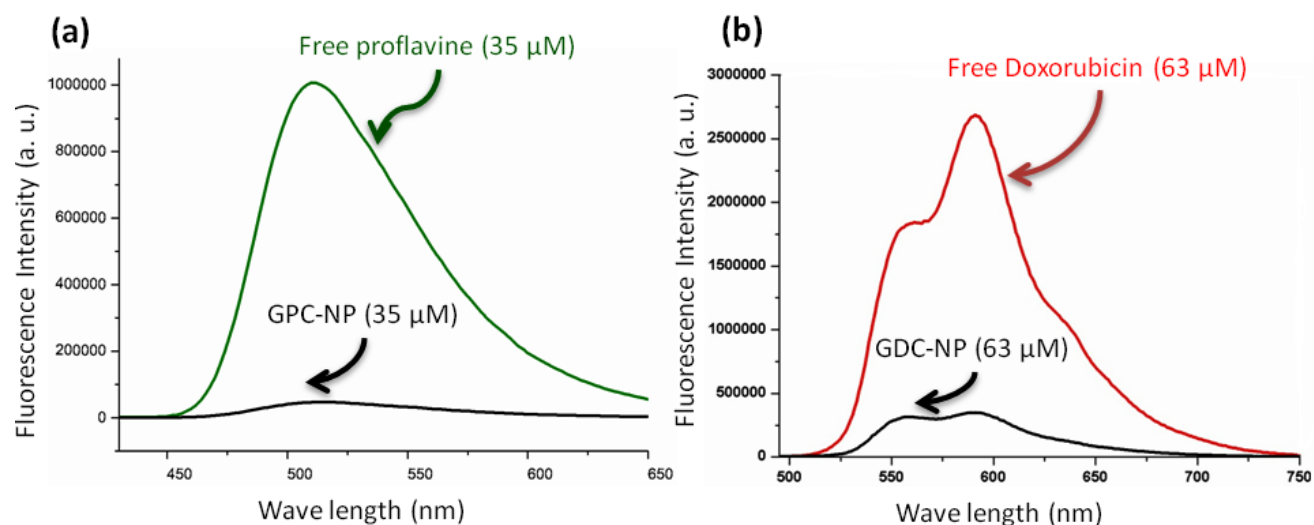


Figure 2.6: Fluorescence emission spectra of GPC-NPs and GDC-NPs showing fluorescence quenching of proflavine and doxorubicin upon stacking on GO surface.

Finally, the presence of cisplatin in the GO-NPs (GPC and GDC) was confirmed by energy dispersion X-ray spectroscopy (EDXS) (**Figure 2.7 and Figure 2.8**). EDXS of GPC and GDC NPs contain platinum in 14.12 weight %, 15.12 weight % respectively. X-ray photoelectron spectroscopy (XPS) (**Figure 2.9**) displayed the peaks of associated elements. The binding energy positions at 75 eV, 285 eV, 400 eV, and 530 eV were assigned to Pt4f, C1s, N1s and O1s. From the XPS spectra we could determine that platinum was present in the +2 oxidation state by the appearance of two platinum peaks at 72.5 at eV and 76.0 eV corresponding to 4f_{7/2} and 4f_{5/2} respectively.

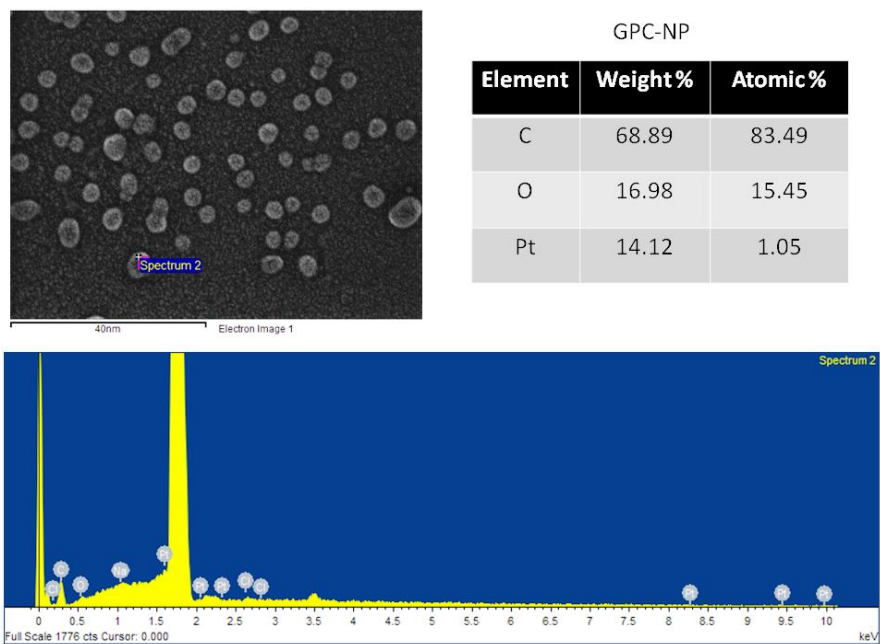


Figure 2.7: EDXS of GPC-NPs from FESEM images showing the presence of cisplatin.

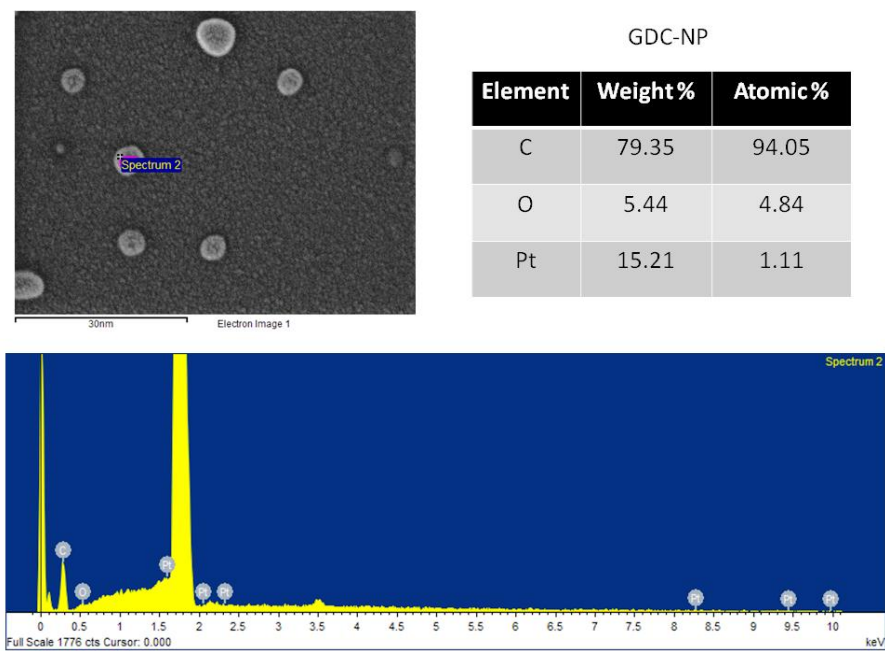


Figure 2.8: EDXS of GDC-NPs from FESEM images showing the presence of cisplatin.

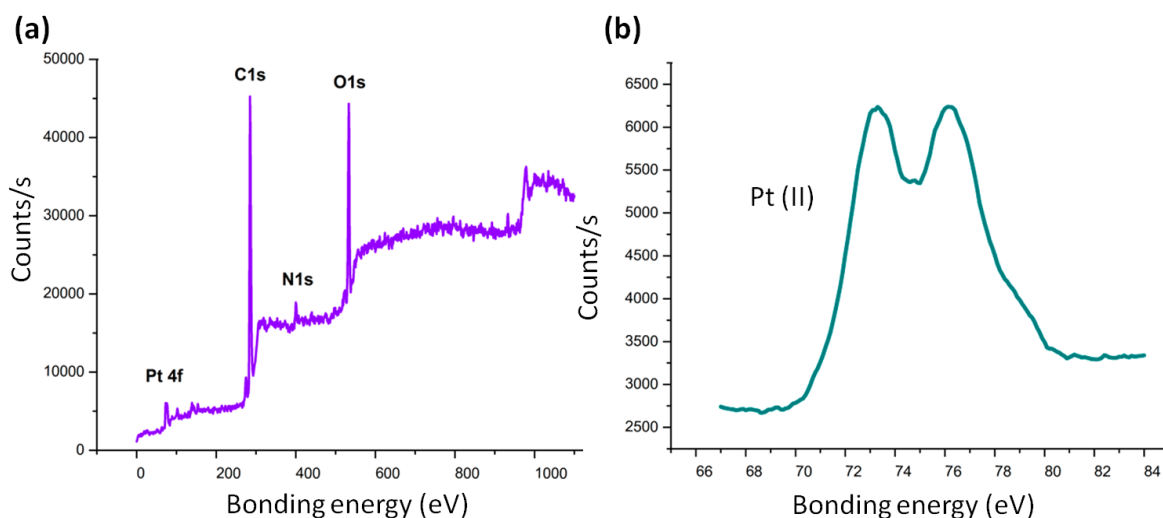


Figure 2.9: (a-b) XPS of GPC-NPs showing the presence of nitrogen from proflavine moiety and Pt(II) from cisplatin.

To validate the cisplatin induced self-assembly, GO was first reacted with aquated cisplatin in ratio-metric manner, followed by monitoring the respective morphological patterns. The FESEM images clearly revealed that 2D-GO-sheets converted into 3D-spherical nanoparticles at weight ratio of GO:CDDP \sim 1:1.5 (**Figure 2.10**).

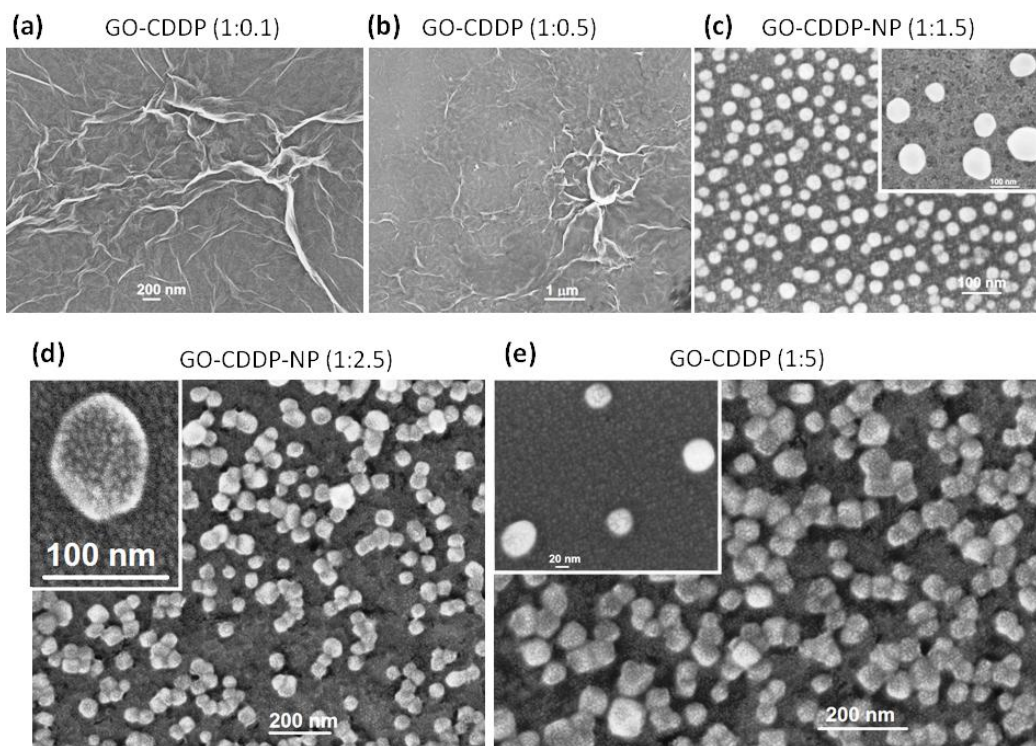


Figure 2.10: (a-e) FESEM images of GO-CDDP composites in different weight ratios to evaluate cisplatin mediated self-assembly.

The presence of cisplatin and GO moiety in the NPs was confirmed by EDXS (**Figure 2.11**) and PXRD (**Figure 2.12**) respectively. Specifically, the appearance of broad peak at $d \sim 6.2 \text{ \AA}$ in 3D-nanoparticles in PXRD demonstrated the stapling of GO sheets into more compact structures by co-ordinating $-\text{COOH}$ groups of GO with Pt moiety in aquated cisplatin as was also discussed earlier in the case of composite NPs.

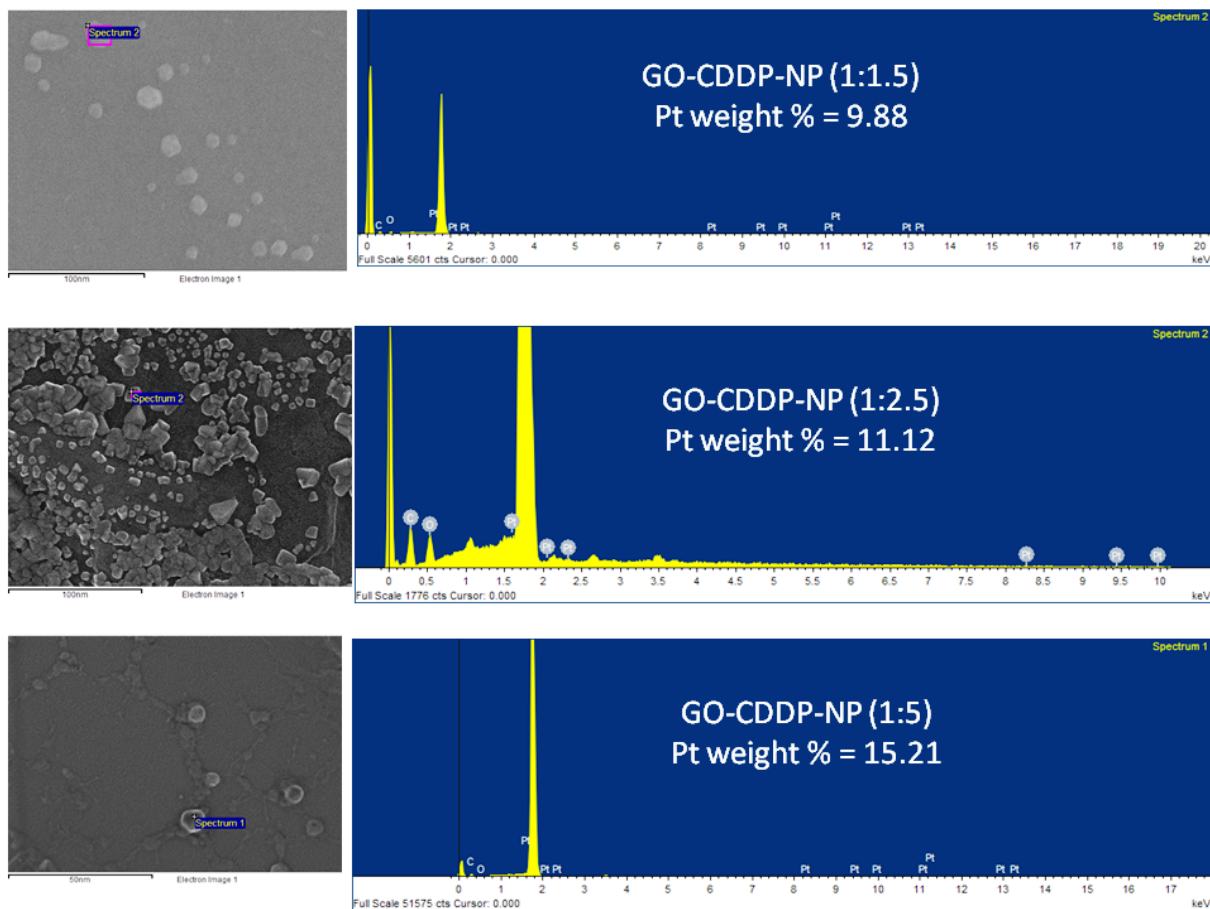


Figure 2.11: EDXS of GO-CDDP-NPs at different weight ratios to show the presence of cisplatin.

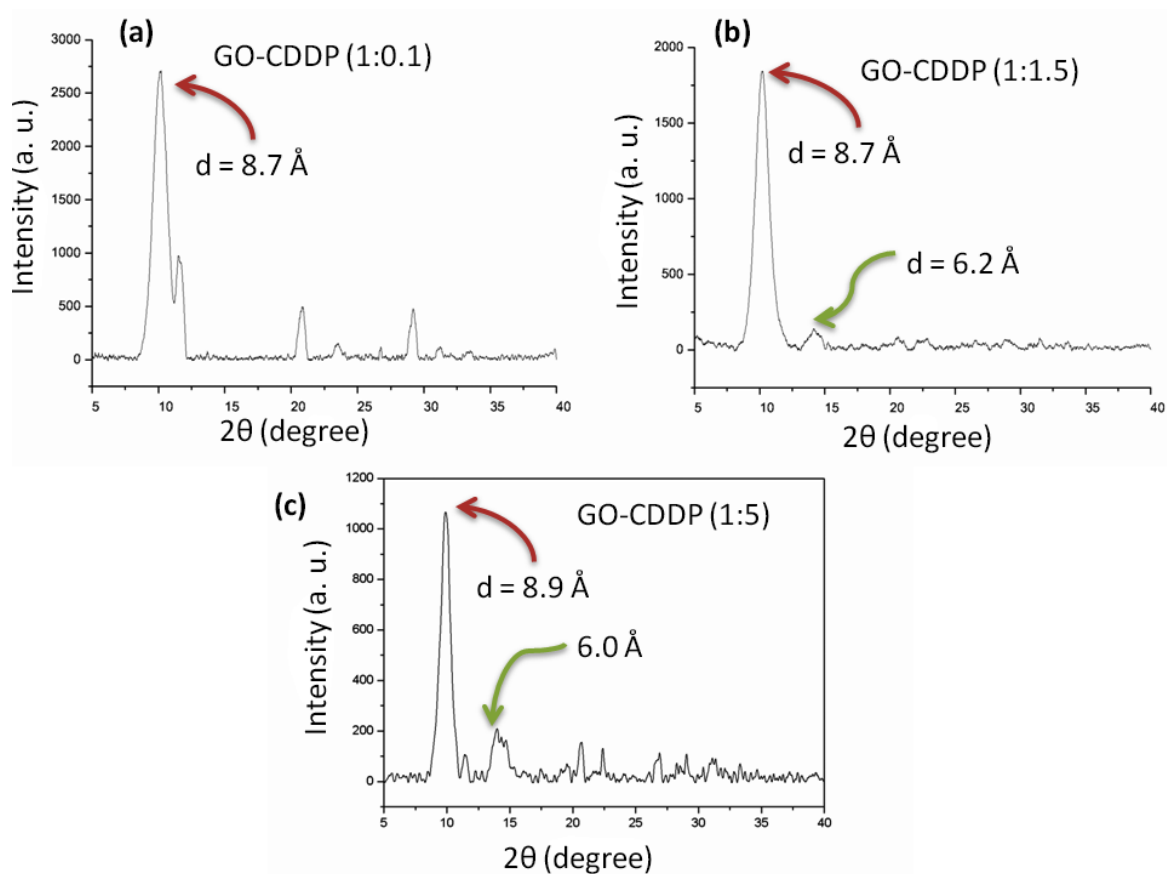


Figure 2.12: PXRD of GO-CDDP composites in different weight ratios.

2D-GO-nano/micro sheets interact with the cellular membrane and internalize inside the cells through different endocytosis mechanism.¹⁸⁻²¹ Notably, to the best of our knowledge, the sub-cellular localization and internalization mechanism of 3D-GO-based spherical nanoparticles in cancer cells are not reported earlier. To investigate the sub-cellular localization, HeLa cervical cancer cells were treated with GPC-NPs (green fluorescent) or GDC-NPs (red fluorescent) in a time-dependent manner (1 h, 3 h and 6 h). The cells were visualized by confocal laser scanning microscopy (CLSM) after staining the lysosomes and nuclei by LysoTracker Red DND-99 (for GPC-NPs) or LysoTracker Green DND-26 (for GDC-NPs) and DAPI (blue fluorescent dye) respectively. The gradual increment of yellow fluorescence after overlapping of green and red fluorescence from 1 h to 3 h to 6 h in CLMS images **Figure 2.13** and **Figure 2.14** evidently demonstrated that both GPC-NPs and GDC-NPs specifically compartmentalized into acidic lysosomes in a time dependent manner.

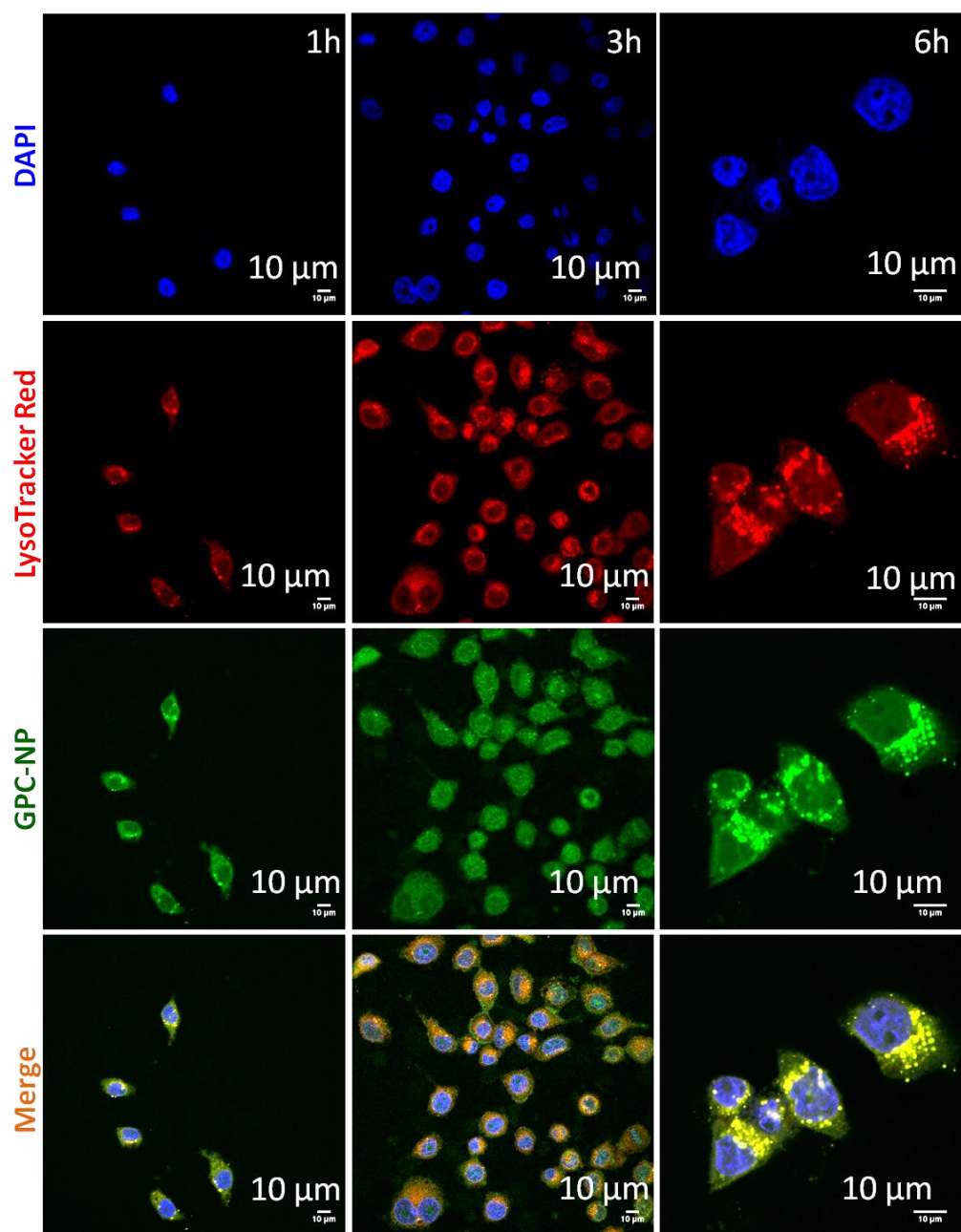


Figure 2.13: CLSM images of HeLa cells after incubating with GPC-NPs at 1h, 3h and 6h time points. Lysosomes and nucleus were stained with LysoTracker Red and DAPI (blue). Merged images show the colocalization of GPC-NPs in lysosomes in a time dependent manner. Scale bar = 10 μm.

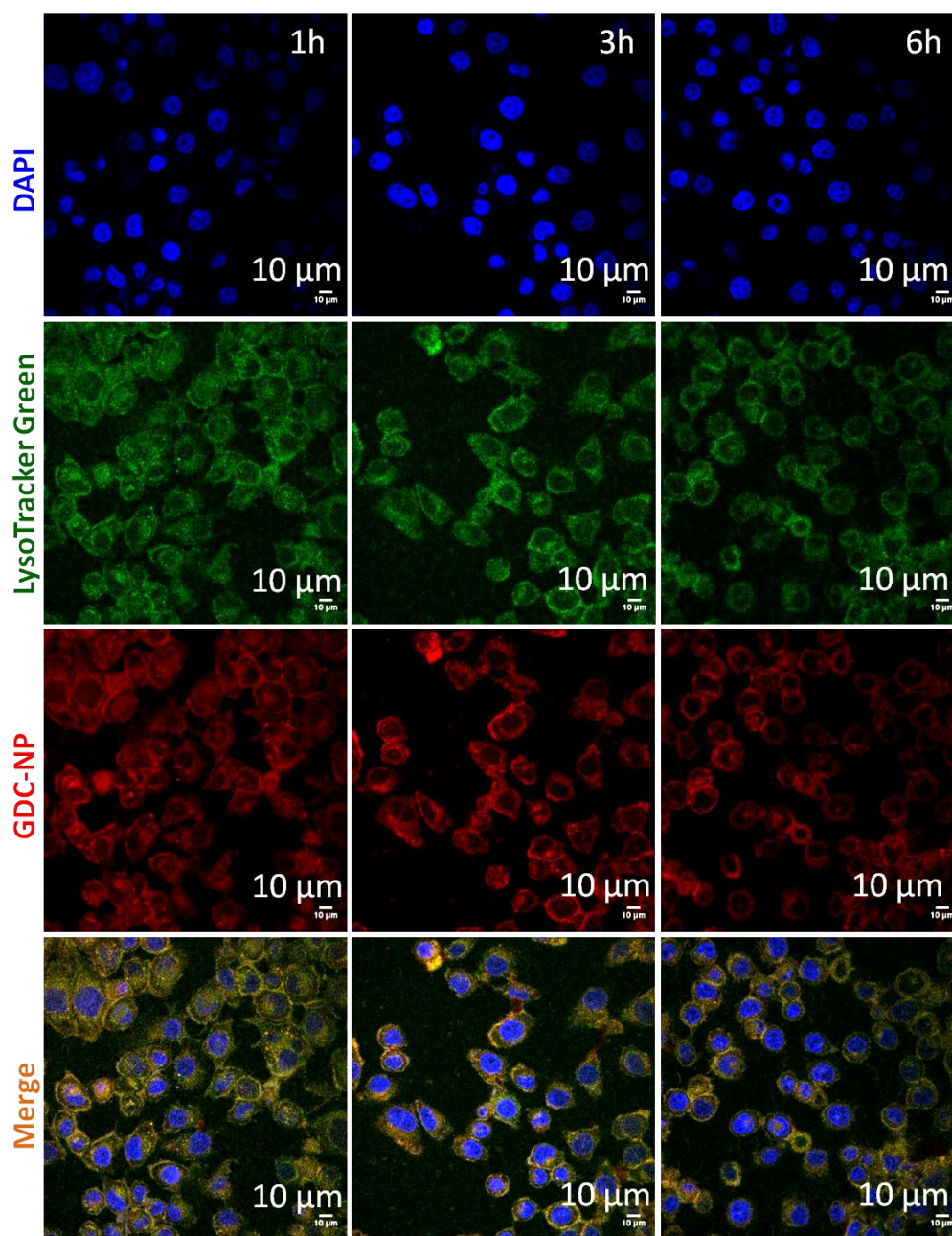


Figure 2.14: CLSM images of HeLa cells after incubating with GDC-NPs at 1h, 3h and 6h time points. Lysosomes and nucleus were stained with LysoTracker Green and DAPI (blue). Merged images show the colocalization of GDC-NPs in lysosomes in a time dependent manner. Scale bar = 10 μm .

To understand the shape-dependency of sub-cellular localization, we further treated HeLa cells with 2D-sheet like GO-Prof (green fluorescent) and GO-Dox (red fluorescent) for 1 h, 3 h and 6 h, followed by staining the lysosomes and nuclei. The CLSM images (**Figure 2.15** and **Figure 2.16**) unambiguously showed that 2D GO-Prof and GO-Dox internalized

into the HeLa cells within 1 h and spread over the cells non-specifically into lysosomes and nucleus.

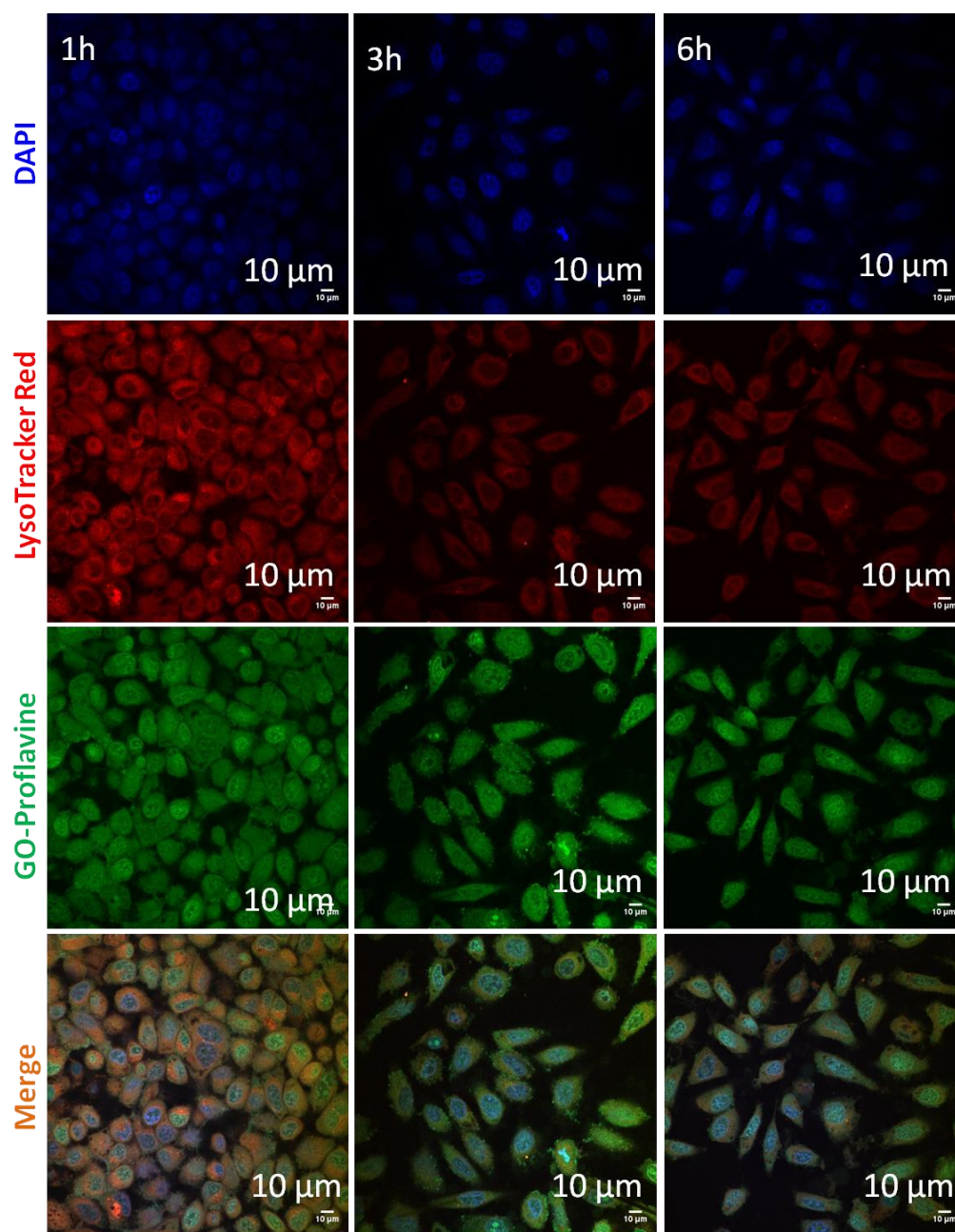


Figure 2.15: CLSM images of HeLa cells after incubating with GO-Proflavine composite at 1h, 3h and 6h time points. Lysosomes and nucleus were stained with LysoTracker Red and DAPI (blue). Merged images show the colocalization of GO-Proflavine in lysosomes in a time dependent manner. Scale bar = 10 μm.

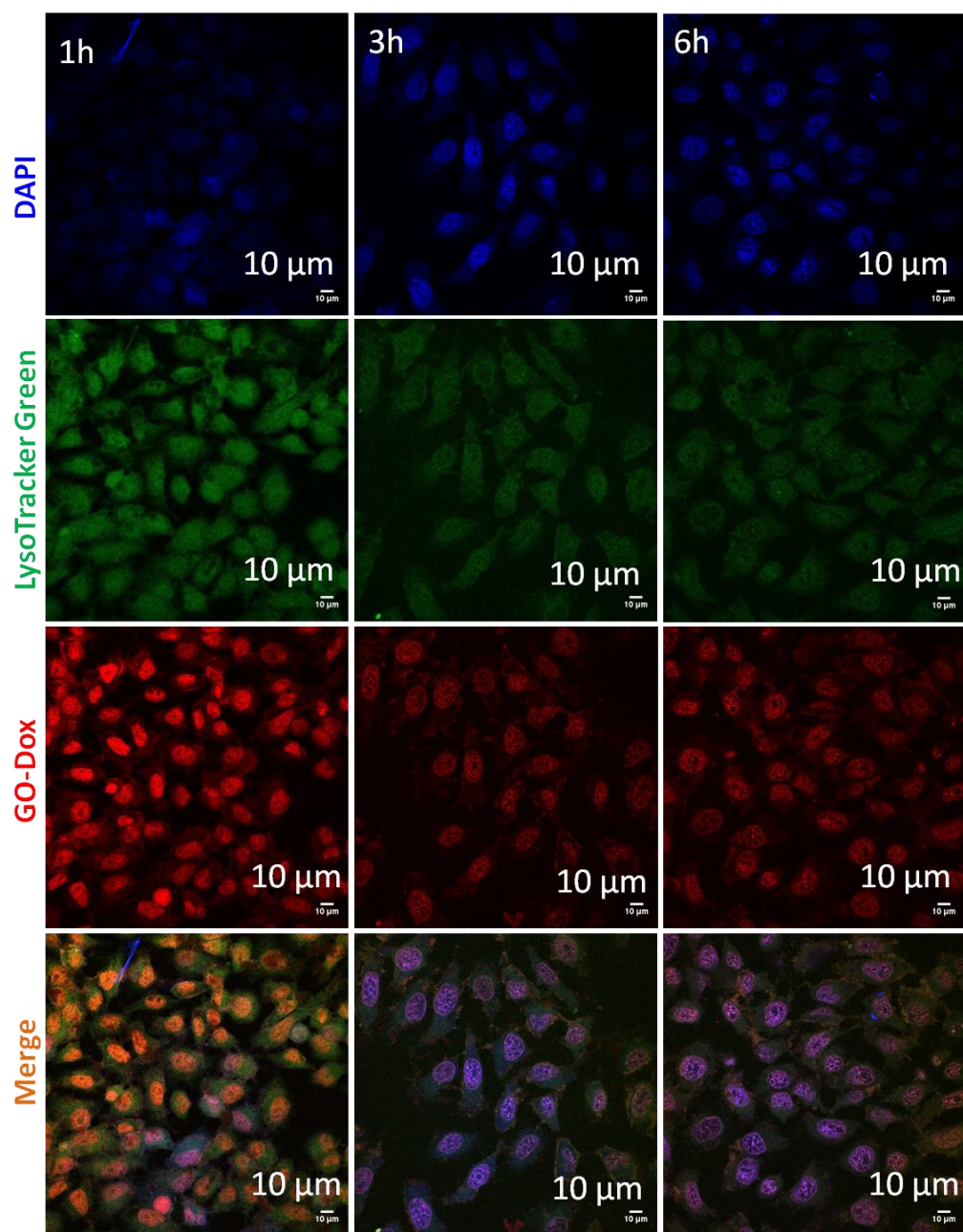


Figure 2.16: CLSM images of HeLa cells after incubating with GO-Dox composite at 1h, 3h and 6h time points. Lysosomes and nucleus were stained with LysoTracker Red and DAPI (blue). Merged images show the colocalization of GO-Dox in lysosomes in a time dependent manner. Scale bar = 10 μm .

Furthermore, we pre-treated the HeLa cells with different endocytosis inhibitors like chlorpromazine (clathrin-mediated endocytosis), genistein (caveoline-mediated endocytosis) and amiloride (macropinocytosis),^{22,23} followed by treatment with GPC-NPs and GDC-NPs. We quantified the number of cells with green fluorescent GPC-NPs (and red fluorescent GDC-NPs)

internalized by flow cytometry (FACS) which clearly delineated that, the number of cells treated with genistein and amiloride internalized the GPC-NPs and GDC-NPs in almost the same amount as without inhibitors (**Figure 2.17a-b**). On the contrary, the number of green (or red) fluorescent cells was dramatically reduced in the chlorpromazine treated cells compared to no inhibitor treated cells. Thus, such FACS based quantification undoubtedly suggested that the spherical GPC-NPs and GDC-NPs were internalized into the HeLa cells by clathrin-mediated endocytosis method and independent of caveolin mediated endocytosis and macropinocytosis.

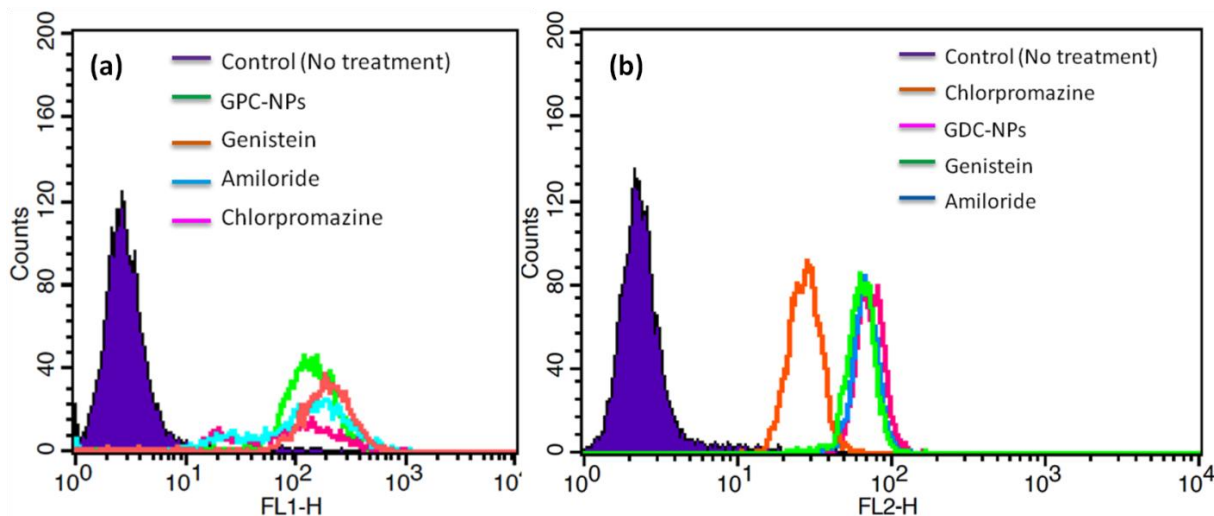


Figure 2.17: FACS analysis of HeLa cells pre-treated with different endocytosis inhibitors followed by (a) GPC-NPs and (b) GDC-NPs treatment.

After localization inside the acidic lysosomes, GO-NPs are expected to release the drugs for an effective damage of DNA. GPC-NPs were incubated into pH = 5.5 buffer (lysosome mimic) in different time points and it was found that GPC-NPs released 54.4 ± 3.99 % of proflavine after 54 h and 21.8 ± 1.19 % of cisplatin after 72 h in a slow and continued manner (**Figure 2.18a**). Since 2D sheets of GO-Prof and GO-Dox were converted into 3D-NPs by cisplatin, one would anticipate that upon release of cisplatin, the spherical nanoparticles should convert back into their sheet like structures. Indeed, the FESEM images showed that at 18 h and 24 h, some spherical nanoparticles converted into sheet-like structures at pH = 5.5 (**Figure 2.19**) and at prolonged incubation (48 h, 54 h and 72 h) the spherical morphology of GPC-NPs was completely transformed into 2D-sheet structures. Similarly, GDC-NPs released 32.7 ± 1.7 % cisplatin and 22.3 ± 1.0 % doxorubicin after 72 h (**Figure 2.18b**) slowly. Time dependent FESEM images also

confirmed the transformation of spherical GDC-NPs into sheet like unassembled structures (Figure 2.20). We propose a plausible mechanism of cisplatin release by breaking Pt-carboxylato bonds in acidic medium to convert spherical structures into disassembled 2D-structures (Figure 2.18c).

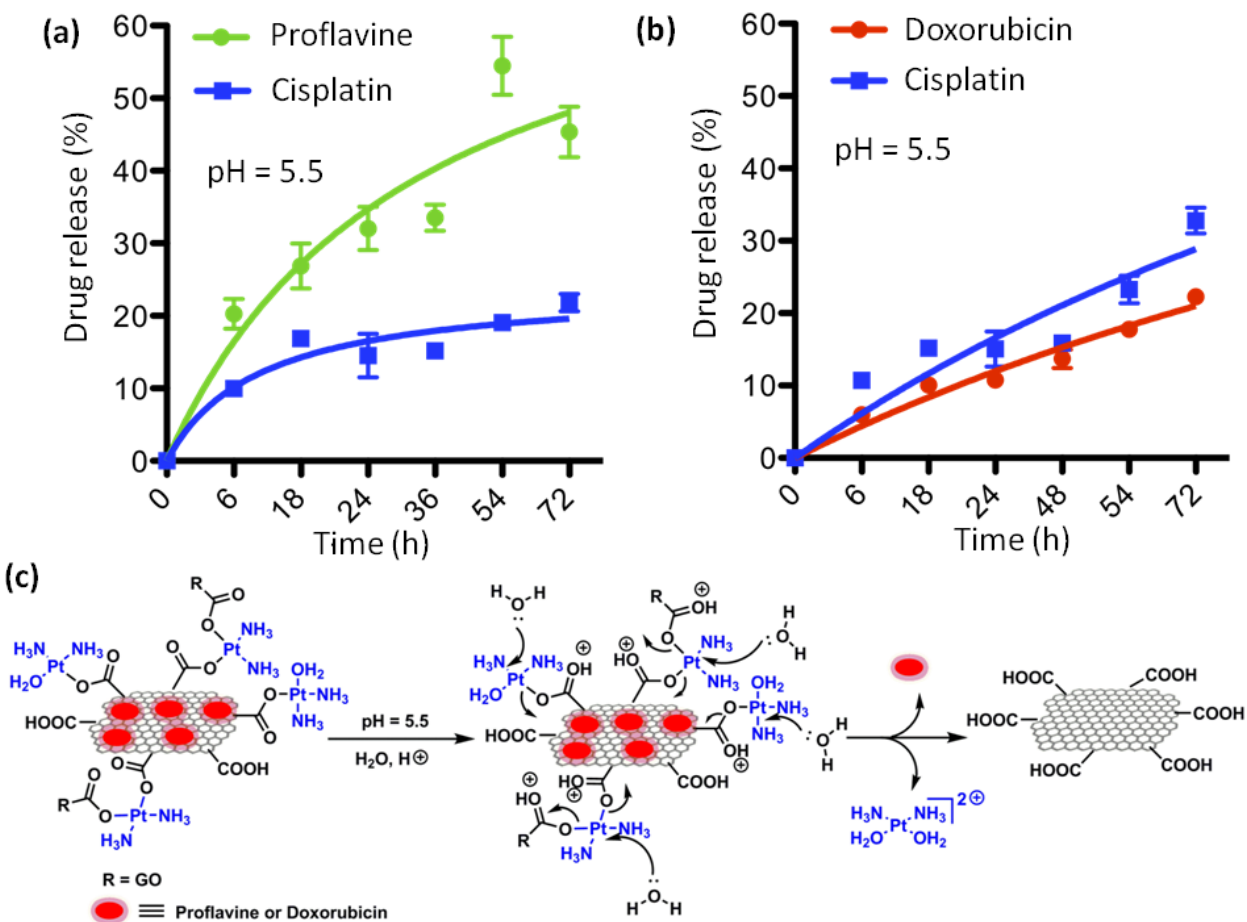


Figure 2.18: (a-b) Time dependent release of proflavine/cisplatin and doxorubicin/cisplatin from GPC-NPs and GDC-NPs respectively at pH = 5.5 mimicking lysosome environment. (c) Plausible mechanism of dual drug release at pH = 5.5 leading to the dis-assembly of spherical nanoparticles into sheet like structures.

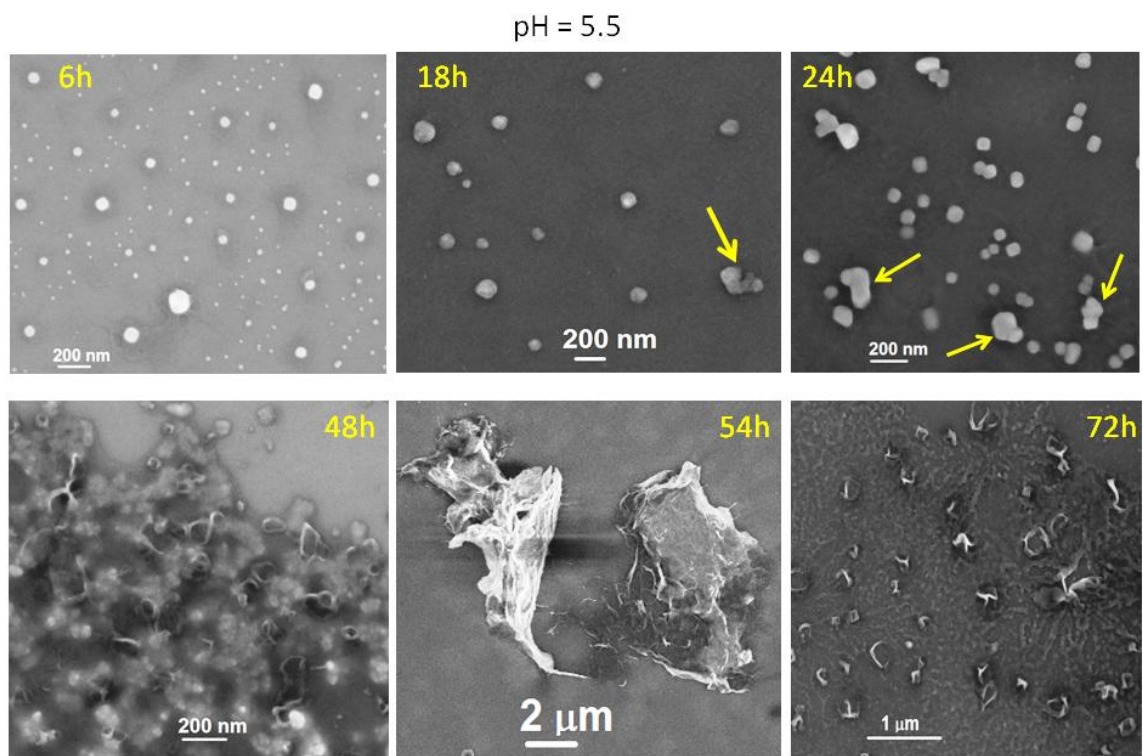


Figure 2.19: FESEM images of GPC-NPs at different time points at pH = 5.5 mimicking lysosome environment.

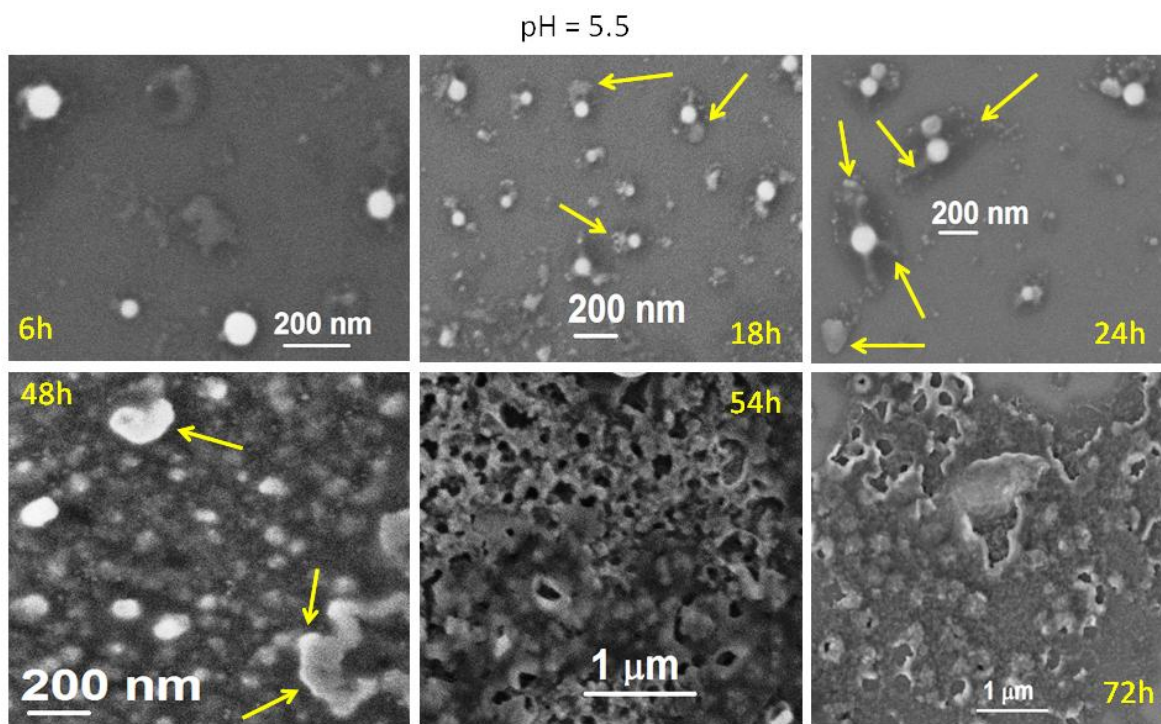


Figure 2.20: FESEM images of GDC-NPs at different time points at pH = 5.5 mimicking lysosome environment.

Whereas, GPC and GDC NPs incubated at pH 7.4 buffer showed very low release of proflavine (14%), cisplatin (10%) and doxorubicin (11%), cisplatin (8%) after 72h (Figure 2.21a-b). The intact spherical structure of GPC NPs (Figure 2.22a-b) and GDC NPs (Figure 2.22c-d) post 54h of incubation in pH 7.4 buffer also correlated with the low release of the cisplatin.

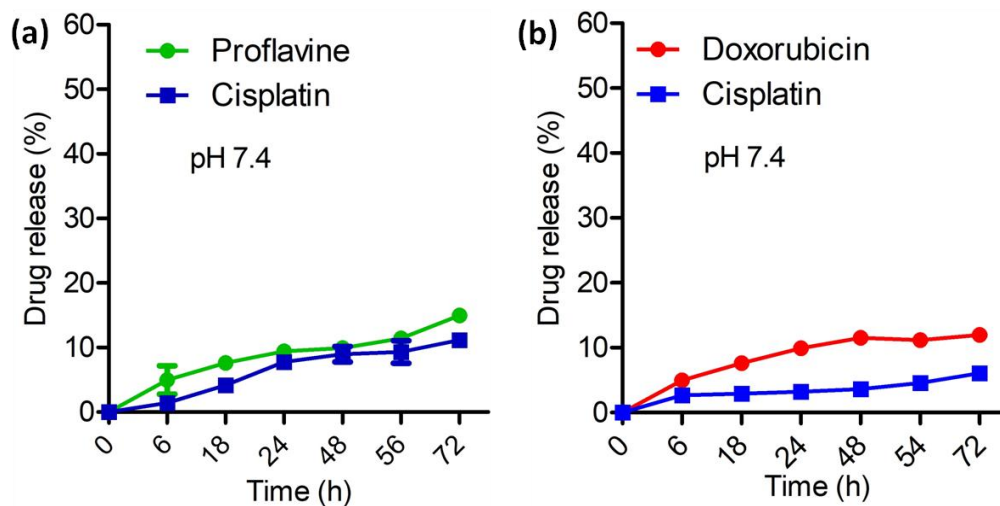


Figure 2.21: Time dependent release of proflavine/cisplatin and doxorubicin/cisplatin from (a) GPC-NPs and (b) GDC-NPs respectively at pH = 7.4

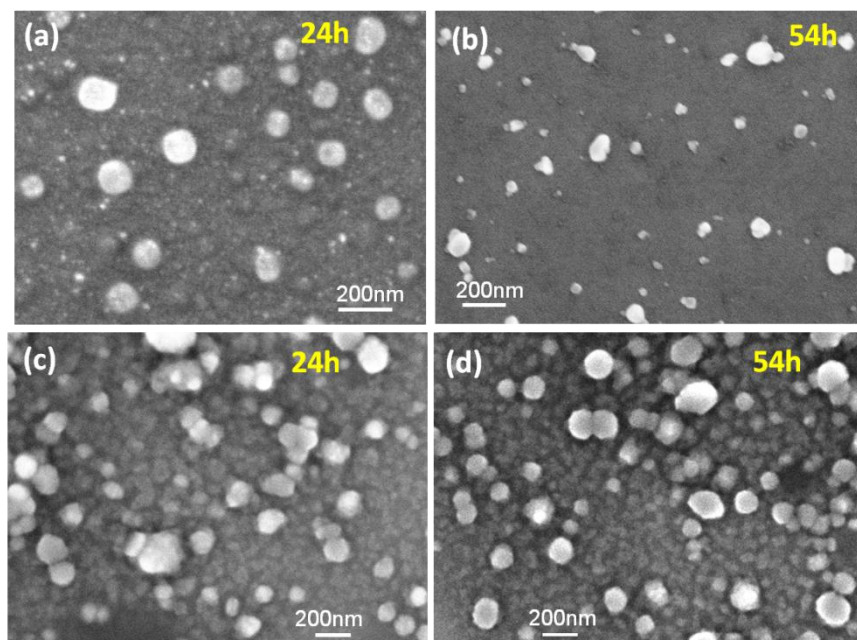


Figure 2.22: FESEM images of GPC-NPs (a-b) and GDC (c-d) after 24h and 54h time points at pH = 7.4.

While inside the cells, followed by drug release, GO-NPs should damage DNA as their sub-cellular target. We evaluated the expression of phosphorylated histone γ H2AX by western blot (DNA damage marker)²⁴ after treating the HeLa cells with GO-NPs for 24 h. The western blot images and quantification evidently exhibited that both GPC-NPs and GDC-NPs increased the expression of γ H2AX by 33.8 and 5.4 folds respectively compared to control cells (**Figure 2.23a and Figure 2.23b**). Cancer cells trigger poly (ADP-ribose) polymerase (PARP) family of proteins followed by DNA damage as repair machinery.²⁵ Further, western blot images and quantification revealed that GPC-NPs and GDC-NPs increased the PARP expression by 11.3 and 2.2 folds in HeLa cells (**Figure 2.23a and Figure 2.23c**). These electrophoresis experiments demonstrated that GO-NPs successfully damaged sub-cellular DNA in cancer cells.

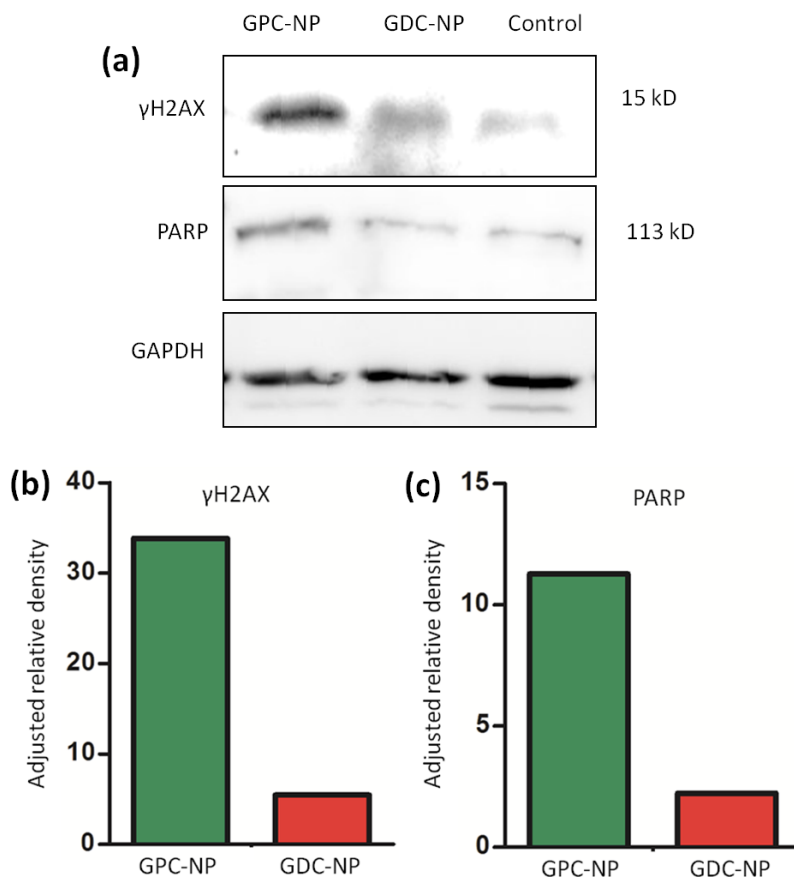


Figure 2.23: (a) Western blot analysis of γ H2AX and PARP after treatment of HeLa cells with GPC-NPs and GDC-NPs. (b-c) Quantification of γ H2AX and PARP after treating HeLa cells with GPC-NPs and GDC-NPs from western blot analysis.

Evading apoptosis (programmed cell death) is one of the hallmarks of cancer.²⁶ Apoptotic and necrotic cells were stained by Annexin V-FITC (green) and PI (red) after treating the HeLa cells

with GO-NPs for 24 h followed by FACS analysis. We observed that, GPC-NPs induced early and late apoptosis in 6.47 % and 21.03 % cells, whereas, GDC-NPs triggered early apoptosis and late apoptosis in 35.18 % and 3.91 % cells respectively (**Figure 2.24**)

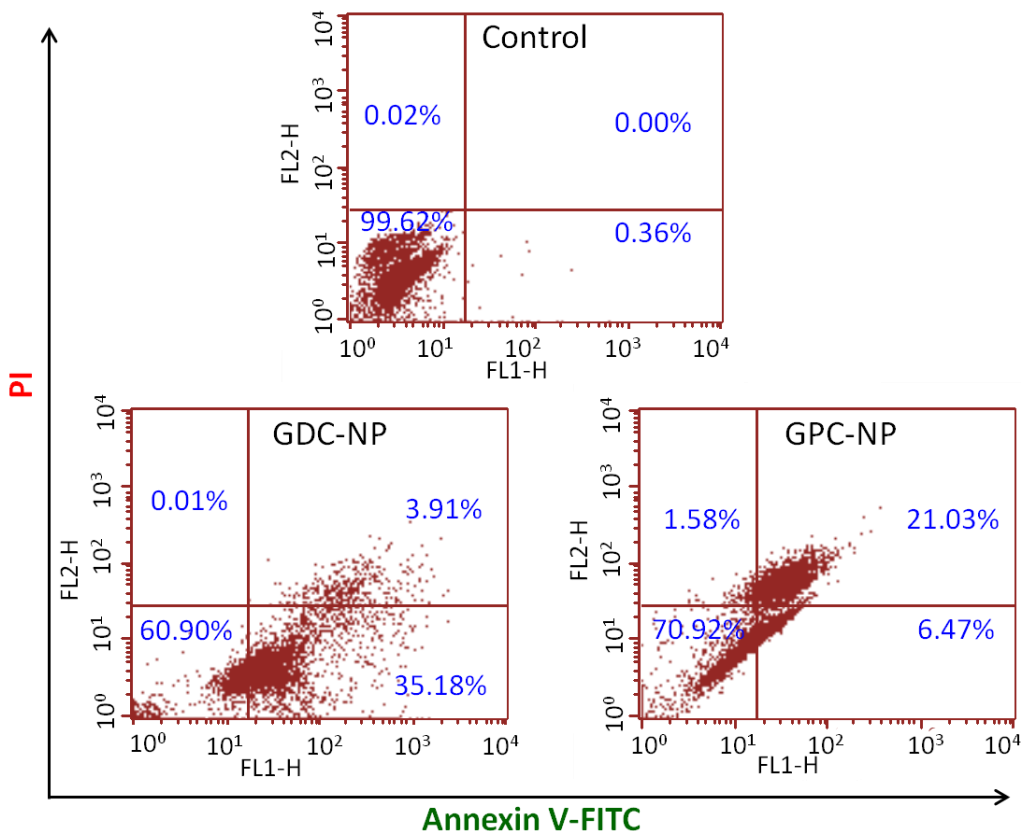


Figure 2.24: FACS analysis of HeLa cells after treatment of HeLa cells with GPC-NPs and GDC-NPs. Apoptotic cells were stained with Annexin V-FITC and necrotic cells were stained with PI.

DNA damage-induced apoptosis leads to cellular death. We finally evaluated cell viability after treatment with GO-NPs in a dose-dependent manner for 48 h by MTT assay. As control, we treated the HeLa cells with combination of free DNA damaging drugs in the same ratio present in GO-NPs. GPC-NPs showed remarkably improved $IC_{50} = 1.91 \pm 0.10 \mu\text{M}$ compared to $IC_{50} = 8.33 \pm 0.79 \mu\text{M}$ for free GO, proflavine, cisplatin cocktail (**Figure 2.25a**). On the other hand, GDC-NPs also demonstrated comparable $IC_{50} = 2.01 \pm 0.05 \mu\text{M}$ in comparison to $IC_{50} = 2.33 \pm 0.06 \mu\text{M}$ for free GO, Dox and cisplatin combination (**Figure 2.25b**). To show that the GO-NPs can very specifically kill cancer cells but not the healthy cells, we further evaluated the toxicity of GO-NPs in healthy L929 fibroblast cells at 24 h post-incubation. Interestingly, GPC-NPs and GDC-NPs

induced only 78.4 ± 9.2 % (at $3.2 \mu\text{M}$) and 97.2 ± 12.2 % cell viability (at $25 \mu\text{M}$) respectively (**Figure 2.26a-b**). Also free GO induced no cytotoxicity in L929 cells (cell viability = 110.5 ± 10.4 %) at 0.2 mg/ml concentration (**Figure 2.26c**)

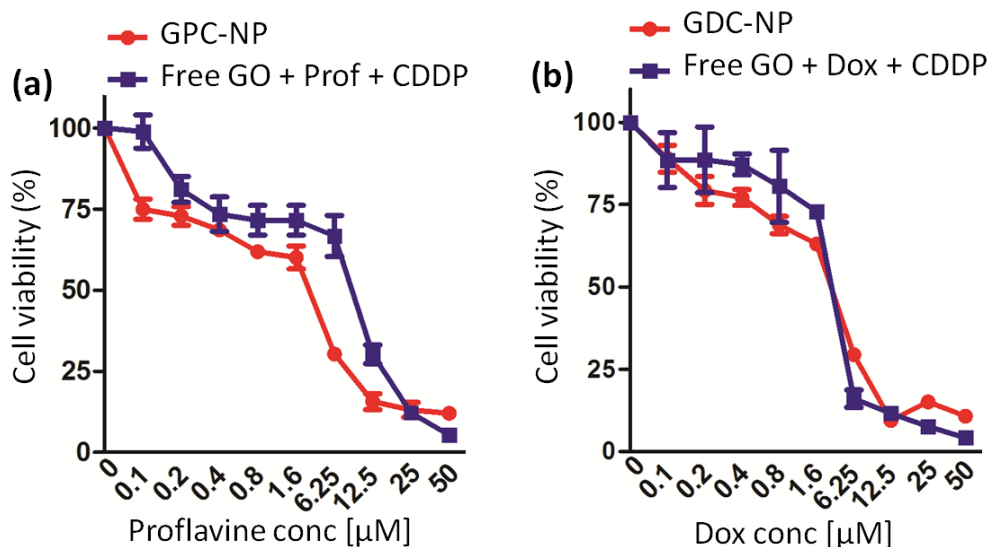


Figure 2.25: Cell viability of GPC-NPs and GDC-NPs in HeLa cells at 48h post-incubation measured by MTT assay.

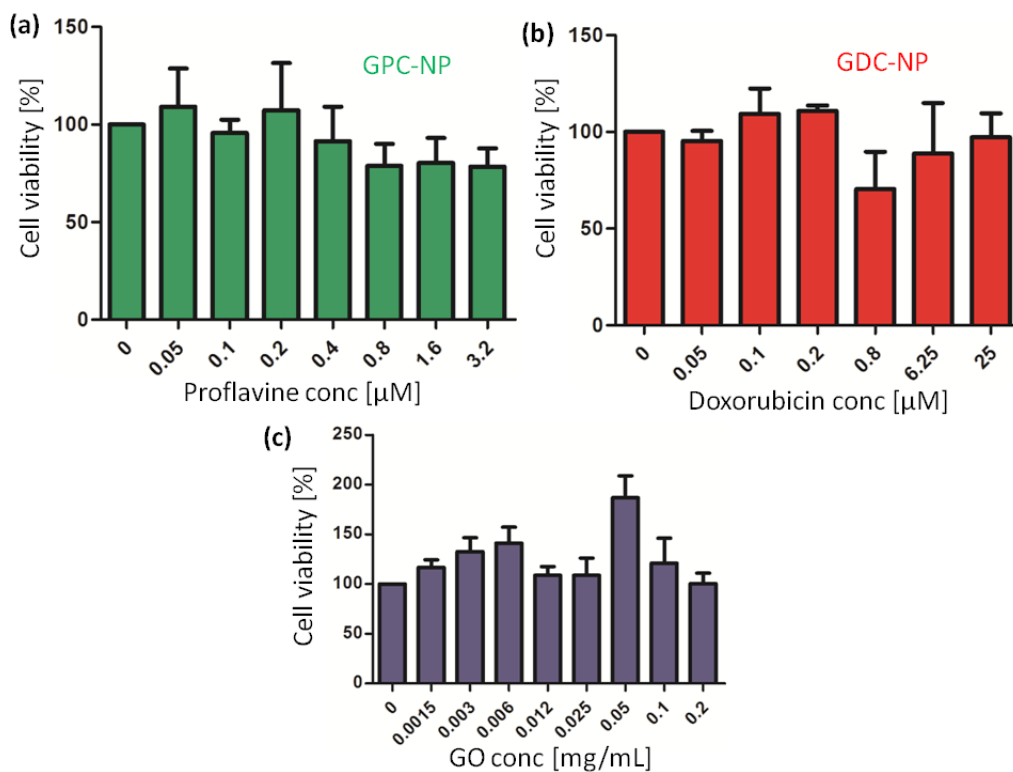


Figure 2.26 (a-b) Concentration dependent cell viability assay of GPC-NPs and GDC-NPs in L929 mouse fibroblast cells respectively at 24h post-incubation. (c) Concentration dependent cell viability assay of GO in L929 mouse fibroblast cells at 24h post-incubation.

2.4 Materials and Methods

2.4.1 Materials:

Graphene oxide (4mg/ml), distilled water, proflavine (3,6- diaminoacridine hydrochloride), sodium dodecyl sulfate (SDS), cisplatin, 3-(4, 5-dimethylthiazol-2-yl)-2,5-diphenyltetrazolium bromide (MTT) and silicon wafer for FE-SEM were acquired from Sigma-Aldrich. Doxorubicin was bought from Selleck Chemicals. DMEM media and DAPI were purchased from HiMedia.. Annexin-V-FITC Staining Kit was purchased from Roche. LysoTrackerTM Red DND-99, LysoTrackerTM Green DND-26, *SlowFade*® Gold Antifade Reagents was procured from Life Technologies. Anti-PARP antibody-clone 7A10, anti-phospho-histone H2AX (Ser139) antibody-clone JBW301, GAPDH antibody were obtained from BioLegend. HeLa cells were obtained from National Centre for Cell Science (NCCS), Pune.

2.4.2 Synthesis of aquated cisplatin (3):

Aquated cisplatin was prepared by using the method described in reference 1.

2.4.3 Synthesis of GO-Prof conjugate (2):

Graphene oxide (1) (4 mg/ml, 250 μ l) was dispersed in distilled water (2 ml). Aqueous solution of proflavine (5 mg, 0.023 mmol) in distilled water (1 ml) was prepared and added to the dispersed graphene oxide solution. The reaction was stirred in dark at room temperature for 24h. To remove un-reacted proflavine, the reaction mixture was dialysed against distilled water through dialysis membrane (MWCO = 1 kDa) for 24 h. Water was lyophilized to obtain GO-Prof conjugate (2).

2.4.4 Synthesis of GO-Prof-CDDP conjugate (4) and GPC-NPs:

1 mg of GO-Prof conjugate (2) was suspended in 1 ml distilled water and aquated cisplatin (3) (5 mg/ml, 0.019 mmol) into it. The reaction mixture was stirred at room temperature for 24h. The reaction mixture was further dialyzed (MWCO = 1 kDa) against water for 6 h to remove excess of aquated cisplatin to obtain GO-Prof-CDDP conjugate (4). 20 μ l of dialyzed solution was further diluted to 1 ml by distilled water for size, shape and morphology characterization.

2.4.5 Synthesis of GO-Dox conjugate (5):

Graphene oxide (1) (4 mg/ml, 250 μ l) was dispersed in distilled water (2 ml). Aqueous solution of doxorubicin (0.5 mg, 0.023 mmol) in distilled water (1 ml) was prepared and added to the dispersed graphene oxide solution. The reaction was stirred at room temperature for 24 h. To

remove un-reacted doxorubicin, the reaction mixture was dialyzed (MWCO = 1kDa) against distilled water through for 24 h. Water was lyophilized to obtain GO-Dox conjugate (5).

2.4.6 Synthesis of GO-Dox-CDDP conjugate (6) and GDC-NPs:

1 mg of GO-Dox conjugate (5) was suspended in 1 ml distilled water and aquated cisplatin (5 mg/ml, 0.019 mmol) was added into it. The reaction mixture was stirred at room temperature for 24h. The reaction mixture was further dialyzed (MWCO = 1 kDa) against water for 6 h to remove excess of aquated cisplatin to obtain GO-Dox-CDDP conjugate (6). 20 μ l of dialyzed solution was further diluted to 1 ml by distilled water for morphological characterization.

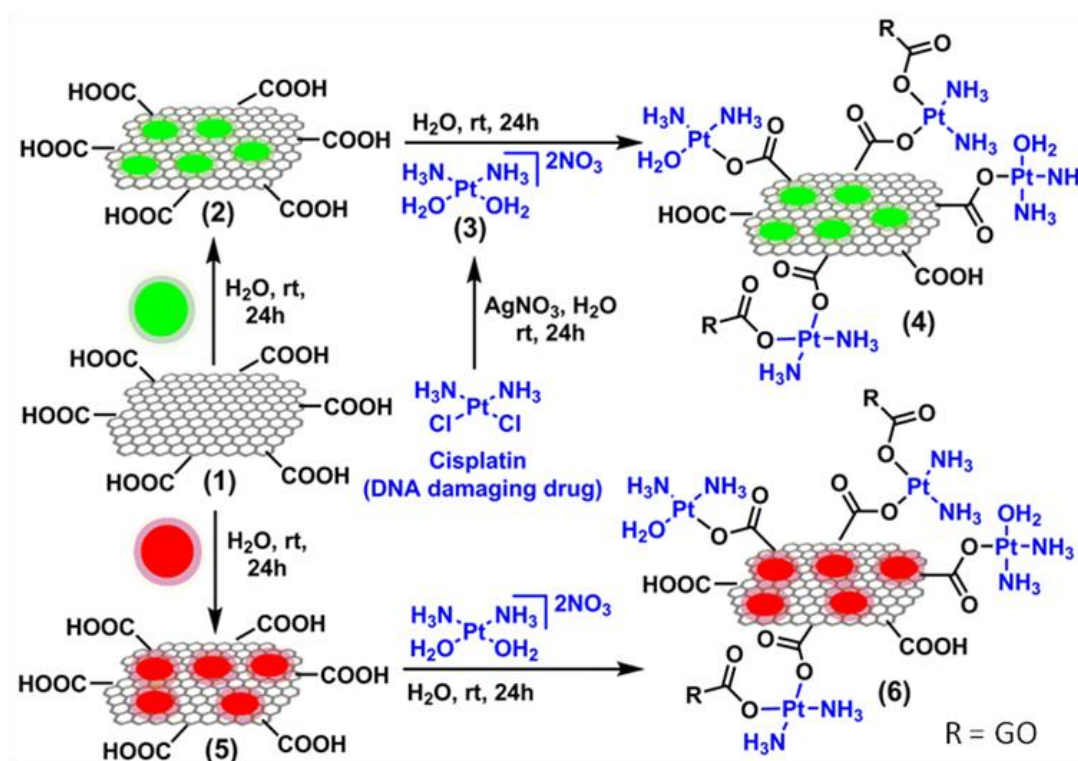


Figure 2.27: Synthesis of: GO-Prof conjugate (2), aquated cisplatin (3), GO-Prof-CDDP (GPC-NPs) conjugate (4), GO-Dox conjugate (5), GO-Dox-CDDP conjugate (GDC-NPs) (6).

2.4.7 Field-Emission Scanning Electron Microscopy (FESEM) of GPC and GDC-NPs:

15 μ l of samples (GO-Prof, GO-Dox, GPC-NPs, GDC-NPs) were diluted in 1 ml water and sonicated for 1 min. 2 μ l of these solutions were placed on a silicon wafer without any dopant and it was allowed to dry at room temperature under vacuum desiccators for 2 h. The FESEM images were taken by using the method described in reference 27.

2.4.8 Atomic Force Microscopy (AFM) of GPC-NPs and GDC-NPs:

15 μl of samples (GO-Prof, GO-Dox, GPC-NPs, GDC-NPs) were diluted in 1 ml water and sonicated for 1 min. Then 10 μl of these solutions were drop casted on mica sheet and dried under the vacuum desiccators for 2 h. AFM images were taken using the method described in reference 27.

2.4.9 Transmission Electron Microscopy (TEM) of GPC-NPs and GDC-NPs:

15 μl of GPC-NPs and GDC-NPs were diluted in 1 ml water and sonicated for 1 min. Then 15 μl of the GO-NPs was drop casted on a copper grid. After 30 min, this sample was absorbed using filter paper and then 15 μl of freshly prepared 0.25% uranyl acetate solution was added on the grid. After 60 seconds, the solution of uranyl acetate was washed three times with 15 μl water. The grid was dried in a dust free environment and images were captured using the method described in reference 27.

2.4.10 Resonance Raman Spectroscopy:

Resonance Raman spectra were collected using a Lab RAM HR 800 (Horiba scientific) using laser excitation wavelength of 532 nm excitation with a 50X objective at room temperature. 532 nm was chosen as the excitation to guarantee a good signal/noise ratio. Prior to analysis the baseline of the spectrum was extracted using the software NGSLabSpec.

2.4.11 Powder X-ray diffraction (PXRD):

Powder X-ray diffraction (PXRD) spectra of GO, GO-Prof, GPC-NPs and GO-CDDP in different concentrations were collected using a Bruker D8-Advance X-ray powder diffractometer (Cu $K\alpha$ radiation; $\lambda=1.5418 \text{ \AA}$) in the range 3-40°(0.010° step size, 175s holding time).

2.4.12 X-ray photoelectron spectroscopy (XPS):

XPS spectra were acquired in an ultra high vacuum equipment (10^{-1} mbar) using a hemispherical electron energy analyzer and an Mg K-alpha X-ray source (1253.6 eV). All samples were measured under the same conditions.

2.4.13 *In vitro* assays:

Cellular internalization, cell viability by MTT assay, apoptosis detection by fluorescence-activated cell sorting (FACS), and Western blot analyses were performed by using the procedure described in reference 27 and reference 28.

2.4.14 Quantification of drug release from GPC-NPs and GDC-NPs:

Quantification of dual drug loading and release from the nanoparticles were determined by the dialysis method described in reference 4.

2.5 Conclusion

In conclusion, the presented work demonstrates the first example of cisplatin mediated self-assembly of 2D GO-sheets into 3D-spherical nanoparticles. In course of the hierarchical self-assembly, aromatic DNA damaging drugs can be loaded along with cisplatin. These composite NPs were taken up by the cancer cells through endocytosis, localized into lysosomes, damaged sub-cellular DNA leading to apoptosis. The NPs exhibited remarkable efficacy in killing cancer cells by keeping healthy cells unperturbed. We envision that our new approach of GO-based nanoparticles have the potential to be translated into clinics in future for combination chemotherapy.

2.6 Salient Features

- This work demonstrates, the first example of a cisplatin mediated hierarchical self assembly of 2D GO sheets to 3D spherical GO nanoparticles (GO-NPs).
- The reaction scheme is robust and carried out in water as the solvent.
- The 3D spherical GO nanoparticles can be co-loaded with Doxorubicin or Proflavin-aromatic DNA damaging drugs along with cisplatin.
- These dual drug loaded GO-NPs endocytosed into cervical cancer HeLa cells through clathrin mediated endocytosis. They homed specifically into the acidic lysosomal compartments of the cells within 6h, as compared to the 2D GO-Pro or GO-Dox sheets which internalized non-specifically into the nucleus as well as lysosomes in 1 h. This displayed the morphological advantage of the spherical size of GO NP's in contrast to 2D sheet.
- The release proflavin or doxorubicin along with cisplatin from the GPC and GDC NPs, led to DNA damage which was conformed my expression of important DNA damage biomarkers like γ H2AX and PARP through western blot analysis.
- The DNA damage triggered apoptosis in HeLa cells and subsequently led to cell death.
- Another interesting aspect of the GO NPs was the fact that they exhibited remarkable efficacy in killing cancer cells, but the healthy cells (L929 fibroblast cells) remained unperturbed.

2.7 References

1. Gonçalves, G.; Vila, M.; Portolés, M.; Vallet-Regi, M.; Gracio, J.; Marques, P. A. A. P. Nano-Graphene Oxide: A Potential Multifunctional Platform for Cancer Therapy. *Adv. Healthcare Mater.* **2013**, *2*, 1072–1090.
2. Kostarelos, K.; Novoselov, K. Exploring the Interface of Graphene and Biology. *Science* **2014**, *344*, 261-263.
3. Sydlik, S. A.; Jhunjhunwala, S.; Webber, M. J.; Anderson, D. G.; Langer, R. *In Vivo* Compatibility of Graphene Oxide with Differing Oxidation States. *ACS Nano* **2015**, *9*, 3866–3874.
4. Jiang, T.; Sun, W.; Zhu, Q.; Burns, N. A.; Khan, S. A.; Mo, R.; Gu, Z. Furin-Mediated Sequential Delivery of Anticancer Cytokine and Small-Molecule Drug Shuttled by Graphene. *Adv. Mater.* **2015**, *27*, 1021-1028.
5. Chung, C.; Kim, Y.; Shin, D.; Ryoo, S.; Hong, B. H.; Min, D. Biomedical Applications of Graphene and Graphene Oxide. *Acc. Chem. Res.* **2013**, *46*, 2211-2224.
6. Zang, L.; Xia, J.; Zhao, Q.; Liu, L.; Zhang, Z. Functional graphene oxide as a nanocarrier for controlled loading and targeted delivery of mixed anticancer drugs. *Small* **2010**, *6*, 537-544.
7. Shao, J.; Lv, W.; Guo, Q.; Zhang, Z.; Xu, Q.; Yang, Q.; Kang, F. Hybridization of graphene oxide and carbon nanotubes at the liquid/air interface. *Chem. Commun.* **2012**, *48*, 3706-3708.
8. Shao, J.; Wu, S.; Zhang, S.; Lv, W.; Su, F.; Yang, Q. Graphene oxide hydrogel at solid/liquid interface. *Chem. Commun.* **2011**, *47*, 5771-5773.
9. Luo, J.; Jang, H. D.; Sun, T.; Xiao, L.; He, Z.; Katsoulidis, A. P.; Kanatzidis, M. G.; Gibson, J. M.; Huang, J. Compression and Aggregation-Resistant Particles of Crumpled Soft Sheets. *ACS Nano* **2011**, *5*, 8943-8949.
10. Kim, J.; Cote, L. J.; Kim, F.; Yuan, W.; Shull, K. R.; Huang, J. Graphene Oxide Sheets at Interfaces. *J. Am. Chem. Soc.* **2010**, *132*, 8180-8186.

11. Shao, J.; Lv, W.; Yang, Q. Self-Assembly of Graphene Oxide at Interfaces. *Adv. Mater.* **2014**, *26*, 5586-5612.
12. Chithrani, B. D.; Ghazani, A. A.; Chan, W. C. W. Determining the Size and Shape Dependence of Gold Nanoparticle Uptake into Mammalian Cells. *Nano Lett.* **2006**, *6*, 662-668.
13. Geng, Y.; Dalhaimer, P.; Cai, S.; Tsai, R.; Tewari, M.; Minko, T.; Discher, D. E. Shape effects of filaments versus spherical particles in flow and drug delivery. *Nat. Nanotechnol.* **2007**, *2*, 249-255.
14. Chaudhuri, P.; Hartouche, R.; Soni, S.; Hentschel, D. M.; Sengupta, S. Shape Effect of Carbon Nanovectors on Angiogenesis. *ACS Nano* **2012**, *4*, 574-582.
15. Chu, Z.; Zhang, S.; Zhang, B.; Zhang, C.; Fang, C.; Rehor, I.; Cigler, P.; Chang, H.; Lin, G.; Liu, R.; Li, Q. Unambiguous Observation of Shape Effects on Cellular Fate of Nanoparticles. *Sci. Rep.* **2014**, *4*, 4495-4503.
16. Srivastava, S Highly Efficient Fluorescent Quenching with Chemically Exfoliated Reduced Graphene oxide. *J. Vac. Sci. Technol B*, **2018**, *36*,
17. Patil, A. J.; Vickery, J. L.; Scott, T. B.; Mann, S. Aqueous Stabilization and Self-Assembly of Graphene Sheets into Layered Bio-Nanocomposites using DNA. *Adv. Mater.* **2009**, *21*, 3159-3164.
18. Yue, H.; Wei, W.; Yue, Z.; Wang, B.; Luo, N.; Gao, Y.; Ma, D.; Ma, G.; Su, Z. The Role of the Lateral Dimension of Graphene oxide in the Regulation of Cellular Responses. *Biomaterials* **2012**, *33*, 4013-4021.
19. Li, Y.; Yuan, H.; Bussche, A.; Creighton, M.; Hurt, R. H.; Kane, A. B.; Gao, H. Graphene Microsheets Enter Cells through Spontaneous Membrane Penetration at Edge Asperities and Corner sites. *Proc. Natl. Acad. Sci. USA* **2013**, *110*, 12295-12300.

20. Linares, J.; Matesanz, M. C.; Vila, M.; Feito, M. J.; Gonçalves, G.; Vallet-Regí, M.; Marques, P. A. A. P.; Portolés, M. T. Endocytic Mechanisms of Graphene Oxide Nanosheets in Osteoblasts, Hepatocytes and Macrophages. *ACS Appl. Mater. Interfaces* **2014**, *6*, 13697-13706.
21. Sun, C.; Wakefield, D. L.; Han, Y.; Muller, D. A.; Holowka, D. A.; Baird, B. A.; Dichtel, W. R. Graphene Oxide Stimulates Cells to Ruffle and Shed Plasma Membranes. *Chem.* **2016**, *1*, 273-286.
22. Koivusalo, M.; Welch, C.; Hayashi, H.; Scott, C. C.; Kim, M.; Alexander, T.; Touret, N.; Hahn, K. M.; Grinstein, S. Amiloride Inhibits Macropinocytosis by Lowering Submembranous pH and Preventing Rac1 and Cdc42 signaling. *J. Cell. Biol.* **2010**, *188*, 547-563.
23. Rejman, J.; Bragonzi, A.; Conese, M. Role of Clathrin- and Caveolae-Mediated Endocytosis in Gene Transfer Mediated by Lipo- and Polyplexes. *Mol. Ther.* **2005**, *12*, 468-474.
24. Kuo, L. J.; Yang, L. γ -H2AX – A Novel Biomarker for DNA Double-strand Breaks. *In Vivo* **2008**, *22*, 305-310.
25. Curtin, N. J. DNA Repair Dysregulation from Cancer Driver to Therapeutic target. *Nat. Rev. Cancer* **2012**, *12*, 801-817.
26. Hanahan, D.; Weinberg, R. A. The Hallmarks of Cancer. *Cell*, **2000**, *100*, 57-70.
27. Sengupta, P.; Basu, S.; Soni, S.; Pandey, A.; Roy, B.; Oh, M. S.; Chin, K. T.; Paraskar, A. S.; Sarangi, S.; Connor, Y.; Sabbisetti, V. S.; Koppam, J.; Kulkarni, A.; Muto, K.; Amarasiriwardena, C.; Jayawardene, I.; Lupoli, N.; Dinulescu, D. M.; Bonventre, J. V.; Mashelkar, R. A.; Sengupta, S. Cholesterol-Tethered Platinum II- Based Supramolecular Nanoparticle Increases Antitumor Efficacy and Reduces Nephrotoxicity. *Proc. Natl. Acad. Sci. U. S. A.* **2012**, *109*, 11294–11299.
28. Mallick, A.; More, P.; Ghosh, S.; Chippalkatti, R.; Chopade, B. A.; Lahiri, M.; Basu, S. Dual Drug Conjugated Nanoparticle for Simultaneous Targeting of Mitochondria and Nucleus in Cancer Cells. *ACS Appl. Mater. Interfaces* **2015**, *7*, 7584-7598.

29. Mallick, A.; More, P.; Syed, M. M. K.; Basu, S. Nanoparticle-Mediated Mitochondrial Damage Induces Apoptosis in Cancer. *ACS Appl. Mater. Interfaces* **2016**, *8*, 13218-13231.

Chapter 3: Polymer Modified GO-Nanoparticles for TOP1 Inhibition and DNA Damage in Cancer Cells.

This chapter has been published as:

Aditi Nandi, Chandramouli Ghosh, and Sudipta Basu. Polymer Conjugated Graphene-oxide Nanoparticles Impair Nuclear DNA and Topoisomerase I in Cancer. *Nanoscale Adv.* **2019**, *1*, 4965-4971.

(Reproduced by the permission from The Royal Society of Chemistry)

3.1 Abstract

Oncogene-associated cellular stresses (DNA damage stress, mitotic stress etc.) are newly proposed common characteristic of tumor cells. Stress sensitization and stress overload in cancer cells are two important approaches to cease cell proliferation and induce apoptosis, making them widely applicable in cancer therapy. Damaging the nuclear DNA and its associated proteins (namely Topoisomerases) with genotoxic drugs have been established as essential targets which can induce DNA damage stress followed by cell death. The adverse effects and solubility issues of DNA damaging drugs limits their use in clinics, hence incorporating the use of nano-scale materials like graphene oxide can greatly improve the solubility, permeability and efficacy of such chemotherapeutic drugs. Previously, we have developed cisplatin containing GO nanoparticles which can encapsulate another aromatic drug. The colloidal stability of these particles is an essential criterion for their efficient use in cancer therapy. To tackle the issue of colloidal stability and achieve multiple drug loading, we have engineered hydrophilic polymer (PEG and PIMA) grafted self-assembled GO nanoparticles containing a hydrophobic topoisomerase inhibitor-SN38 and cisplatin simultaneously. A combination of confocal microscopy, gel electrophoresis, and flow cytometry studies revealed that the GO-PEG-SN38-CDDP NPs and GO-PIMA_Ed-SN38-CDDP NPs endocytosed into the acidic lysosomes of HeLa (cervical cancer) cells within 6h leading to subsequent DNA damage and finally apoptosis. They also demonstrated remarkably greater cytotoxicity towards HeLa cells. Hence, this nano-platform can be used for strategic impairment of multiple cellular targets in next generation combinational chemotherapy.

3.2 Introduction

Cancer is a multifactorial disease having extremely complex origins and developmental stages.¹ As the underlying mechanisms of cancer progression were investigated, it was revealed that DNA played a critical role in tumorigenesis.² The nuclear DNA dictates important regulatory processes such as replication and transcription which directly affect cell proliferation, metabolism, gene activation, and cell cycle management. Thus given the importance of the DNA, it has been established as the main target and interaction site of many chemotherapeutic drugs.³ Genotoxic agents used in chemotherapy, which is the mainstay treatment for cancer today, target rapidly proliferating cancer cells by directly or indirectly damaging the DNA, and leads to eradication of tumor cells.⁴⁻⁶ While chemotherapy has been successful for the treatment

of different cancers, its effectiveness is often hampered in the long run by the onset of drug resistance.⁷⁻⁹ Thus, identification of new suitable targets in the cellular micro-environment will help enhance the therapeutic outcome of the chemotherapeutic drugs.¹⁰⁻¹²

In recent years, Topoisomerases have been proven to be viable therapeutic target for anticancer drugs because of their essential biophysical properties.^{13-14,16} These ubiquitous enzymes belong to a protein super-family that are responsible for maintain DNA topology by relaxing the DNA supercoils generated during DNA replication, DNA transcription, chromosome condensation-decondensation and segregation.¹⁵ The regulatory activity to conserve the DNA helicity involves co-ordinately cleaving, exploiting and re-ligating the double strand.¹⁷⁻²⁰ Topoisomerase I (TOP1) is a type I Topoisomerase encoded by the human genome, which resolves the torsional stress by introducing a reversible single strand break. This allows the rotation of the cleaved DNA strand across the intact strand, followed by re-ligation to restore the integrity of the double stranded DNA.²¹⁻²³ The transient reversible cleavable complex of TOP1 and DNA strand has been a vulnerable target of various novel antitumor drugs of which camptothecins are an important class. Camptothecin and its derivatives have been identified as effective Topoisomerase I inhibitors and have advanced to the frontline in clinics, for its utility against various types of cancers. Unfortunately, their use is limited because of dose limiting cytotoxicity resulting in myelosuppression, neutropenia and also erratic drug bio-distribution.²⁴⁻²⁷ Nonetheless, the additive and synergistic interactions of TOP 1 inhibitors with other cytotoxic DNA damaging drugs have been tested and have shown improved activity in several malignancies.²⁸⁻³⁰ This concept of “combination therapy”, based on simultaneous administration of multiple therapeutic drugs is regarded as an efficient solution for cancer treatment,³¹⁻³² but co-loading multiple drugs in a single carrier combined with their controlled release poses a major hurdle in next-generation combination therapy.

Inclusion of nanotechnology in the treatment of cancer has led to the discovery of nano-materials with distinctive advantageous properties such as: enhanced drug encapsulation, controlled release, increased tumor accumulation and reduced side effects, which potentiated good biomedical application.³³⁻³⁷ Lately, graphene oxide (GO) has garnered great interest owing to its biocompatibility and plethora of applications specially in cancer treatment for delivery of anti-neoplastic drugs, biomolecules (gene, siRNA), small molecules and diagnostic sensors.³⁸⁻⁴⁸ The superiority of GO stems from its unique 2D structure combined with oxygen functionalities

present on the sp^3 domains of the carbon framework, which confer GO with intriguing physical and chemical properties. This panoply of features like high aspect ratio, chemical versatility, ability to load aromatic anti-cancer drugs, molecules via π - π stacking and hydrophobic interactions, make GO stand out as a desirable platform for cancer therapy^{39,49}

Taking advantage of the characteristics of GO, in Chapter 2 we successfully synthesised cisplatin-mediated self-assembled spherical 3D GO nanoparticles from 2D sheets. The nanoparticles could be co-loaded with another hydrophilic aromatic drug along with cisplatin, enabling dual drug encapsulation in a single GO nano-platform.⁵⁰ These dual drug GO nanoparticles effectively killed cervical cancer cells, but were accompanied by compromised colloidal stability in water. Thus the challenge at hand was to enhance the aqueous dispersibility of GO nanoparticles for efficient use and evaluate the ability of the nanoparticles to package hydrophobic drugs along with cisplatin in a single vector.

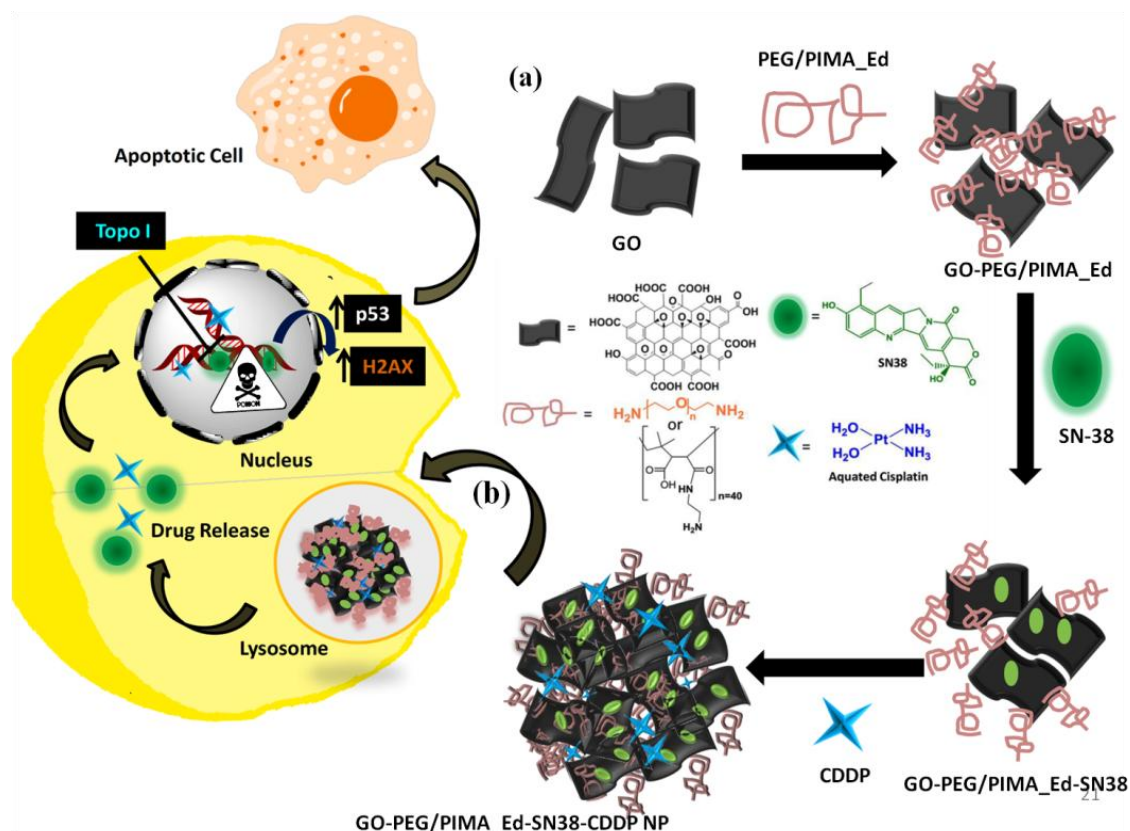
Polymers are the most common materials to engineer nanoparticles for drug delivery. Polymeric nanoparticles can be constructed from synthetic polymers or natural polymers like chitosan. The use of natural polymers helps enhance the biocompatibility of the nanocarriers. Polymers have also been employed for coating/ surface modification of various nanoparticles to increase their stability in biological fluids.³⁵ They also provide a physical barrier to suppress non-specific interactions with the blood components thus, enhancing the stability and efficacy.⁵¹ Another advantage of polymer coating of nanoparticles, is the possibility of further functionalisation of the polymers with small molecules to achieve a multifunctional nanocarrier.

In this chapter, we developed polyethylene glycol (GO-PEG-SN-38-CDDP) and poly(isobutylene-alt-maleic anhydride) conjugated ethylenediamine (GO-Pima_Ed-SN-38-CDDP) modified self-assembled graphene oxide nanoparticles (GO-PEG-SN-38-CDDP and GO-Pima_Ed-SN-38-CDDP) to cope with the issue of compromised aqueous colloidal stability. The PEG and PIMA_Ed modified GO-NPs can concertedly load a DNA Topoisomerase inhibitor (SN-38) and cisplatin, a DNA damaging agent. The polymer modified GO nanoparticles, GO-PEG-SN-38-CDDP and GO-Pima_Ed-SN-38-CDDP were found to be spherical having a diameter of 114nm and 180nm respectively, which was assessed by dynamic light scattering (DLS), field emission scanning electron microscopy (FESEM), and atomic force microscopy (AFM). The nanoparticles were taken up by cervical cancer HeLa cells through endocytosis and

temporarily confined into the acidic lysosomes, followed by the release of TOP1 inhibitor and DNA damaging drug in a controlled manner spanning over 72h. Confocal laser scanning microscopy and gel electrophoresis were employed to evaluate the simultaneous DNA damage along with Topoisomerase I (TOP1) inhibition, which eventually led to induction of programmed cell death (apoptosis) in HeLa cells. Dose-dependent treatment of HeLa cells with GO-PEG-SN-38-CDDP and GO-Pima_Ed-SN-38-CDDP displayed escalated cell death at 48h as compared to the free dual drug combination. These modified self-assembled nano-scale GO platforms with higher aqueous dispersibility can be viewed as a versatile construct to load different drug combinations having specific targets in the cellular milieu, thus enhancing their therapeutic efficacy for future combination chemotherapy.

3.3 Result and Discussion

3.3.1 Synthesis and characterization of GO-PEG-SN-38-CDDP and GO-PIMA_Ed-SN-38-CDDP nanoparticles: Sequential conjugation of hydrophilic polymer followed by stacking of hydrophobic drug and self-assembly into spherical nanoparticles with aquated cisplatin (CDDP) are represented in **scheme 1**. Surface alteration of GO with polymers like polyethylene glycol (PEG) and poly(isobutylene-alt-maleic anhydride) conjugated ethylenediamine (PIMA_Ed) was employed to enhance the colloidal stability. PEG is the most widely used non-ionic hydrophilic polymer having stealth behaviour to functionalize nano-scale materials. It not only helps increase the blood circulation time of nanoparticles but also reduces their tendency to aggregate in water and physiological solutions.⁵²⁻⁵⁵



Scheme 1: (a) Synthesis GO-PEG-SN38-CDDP and GO-PIMA_Ed-SN38-CDDP NPs (b) representation of cellular internalization and the mechanism of action of GO-PEG-SN38-CDDP and GO-PIMA_Ed-SN38-CDDP NPs.

Poly(isobutylene-alt-maleic anhydride) (PIMA) is another interesting polymer template used for modifying nanomaterials. It contains labile anhydride functional groups which can be easily conjugated to reactive moieties and drug molecules.⁵⁶ The poly(isobutylene-alt-maleic anhydride) conjugated ethylenediamine (PIMA_Ed) (10, **Figure 3.1**) polymer platform was synthesized via nucleophilic addition of N-Boc-ethylenediamine (8, **Figure 3.1**) on PIMA (7, **Figure 3.1**), followed by Boc-deprotection (9, **Figure 3.1**) and characterized by FTIR (**Figure 3.2b**) and ¹H NMR. The intrinsic peaks for PIMA at 1850 cm⁻¹, 1750 cm⁻¹, 1080 cm⁻¹ and 910 cm⁻¹ denote C=O and C-O stretching frequency of anhydride functionality. Reduction of the characteristic peaks combined with the appearance of broad O-H stretching resonance of carboxylic acid at around 3000-3600cm⁻¹ indicated anhydride ring opening by ethylenediamine. The incorporation of ethylenediamine was further confirmed by the presence of a peak at 1670 cm⁻¹ and 1560 cm⁻¹ which correspond to C=O stretching and N-H bending of amides

respectively.⁵⁷ The appearance of peak in the ¹H NMR spectra of conjugate 9 at $\delta=1.39$ which is characteristic for N-Boc protons and $\delta=8.32$, confirmed the incorporation of N-Boc-ethylenediamine into PIMA via amide bond formation (**Figure A 3.1**). Further, Boc- deprotection to get the desired PIMA-ethylenediamine (PIMA_Ed) conjugate was confirmed by the disappearance of the Boc peak in the ¹H NMR spectra of conjugate 10 (**Figure A 3.2**). The two hydrophilic polymers PEG (**2**, **Figure 3.1**) and PIMA_Ed (**10**, **Figure 3.1**) were covalently linked to carboxylic acid (-COOH) groups on GO (**1**, **Figure 3.1**) via EDC catalyzed amide coupling to yield GO-PEG (**3**, **Figure 3.1**) and GO-PIMA_Ed (**11**, **Figure 3.1**) respectively in a 1:5 weight ratio in water. The grafting of PEG or PIMA_Ed onto graphene oxide was assessed by FTIR (**Figure 3.2a and 3.2b**). The IR spectra of GO displayed signature peaks at 1720 cm⁻¹ corresponding to C=O stretching, a broad intense peak for O-H stretching resonance of carboxylic acid around 3400 cm⁻¹ and C-O peak at 1050 cm⁻¹.

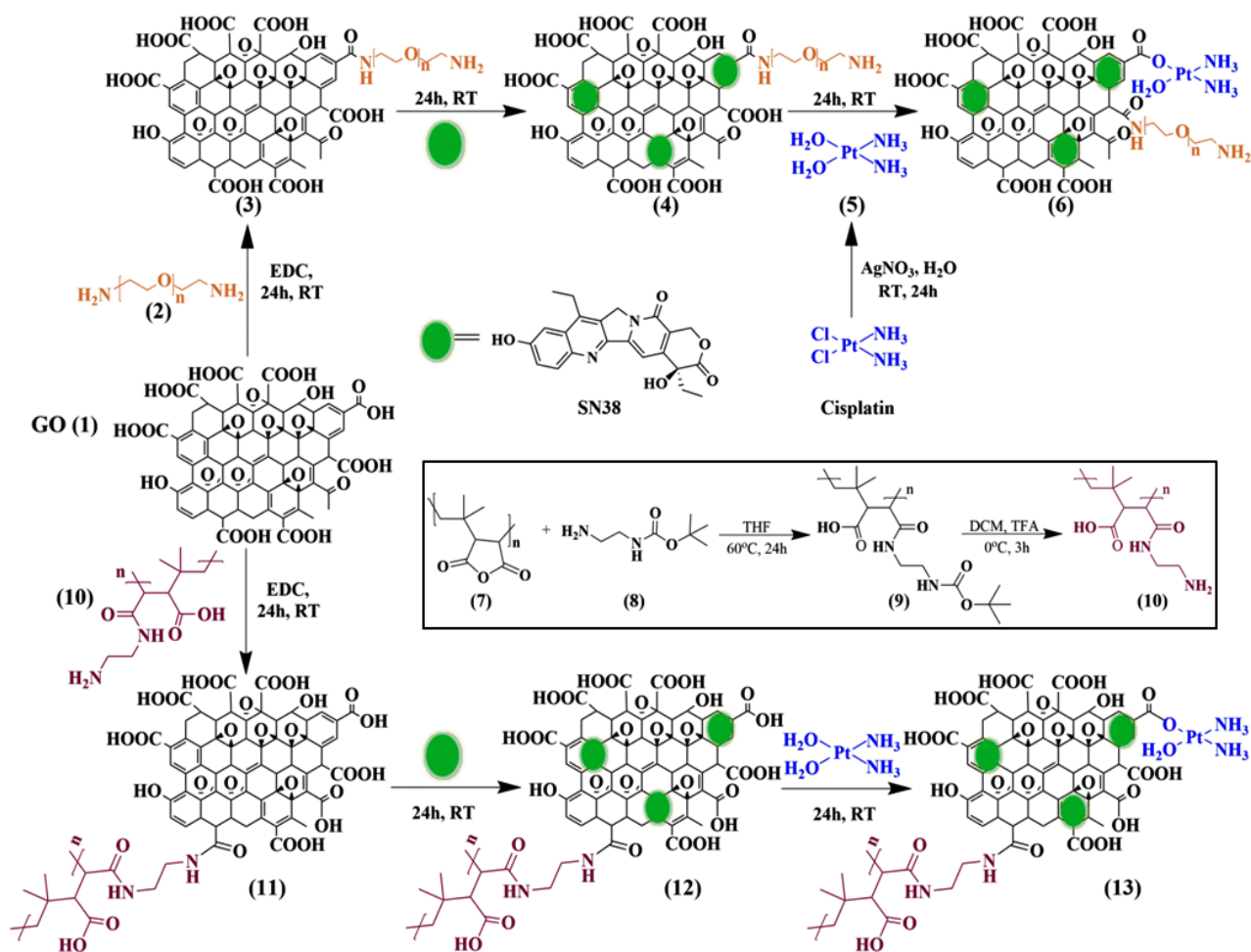


Figure 3.1: Synthesis of GO-PEG-SN38-CDDP and GO-PIMA_Ed-SN38-CDDP NPs.

The IR spectra of GO-PEG and GO-PIMA_Ed confirmed the amide bond formation by the appearance of new peaks at 1640 cm^{-1} and around 1530 cm^{-1} which are contributed by the C=O stretching and N-H bending of amides respectively. The increase in layer thickness of GO-PEG and GO-PIMA_Ed compared to pristine GO (3.9 and 6.9 vs 1.8 nm respectively) (**Figure.3.2 c-e**) visualized by atomic force microscopy (AFM) also confirmed the attachment of PEG and PIMA_Ed polymer on GO.⁵⁸

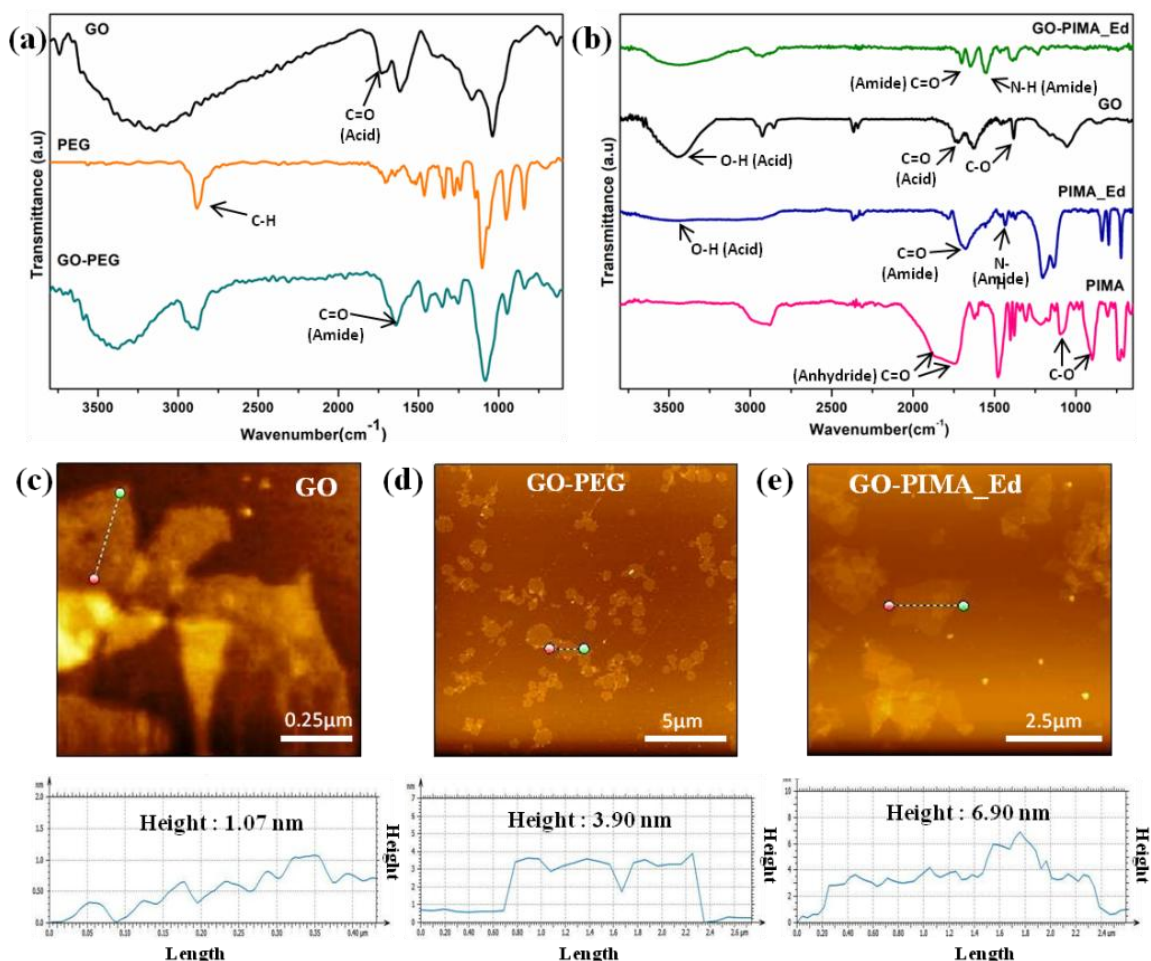


Figure 3.2: IR characterization of (a) GO-PEG, (b) PIMA_Ed and GO-PIMA_ED. Representative AFM images with height profiles (c) GO, (d) GO-PEG, (e) GO-PIMA_ED.

For simultaneous DNA damage and Topoisomerase I inhibition we chose cisplatin (CDDP)- which is the most widely used FDA approved platinum containing drug and SN38 an active metabolite of Irinotecan, which is derived from camptothecin and frequently used in clinics for

chemotherapy.⁵⁹⁻⁶³ The combined use of SN38 and CDDP has been studied for human small cell lung cancer and has shown good therapeutic synergy²⁸⁻³⁰. Dose dependent nephrotoxicity associated with cisplatin and low solubility of SN38 coupled with side effects such as neutropenia and anaemia limit their use.^{60,62} Thus to overcome these drawbacks and ameliorate the therapeutic efficacy of the drug combination regime, we hypothesized their incorporation in a single nanoscale material which can help achieve the desirable target.

SN38 was stacked onto 2D PEG/ PIMA_Ed modified graphene oxide (GO) by Π - Π stacking interaction. SN38 dissolved in DMSO was reacted with an aqueous solution of GO-PEG and GO-PIMA_Ed (**4 and 12 in Figure 3.1**) in a 1:0.5 weight ratio for 24h followed by centrifugation to remove excess SN38. Electron microscopy based visualization of GO-PEG-SN38 and GO-PIMA_Ed-SN38 revealed the conserved 2D sheet structure like that of GO (**Figure 3.3 a-b**). Aquated cisplatin (**5, Figure 3.1**) was further added in a 1:5 weight ratio and reacted for 24h which helped mediate the self-assembly into GO-PEG-SN38-CDDP and GO-PIMA_Ed-SN38-CDDP nanoparticles (**6 and 13, Figure 3.1**). The notable morphological change from 2D sheets to 3D spherical nanoparticles with diameter less than 200nm was elucidated by field emission electron microscopy (FESEM) (**Figure 3.3c-d**).

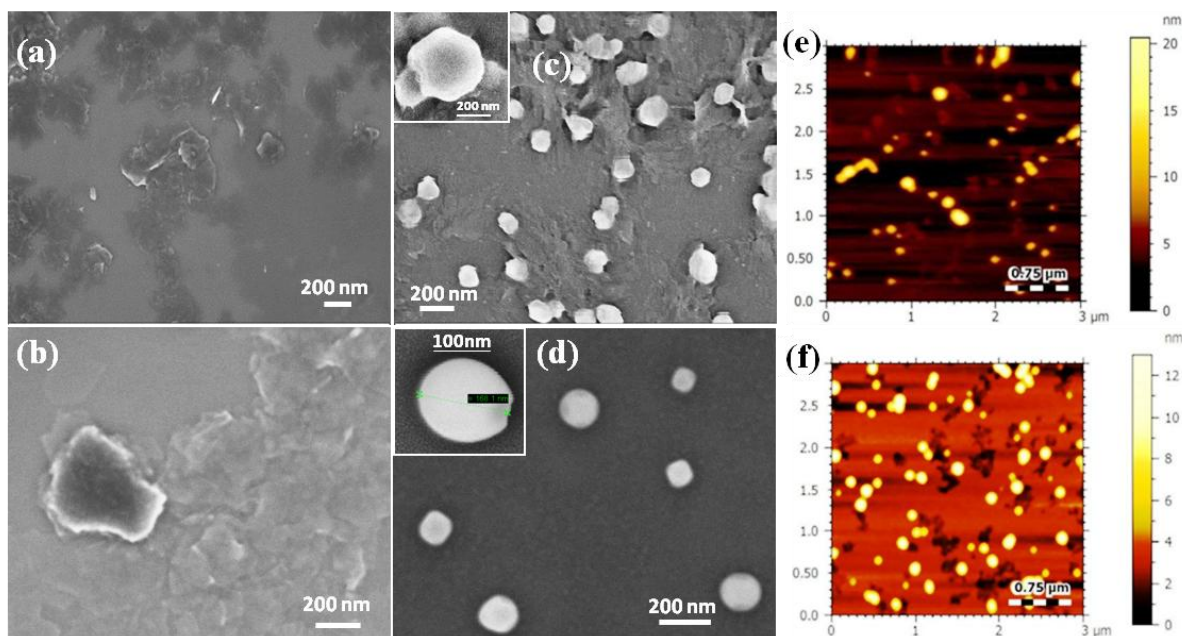


Figure 3.3: (a-b) FESEM images of GO-PEG-SN38 and GO-PIMA_Ed-SN38 (c-d) FESEM images of GO-PEG-SN38-CDDP NPs and GO-PIMA_Ed-SN38-CDDP NPs (e-f) AFM images of GO-PEG-SN38-CDDP and GO-PIMA_Ed-SN38-CDDP NPs.

AFM images also confirmed the spherical shape of into GO-PEG-SN38-CDDP and GO-PIMA_Ed-SN38-CDDP with size around 180 nm and 200 nm respectively (**Figure 3.3 e-f**). Successful stacking of SN38 on GO-PEG and GO-PIMA_Ed by hydrophobic and Π - Π interaction was evaluated by the drastic quenching in fluorescence emission (λ_{max} -560 nm) of SN38 when in close proximity to GO as compared to free SN38 at the same concentration (**Figure 3.4 a-b**). Raman spectroscopy, which is one of the best techniques to identify graphene and its derivatives, established the presence of GO moiety in GO-PEG-SN38-CDDP and GO-PIMA_Ed-SN38-CDDP by the appearance of the characteristic D and G bands centred at 1350cm^{-1} and 1590cm^{-1} respectively (**Figure 3.4c**).⁶⁴ To validate the presence of cisplatin, energy dispersive X-ray spectroscopy was carried out on single particles, which showed approximately 19.58 wt% of platinum (Pt) composition in the nanoparticles (**Figure 3.4d**).

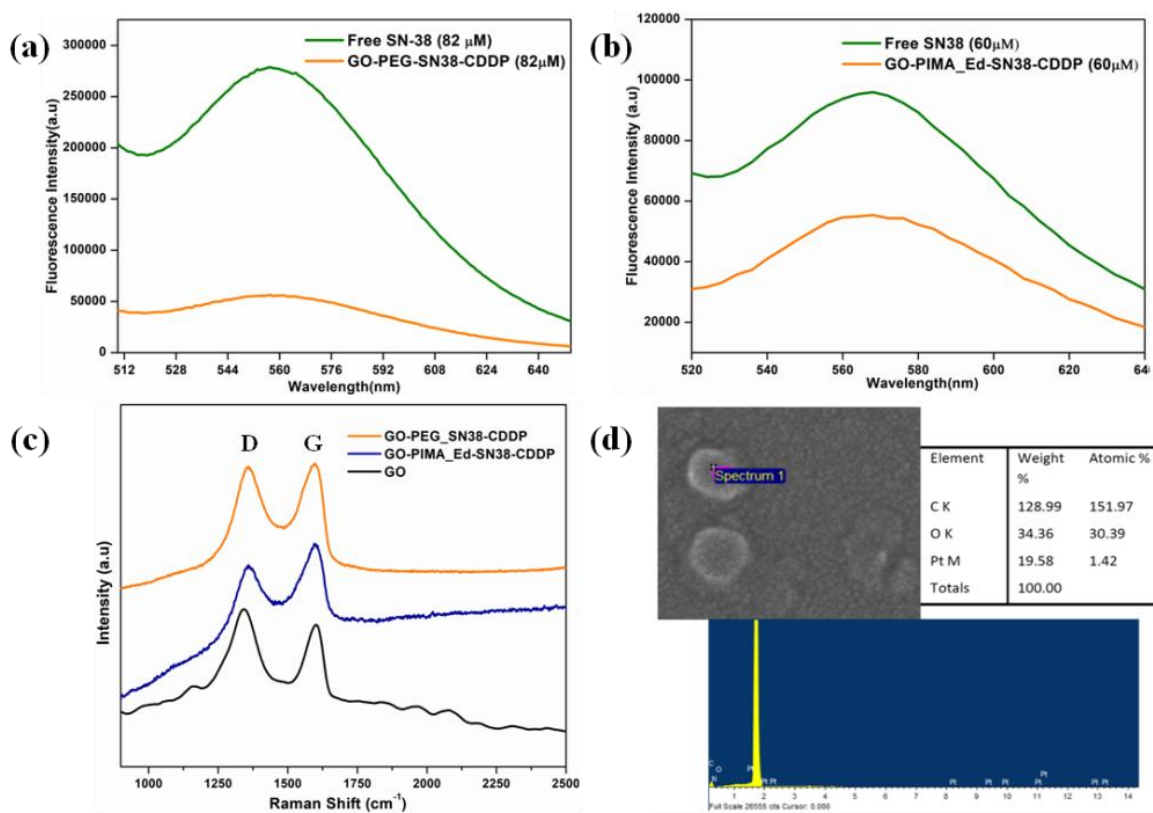


Figure 3.4: Fluorescence quenching of SN38 in (a) GO-PEG-SN38-CDDP and (b) GO-PIMA_Ed-SN38-CDDP NPs vs. Free SN38 (λ_{max} -560 nm), (c) Single particle resonance Raman spectra of GO-PEG-SN38-CDDP, GO-PIMA_Ed-SN38-CDDP NPs and GO, (d) EDAX of GO-PEG-SN38-CDDP.

Moreover, confirmation for the co-encapsulation of cisplatin (CDDP) and SN38 along with the determination of their loading concentration in GO-PEG-SN38-CDDP and GO-PIMA_Ed-SN38-

CDDP NPs was done by UV-Visible spectroscopy. From the absorbance vs. conc. calibration curve of SN38 ($\lambda_{\text{max}} = 387\text{nm}$) and CDDP ($\lambda_{\text{max}} = 706\text{nm}$) (**Figure 3.5 a-b**), the loading of SN38 in GO-PEG-SN38-CDDP NP was found to be $1364 \mu\text{M}$ ($535\mu\text{g/ml}$) and CDDP was $1100 \mu\text{M}$ ($330 \mu\text{g/ml}$), whereas for GO-PIMA_Ed-SN38-CDDP NP it was calculated to be $1321 \mu\text{M}$ ($518 \mu\text{g/ml}$) SN38 and $1290 \mu\text{M}$ ($387 \mu\text{g/ml}$) CDDP (**Figure 3.5c-d**).

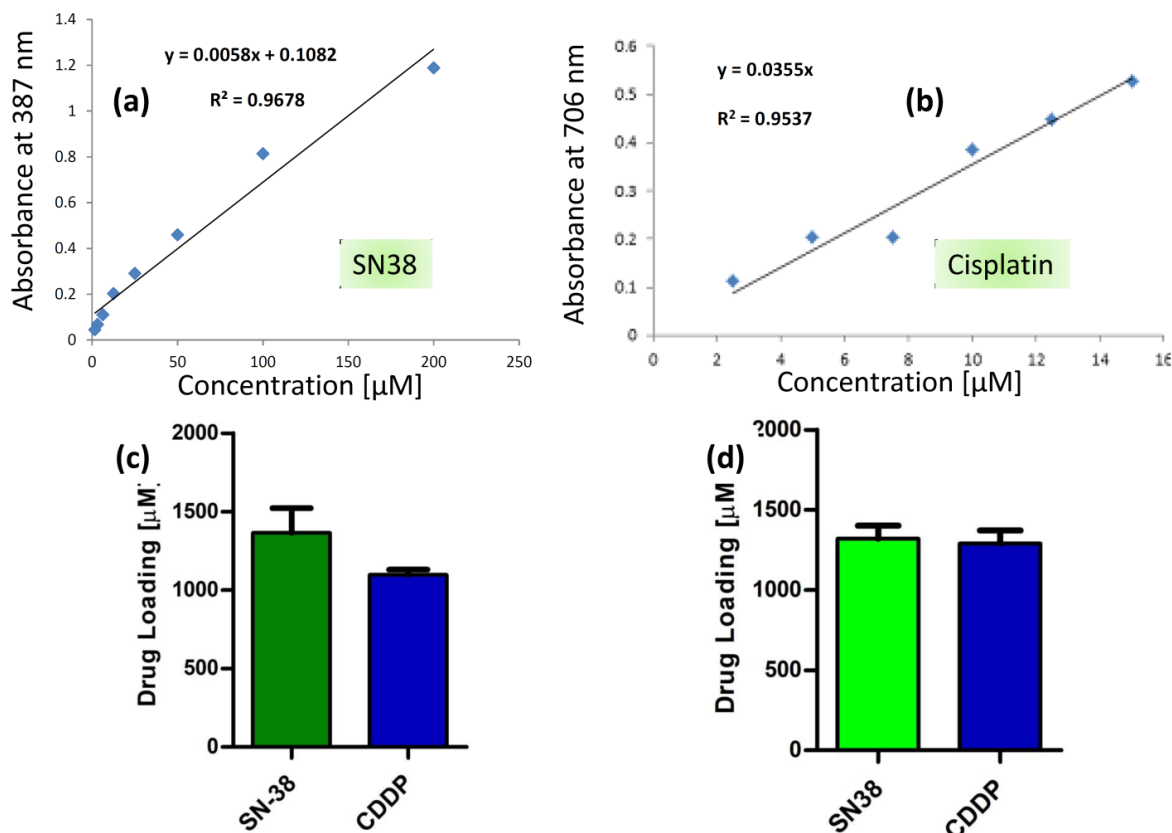


Figure 3.5: Standard curve of (a)SN38, (b) Cisplatin, (c) Loading of SN38 and CDDP in GO-PEG-SN38-CDDP (c) and GO-PIMA_Ed-SN38-CDDP(d).

Lastly, we studied the time dependent dispersibility of GO-PEG-SN38-CDDP and GO-PIMA_Ed-SN38-CDDP NPs in water. The results displayed enhanced colloidal stability for over 140 min as compared to unmodified GO-SN38-CDDP NP, which agglomerate in water within 10 min (**Figure 3.6**).

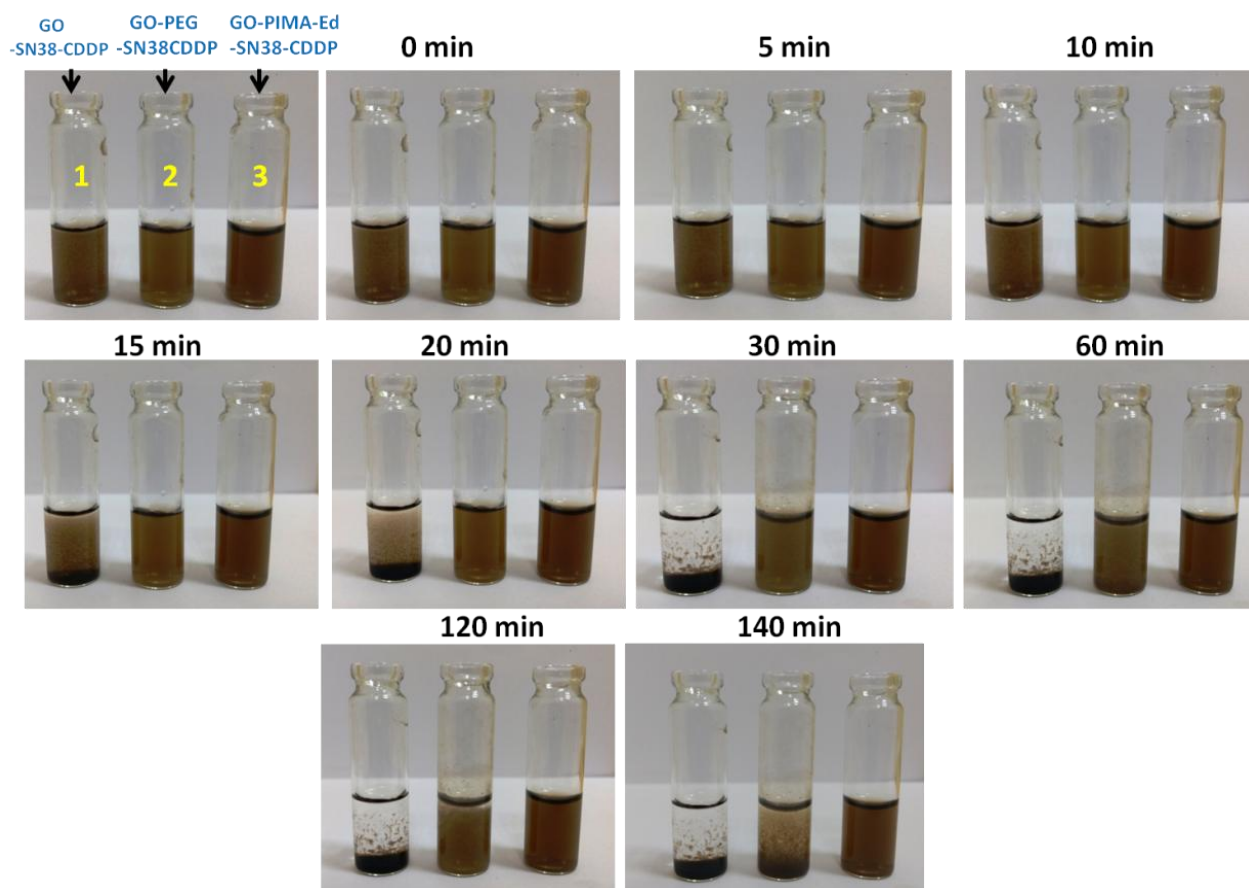


Figure 3.6: Time dependent colloidal stability of GO-PEG-SN38-CDDP and GO-PIMA_Ed-SN38-CDDP NPs vs. unmodified GO-SN38-CDDP NPs.

3.3.2 Cellular internalisation: According to our assumption shown in **scheme 1(b)**, the engineered GO-PEG-SN38-CDDP and GO-PIMA_Ed-SN38-CDDP NPs would internalize into cancer cells and home into the acidic lysosomal compartment in the cellular micro-environment⁵⁰. To check our hypothesis, we incubated HeLa cervical cancer cells with the two green fluorescent GO-polymer NPs in a time dependent manner. The lysosomes were stained with LysoTracker Red DND-99 and thereafter viewed under a confocal scanning laser microscope (CLSM). The fluorescence microscopy images clearly showed the cellular uptake and time dependent lysosomal co-localisation of green fluorescent GO-PEG-SN38-CDDP and GO-PIMA_Ed-SN38-CDDP NPs into red fluorescently labelled lysosomes, by the gradual increase of yellow intensity due to overlapping of green and red fluorescence from 1h to 3h to 6h. Quantification of the confocal images for the extent of overlap of red and green fluorescent signals confirmed the time dependent localisation of the nanoparticles into the lysosomes with

15%, 25% and 45% colocalisation volume for GO-PEG-SN38-CDDP (Figure 3.7) and 11%, 23% and 37% for GO-PIMA_Ed-SN38-CDDP NPs (Figure 3.8).

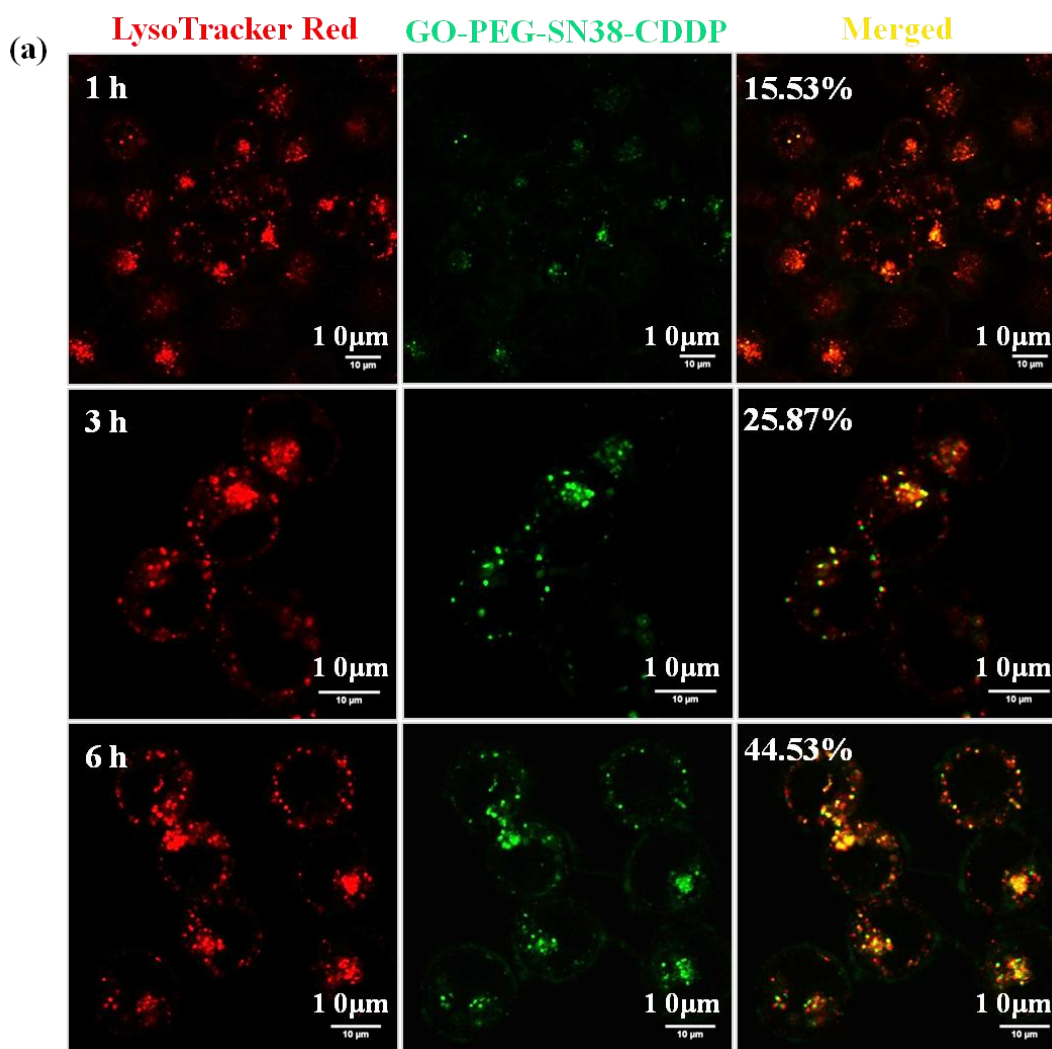


Figure 3.7: Representative confocal scanning laser microscope images of HeLa cells post incubation with green fluorescent GO-PEG-SN38-CDDP NPs for 1h, 3h, and 6h. The lysosomes were stained with LysoTracker DND-99 (red fluorescence). The yellow merged regions areas the colocalization of GO-PEG-SN38-CDDP NPs into the lysosomes. [Inset is the % colocaliation volume]. Scale bar =10 μm.

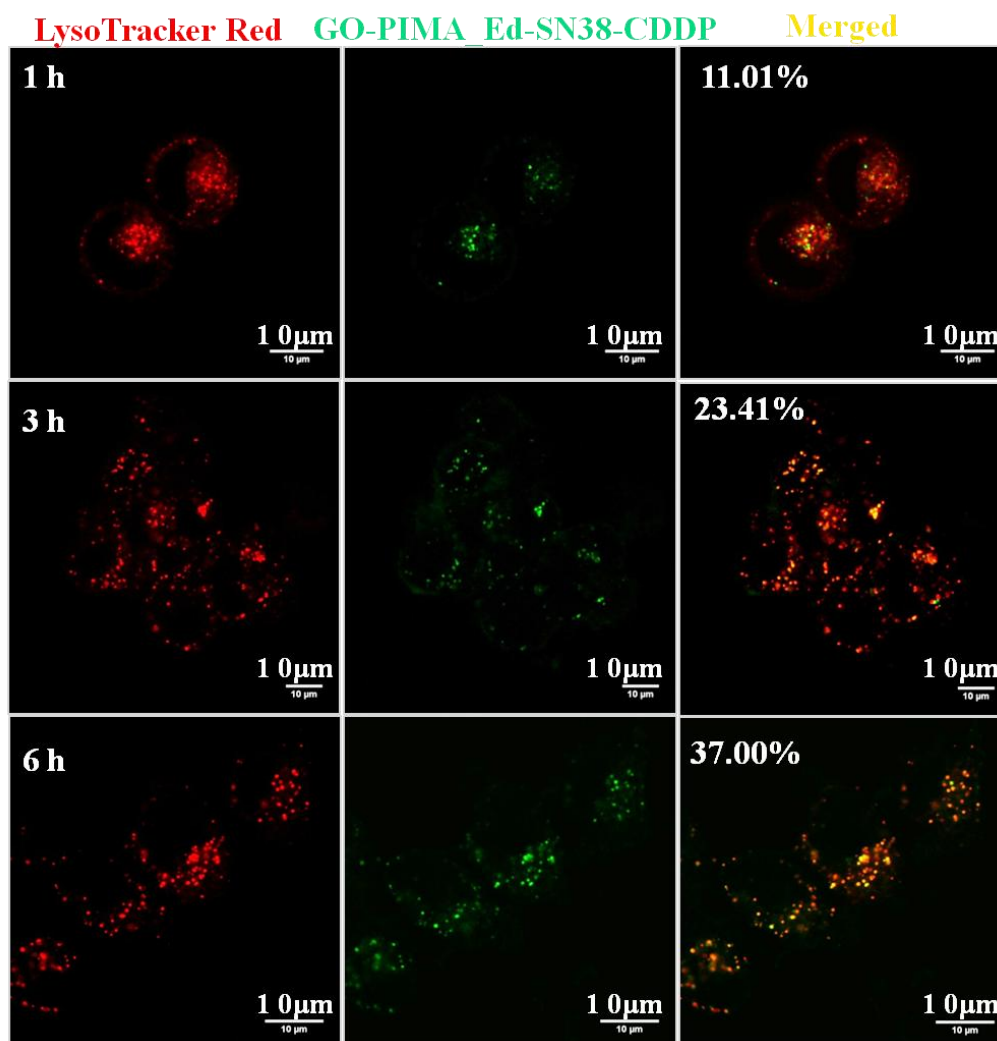


Figure 3.8 Representative confocal scanning laser microscope images of HeLa cells post incubation with green fluorescent GO-PIMA_Ed-SN38-CDDP NPs for 1h, 3h, and 6h. The lysosomes were stained with LysoTracker DND-99 (red fluorescence). The yellow merged areas depict the colocalization of GO-PEG-SN38-CDDP NPs into the lysosomes. [Inset is the % colocaliation volume]. Scale bar =10 μm .

The engulfment of nano-scale materials by cells through different endocytotic pathways vary depending upon the size and shape of the nanoparticles. To determine the mechanism of endocytosis, GO-PEG-SN38-CDDP and GO-PIMA_Ed-SN38-CDDP NPs, HeLa cells were pre-treated with different endocytosis pathway inhibitors like chlorpromazine (clathrin dependent endocytosis), genistein (caveolin dependendent endocytosis) and amiloride (macropinocytosis) for 45min. This was followed by incubation with green fluorescent GO-PEG-SN38-CDDP and GO-PIMA_Ed-SN38-CDDP NPs at (2 $\mu\text{g}/\text{ml}$ of SN38) for 2h, after which the lysosomes were stained with LysoTracker Red DND-99. Observation using confocal microscopy (**Figure 3.9 and**

Figure 3.10) revealed that cells treated with genistein and amiloride showed no significant variation in the lysosomal homing of both GO-Polymer NPs compared to no inhibitor treated control cells, which was clear from the yellow colour fluorescence intensity obtained by merging of green and red fluorescence signal from nanoparticles and lysosomes. On the contrary, a notable reduction in the colocalisation (yellow colour intensity) was seen for cells treated with chlorpromazine and incubated with GO-PEG-SN38-CDDP and GO-PIMA_Ed-SN38-CDDP NPs. The image based quantification for colocalisation volume [(12% chlorpromazine, 41% amiloride and 27% genistein vs 39% non-treated control for GO-PEG_SN38-CDDP) and for (GO-PIMA_Ed-SN38-CDDP chlorpromazine-16%, amiloride-35% and genistein 31% vs 41% control cells)] also supported the cellular uptake through clathrin dependent endocytosis for both the nanoparticles by showing lower percentage of overlap in contrast to control and other inhibitor treated cells.⁶⁵

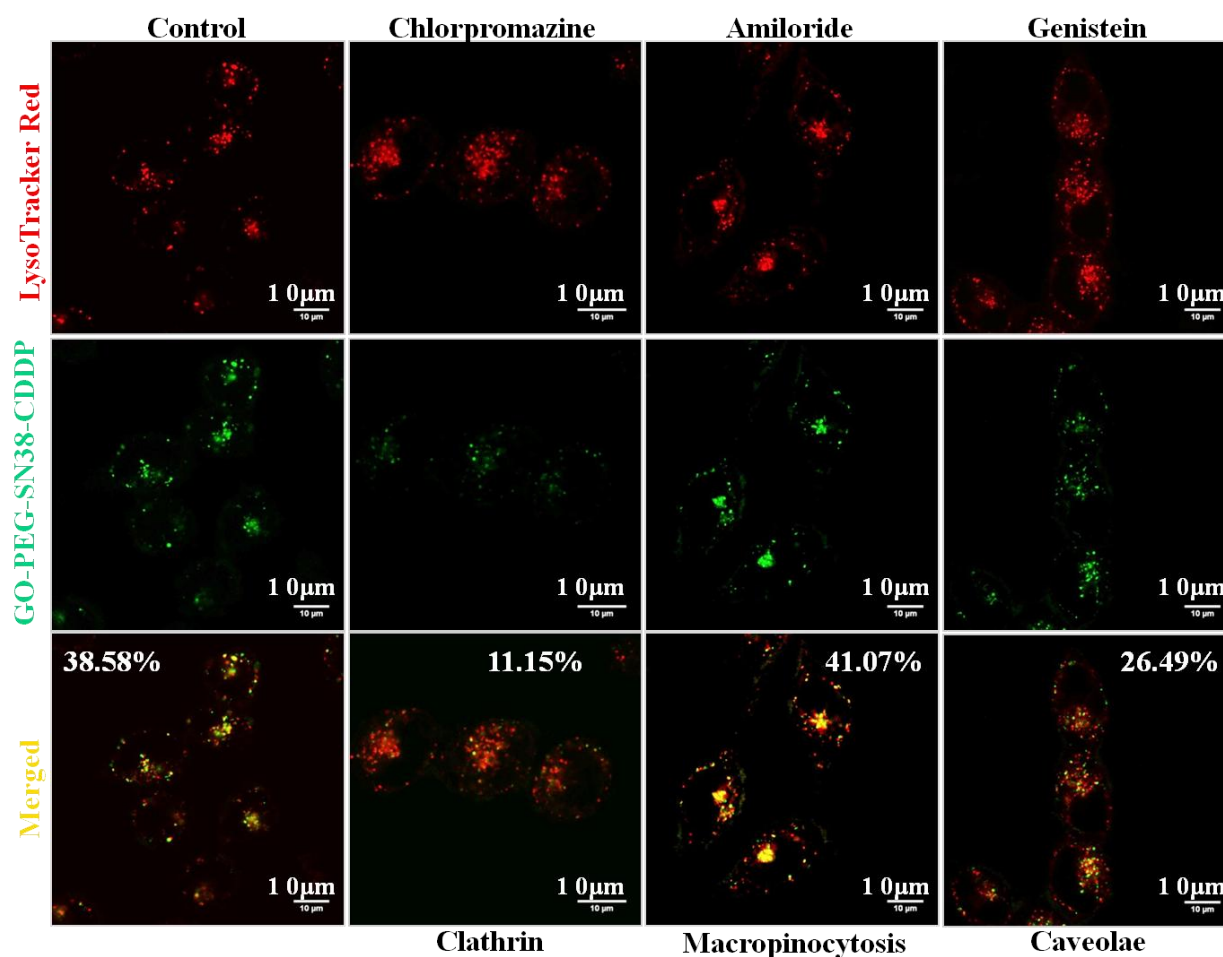


Figure 3.9: Confocal scanning laser microscope images of HeLa cells pre-treated with endocytosis inhibitors (chlorpromazine, genistein and amiloride) followed by GO-PEG-SN38-CDDP NPs

(green). Lysosomes of HeLa cells were stained with LysoTracker Red DND-99 dye. Scale bar = 10 μm .

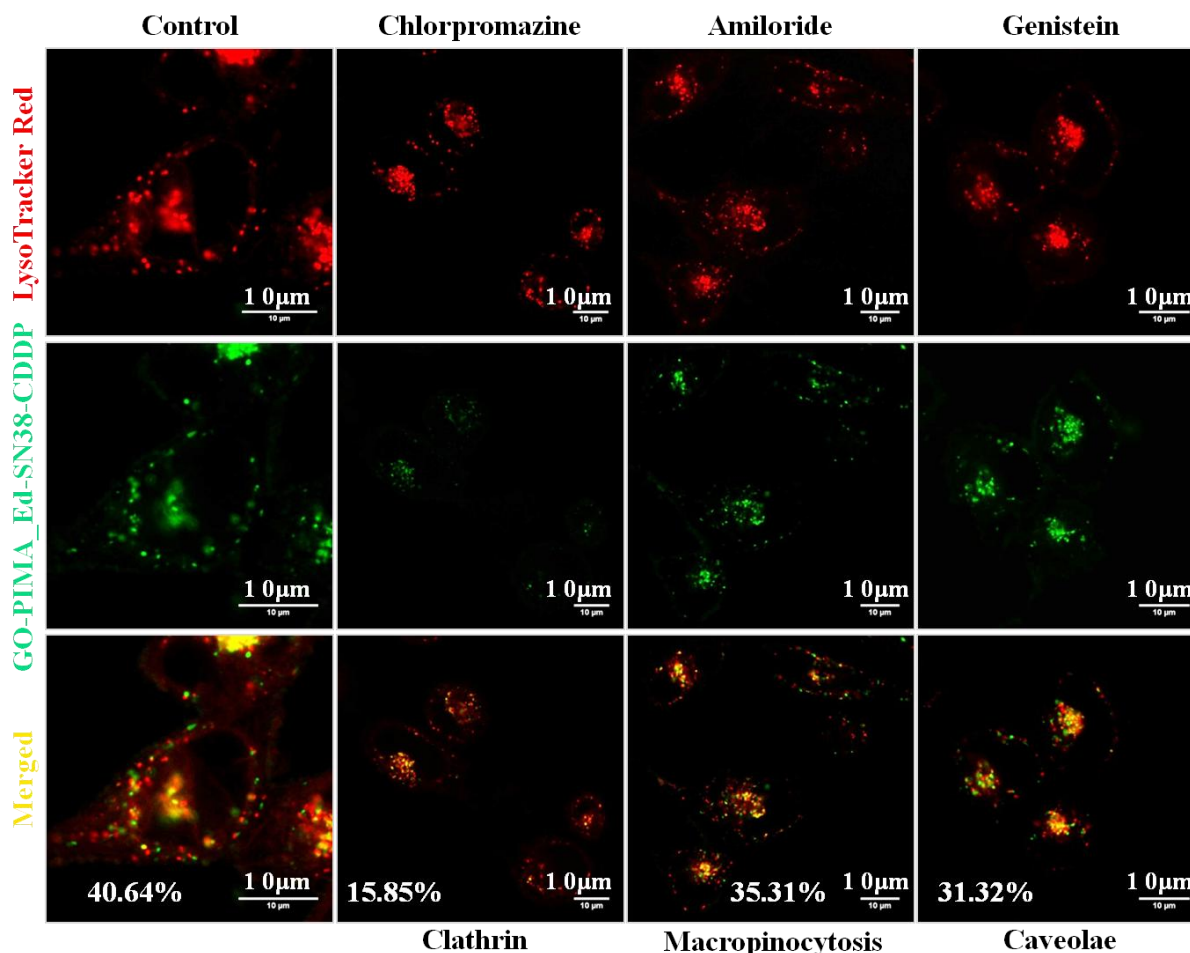


Figure 3.10: Confocal scanning laser microscope images of HeLa cells pre-treated with endocytosis inhibitors (chlorpromazine, genistein and amiloride) followed by GO-PIMA_Ed-SN38-CDDP NPs (green). Lysosomes of cells were stained with LysoTracker Red DND-99 dye. Scale bar = 10 μm .

3.3.3 Drug release: Post the localisation into acidic lysosomal compartment inside the cellular milieu, GO-PEG-SN38-CDDP and GO-PIMA_Ed-SN38-CDDP NPs are anticipated to release their drug payloads for effective DNA damage and Topoisomerase I (TOP1) inhibition. To study the release of SN38 and cisplatin, GO-PEG-SN38-CDDP and GO-PIMA_Ed-SN38-CDDP NPs were incubated in acidic buffer (pH 5.5: mimic of acidic lysosomal pH) over 72h. The release was monitored and quantified at different time intervals by UV-Visible spectroscopy and it was found that GO-PEG-SN38-CDDP (**Figure 3.11a**) released of 47% of SN38 and 36% CDDP after 72h and 54h, whereas GO-PIMA_Ed-SN38-CDDP NP (**Figure 3.11b**) released 50%, 22% of SN38 and CDDP respectively in a slow and sustained manner. Higher release of SN38 compared

to CDDP can be attributed to the weaker aromatic Π - Π stacking interaction between GO and SN38 as compared to stronger coordinate linkage between cisplatin and -COOH of graphene oxide. Alternately, quantification of dual drug release at physiological pH of 7.4 revealed only 21% of SN38, 13% CDDP release from GO-PEG-SN38-CDDP (**Figure 3.11a**) and 34% SN38, 10% CDDP for GO-PIMA_Ed-SN38-CDDP NPs even after 72h (**Figure 3.11b**). The drug release profiles in buffer pH 5.5 and pH 7.4 indicated that the nanoparticles released the chemotherapeutic payload better when in the acidic lysosomes rather than when in blood circulation, which is required for efficient targeting of tumor tissues and not healthy tissues through passive transport by EPR effect.

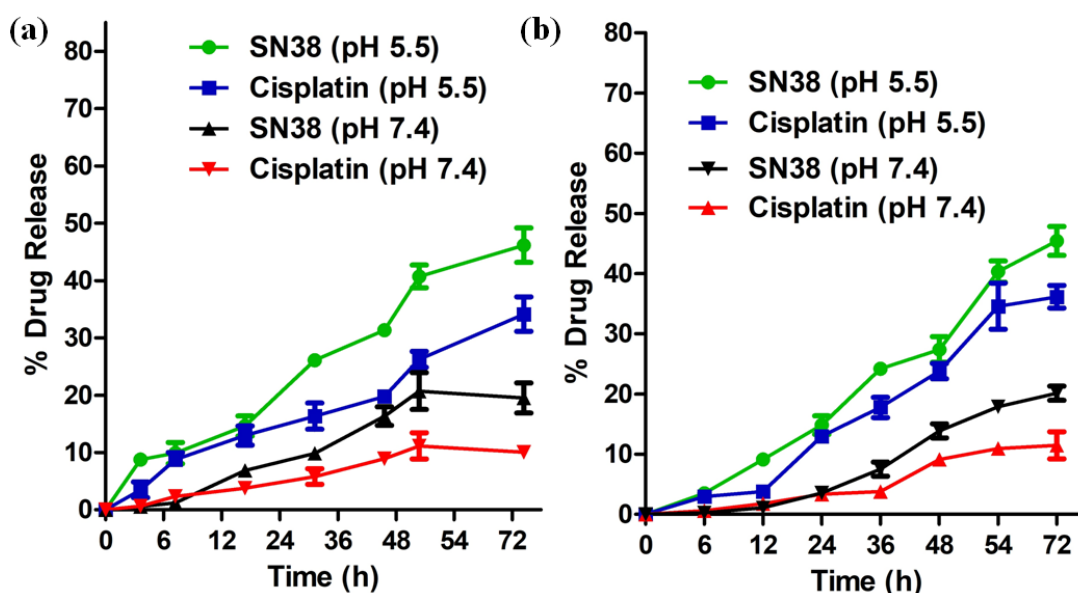


Figure 3.11: Drug release profiles of SN38 and Cisplatin at pH 5.5 and pH 7.4 from (a) GO-PEG-SN38-CDDP NPs, and (b) GO-PIMA_Ed-SN38-CDDP NPs.

3.3.4 DNA damage and Topoisomerase I inhibition: We hypothesized that acidic environment triggered release of SN38 and CDDP from the GO-PEG-SN38-CDDP and GO-PIMA_Ed-SN38-CDDP NPs would lead to concurrent TOP1 inhibition along with DNA impairment. To account for topoisomerase I inhibition due to SN38, HeLa cells were treated with GO-PEG-SN38-CDDP and GO-PIMA_Ed-SN38-CDDP separately for 24h followed by western blot assay for the extracted proteins. The gel electrophoresis image (**Figure 3.12a**) and analogous quantification plot (**Figure 3.12b**) clearly showed the downregulation of TOP1 as compared to non-treated control cells.

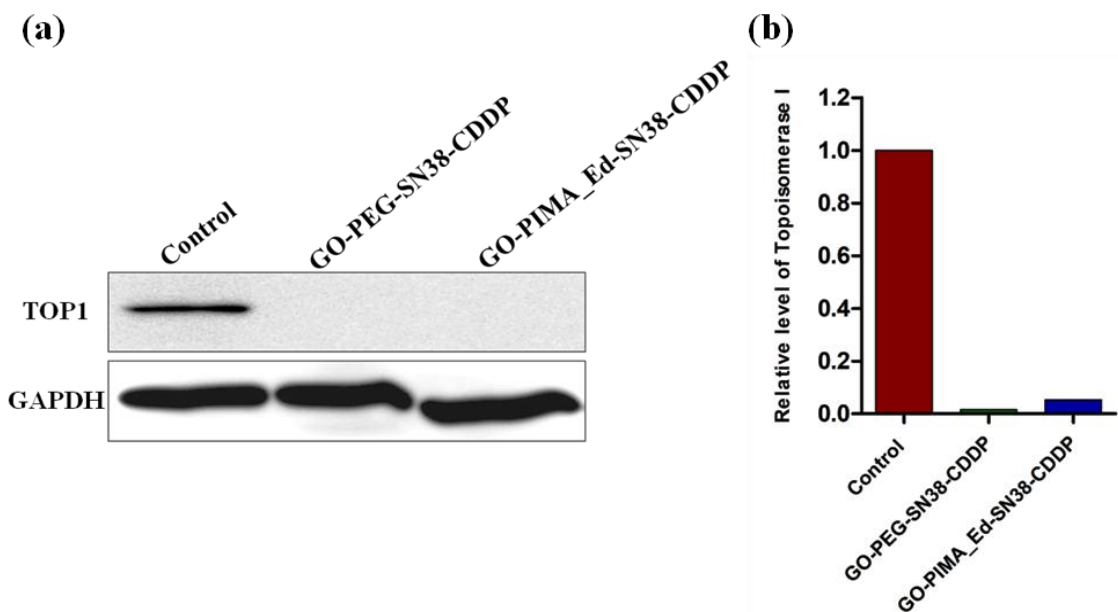


Figure 3.12: (a) Western blot image for Topoisomerase I (TOP1) after treatment with GO-PEG-SN38-CDDP NPs and GO-PIMA_Ed-SN38-CDDP NPs, (b) Quantification for expression of TOP1 from western blot.

For determining the DNA damaging ability, we gauged the expression of γ H2AX and p53-which are important DNA damage biomarkers by immunofluorescence assay.^{66,67} Cervical cancer HeLa cells were treated incubated with GO-PEG-SN38-CDDP and GO-PIMA_Ed-SN38-CDDP NPs for 24h followed by treatment with anti- γ H2AX, anti-p53 primary antibody separately and red fluorescently labelled Alexa-549 secondary antibody. The nucleus of the treated cells were stained with DAPI (blue fluorescence) after which the expression of γ H2AX and p53 was visualised by confocal microscopy. **(Figure 3.13a)** displayed increased expression of γ H2AX through higher red fluorescence signal (indicating DNA damage) as compared to non-treated control cells, which showed negligible DNA damage. Fluorescence signal based quantification also revealed that GO-PEG-SN38-CDDP and GO-PIMA_Ed-SN38-CDDP caused 5.0 fold and 6.4 fold increase in γ H2AX expression **(Figure 3.13b)**.

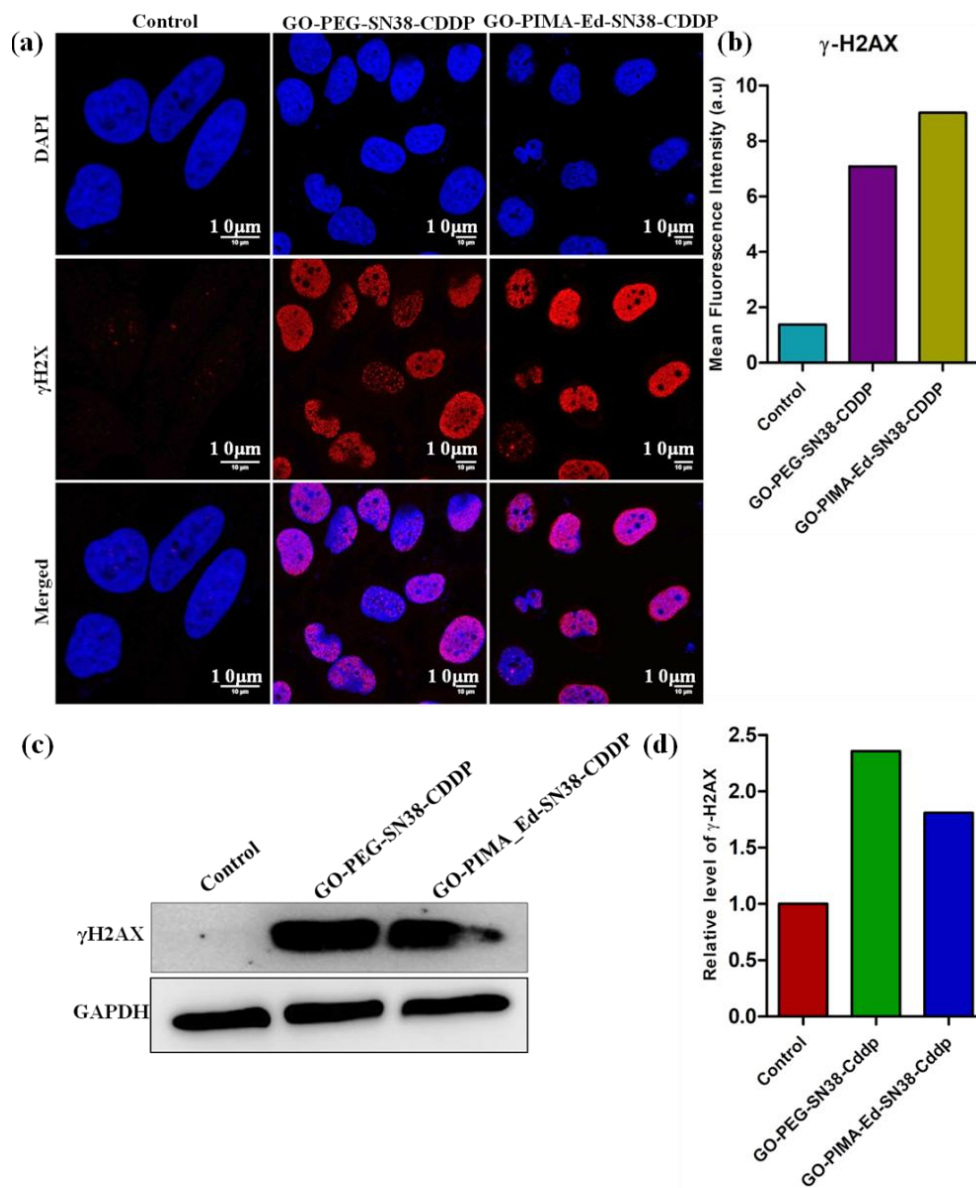


Figure 3.13: (a) Confocal microscope images of HeLa cells to visualize γ -H2AX as DNA damage biomarker post 24h treatment with GO-PEG-SN38-CDDP and GO-PIMA_Ed-SN38-CDDP NPs. γ -H2AX was stained with the Alexa Fluor 594-labeled secondary antibody (red fluorescent), the nuclei of HeLa cells were stained with DAPI (blue). (b) Quantification for expression of γ -H2AX from fluorescence images. (c) Western blot image for the expression of γ -H2AX in HeLa cells. (d) Quantification of γ -H2AX from western blot.

Moreover, western blot analysis for expression of γ H2AX (**Figure 3.13c-d**) asserted the nuclear DNA damage of HeLa cells post 24h treatment. 2.3 fold and 1.8 fold amplification of the γ H2AX expression for GO-PEG-SN38-CDDP and GO-PIMA_Ed-SN38-CDDP was evident from the gel electrophoresis image. Upregulation of p53 by immunofluorescence assay (**Figure 3.14a**) also confirmed the cellular stress generated from DNA damage. The quantification

(Figure 3.14b) revealed a 4.0 and 5.0 fold increase for GO-PEG-SN38-CDDP and GO-PIMA_Ed-SN38-CDDP NP treated cells compared to control cells. Since DNA damage is a nuclear phenomena, the overlapping of red fluorescence signal (appearing because of over expression of γ H2AX and p53) with blue DAPI stained nucleus confirmed the claim of DNA damage upon nanoparticle treatment. Western blot images along with its quantification (Figure 3.14c-d) showed significant increase (6.3 fold and 6.4 fold) in p53 expression.

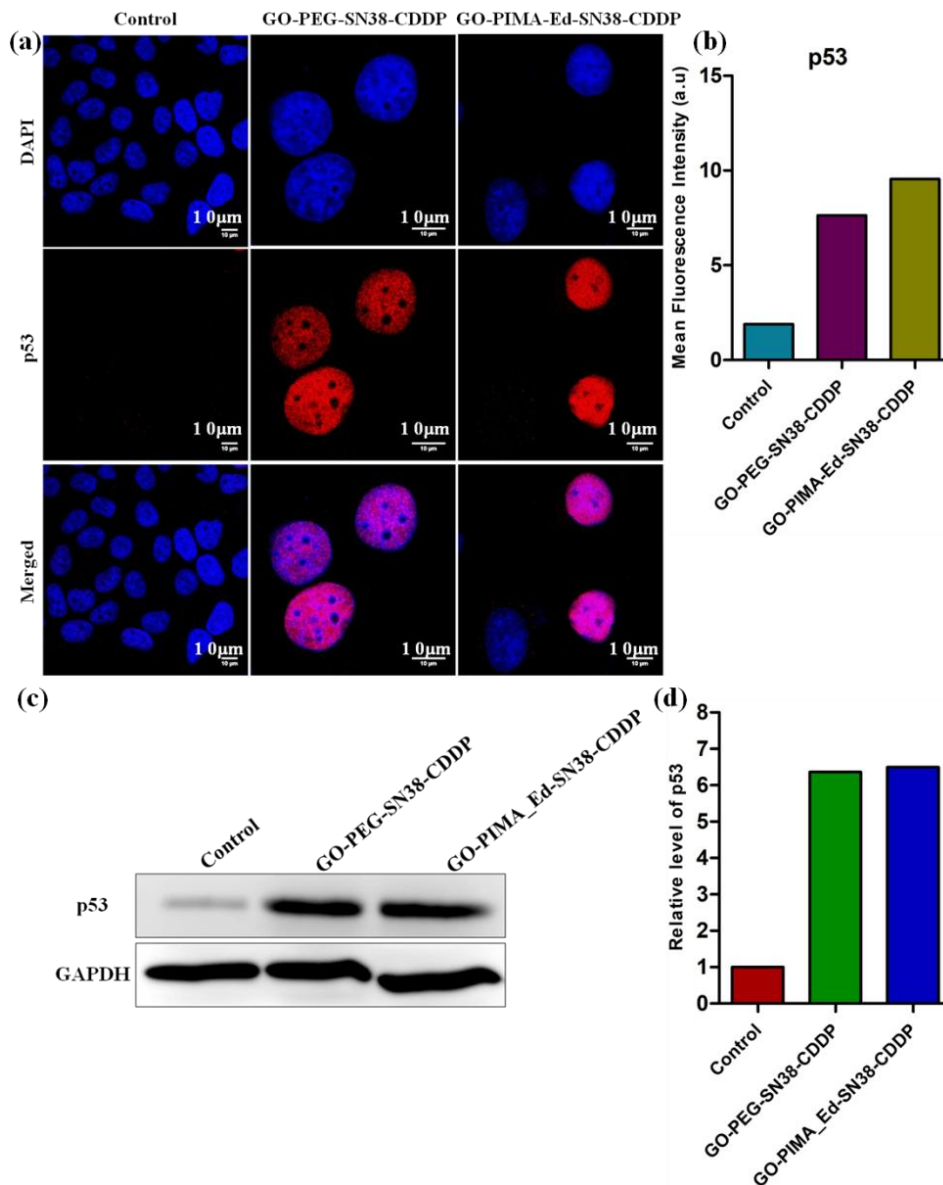


Figure 3.14: (a) Confocal microscope images of HeLa cells to visualize p53 as DNA damage and apoptosis biomarker post 24h treatment with GO-PEG-SN38-CDDP and GO-PIMA_Ed-SN38-CDDP NPs. p53 was stained with the Alexa Fluor 594-labeled secondary antibody (red fluorescent) and the nuclei of cells were stained with DAPI (blue). (b) Quantification for expression of p53 from fluorescence images. (c) Western blot image for the expression of p53 in HeLa cells. (d) Quantification of p53 from western blot.

As a consequence of DNA damage, the cellular repair machinery through poly-ADP ribose (PARP) family of proteins gets triggered in cells. Assessment of the expression of PARP post treatment with GO-PEG-SN38-CDDP and GO-PIMA_Ed-SN38-CDDP NPs by western blot clearly showed the reduction (1.6 fold and 1.4 fold) in expression of the protein (**Figure 3.15a and b**). The downregulation of PARP expression as compared to untreated cells can be attributed to its cleavage because of DNA damage. The subsequent 3.0 fold (GO-PEG-SN38-CDDP) and 2.0 fold (GO-PIMA_Ed-SN38-CDDP) increase in the expression of cleaved PARP (an important cellular marker for apoptosis) facilitates the cellular disassembly during programmed cell death (**Figure 3.15c-d**).^{68,69} Thus the western blot and confocal images demonstrated, successful DNA damage as well as the onset of apoptosis in HeLa cells upon treatment with GO-PEG-SN38-CDDP and GO-PIMA_Ed-SN38-CDDP NPs.

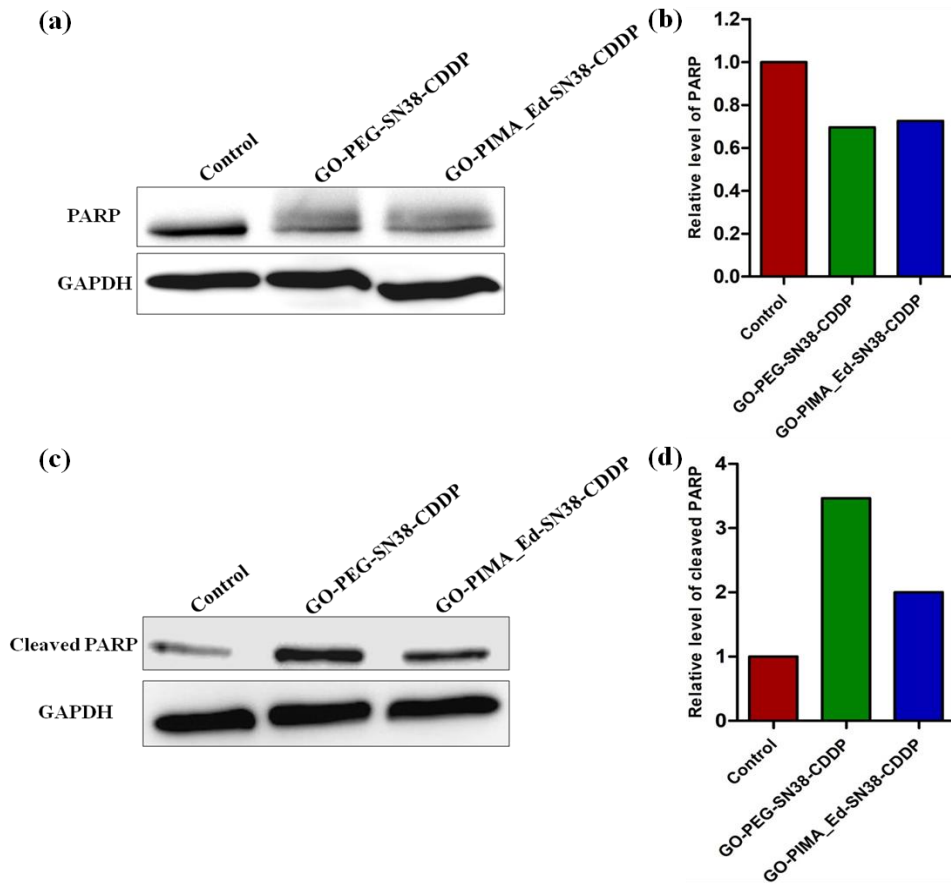


Figure 3.15: Western blot images and corresponding quantification for the expression of (a-b) PARP and (c-d) Cleaved PARP in HeLa cells after treatment with GO-PEG-SN38-CDDP and GO-PIMA_Ed-SN38-CDDP NPs for 24h.

3.3.5 Apoptosis and cell death: Evading apoptosis is an important phenotype of cancer cells. We estimated the apoptosis inducing ability of GO-PEG-SN38-CDDP and GO-PIMA_Ed-SN38-CDDP NPs by flow cytometry. HeLa cells were treated with the respective nanoparticles for 24h and 48h and co-stained with Annexin V-FITC which binds to the phosphatidylserine on apoptotic cell surface and PI which binds to the DNA of cells undergoing late apoptosis or necrosis cells. From the flow cytometry analysis (**Figure 3.16**) we observed that in comparison to non-treated control cells, HeLa cells treated with GO-PEG-SN38-CDDP NP for 24h showed 50.45% and 43.89% cells in early and late apoptotic stage. After 48h of incubation the percentage of HeLa cells undergoing late apoptosis increased to 74.13% (20.65% cells in early apoptosis). Similar results were obtained for GO-PIMA_Ed-SN38-CDDP NPs where after 24h incubation 41.30% and 49.88% cells were in early and late apoptosis, whereas 27.90% and 71.54% cells were in the early and late apoptotic state after 48h.

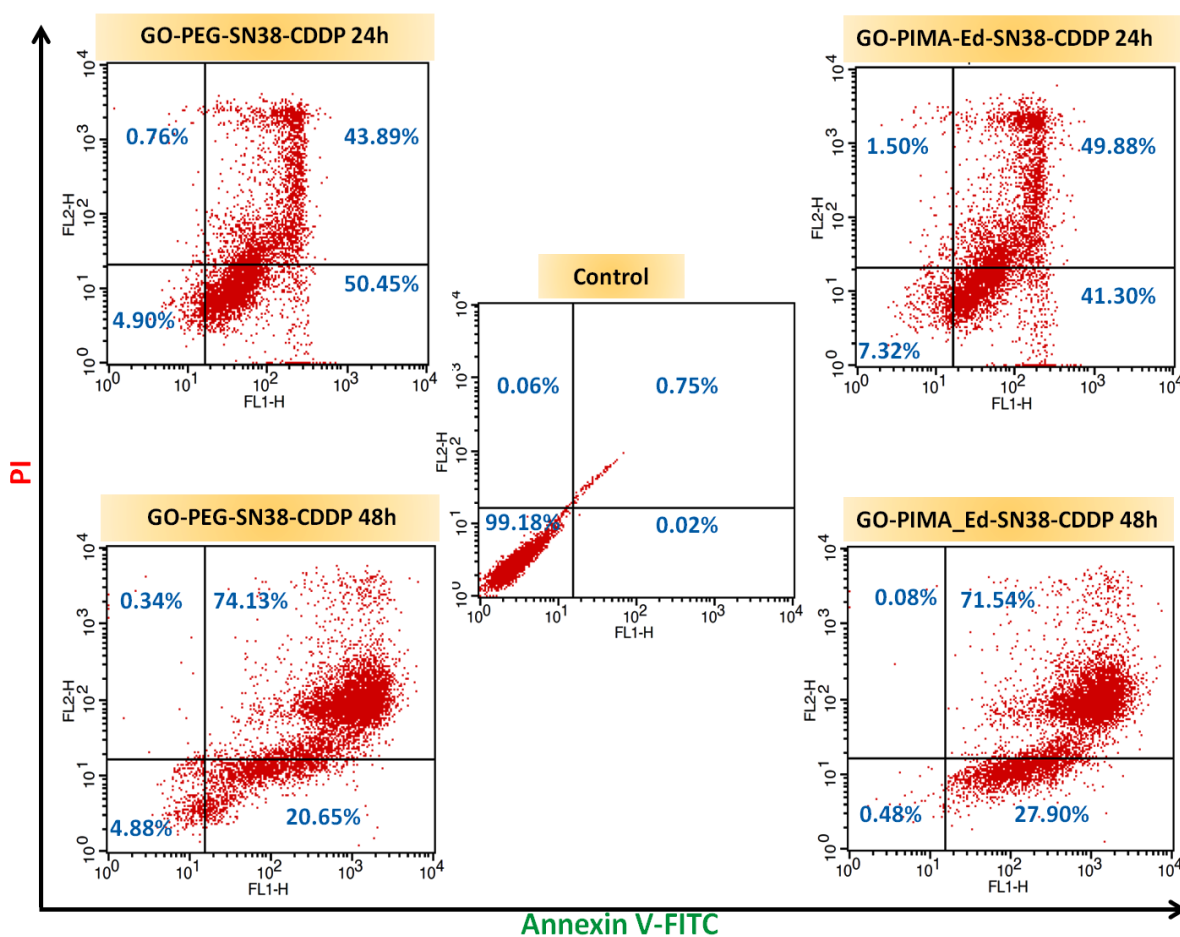


Figure 3.16: FACS analysis of HeLa cells for induction of apoptosis after 24h treatment with GO-PEG-SN38-CDDP and GO-PIMA_Ed-SN38-CDDP NPs.

DNA damage driven apoptosis was further confirmed by cleavage of caspase 3 an important executioner of apoptosis using western blot analysis (**Figure 3.17a**).⁷⁰ The decrease in expression of caspase 3 by 3.0 fold and 2.3 fold (**Figure 3.17b**) and corresponding increase in expression of cleaved caspase 3 by 3.0 fold and 1.8 fold (**Figure 3.17a** and **3.17c**) as compared to control cells, displayed the ability of GO-PEG-SN38-CDDP and GO-PIMA_Ed-SN38-CDDP NPs to successfully induce apoptosis in cervical cancer HeLa cells.

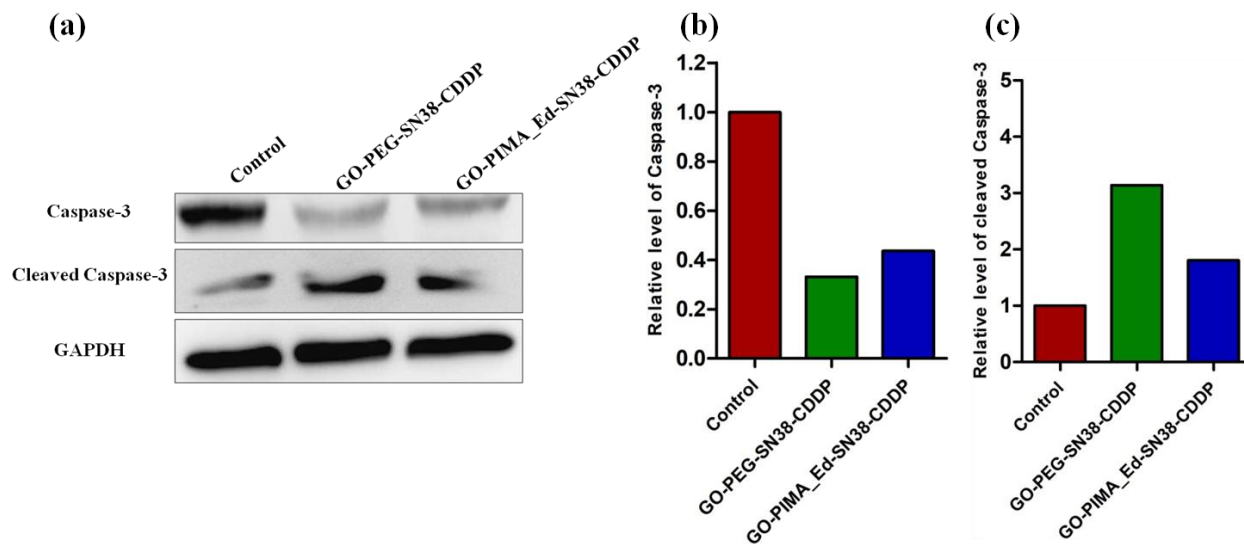


Figure 3.17: (a) Western blot analysis for expression of caspase 3 and cleaved caspase 3 in HeLa cells as markers for apoptosis. (b-c) Quantification of caspase 3 and cleaved caspase 3. post treatment with GO-PEG-SN38-CDDP NPs and GO-PIMA_Ed-SN38-CDDP NPs.

Lastly, since our GO-polymer based nanoparticles effectively caused TOP 1 inhibition, DNA lesions and activated apoptosis in HeLa cells, we wanted to evaluate the cell killing efficacy by cell MTT assay. GO-PEG-SN38-CDDP and GO-PIMA_Ed-SN38-CDDP NPs were incubated with HeLa cells for 48h in a dose dependent manner. As a control, we treated cells with the free drug combination of SN38 and CDDP in the same concentration as present in the respective nanoparticles. MTT data revealed that GO-PEG-SN38-CDDP NPs (**Figure 3.18a**) and GO-PIMA_Ed-SN38-CDDP NPs (**Figure 3.18b**) killed 50% cells at lower concentration of 1.5 μM and 2.5 μM (lower IC_{50} value) as compared to free drug cocktail which displayed a higher IC_{50} value of 6.25 μM . Thus, we can say that our GO-PEG-SN38-CDDP and GO-PIMA_Ed-SN38-CDDP NPs showed significant cell killing efficacy in HeLa cells.

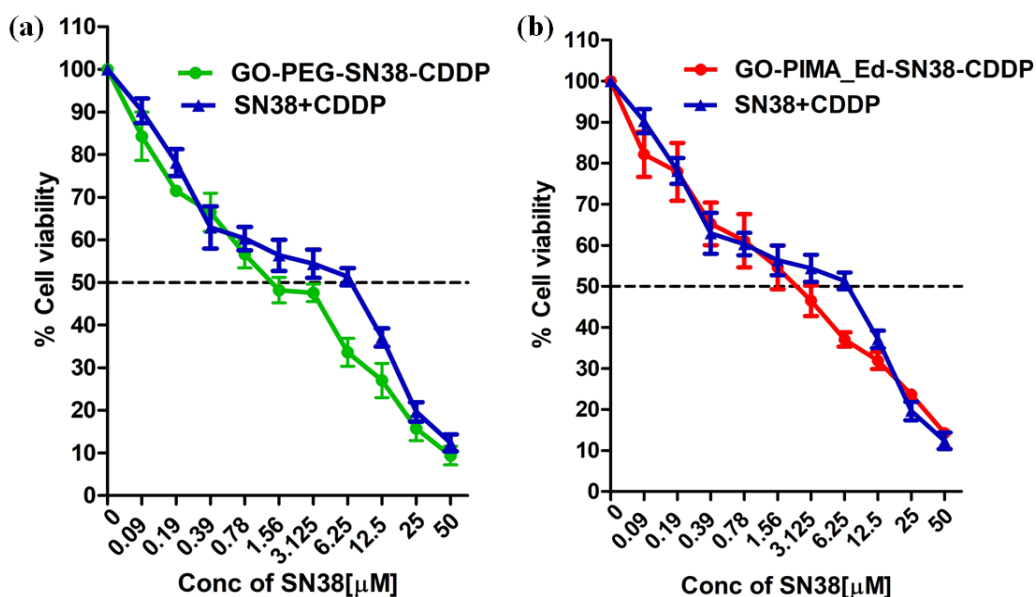


Figure 3.18: Cell viability of HeLa cells at 48 h post-incubation with concentration dependent (a) GO-PEG-SN38-CDDP NPs and (b) GO-PIMA_Ed-SN38-CDDP NPs quantified by MTT assay.

3.4 Experimental Section

3.4.1 Materials: Graphene oxide (4mg/ml), 1-Ethyl-3-(3-dimethylaminopropyl)carbodiimide hydrochloride (EDC), Poly(isobutylene-alt-maleic anhydride) (average $M_w \sim 6000$), Poly(ethyleneglycol)bis(amine) (average $M_n \sim 3400$), Triethylamine, silicon wafer for FESEM, 8 well LabTek chamber slides and solvents needed for synthesis were purchased from Sigma-Aldrich. Anticancer drug SN38 was bought from Selleck Chemicals and was used without any further purification. Gibco-DMEM (Dulbecco's Modified Eagle Meduim), fetal bovine serum (FBS), LysoTrackerTM Green DND-99, were procured from ThermoFisher Scientific. MTT, SDS, 96 well plates, and 6 well plates were purchased from HiMedia. Sterile centrifuge tubes, tissue culture flasks were bought from Tarsons Pvt. Ltd. Annexin-V-FITC Staining Kit was purchased from Biologend along with anti-PARP antibody, anti-phospho-histone H2AX, GAPDH antibody, antigoat anti-mouse IgG antibody, HRP conjugate and rabbit. Anti-Topoisomerase I was purchased from Abcam, Anti-caspase 3 and anti-cleaved caspase 3 were obtained from Cell Signalling respectively. TCS Leica SP8 machine was employed for fluorescence confocal imaging. Apoptosis and cell cycle assay was carried out using BD FACS flow cytometer.

3.4.2 Synthesis of poly(isobutylene-alt-maleic anhydride) conjugated ethylenediamine: 300 mg (1.94mmol of monomer) of poly(isobutylene-alt-maleic anhydride) (**7, Figure 3.1**) was placed in a round bottom flask and dissolved in 5ml anhydrous THF. 2.34 mmol N-Boc-ethylenediamine (**8, Figure 3.1**) dissolved in 3 ml THF was quickly injected, sonicated for a few seconds and then kept at 60 °C under vigorous stirring. For quantitative reaction of maleic anhydride with the primary amine, the reaction mixture was concentrated roughly up to one fifth of the original volume using rotavapor system under a reduced pressure after 3 hours of reaction. Further, the concentrated solution was left overnight at 60 °C under stirring conditions. Finally, THF was completely evaporated and the resultant polymer was washed with chilled diethylether and dried under to yield a yellowish powder (**9, Figure 3.1**). The compound was further dissolved in 3 mL Dichloromethane (DCM) and kept in an ice bath, to which 1.5 ml of TFA was added dropwise. The reaction mixture was stirred at RT for 3h. Finally, the solvent was evaporated under vacuum and remaining viscous liquid was washed with chilled diethylether to get Boc-protected poly(isobutylene-alt-maleic anhydride)-ethylenediamine conjugate which was dried under vacuum (**10, Figure 3.1**). Yield~80%

3.4.3 Synthesis of GO-Peg-SN38-CDDP and GO-PIMA_Ed-SN38-CDDP nanoparticles:

Poly(ethyleneglycol)bis(amine) (PEG) and poly(isobutylene-alt-maleic anhydride)-ethylenediamine (PIMA-Ed) was covalently linked to Graphene oxide through EDC coupling chemistry as per reports.⁵⁷ Briefly, Graphene oxide (4 mg/ml, 250 µL) was dispersed in distilled water (2 mL) followed by addition of 5mg poly(ethyleneglycol)bis(amine) (PEG) or 5mg poly(isobutylene-alt-maleic anhydride)-ethylenediamine (PIMA_Ed) and EDC·HCl (4mg) for sonication at room temperature for 30min. The solution was then kept for stirring at room temperature overnight. The product GO-PEG was dialysed (MW cut off:1000D) against distilled water for 2 days whereas, GO-PIMA_Ed was dialysed as well as centrifuged and washed with water to remove unreacted PIMA_Ed polymer

Next, SN38 dissolved in minimum amount of DMSO was stacked on the modified 2D sheets in a 1:0.5 weight ratio in water for 24h followed by dialysed against distilled water for 1 day to remove DMSO and also centrifugation to remove unbound SN38.⁵² The obtained GO-PEG-SN38 and GO-PIMA_Ed-SN38 was then reacted with aquated cisplatin (CDDP) (5mg/ml) in 1:5 weight ratio in water for 24 h at room temperature to self-assemble the 2D sheets into 3D spherical nanoparticles. Excess aquated cisplatin was excluded by dialysis for 6-8 hrs against

distilled water which yielded the GO-PEG-SN38-CDDP and GO-PIMA_Ed-SN38-CDDP nanoparticles.⁵⁰

3.4.4 Characterization: Fourier transform infrared (FTIR) spectroscopy was performed using a NICOLET 6700 FTIR from Thermo Scientific.

3.4.5 Estimation of size, shape and morphology by FESEM and AFM: The morphology of GO-PEG-SN38-CDDP and GO-PIMA_Ed-SN38-CDDP nanoparticles was observed using field-emission scanning electron microscopy (FESEM) and atomic force microscopy, by spotting the samples on a silicon wafer and mica sheet respectively.⁵⁰

3.4.6 Raman Spectroscopy: Raman spectra for GO-PEG-SN38-CDDP and GO-PIMA_Ed-SN38-CDDP were recorded with Lab RAM HR 800 instrument using laser excitation wavelength of 532 nm with 50X objective.

3.4.7 Quantification of drug loading in nanoparticles: Loading of the individual drugs SN38 (387nm), Cisplatin (707 nm) in GO-Peg-SN38-CDDP and GO-Pima_Ed-SN38-CDDP was estimated by UV-visible spectroscopy and the drug loading efficiency was calculated.⁴⁸ Ratio of loading of SN38: CDDP in GO-PEG-SN38-CDDP is 1:0.8 and in GO-PIMA_ED-SN38-CDDP is 1:0.97.

3.4.8 Fluorescence spectroscopy: Steady state fluorescence of for fluorescent drug SN38 was recorded using a HORIBA Fluoromax-4, emission spectra for SN38 was recorded at $\lambda_{\max} = 560\text{nm}$.

3.4.9 Cellular internalisation by confocal laser scanning microscopy (CLSM): 2×10^4 were seeded in a labtek chamber and were kept at optimum temperature and CO_2 conditions for adherence. Cells were then treated with green fluorescent GO-Peg-SN38-CDDP NP (SN38:CDDP = $2\mu\text{g mL}^{-1}$: $1.22\mu\text{g mL}^{-1}$) and GO-Pima_Ed-SN38-CDDP NP (SN38:CDDP = $2\mu\text{g mL}^{-1}$: $1.4\mu\text{g mL}^{-1}$) for 1h, 3h, and 6h. After incubation, the cells were cleaned with phosphate saline buffer, treated with LysoTracker Red DND 99 and observed using Leica SP8 confocal microscope.⁵⁰

3.4.10 Study of endocytosis pathway: 2×10^4 HeLa cells were allowed to attach in 8 well LabTek and then pre-incubated with inhibitors: Chlorpromazine ($10 \mu\text{g mL}^{-1}$), 5-(N-ethyl-N-isopropyl)-Amiloride (1 mM) and Genistein ($200 \mu\text{M}$) for 30 min. After 30 min, media was removed, washed with PBS and replaced with fresh DMEM. GO-Peg-SN38-CDDP (SN38:CDDP = $2 \mu\text{g mL}^{-1}$: $1.22 \mu\text{g mL}^{-1}$) and GO-Pima_Ed-SN38-CDDP NPs (SN38:CDDP = $2 \mu\text{g mL}^{-1}$: $1.4 \mu\text{g mL}^{-1}$) were added and incubated for 2 h. The cells were washed with phosphate saline buffer (PBS) stained with LysoTracker Red DND 99, followed by which they were imaged using Leica SP8 confocal microscope.⁷¹

3.4.11 Detection of γH2AX by immunostaining: 5×10^5 cervical cancer cells were seeded on coverslips and kept to adhere overnight at optimum conditions. IC_{50} value GO-Peg-SN38-CDDP (SN38:CDDP = $1.5 \mu\text{M}$: $1.2 \mu\text{M}$) and GO-Pima_Ed-SN38-CDDP NPs were added (SN38:CDDP = $2.5 \mu\text{M}$: $2.4 \mu\text{M}$) and incubated for 24h. Cells were treated with primary antibody solution (γH2AX , PARP in 1:100 dilution) led by incubation with Alexa Flour-594 conjugated secondary antibody (1:500 dilution). The slides were imaged using Leica SP8 confocal microscope.⁴⁸

3.4.12 Western blot analysis: 1×10^6 HeLa cells were treated with GO-Peg-SN38-CDDP NPs (SN38:CDDP= $1.5 \mu\text{M}$: $1.2 \mu\text{M}$) and GO-Pima_Ed-SN38-CDDP NPs (SN38:CDDP= $2.5 \mu\text{M}$: $2.4 \mu\text{M}$) for 24 h at their inhibitory concentration, after which cells were lysed to obtain the protein lysate and separated using SDS-PAGE. The desired proteins were further treated with respective primary and secondary antibodies and visualized by ImageQuant LAS 4000 using Chemiluminescent HRP Substrate.⁵⁰

3.4.13 Apoptosis detection by FACS: After 24 h treatment with GO-Peg-SN38-CDDP (SN38:CDDP= $1.5 \mu\text{M}$: $1.2 \mu\text{M}$) and GO-Pima_Ed-SN38-CDDP (SN38:CDDP= $2.5 \mu\text{M}$: $2.4 \mu\text{M}$) NP at their corresponding IC_{50} concentrations, HeLa- cervical cancer cells were washed trypsinised and stained with Annexin V-FITC and PI (Dead Cell Apoptosis Kit). The cells were analysed for apoptosis using BD Accuri™ C6 flow cytometer.⁵⁰

3.4.14 Cell viability assay: 5×10^3 HeLa cells were incubated with GO-Peg-SN38-CDDP and GO-Pima_Ed-SN38-CDDP NP in a concentration dependent manner. The viable cells were estimated using MTT reagent as described previously.⁵⁰

3.5 Conclusion

In the current study we have successfully designed polymer functionalized self-assembled graphene oxide (GO) spherical nanoparticles which can encompass SN38 (Topoisomerase I inhibitor) and cisplatin (DNA cross-linker). We modified parental GO 2D sheets with hydrophilic polymers like PEG and PIMA_Ed and self-assembled the sheets into 3D spherical nanoparticles via. cisplatin. The as formed GO-PEG-SN38-CDDP and GO-PIM_Ed-SN38-CDDP nanoparticles displayed enhanced aqueous colloidal stability, which is an important aspect for effective biomedical application of nano-scale materials. The average diameter of the nanoparticles was around 180nm-200nm which can facilitate their accumulation specifically into tumor tissues through enhanced permeability and retention effect. The GO-PEG-SN38-CDDP and GO-PIM_Ed-SN38-CDDP NPs were taken up by HeLa cells through clathrin mediated endocytosis, into the acidic lysosomes within 6h and triggered the release of drugs SN38 and CDDP. The drug induced DNA damage and TOP1 inhibition triggered apoptosis in cancer cells which was confirmed by western blot and flow cytometry analysis. Further, the nanoparticles demonstrated improved HeLa cell killing efficacy in comparison to the corresponding free drug cocktail. Thus, our strategy represents a safer design to improve the dispersibility of GO nanoparticles and their potential usage in clinics for future chemotherapy.

3.6 Salient Features

- We achieved improved aqueous colloidal stability of the GO-NPs, by modifying pristine GO with hydrophilic polymers PEG and ethylenediamine conjugated PIMA (PIMA_Ed) which was then self assembled into into 3-dimensional spherical nanoparticles (GO-PEG-NPs and GO-PIMA-Ed NPs) through cisplatin cross-linking.
- The nanoparticles were stacked with SN38-a Topoisomerase I inhibitor along with cisplatin.
- The GO-PEG-SN38-CDDP NPs and GO-PIMA- NPs were taken up by HeLa cells through clathrin-induced endocytosis, into the acidic lysosomes within 6h and triggered the release of SN38 and cisplatin as payloads.
- The nanoparticles induced DNA damage and Topoisomerase I inhibition prompted apoptosis in cancer cells which was confirmed by western blot and flow cytometry analysis.
- The GO-polymer-NPs demonstrated improved HeLa cell killing efficacy in comparison to the free drug cocktail.

3.7 Appendix

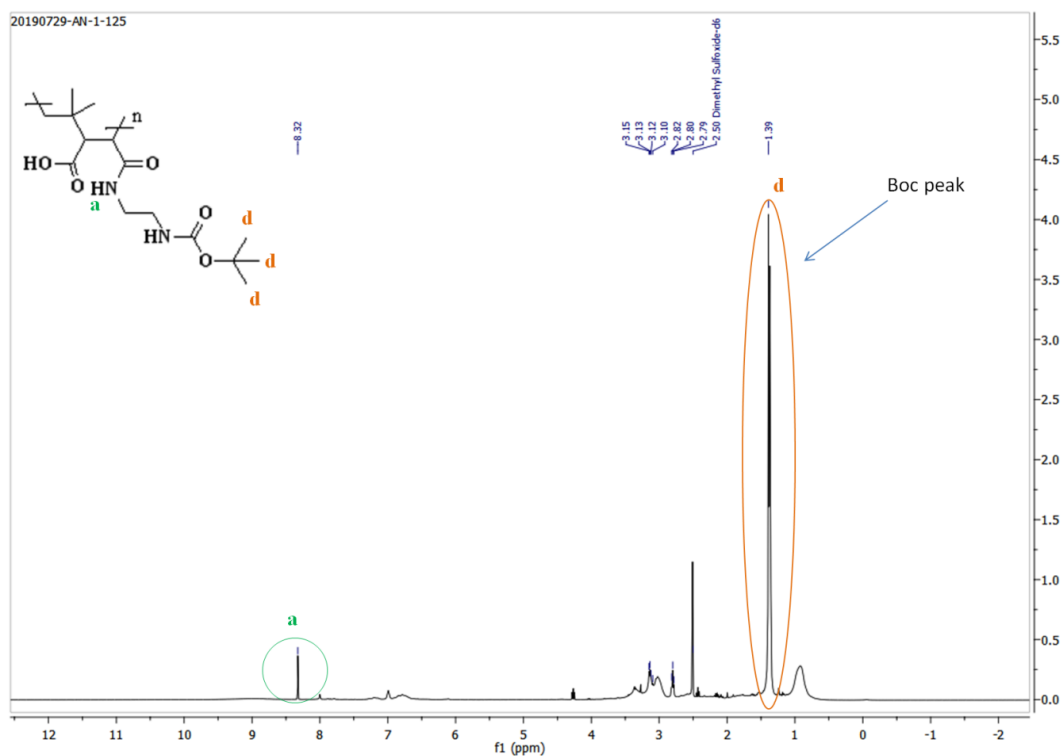


Figure A 3.1: ^1H NMR of PIMA_Boc-ethylenediamine-conjugate 9.

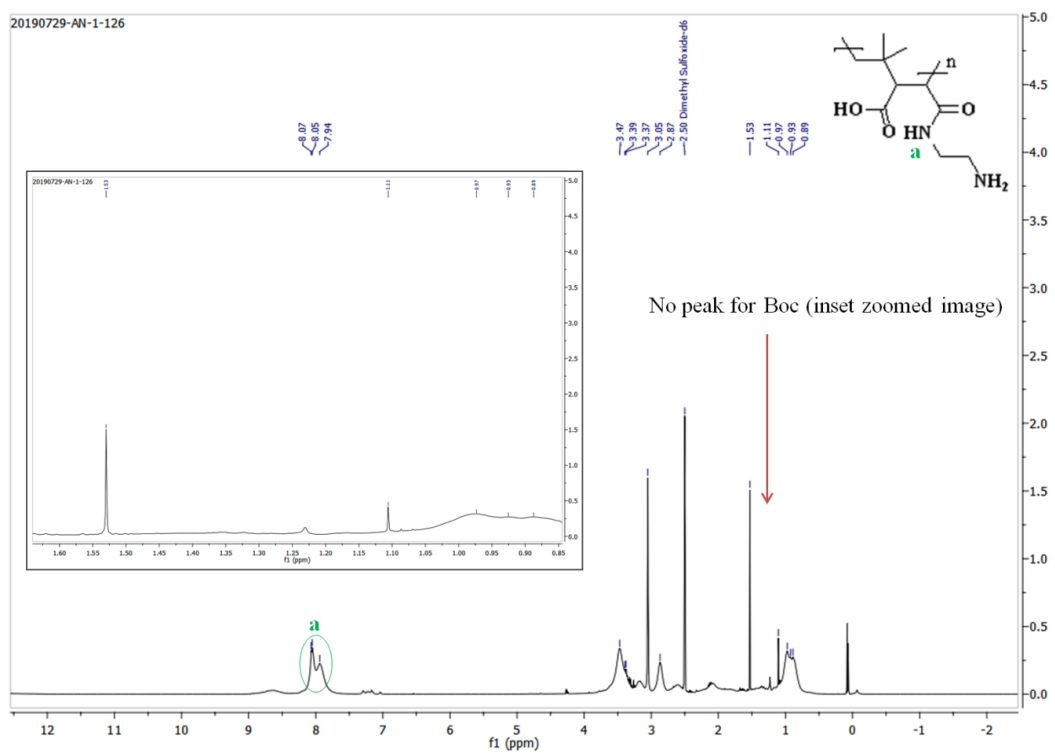


Figure A 3.2: ^1H NMR of PIMA_ethylenediamine-conjugate 10.

3.8 References

1. Kumar, B.; Singh, S.; Skvortsova, I.; Kumar, V. Promising Targets in Anti-cancer Drug Development: Recent Updates. *Curr. Med. Chem.* **2017**, *24*, 4729-4752.
2. Gorjánácz, M. Nuclear Assembly as a Target for Anti-Cancer Therapies. *Nucl. (United States)* **2014**, *5*, 47–55.
3. Pan, L.; Liu, J.; Shi, J. Cancer Cell Nucleus-Targeting Nanocomposites for Advanced Tumor Therapeutics. *Chem. Soc. Rev.* **2018**, *47*, 6930–6946.
4. Luo, J.; Solimini, N. L.; Elledge, S. J. Principles of Cancer Therapy: Oncogene and Non-Oncogene Addiction. *Cell* **2009**, *136*, 823–837.
5. DeVita, V. T.; Chu, E. A History of Cancer Chemotherapy. *Cancer Res.* **2008**, *68*, 8643–8653.
6. Hoelder, S.; Clarke, P. A.; Workmann, P. Discovery of Small Molecule Cancer Drugs: Successes, Challenges and Opportunities. *Mol. Oncol.* **2012**, *6*, 155-176.
7. Housman, G.; Byler, S.; Heerboth, S.; Lapinska, K.; Longacre, M.; Snyder, N.; Sarkar, S. Drug Resistance in Cancer: An Overview. *Cancers (Basel)*. **2014**, *6*, 1769–1792.
8. Luqmani, Y. A. Mechanisms of Drug Resistance in Cancer Chemotherapy. *Med. Princ. Pract.* **2005**, *14*, 35–48.
9. Yardley, D. A. Drug Resistance and the Role of Combination Chemotherapy in Improving Patient Outcomes. *Int. J. Breast Cancer* **2013**, *2013*, 1–15.
10. Tsuruo, T.; Naito, M.; Tomida, A.; Fujita, N.; Mashima, T.; Sakamoto, H.; Haga, N. Molecular Targeting Therapy of Cancer: Drug Resistance, Apoptosis and Survival Signal. *Cancer Sci.* **2003**, *94*, 15–21.
11. Zimmermann, G. R.; Lehár, J.; Keith, C. T. Multi-Target Therapeutics: When the Whole Is Greater than the Sum of the Parts. *Drug Discov. Today* **2007**, *12*, 34–42.

12. Novotny, L.; Szekeres, T. Cancer Therapy: New Targets for Chemotherapy. *Hematology* **2003**, *8*, 129–137.
13. Topcu, Z. DNA Topoisomerases as Targets for Anti-Cancer Drugs. *J. Clin. Pharm. Ther.* **2001**, *26*, 405–416.
14. Delgado, J. L.; Hsieh, C.-M.; Chan, N.-L.; Hiasa, H. Topoisomerases as Anticancer Targets. *Biochem. J.* **2018**, *475*, 373–398.
15. Wang, J. C. Cellular Roles of DNA Topoisomerases: A Molecular Perspective. *Nat. Rev. Mol. Cell Biol.* **2002**, *3*, 430–440.
16. Pommier, Y. Drugging Topoisomerases: Lessons and Challenges. *ACS Chem. Biol.* **2013**, *8*, 82–95.
17. Pommier, Y.; Sun, Y.; Huang, S. Y. N.; Nitiss, J. L. Roles of Eukaryotic Topoisomerases in Transcription, Replication and Genomic Stability. *Nat. Rev. Mol. Cell Biol.* **2016**, *17*, 703–721.
18. Vos, S. M.; Tretter, E. M.; Schmidt, B. H.; Berger, J. M. All Tangled up: How Cells Direct, Manage and Exploit Topoisomerase Function. *Nat. Rev. Mol. Cell Biol.* **2011**, *12*, 827–841.
19. Ghilarov, D. A.; Shkundina, I. S. DNA Topoisomerases and Their Functions in a Cell. *Mol. Biol.* **2012**, *46*, 47-57.
20. Wang, J. C. Cellular Roles of DNA Topoisomerases: A Molecular Perspective. *Nat. Rev. Mol. Cell Biol.* **2002**, *3*, 430–440.
21. Nitiss, J. L. DNA Topoisomerases in Cancer Chemotherapy: Using Enzymes to Generate Selective DNA Damage. *Curr. Opin. Investig. Drugs* **2002**, *3*, 1512-1516.
22. Chen, S. H.; Chan, N.-L.; Hsieh, T. New Mechanistic and Functional Insights into DNA Topoisomerases. *Annu. Rev. Biochem.* **2013**, *82*, 139–170.

23. Dekker, N. H.; Rybenkov, V. V.; Duguet, M.; Crisona, N. J.; Cozzarelli, N. R.; Bensimon, D.; Croquette, V. The Mechanism of Type IA Topoisomerases. *Proc. Natl. Acad. Sci.* **2002**, *99*, 12126–12131.
24. Pommier, Y.; Leo, E.; Zhang, H.; Marchand, C. DNA Topoisomerases and Their Poisoning by Anticancer and Antibacterial Drugs. *Chem. Biol.* **2010**, *17*, 421–433.
25. Pommier, Y. DNA Topoisomerase I Inhibitors: Chemistry, Biology, and Interfacial Inhibition. *Chem. Rev.* **2009**, *109*, 2894–2902.
26. Pommier, Y. Topoisomerase I Inhibitors: Camptothecins and Beyond. *Nat. Rev. Cancer* **2006**, *6*, 789–802.
27. Beretta, G. L.; Perego, P.; Zunino, F. Targeting Topoisomerase I: Molecular Mechanisms and Cellular Determinants of Response to Topoisomerase I Inhibitors. *Expert Opin. Ther. Targets* **2008**, *12*, 1243–1256.
28. Kanzawa, F.; Koizumi, F.; Koh, Y.; Nakamura, T.; Tatsumi, Y.; Fukumoto, H.; Saijo, N.; Yoshioka, T.; Nishio, K. In Vitro Synergistic Interactions between the Cisplatin Analogue Nedaplatin and the DNA Topoisomerase I Inhibitor Irinotecan and the Mechanism of This Interaction. *Clin. Cancer Res.* **2001**, *7*, 202–209.
29. Fukuda, M.; Nishio, K.; Kanzawa, F.; Ogasawara, H.; Ishida, T.; Arioka, H.; Bojanowski, K.; Oka, M.; Saijo, N. Synergism between Cisplatin and Topoisomerase I Inhibitors, NB-506 and SN-38, in Human Small Cell Lung Cancer Cells. *Cancer Res.* **1996**, *56*, 789–793.
30. Minagawa, Y.; Kigawa, J.; Ishihara, H.; Itamochi, H.; Terakawa, N. Synergistic Enhancement of Cisplatin Cytotoxicity by SN-38, an Active Metabolite of CPT-11, for Cisplatin-resistant HeLa Cells. *Jpn. J. Cancer Res.* **1994**, *85*, 966–971.
31. Mokhtari, R. B.; Homayouni, T. S.; Baluch, N.; Morgatskaya, E.; Kumar, S.; Das, B.; Yeger, H. Combination Therapy in Combating Cancer. *Oncotarget* **2017**, *8*, 38022–38043.
32. Hu, Q.; Sun, W.; Wang, C.; Gu, Z. Recent advances of cocktail chemotherapy by combination drug delivery systems. *Adv. Drug Deliv. Rev.* **2016**, *98*, 19–34.

33. Ferrari, M. Cancer Nanotechnology: Opportunities and Challenges. *Nat. Rev. Cancer* **2005**, *5*, 161–171.
34. Shi, J.; Kantoff, P. W.; Wooster, R.; Farokhzad, O. C. Cancer Nanomedicine: Progress, Challenges and Opportunities. *Nat. Rev. Cancer* **2017**, *17*, 20-37.
35. Peer, D.; Karp, J. M.; Hong, S.; Farokhzad, O. C.; Margalit, R.; Langer, R. Nanocarriers as an Emerging Platform for Cancer Therapy. *Nat. Nanotechnol.* **2007**, *2*, 751–760.
36. Barreto, J. A.; O'Malley, W.; Kubeil, M.; Graham, B.; Stephan, H.; Spiccia, L. Nanomaterials: Applications in Cancer Imaging and Therapy. *Adv. Mater.* **2011**, *23*, H18–H40.
37. Sun, T.; Zhang, Y. S.; Pang, B.; Hyun, D. C.; Yang, M.; Xia, Y. Engineered Nanoparticles for Drug Delivery⁰ in Cancer Therapy. *Angew. Chemie - Int. Ed.* **2014**, *53*, 12320–12364.
38. Gonçalves, G.; Vila, M.; Portolés, M. T.; Vallet-Regi, M.; Gracio, J.; Marques, P. A. A. P. Nano-Graphene Oxide: A Potential Multifunctional Platform for Cancer Therapy. *Adv. Healthcare Mater.* **2013**, *2*, 1072–1090.
39. Chung, C.; Kim, Y. K.; Shin, D.; Ryoo, S. R.; Hong, B. H.; Min, D. H. Biomedical Applications of Graphene and Graphene Oxide. *Acc. Chem. Res.* **2013**, *46*, 2211–2224.
40. Feng, L.; Wu, L.; Qu, X. New Horizons for Diagnostics and Therapeutic Applications of Graphene and Graphene Oxide. *Adv. Mater.* **2013**, *25*, 168–186.
41. Kostarelos, K.; Novoselov, K. S. Exploring the Interface of Graphene and Biology. *Science* **2014**, *344*, 261–263.
42. Sydlik, S. A.; Jhunjhunwala, S.; Webber, M. J.; Anderson, D. G.; Langer, R. In Vivo Compatibility of Graphene Oxide with Differing Oxidation States. *ACS Nano* **2015**, *9*, 3866–3874
43. Lu, C. H.; Yang, H. H.; Zhu, C. L.; Chen, X.; Chen, G. N. A Graphene Platform for Sensing Biomolecules. *Angew. Chem. Int. Ed.* **2009**, *48*, 4785–4787.

44. Jiang, T.; Sun, W.; Zhu, Q.; Burns, N. A.; Khan, S. A.; Mo, R.; Gu, Z. Furin-Mediated Sequential Delivery of Anticancer Cytokine and Small-Molecule Drug Shuttled by Graphene. *Adv. Mater.* **2015**, *27*, 1021–1028.
45. Kim, H.; Namgung, R.; Singha, K.; Oh, I. K.; Kim, W. J. Graphene Oxide-Polyethylenimine Nanoconstruct as a Gene Delivery Vector and Bioimaging Tool. *Bioconjug. Chem.* **2011**, *22*, 2558–2567.
46. Zhang, L.; Xia, J.; Zhao, Q.; Liu, L.; Zhang, Z. Functional Graphene Oxide as a Nanocarrier for Controlled Loading and Targeted Delivery of Mixed Anticancer Drugs. *Small* **2010**, *6*, 537–544.
47. Mallick, A.; Nandi, A.; Basu, S. Polyethylenimine Coated Graphene Oxide Nanoparticles for Targeting Mitochondria in Cancer Cells. *ACS Appl. Bio Mater.* **2019**, *2*, 14–19.
48. Nandi, A.; Ghosh, C.; Bajpai, A.; Basu, S. Graphene Oxide Nanocells for Impairing Topoisomerase and DNA in Cancer Cells. *J. Mater. Chem. B* **2019**.
49. Dreyer, D. R.; Park, S.; Bielawski, C. W.; Ruoff, R. S. The Chemistry of Graphene Oxide. *Chem. Soc. Rev.* **2010**, *39*, 228–240.
50. Nandi, A.; Mallick, A.; More, P.; Sengupta, P.; Ballav, N.; Basu, S. Cisplatin-Induced Self-Assembly of Graphene Oxide Sheets into Spherical Nanoparticles for Damaging Sub-Cellular DNA. *Chem. Commun.* **2017**, *53*, 1409–1412.
51. Knop, K.; Hoogenboom, R.; Fischer, D.; Schubert, U.S. Poly(ethyleneglycol) in Drug Delivery: Pros and Cons as Well as Potential Alternatives. *Angew. Chem. Int. Ed.* **2010**, *49*, 6288–6308.
52. Shi, S.; Chen, F.; Ehlerding, E. B.; Cai, W. Surface Engineering of Graphene-Based Nanomaterials for Biomedical Applications. *Bioconjugate Chem.* **2014**, *25*, 1609–1619.
53. Liu, Z.; Robinson, J. T.; Sun, X.; Dai, H. PEGylated Nanographene Oxide for Delivery of Water-Insoluble Cancer Drugs. *J. Am. Chem. Soc.* **2008**, *130*, 10876–10877.

54. Wang, Y.; Li, Z.; Wang, J.; Li, J.; Lin, Y. Graphene and Graphene oxide: Biofunctionalization and Applications in Biotechnology. *Trends Biotechnol.* **2011**, *29*, 205-212.
55. Xu, M.; Zhu, J.; Wang, F.; Xiong, Y.; Wu, Y.; Wang, Q.; Weng, J.; Zhang, Z. Chen, W.; Liu, S. Improved In Vitro and In Vivo Biocompatibility of Graphene Oxide through Surface Modification: Poly(Acrylic Acid)-Functionalization is Superior to PEGylation. *ACS Nano* **2016**, *10*, 3267–328.
56. Lin, C.-A. J.; Sperling, R. A.; Li, J. K.; Yang, T.-Y.; Li, P.-Y.; Zanella, M.; Chang, W. H.; Parak, W. J. Cover Picture: Design of an Amphiphilic Polymer for Nanoparticle Coating and Functionalization. *Small* **2008**, *4*, 301–301.
57. Peng, E.; Choo, E. S. G.; Sheng, Y.; Xue, J. M. Monodisperse Transfer of Superparamagnetic Nanoparticles from Non-Polar Solvent to Aqueous Phase. *New J. Chem.* **2013**, *37*, 2051–2060.
58. Xu, Z.; Wang, S.; Li, Y.; Wang, M.; Shi, P.; Huang, X. Covalent Functionalization of Graphene Oxide with Biocompatible Poly(Ethylene Glycol) for Delivery of Paclitaxel. *ACS Appl. Mater. Interfaces*, **2014**, *6*, 17268–17276.
59. Kelland, L. The Resurgence of Platinum-Based Cancer Chemotherapy. *Nat. Rev. Cancer* **2007**, *7*, 573–584.
60. Yao, X.; Panichpisal, K.; Kurtzman, N.; Nugent, K. Cisplatin Nephrotoxicity: A Review. *Am. J. Med. Sci.* **2007**, *334*, 115–124.
61. Sengupta, P.; Basu, S.; Soni, S.; Pandey, A.; Roy, B.; Oh, M. S.; Chin, K. T.; Paraskar, A. S.; Sarangi, S.; Connor, Y.; Sabbisetti, V. S.; Koppam, J.; Kulkarni, A.; Muto, K.; Amarasiriwardena, C.; Jayawardene, I.; Lupoli, N.; Dinulescu, D. M.; Bonventre, J. V.; Mashelkar, R. A.; Sengupta, S. Cholesterol-Tethered Platinum II-Based Supramolecular Nanoparticle Increases Antitumor Efficacy and Reduces Nephrotoxicity. *Proc. Natl. Acad. Sci.* **2012**, *109*, 11294–11299.
62. Pizzolato, J. F.; Saltz, L. B. The Camptothecins. *Lancet* **2003**, *361*, 2235–2242.

63. Liu, X.; Huang, Q.; Yang, C.; Zhang, Q.; Chen, W.; Shen, Y.; Sui, M. A Multi-Stimuli Responsive Nanoparticulate SN38 Prodrug for Cancer Chemotherapy. *J. Mater. Chem. B* **2017**, *5*, 661–670.
64. Claramunt, S.; Varea, A.; López-Díaz, D.; Velázquez, M. M.; Cornet, A.; Cirera, A. The Importance of Interbands on the Interpretation of the Raman Spectrum of Graphene Oxide. *J. Phys. Chem. C* **2015**, *119*, 10123–10129.
65. Linares, J.; Matesanz, M. C.; Vila, M.; Feito, M. J.; Gonçalves, G.; Vallet-Regí, M.; Marques, P. A. A. P.; Portolés, M. T. Endocytic Mechanisms of Graphene Oxide Nanosheets in Osteoblasts, Hepatocytes and Macrophages. *ACS Appl. Mater. Interfaces* **2014**, *6*, 13697–13706.
66. Kuo, L. J.; Yang, L. X. γ -H2AX-A Novel Biomaker for DNA Double-Strand Breaks. *In Vivo*. **2008**, *22*, 305–310.
67. Fridman, J. S.; Lowe, S. W. Control of Apoptosis by P53. *Oncogene* **2003**, *22*, 9030–9040.
68. Boulares, A. H.; Yakovlev, A. G.; Ivanova, V.; Stoica, B. A.; Wang, G.; Iyer, S.; Smulson, M. Role of Poly(ADP-Ribose) Polymerase (PARP) Cleavage in Apoptosis. *J. Biol. Chem.* **2002**, *274*, 22932–22940.
69. Curtin, N. J. DNA Repair Dysregulation from Cancer Driver to Therapeutic Target. *Nat. Rev. Cancer* **2012**, *12*, 801–817.
70. Porter, A. G.; Jänicke, R. U. Emerging roles of caspase-3 in apoptosis. *Cell Death Differ.* **1999**, *6*, 99-104.
71. Ghosh, C.; Nandi, A.; Basu, S. Supramolecular Self-Assembly of Triazine-Based Small Molecule: Targeting Endoplasmic Reticulum in Cancer Cells. *Nanoscale* **2019**, *8*, 1–3.

Chapter 4: Graphene oxide Nanocells for Impairing Topoisomerase and DNA in Cancer Cells.

This chapter has been published as:

Aditi Nandi, Chandramouli Ghosh, Aman Bajpai and Sudipta Basu. Graphene oxide Nanocell for Impairing Topoisomerase and DNA in Cancer Cells. *J. Mater. Chem. B*, **2019**,7, 4191-4197.

(Reproduced by the permission from The Royal Society of Chemistry)

4.1 Abstract

DNA Topoisomerases and nuclear DNA are recognized as important targets for cancer therapy. However, DNA Topoisomerase inhibitors and DNA damaging drugs demonstrate a large window of side effects in the clinics. Graphene oxide based biocompatible and biodegradable nano-scale materials have the potential to overcome this complication. However, encompassing different Topoisomerase inhibitors along with DNA damaging drug into 2D-graphene oxide remains a main challenge. To address this, in this manuscript, we have engineered a self-assembled spherical 3D-graphene oxide nanoparticle coated with lipid (GO-Nanocell) which can concomitantly load and release multiple Topoisomerase inhibitors (topotecan and doxorubicin) and DNA damaging drug (cisplatin) in a controlled manner. Fluorescence confocal microscopy confirmed that these GO-Nanocells were taken up by the HeLa cervical cancer cells and homed into lysosomes temporally over 6h. A combination of confocal microscopy, gel electrophoresis, and flow cytometry study revealed that these GO-Nanocells damaged nuclear DNA along with Topoisomerase inhibition leading to induction of apoptosis through cell cycle arrest in G2-M phase. These GO-Nanocells killed HeLa cancer cells with remarkably greater efficacy compared to free drug cocktail at 48 h post-incubation. These self-assembled GO-Nanocells can serve as a nanoscale tool to perturb multiple therapeutically important sub-cellular targets simultaneously for improved efficacy in future cancer chemotherapy.

4.2 Introduction

Cancer is the second leading deadliest disease in the whole world.^{1, 2} Chemotherapy using small molecule cytotoxic drugs is highly effective in eradicating cancer where surgical removal is not possible.³⁻⁵ However, collateral damage of healthy cells leading to severe side effects to the patients is a foremost setback for the chemotherapy strategy.⁶ As a result, novel targets inside cancer cells need to be impaired for improved therapeutic efficacy. In this context, in recent years, DNA Topoisomerases, which are instrumental in solving topological problems in replication, transcription and genomic stability, have gained lots of attention.⁷⁻¹² Furthermore, Topoisomerases (Topoisomerase I and II) are implicated in different types of cancers leading to the development of topoisomerase inhibitors as anti-cancer drugs.¹³⁻¹⁶ Although topoisomerase inhibitors showed dose-dependent toxicity to bone-marrow progenitor and intestinal cells, they

are extensively used as mono- or in combination therapy with DNA damaging drugs for improved therapeutic efficacy.¹⁷⁻²¹

Nevertheless, drug combinations have augmented side-effects as well as unpredictable bio-distribution leading to attrition in effective dose reaching to the diseased tissues. Hence, the packaging of multiple drugs in optimal concentrations in a single vector with controlled release remains a major challenge in next-generation chemotherapy.

In the past decade, nano-materials have transformed the traditional cancer chemotherapy by encasing and transporting multiple therapeutic payloads (small molecules, biologics, and nucleic acids) into tumor tissues in critical dosages with proper release strategies and reduced side effects.²²⁻²⁵ In this regard, recently, different carbon materials have gained a lot of attention as nano-scale vectors for drug delivery, biosensing as well as theranostic probes for biomedical applications due to their exceptional structures and biocompatibility.²⁶⁻³² The unique aromatic and 2-dimensional structure of graphene and graphene oxide (GO) have been judiciously used to stack aromatic anti-cancer drugs and nucleic acids by π - π interactions.³³⁻³⁶ However, it remains a key task to integrate multiple therapeutic payloads beyond the GO surface with optimum loading and controlled release profiles. Despite some recent advancements in developing surface modified GO for various small molecules, small molecule-siRNA and small molecule-cytokine combination in cancer therapy, the field remains in its infancy to impair multiple targets simultaneously inside the cancer cells using GO as nano-platform.

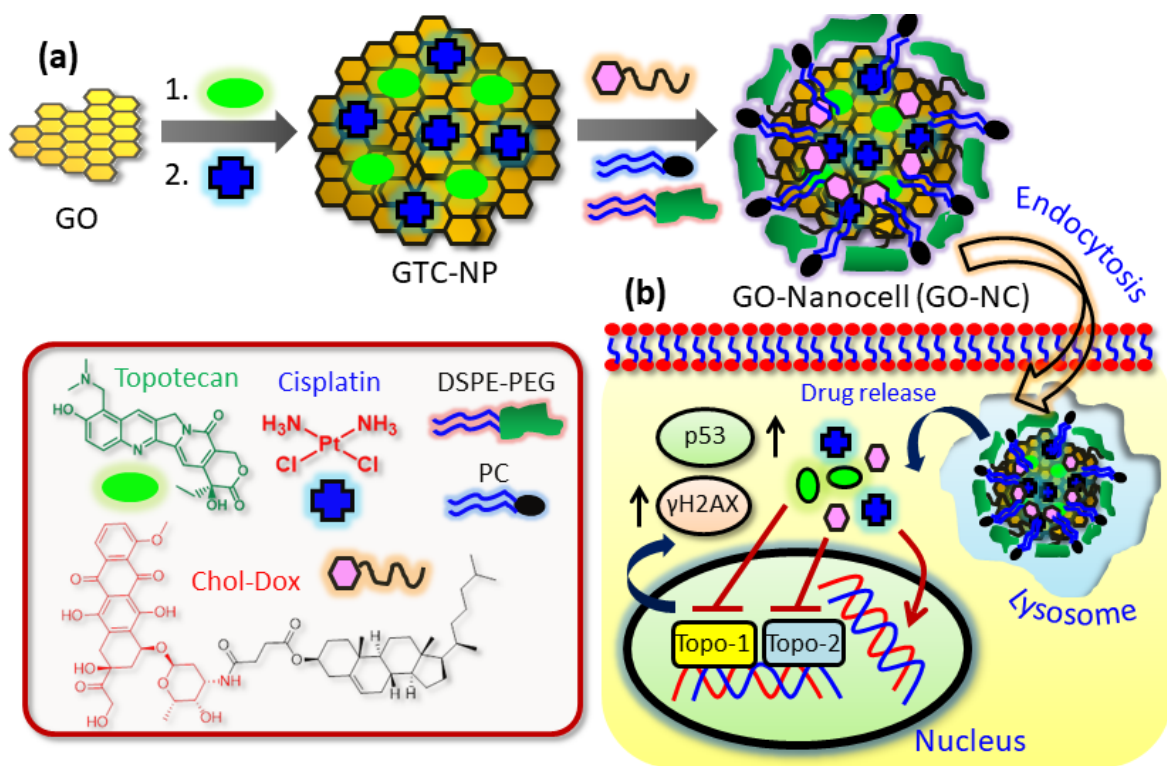
To address this, in this chapter, we have engineered a lipid coated self-assembled graphene oxide nanoparticle (GO-Nanocell) which can concurrently encompass DNA Topoisomerase inhibitors (Topotecan and Doxorubicin) and DNA damaging agent (Cisplatin) in a single nanoparticle. These GO-Nanocells (GO-NCs) were spherical in shape with a diameter of 151 nm confirmed by light scattering (DLS) and electron microscopy (AFM and FESEM). These GO-NCs were temporally internalized into the sub-cellular lysosomes of HeLa cervical cancer cells within 6h and released the Topoisomerase inhibitors and DNA damaging drugs in a controlled manner over 72 h. DNA Topoisomerases were inhibited in a synchronized manner with DNA damage by GO-NCs visualized by confocal laser scanning microscopy (CLSM) and gel electrophoresis. This GO-NC mediated simultaneous impairment of DNA Topoisomerases, and nuclear DNA prompted programmed cell death (apoptosis) through cell cycle arrest in G2-M phase leading to

remarkably augmented HeLa cancer cell death at 48 h compared to free inhibitors and drug combinations. These GO-NCs can be further explored as a platform to target multiple oncogenic proteins simultaneously to improve the therapeutic efficacy for next-generation combination cancer therapy.

4.3 Result and Discussion

4.3.1 Engineering GO Nanocell: To inhibit Topoisomerase I and II in cancer cells, we have chosen topotecan (Topo) and doxorubicin (Dox) respectively due to their extensive use in clinics as anti-cancer drugs.¹⁴⁻¹⁶ Moreover, Topoisomerase I and II have overlapping functions leading to inefficient inhibition of their catalytic activity by single inhibitors.¹⁶ Hence, we rationalized to combine both topoisomerase inhibitors for improved efficiency. To damage nuclear DNA simultaneously, we have chosen cisplatin (CDDP) as FDA approved drug used to treat different types of cancers.^{42, 43} Moreover, cisplatin has been used in combination with both topotecan and doxorubicin to cure multiple types of malignancies including cervical cancer.^{17, 19, 20} Although, cisplatin, doxorubicin and topotecan have no over-lapping toxicity profile, individually, they show dose-dependent nephron-, neuro-, cardio-toxicity along with myelosuppression respectively.⁴⁴⁻⁴⁷ Hence, we hypothesized to use these anti-cancer drugs to inhibit nuclear Topoisomerases and DNA in cancer cells using a single nano-scale material for augmented therapeutic efficacy.

First, topotecan (**2**) was loaded on 2-dimensional GO (**1**) surface by aromatic π - π interaction (**Scheme 1a, Figure 4.1**) by mixing GO and topotecan in 1:1 weight ratio in water for 24 h to obtain GO-Topotecan (GT, **3**).



Scheme 1: (a) Scheme of engineering GO-Nanocells. (b) Schematic representation of cellular internalization and the mechanism of action of GO-Nanocells.

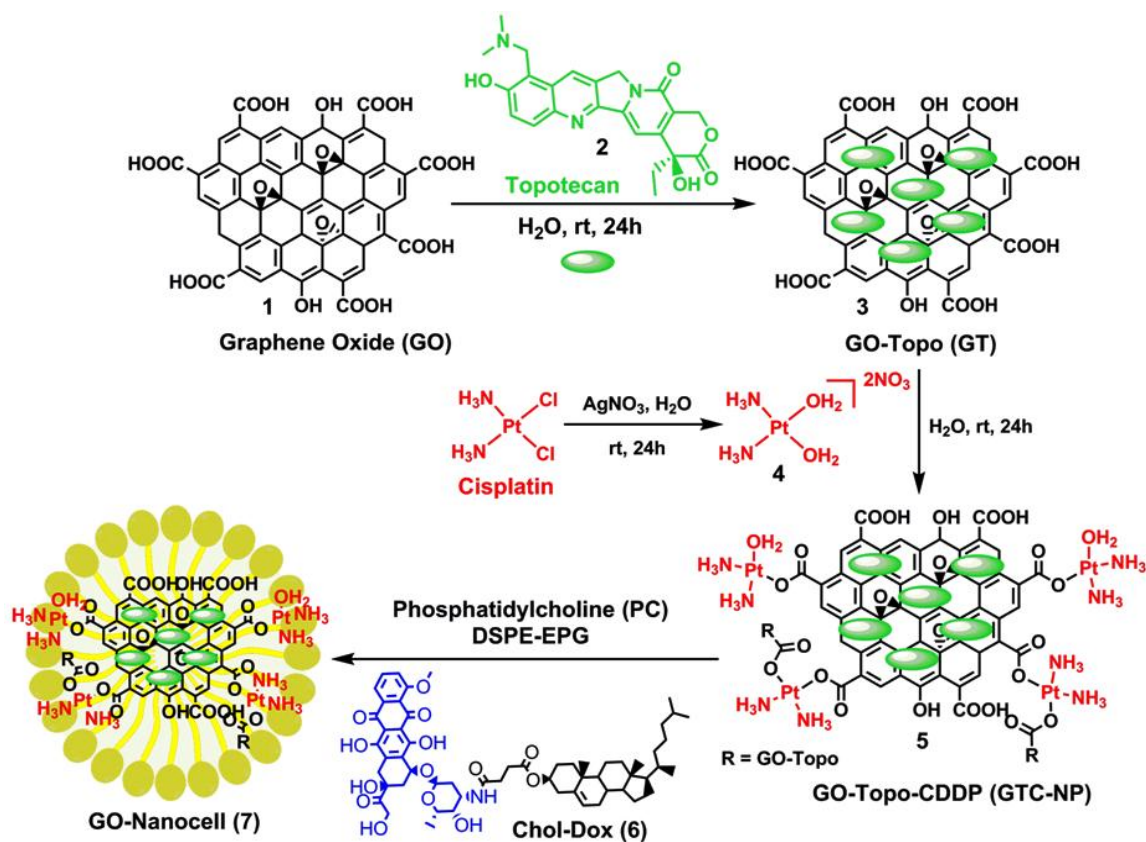


Figure 4.1: Synthetic scheme of GO-Nanocell.

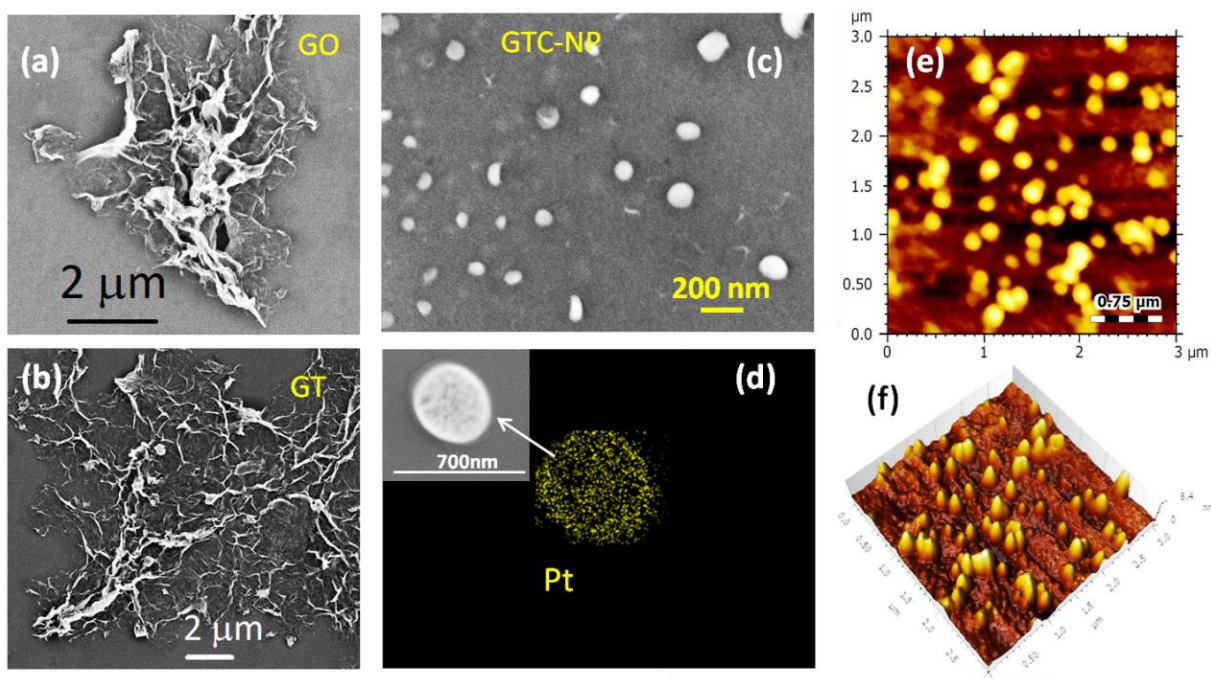


Figure 4.2: (a-c) FESEM images of GO, GT and GTC-NPs respectively. (d) Elemental mapping of Pt from FESEM, (e,f) 2-D and 3D AFM images of GTC-NPs respectively

The morphology of GT was visualized by field emission scanning electron microscopy (FESEM), which revealed that GT preserved the 2D-sheet like morphology as GO (**Figure 4.2a-b**). The existence of GO in GT was established by the characteristic D and G bands in resonance Raman spectroscopy (**Figure 4.3a**). The stacking of topotecan on 2D-GO surface was confirmed by the remarkable quenching of fluorescence emission intensity of free topotecan at $\lambda_{\text{max}} = 525$ nm (**Figure 4.4a**). GT was further reacted with aquated cisplatin (**4**, **Figure 4.1**) in 1:5 weight ratios in water for another 24 h to afford GO-Topotecan-CDDP (**5**, **Figure 4.1**). It was observed that GO-Topotecan-CDDP composite formed spherical nanoparticle (GTC-NP) having a size range from 80-90 nm, which was in agreement with our previous study.^{37, 40} The spherical morphology of GTC-NPs was determined via FESEM and atomic force microscopy (AFM) (**Figure 4.2c, e-f**). The existence of cisplatin in GTC-NPs was confirmed by elemental mapping of Pt by FESEM based energy dispersive X-ray spectroscopy (EDAX) (**Figure 4.2d**). Presence of GO and topotecan in GTC-NPs was further confirmed by characteristic D/G band in resonance Raman spectroscopy and fluorescence emission quenching spectra respectively (**Figure 4.3b, 4.4b**).

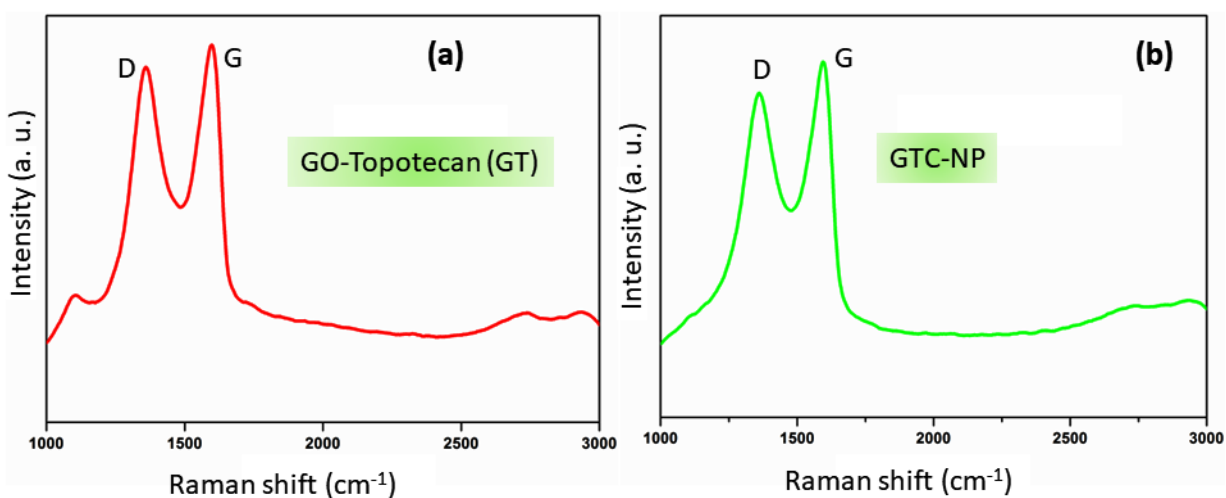


Figure 4.3: (a, b) Resonance Raman spectra of GT and GTC-NPs confirming the presence of GO moiety.

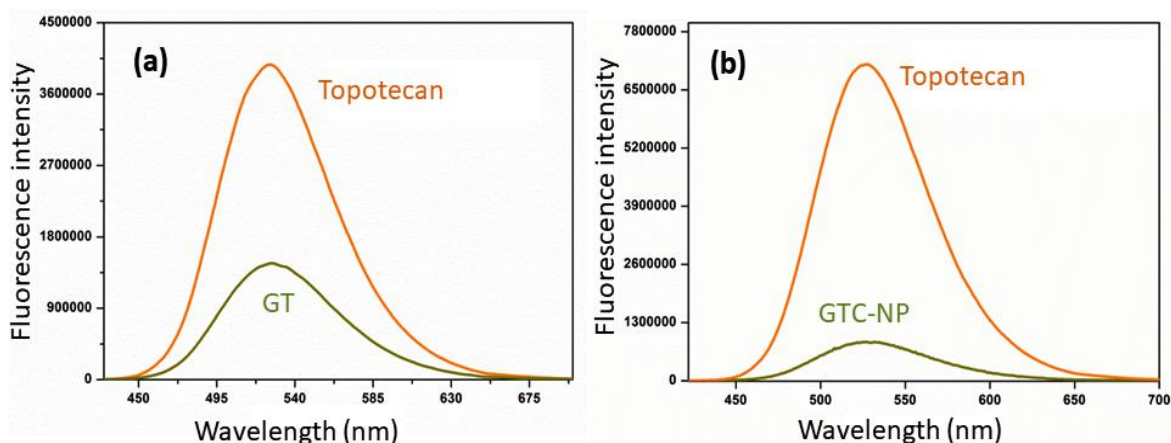


Figure 4.4: (a, b) Fluorescence emission spectra of GT and GTC-NPs confirming the stacking of topotecan on GO.

Finally, to introduce Topoisomerase II inhibitor, doxorubicin, we synthesized cholesterol-doxorubicin conjugate through a succinic acid linker.³⁸ We coated the GTC-NPs with cholesterol-doxorubicin (Chol-Dox) conjugate (**6**, **Figure 4.1**) using phosphatidylcholine (PC) and DSPE-PEG₂₀₀₀ by employing the lipid film hydration-extrusion technique⁴⁸ to engineer GO-Nanocell (GO-NC).

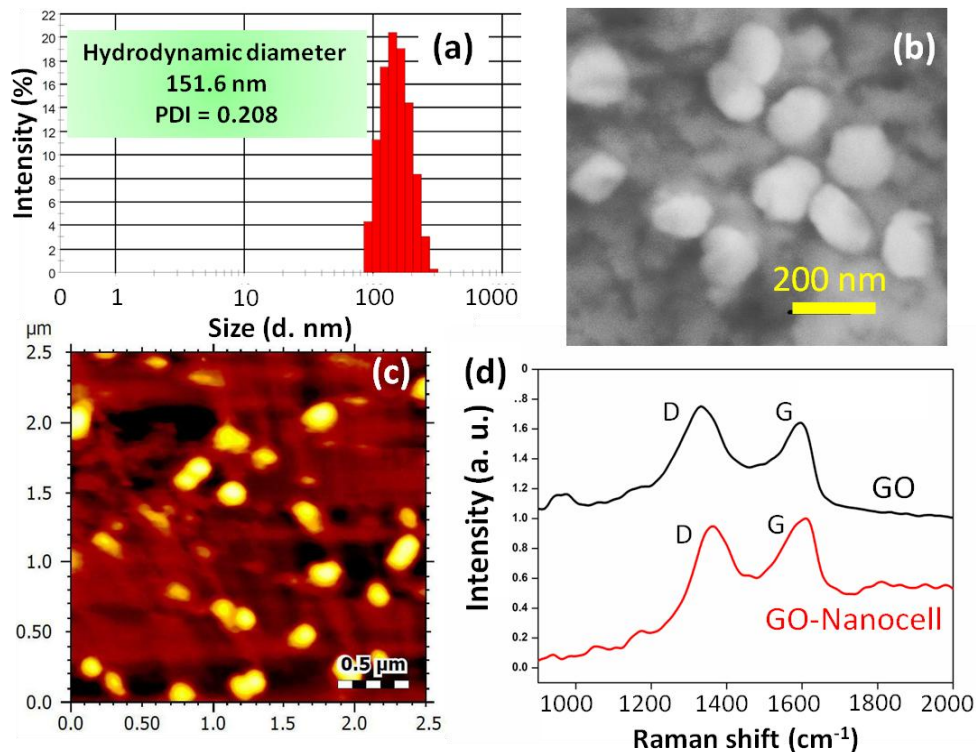


Figure 4.5: Characterization of GO-Nanocells by (a) dynamic light scattering (DLS), (b) FESEM and (c) AFM. (d) Single particle resonance Raman spectra of GO-Nanocells and GO.

Dynamic light scattering (DLS) of GO-NCs revealed that the hydrodynamic diameter of GO-NCs was 151.6 nm with a polydispersity index (PDI) = 0.298 (**Figure 4.5a**), which indicated that the GO-NCs are mono-dispersed with suitable size range for accumulating into tumor tissues by leaky vasculature.⁴⁹ FESEM and AFM images also confirmed that the spherical morphology of GTC-NPs was retained in GO-NC (**Figure 4.5b,c**). Single particle resonance Raman spectra of GO-NCs demonstrated characteristic D and G bands at 1350 cm^{-1} and 1590 cm^{-1} respectively which unequivocally established the existence of GO in GO-NCs (**Figure 4.5d**).

The presence of topotecan and doxorubicin in GO-NCs was determined by UV-Vis spectroscopy having a representative absorbance peak at $\lambda_{\text{max}} = 389$ nm and 480 nm respectively (**Figure 4.6a**). Furthermore, the incorporation of topotecan in GO-NCs was validated by the reduction of fluorescence emission intensity at $\lambda_{\text{max}} = 525$ nm compared to free topotecan (**Figure 4.6b**). We finally confirmed the occurrence of cisplatin in GO-NCs by EDAX measurement showing 8.56 weight % of Pt in GO-NCs (**Figure 4.7**). We also evaluated the loading of topotecan, doxorubicin and cisplatin in GO-NCs by UV-Vis spectroscopy at distinctive $\lambda_{\text{max}} = 389$ nm, 480 nm, and 706 nm respectively (**Figure 4.8a-c**). It was estimated that GO-NCs contained 120.5 $\mu\text{g}/\text{mL}$ of doxorubicin, 291 $\mu\text{g}/\text{ml}$ of topotecan and 198 $\mu\text{g}/\text{ml}$ of cisplatin (**Figure 4.8d**).

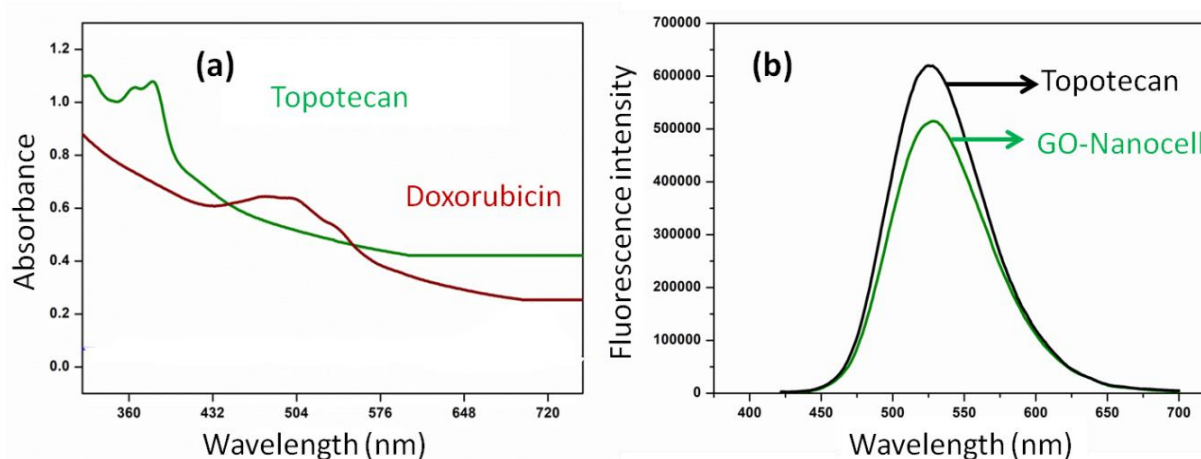
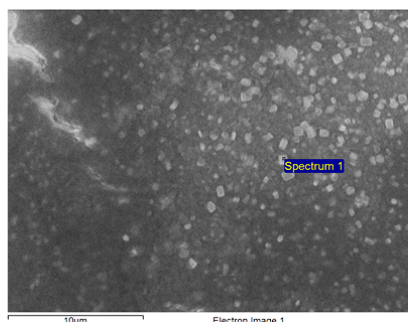


Figure 4.6: (a) UV-Vis spectra of GO-Nanocells confirming the presence of topotecan and doxorubicin. (b) Fluorescence emission spectra of GO-Nanocell exhibiting the stacking of topotecan on GO surface.



Element	Weight%	Atomic%
C K	33.42	42.61
N K	8.83	9.65
O K	49.19	47.07
Pt M	8.56	0.67
Totals	100.00	

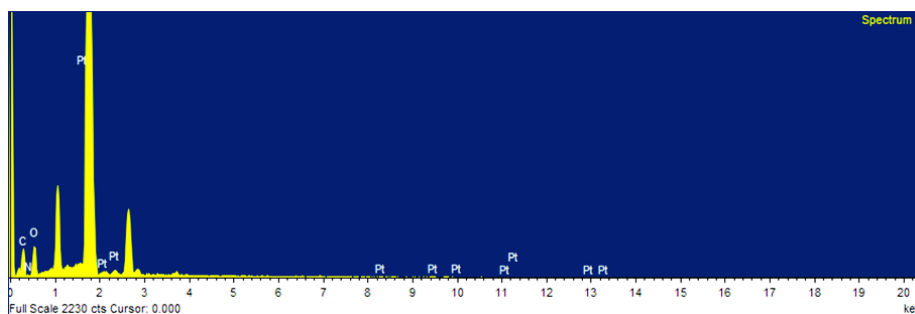


Figure 4.7:EDAX of GO-Nanocell from FESEM confirming the presence of cisplatin.

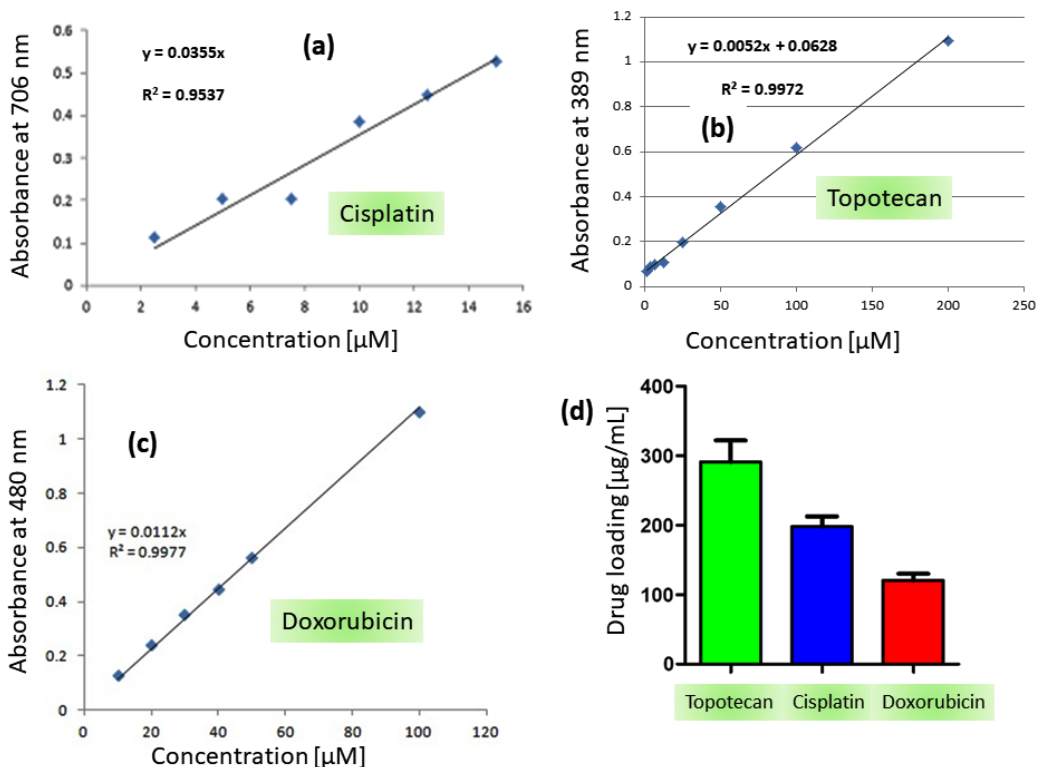


Figure 4.8: (a-c) Absorbance versus concentration graph of cisplatin, topotecan and doxorubicin respectively determined by UV-Vis spectra. (d) Loading of topotecan, cisplatin and doxorubicin in GO-Nanocell.

4.3.2 Cellular internalization: We hypothesized that GO-NCs would be internalized into the cancer cells and home into lysosomes (**Scheme 1b**). To validate our hypothesis, we have incubated the HeLa cervical cancer cells with GO-NCs at different time points (1h, 3h, and 6h) and co-stained the lysosomes with LysoTracker Green DND-26 dye. The cells were then observed under a confocal fluorescence laser scanning microscope (CLSM). The fluorescence microscopy images revealed that GO-NCs (red fluorescently labeled due to the presence of doxorubicin) slowly entered into the HeLa cells and localized into lysosomes in a time-dependent manner leading to the merged yellow areas after overlapping green and red fluorescence signals (**Figure 4.9**).

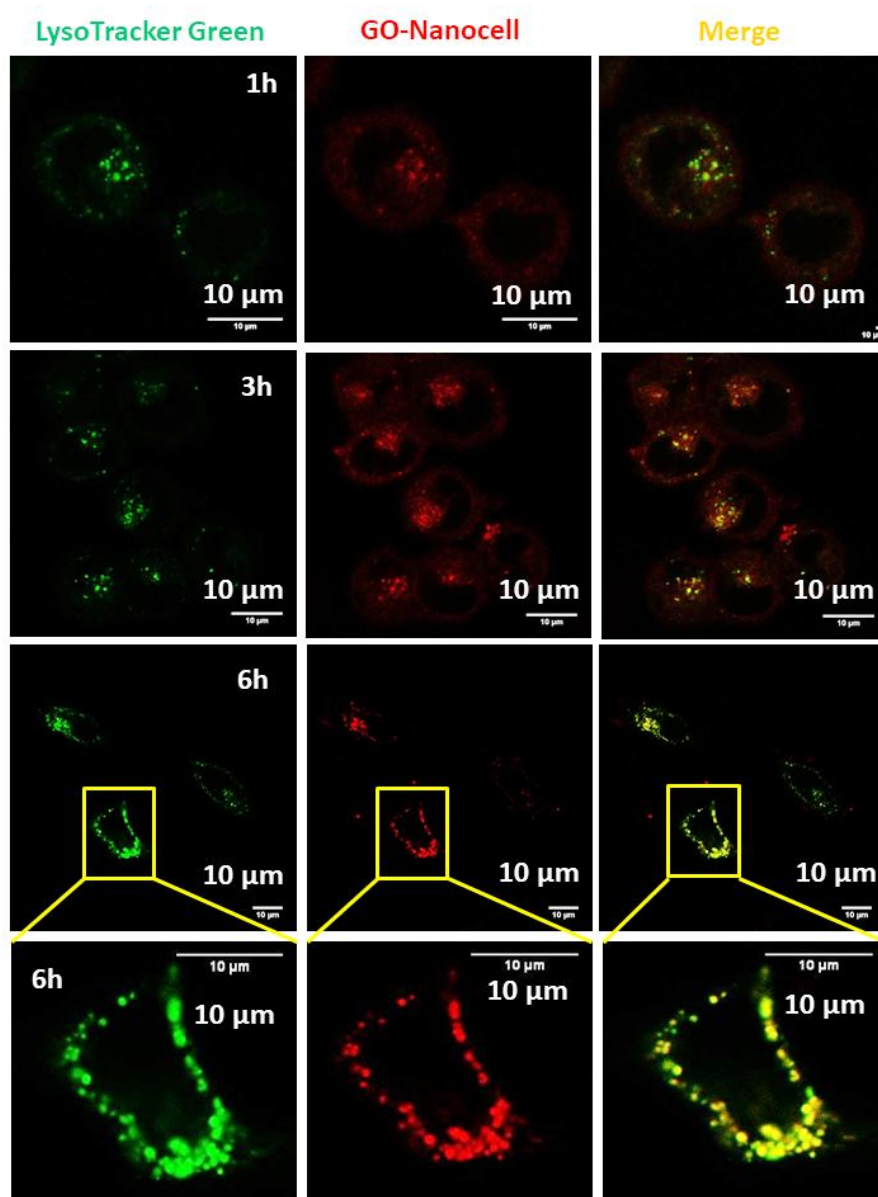


Figure 4.9: Confocal laser scanning microscopy (CLSM) images of HeLa cells treated with GO-Nanocells (red fluorescence) at 1 h, 3 h and 6 h time points. The cells were co-stained with LysoTracker DND-26 (green fluorescence). The yellow regions show the co-localization of GO-Nanocells into the lysosomes. Scale bar = 10 μm .

Further quantification from confocal microscopy through Mander's and Pearson's coefficients also confirmed that GO-NCs localized into lysosomes with 13%, 20% and 42% colocalization volume at 1h, 3h and 6h time points respectively (**Table 1**). We further evaluated the retention time of the GO-NCs into lysosomes by incubating them for higher time points (12h and 24h). The CLSM images clearly showed that the GO-NCs were retained in the lysosomes for 12 h and 24 h with nearly 36% and 31% volume colocalization (**Figure 4.10, Table 1**). This fluorescence confocal microscopy showed that GO-NCs internalized into the HeLa cells temporally and homed into lysosomes within 6 h and retained there for 24 h.

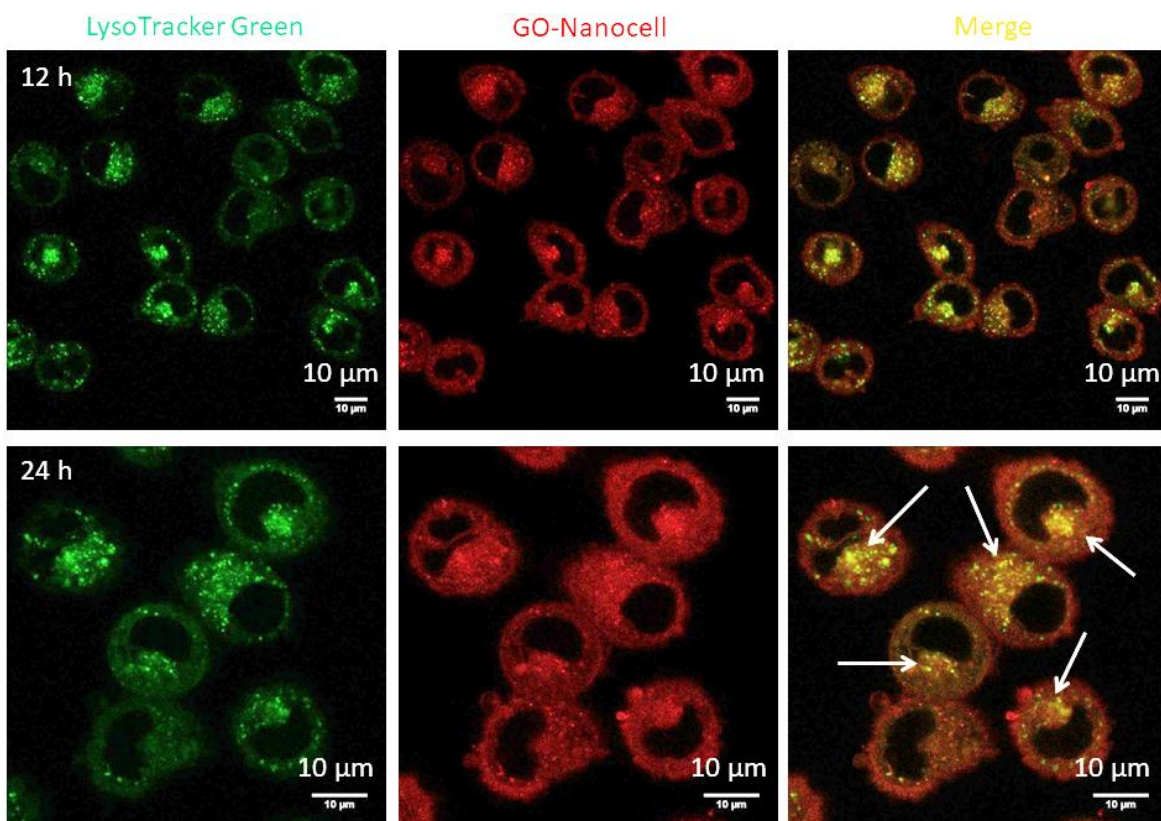


Figure 4.10: CLSM images of HeLa cells at 12 h and 24 h post incubation with GO-Nanocells (red fluorescence). Lysosomes were stained with fluorescently labelled LysoTracker Green DND-26. Scale bar = 10 μm .

Time	Pearson's Correlation Coefficient	Mander's Coefficients (TM1 Fraction of C1 overlapping C2)	Mander's Coefficients (TM2 Fraction of C2 overlapping C1)	% Volume Colocalization
1h	0.3157	0.6101	0.6074	13.02%
3h	0.4028	0.6689	0.7061	19.94%
6h	0.8811	0.9167	0.6388	42.19%
12h	0.7707	0.544	0.8510	36.20%
24h	0.6569	0.6124	0.6209	31.34%

Table 3: Quantification of % volume colocalization of GO-Nanocells into lysosomes of HeLa cells in different time points (1h, 3h, 6h, 12h and 24h) from confocal microscopy.

Sub-cellular lysosomes are acidic.⁵⁰ Hence, after localization of GO-NCs into lysosomes in HeLa cells, the topoisomerase inhibitors and DNA damaging agent should be released from GO-NCs in acidic milieu. To evaluate the release of inhibitors and DNA damaging drugs, GO-NCs were incubated into the buffer of pH = 5.5 over 72 h and the released drugs in each time interval was quantified by UV-Vis spectroscopy. It was observed that after 72 h, 41%, 22% and 18% of topotecan, doxorubicin, and cisplatin were released respectively from GO-NCs in a slow and continuous manner (**Figure 4.11a**). We rationalized that, as topotecan was attached with GO-NCs by weak aromatic π - π stacking, the release of topotecan was faster compared to doxorubicin which was linked with the stronger amide covalent bonding at the acidic environment. Furthermore, cisplatin was attached to GO by much stronger coordination linkage leading to the slowest released drug from GO-NCs. To make sure that GO-NCs should not release its payload in blood circulation before reaching the tumor tissues by passive targeting, we also incubated GO-NCs in physiological pH (pH = 7.4) for 72 h and quantified the drug release profile. Interestingly, it was found that only 17%, 13% and 10% of topotecan, cisplatin and doxorubicin were released from GO-NCs even after 72 h respectively (**Figure 4.11b**). These remarkable difference in release profiles in acidic and physiological pH indicated that GO-NCs would release the payload much better in acidic lysosomes compared to blood circulation or non-cancerous milieu in a controlled and slow fashion which would be ideal for tumor tissue targeting compared to healthy tissues.

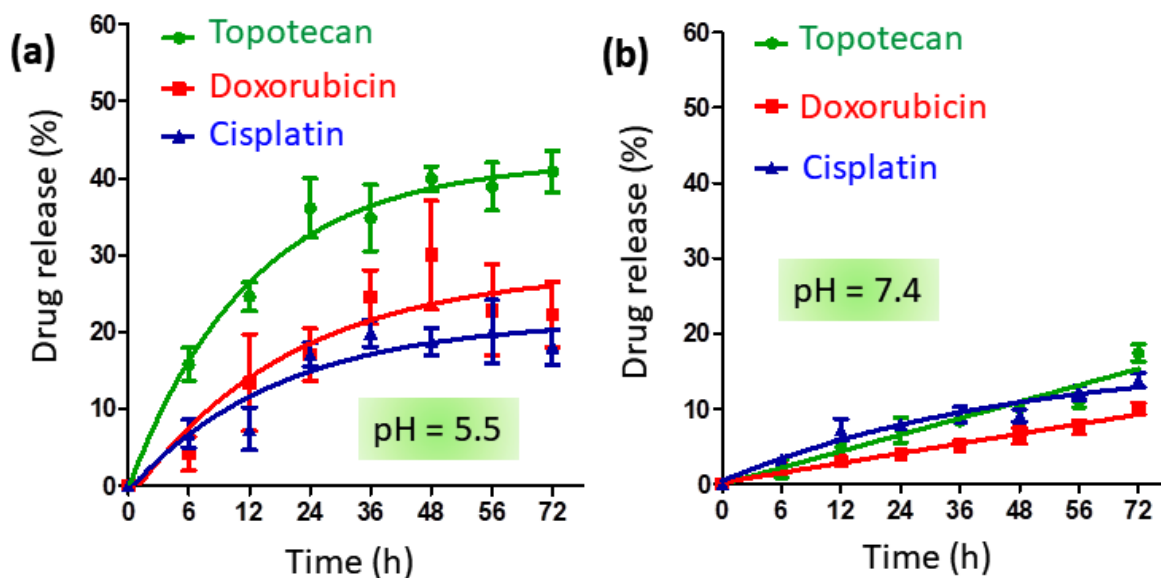


Figure 4.11: (a, b) Release profile of different drugs from GO-Nanocells at pH = 5.5 and 7.4 respectively over 72 h.

4.3.3 DNA damage and Topoisomerase Inhibition: After transport into the cancer cells, GO-NCs should be able to damage nuclear DNA and inhibit topoisomerases. To estimate the nuclear DNA damage, we evaluated the expression of γ H2AX as one of the DNA damage markers.⁵¹ The HeLa cells were incubated with GO-NCs for 24 h followed by the treatment with γ H2AX specific primary antibody which was further detected by Alexa Fluor 594 (red fluorescence) tagged secondary antibody. The nucleus of the cells was co-stained by blue fluorescent dye DAPI. The cells were visualized by fluorescence confocal microscopy. The CLSM images of the control cells showed a negligible signal for γ H2AX (**Figure 4.12**, upper panel). In contrast, the microscopy images of GO-NC treated cells showed a significant increase (3.7 folds) in the red fluorescent signal confirming the much-increased expression of γ H2AX (**Figure 4.12**, lower panel, and **Figure 4.14a**). Furthermore, the red fluorescence signals from γ H2AX colocalized into the nucleus leading to purple fluorescence signals by overlapping with blue fluorescence signals of DAPI which confirmed that GO-NCs damaged the nuclear DNA.

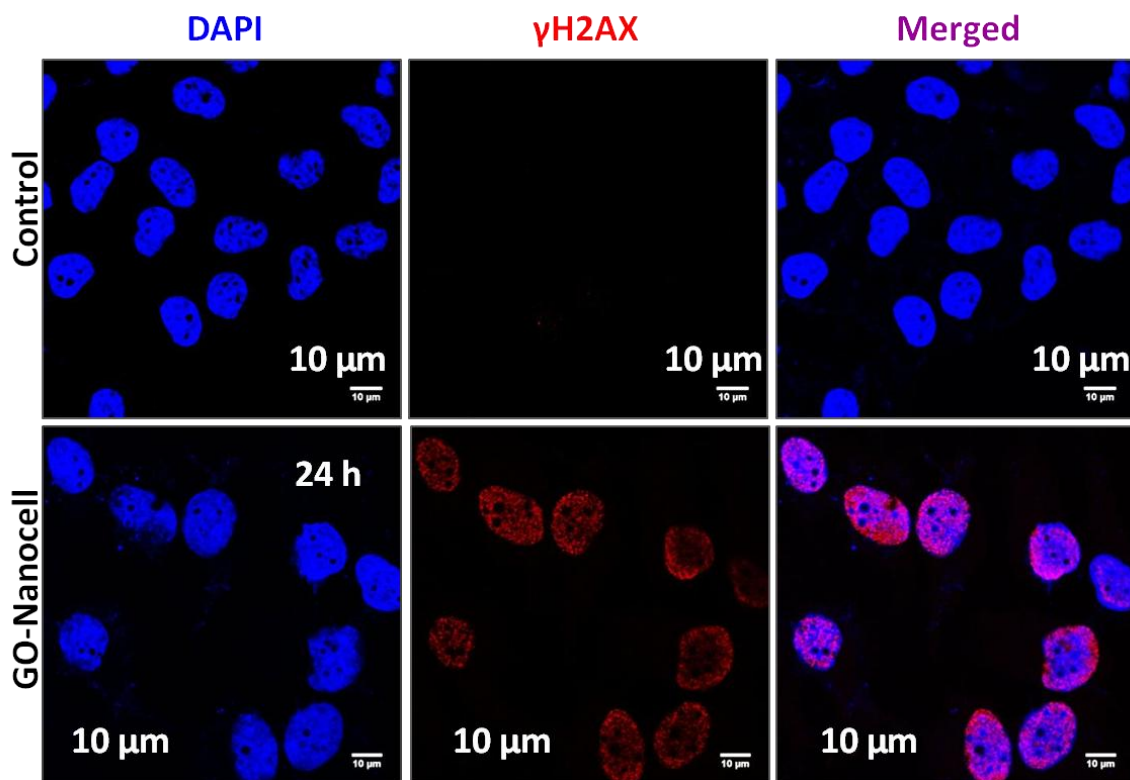


Figure 4.12: CLSM images of HeLa cells treated with GO-Nanocells for 24h followed by incubation with the γ H2AX antibody labeled with Alexa Fluor 594 dye (red fluorescence). The nuclei were stained with blue fluorescent DAPI. Scale bar = 10 μ m.

To further confirm the nuclear DNA damage, we evaluated the expression of γ H2AX and p53 via gel electrophoresis. The HeLa cells were treated with GO-NCs for 24 h followed by the separation of the proteins under electrophoresis and visualized by Western blot analysis. It was observed that the untreated control cells hardly showed any expression of γ H2AX and p53. However, GO-NCs increased the expression of γ H2AX (**Figure 4.13a**) and p53 significantly (**Figure 4.13b**). The quantification of the protein expression also validated that GO-NC treated cell amplified the expression of γ H2AX and p53 by 6.9 and 4.3 folds respectively compared to the non-treated control cells (**Figure 4.14b and c**). Cellular DNA damage triggers the repair mechanism through poly (ADP-ribose) polymerase (PARP).⁵² We also assessed the expression of PARP after treatment with GO-NCs by Western blot, which demonstrated that PARP expression was reduced by 1.8 fold due to cleavage as a result of DNA damage (**Figure 4.13c** and **Figure 4.14d**). Finally, we estimated the inhibition of Topoisomerase I by gel electrophoresis after treatment of HeLa cells for 24 h with GO-NCs. Interestingly; GO-NCs reduced the expression of Topoisomerase I by 3.4 folds compared to the control cells, which

confirmed that GO-NCs inhibited Topoisomerase I in HeLa cells (**Figure 4.13d** and **Figure 4.14e**). The confocal imaging and immune-blotting experiments explicitly established that GO-NCs inhibited Topoisomerase along with nuclear DNA damage in HeLa cells.

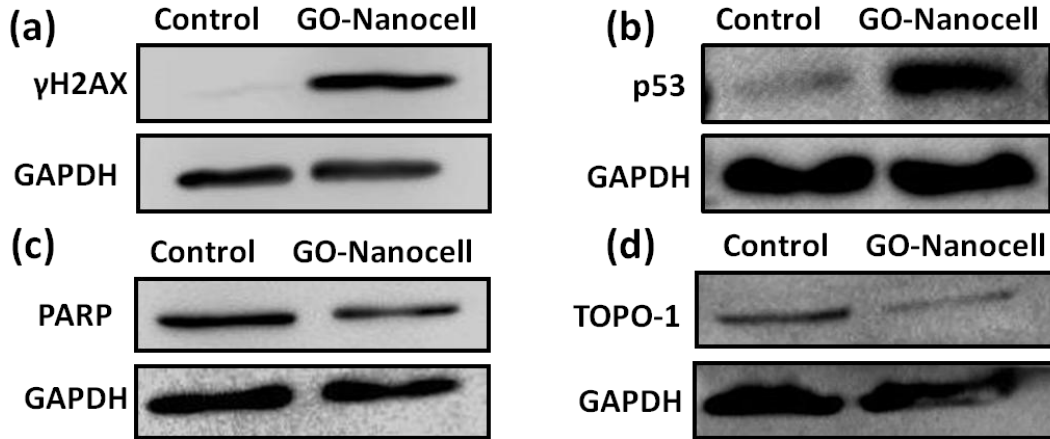


Figure 4.13: Western blot analysis of (a) γ H2AX, (b) p53, (c) PARP and (d) TOPO-1 in HeLa cells after treatment with GO-Nanocells for 24 h.

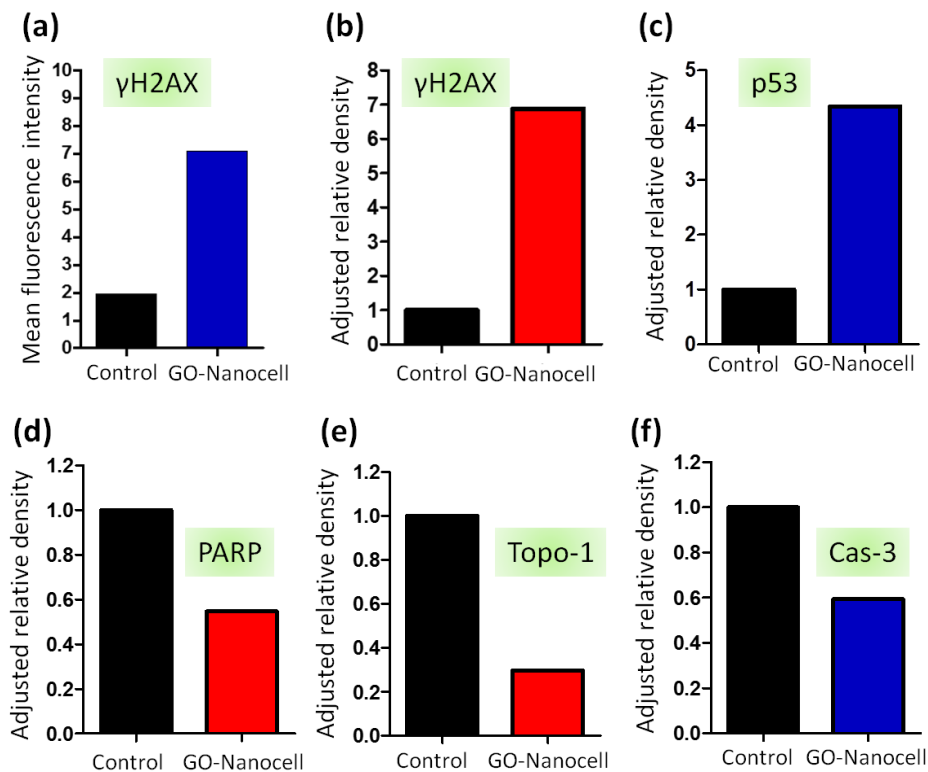


Figure 4.14: HeLa cells were treated with GO-Nanocells for 24 h and (a, b) γ H2AX expression was quantified from confocal microscopy and Western blot analysis respectively and (c-f) quantification of p53, PARP, Topo-1 and Cas-3 from Western blot analysis respectively.

4.3.4 Cell cycle arrest, apoptosis induction and cell death: GO-Nanocell mediated inhibition of topoisomerase and DNA damage would lead to the cell cycle arrest in cancer cells. Flow cytometry analysis was used to evaluate the cell cycle arrest after treating HeLa cells with GO-NCs for 24 and 48 h followed by propidium iodide (PI) to label the cellular DNA. The flow cytometry analysis revealed that 65%, 11%, and 5% control cells were in G₁, S and G₂-M phase of cell cycle respectively. However, after treatment with GO-NCs for 24 h, 21.5%, 4%, and 41.5% of cells were found in G₁, S and G₂-M phase respectively. Similarly, at 48 h post-incubation with GO-NCs, 10.5%, 11%, and 47.5% cells were in G₁, S and G₂-M phase of cell cycle (**Figure 4.15**). The flow cytometric analysis indicated that GO-NC mediated DNA damage and Topoisomerase inhibition led the HeLa cells to be arrested in the G₂-M phase of the cell cycle.

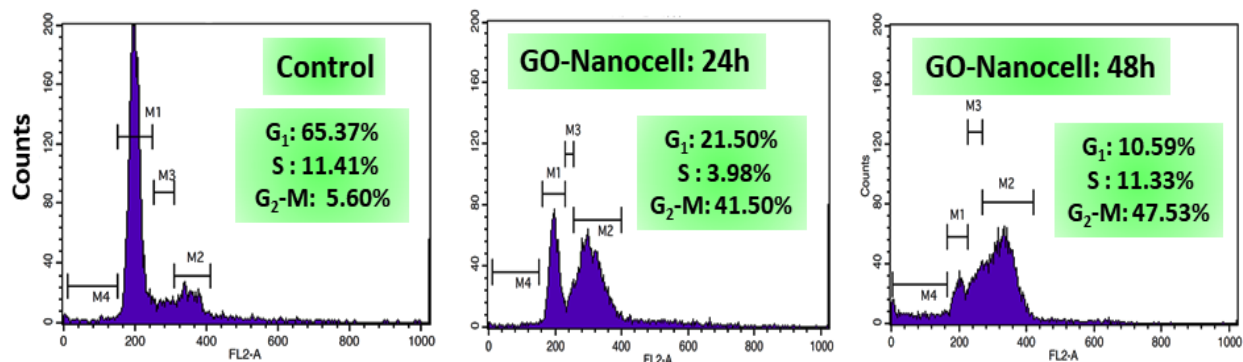


Figure 4.15: Cell cycle analysis of HeLa cells via flow cytometry after treatment with GO-Nanocells for 24 h and 48 h. The cellular DNA was stained by red fluorescent propidium iodide (PI).

The cell cycle arrest by GO-NCs would lead to the programmed cell death (apoptosis) in HeLa cells. To estimate apoptosis, we treated HeLa cells with GO-NCs for 24 h and 48 h. The apoptotic cells and necrotic cells were stained by green fluorescent FITC labelled Annexin V and red fluorescent propidium iodide (PI) respectively followed by flow cytometric analysis to count the cells in different stages. We observed that at 24 h, GO-NCs induced nearly 21% cells into early and only 6% cells in later apoptosis (**Figure 4.16**). However, interestingly, at 48 h, GO-NCs triggered early apoptosis in 22% cells along with 54.5% cells into late apoptosis.

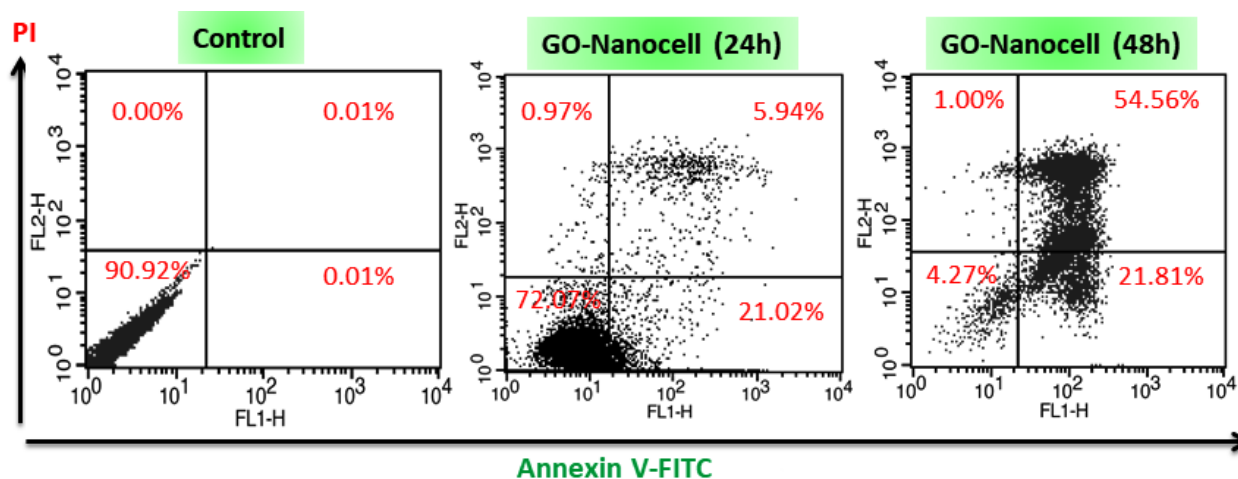


Figure 4.16: Induction of apoptosis in HeLa cells at 24 h and 48 h postincubation with GO-Nanocells determined by flow cytometry analysis.

Moreover, induction of apoptosis into cancer cells would lead to the cleavage of effector caspase 3. Hence, we measured the expression of caspase-3 in HeLa cells by gel electrophoresis after treatment with GO-NCs for 24 h. The immune-blotting demonstrated that GO-NCs reduced the expression of caspase-3 by 1.7 folds compared to control cells (**Figure 4.17a, Figure 4.14f**). These flow cytometry and western blot analysis demonstrated that GO-NCs induced early and late apoptosis in HeLa cells at 24 h and 48 h post-incubation.

Finally, we evaluated the efficacy of GO-NCs in HeLa cervical cancer cell killing by cell viability assay. HeLa cells were treated with GO-NCs in a dose-dependent manner over 24 h and 48h followed by incubation with MTT reagents. As a control, we treated the cells with the combination of topotecan, doxorubicin, and cisplatin in the same ratio present in GO-NCs for 24 h and 48 h. Interestingly, at 24 h, GO-NCs showed 50% cell death at 3 μM concentration of topotecan which is very nearly similar as the 50% cell death induced by the free drug combinations at 2.85 μM (**Figure 4.17b-c**). Although, GO-NCs showed much higher cell killing ability (cell viability = 1.9%) compared to free drug combination (cell viability = 11.3%) at 70 μM concentration of topotecan, at 48h post-incubation, GO-NCs demonstrated far better efficacy with much lower IC_{50} = 1.03 μM compared to IC_{50} = 4.3 μM induced by free drug combination. Moreover, at higher concentration (70 μM), GO-NCs showed much better cell killing (cell viability = 1.4 %) compared to free drug combination (cell viability = 9.5 %). From these cell viability assays, it was evident that GO-NCs demonstrated augmented efficacy in HeLa cervical cancer cell killing at 48 h compared to the free drug cocktail.

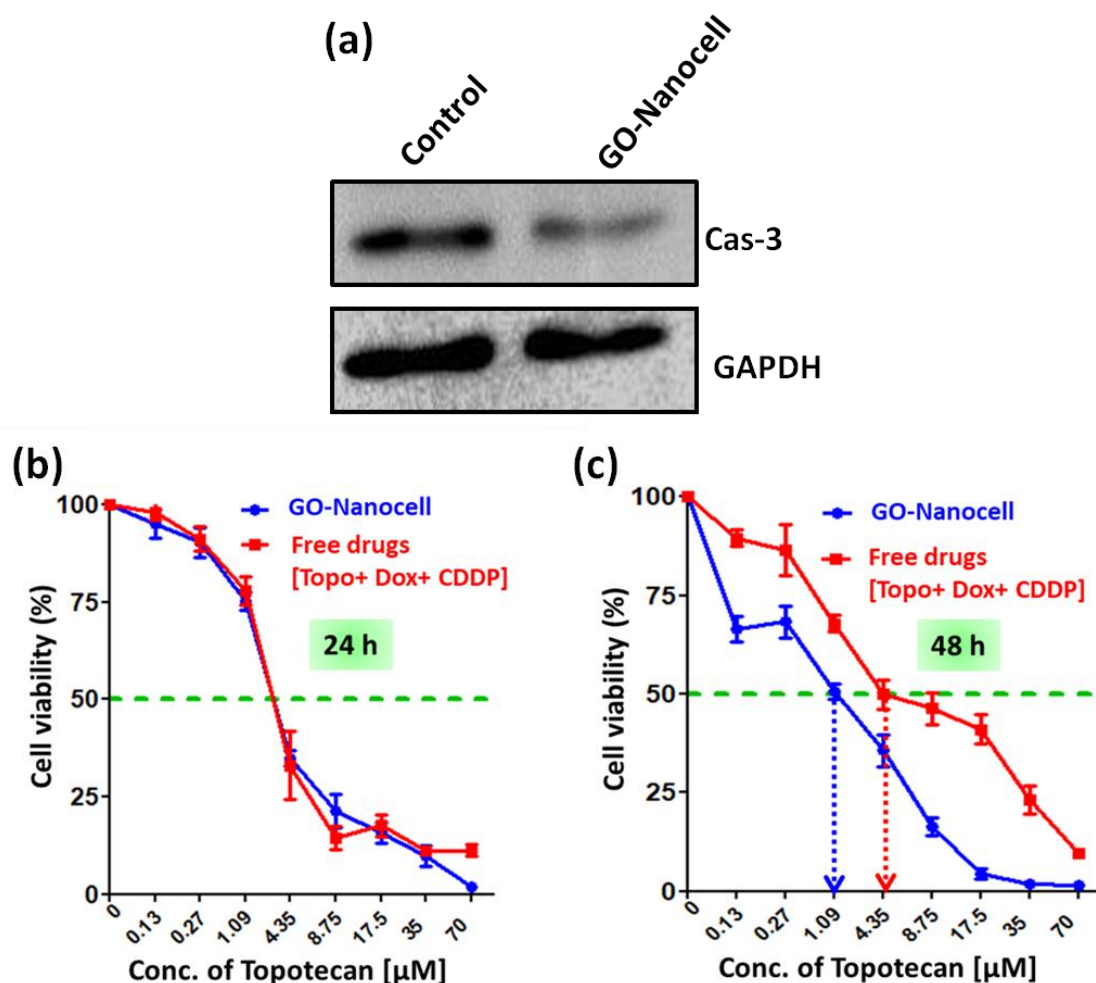


Figure 4.17: (a) Western blot analysis of caspase-3 in HeLa cells as a marker for apoptosis after treatment with GO-Nanocells for 24 h. (b) Viability of HeLa cells at 24 h and (c) 48 h post-incubation with GO-Nanocells quantified by MTT assays.

4.4 Materials and Methods

4.4.1 Reagents: Graphene oxide (4 mg/mL), Cisplatin and silicon wafer for FESEM were bought from Sigma-Aldrich. Topotecan and Doxorubicin were bought from Selleck Chemicals. DMEM media and 3-(4, 5-dimethylthiazol-2-yl)-2,5-diphenyltetrazolium bromide (MTT) were purchased from HiMedia. Annexin-V-FITC Staining Kit was purchased from Roche. LysoTracker™ Green DND-26 and *SlowFade*® Gold Antifade Reagent were procured from Life Technologies.

4.4.2 Synthesis of Graphene oxide-Topotecan-Cisplatin nanoparticles (GTC NPs): The GTC nanoparticles were prepared according to previously reported strategy³⁷. Briefly, graphene oxide

(4 mg/mL, 250 μ l) was dispersed in distilled water (2 ml). An aqueous solution of Topotecan (1.0 mg) in distilled water (1 ml) was prepared and added to the dispersed graphene oxide solution. The reaction was stirred at room temperature for 24 h. To remove unreacted topotecan, the reaction mixture was dialyzed against distilled water through dialysis membrane (MWCO= 1000 Dalton) for 6 h and then centrifugation at 4000 rpm. Further aquated cisplatin (5 mg/ml) was added to graphene oxide-topotecan conjugate and stirred at room temperature for 24 h. After completion of the reaction, the mixture was again dialyzed to remove excess of aquated cisplatin.

4.4.3 Synthesis of Cholesterol-Doxorubicin Conjugate: Doxorubicin was conjugated with cholesterol through a succinic acid linker in two steps by previously reported scheme.³⁸ Characterization in appendix (**Figure A 4.1 to 4.6**)

Characterization of cholesterol-succinic acid linker conjugate

¹H NMR: (400 MHz, Chloroform-d) δ = 5.37(1H, d, J = 4 Hz), 4.67 – 4.59 (1H, m, J = 11.8 Hz), 2.67 (2H, t, J = 6.8 Hz), 2.60 (2H, t, J = 6.9 Hz), 2.30 (2H, d, J = 8 Hz), 2.05 – 1.93 (2H, m), 1.86 (1H, d, 2.4 Hz), 1.75– 1.78 (2H, m), 1.68 – 1.42 (8H, m), 1.40 – 1.20 (5H, m), 1.18 – 1.04 (8H, m), 1.04 (3H, s), 0.91 (3H, d, J = 6.4 Hz), 0.87 (3H, d, J = 1.8 Hz), 0.85 (3H, d, J = 1.8 Hz), 0.67 (3H, s).

¹³C NMR: (100 MHz, Chloroform-d) δ = 177.6, 171.6, 139.6, 122.8, 77.4, 77.1, 76.8, 74.7, 56.8, 56.3, 50.1, 42.4, 39.8, 39.6, 38.1, 37.1, 36.7, 36.3, 35.9, 32.0, 29.4, 29.1, 28.4, 28.1, 27.8, 24.4, 23.9, 22.9, 22.7, 19.4, 18.8, 12.0.

MALDI-TOF: m/z: for C₃₁H₅₀O₄, calculated = 509.3709, observed = 509.3606

Characterization of conjugate (6) chol-dox

¹H NMR: (400 MHz, Chloroform-d) δ = 8.05 (1H, d, J = 8 Hz), 7.78 (1H, t, J = 8.0 Hz), 7.40 (1H, d, J = 8.0 Hz), 6.8 (1H, t, J = 7.9 Hz) 5.94 (1H, d, J = 8.0 Hz), 5.53 (1H, s), 5.35 – 5.29 (2H, m), 4.76 (2H, s), 4.61– 4.53 (2H, m), 4.16 – 4.05 (6H, m), 3.68 (1H, d, J = 2.2 Hz), 3.3 (1H, d, J = 20 Hz), 3.0 (1H, d, J = 16 Hz), 2.28 (2H, d, J = 7.6 Hz), 1.80 – 1.54 (20H, m), 1.29 – 1.25 (8H, m), 1.16–1.06 (6H, m), 0.97 (5H, s), 0.87 (10H, dd, J = 8.4 Hz 1.6 Hz), 0.67 (3H, s).

13C NMR: (100 MHz, Chloroform-d) δ = 214.1, 187.2, 186.9, 173.2, 171.3, 161.2, 156.3, 155.8, 139.6, 135.7, 135.3, 133.7, 122.9, 121.0, 118.5, 111.5, 100.8, 77.1, 74.5, 69.7, 69.0, 67.2, 66.32, 65.7, 56.8, 56.8, 56.2, 50.1, 45.5, 42.4, 39.8, 39.6, 38.1, 37.0, 36.7, 36.3, 35.9, 31.9, 30.0, 29.8, 28.3, 28.1, 27.8, 24.4, 23.9, 22.9, 22.7, 21.1, 19.4, 18.8, 17.0, 12.0.

MALDI-TOF: m/z for calculated for $C_{58}H_{77}NO_{14}Na^+$, calculated = 1034.5344, observed = 1034.7263

4.4.4 Synthesis of GO-Nanocell: In a round bottom flask, L- α -phosphatidylcholine (PC), Cholesterol-Doxorubicin conjugate and 1,2-distearoyl-*sn*-glycero-3-phosphoethanolamine-N-[amino(polyethyleneglycol)2000] (DSPE-PEG) were dissolved in dichloromethane (5 mL) in a weight ratio of 7:2:0.7. The organic solvent was slowly evaporated into a thin and uniform film with the help of a rotary evaporator. After thorough drying under high vacuum, the film was hydrated with the aqueous suspension of GTC-NPs at 60°C for 2 h. The formed GO-Nanocells was first passed through a small Sephadex G-25 column and extruded through 200 nm Whatmann polycarbonate membrane at 60°C to obtain mono-dispersed GO-Nanocells. The GO-Nanocells were stored at 4°C for further use.

4.4.5 Determination of size, shape, and morphology: The size, shape, and morphology of GO-Nanocells were determined by light scattering and electron microscopy like atomic force microscopy (AFM) and field-emission scanning electron microscopy (FESEM). The samples were prepared using the method described previously.³⁹

4.4.6 Resonance Raman Spectroscopy: Resonance Raman spectra were collected using a Lab RAM HR 800 (Horiba Scientific) using a laser excitation wavelength of 532 nm excitation with a 50X objective at room temperature. 532 nm was chosen as the excitation to guarantee a good signal/noise ratio. Before analysis, the baseline of the spectrum was extracted using the software NGSLabSpec.

4.4.7 Quantification of drug loading in GO-Nanocell: Loading of individual drugs like Topotecan (λ_{max} = 389 nm), Doxorubicin (λ_{max} = 480 nm), Cisplatin (λ_{max} = 707 nm) in GO-Nanocell was determined *via* UV-visible spectroscopy using the methods described in previous reports.^{39, 40}

Drug loading efficiency (%) = $\frac{\text{Amount of drug loaded in nanoparticle} \times 100}{\text{The total amount of drug used}}$

4.4.8 Fluorescence spectroscopy: Steady-state fluorescence spectroscopy was recorded using a Fluoromax-4 (HORIBA scientific, USA). The GO-Nanocell was suspended in water, and the emission spectra for Topotecan was checked at $\lambda_{\text{max}} = 525$ nm. The fluorescence spectra of free topotecan in the same concentration was also checked at emission wavelength $\lambda_{\text{max}} = 525$ nm.

4.4.9 Cellular internalization by confocal laser scanning microscopy (CLSM): 2×10^4 HeLa cells were used for cellular internalization study. Upon attachment, cells were treated with GO-Nanocell (topotecan :CDDP : doxorubicin = $2 \text{ mg ml}^{-1} : 1.4 \text{ mg ml}^{-1} : 0.8 \text{ mg ml}^{-1}$) for 24h, 12h, 6h, 3h, and 1h. Cells were counter-stained with Lysotracker Green DND 26 after washing with PBS. Cells were visualized by Leica SP8 confocal microscope⁴⁰

4.4.10 Detection of γ H2AX by immunostaining: 5×10^5 HeLa cells were used for this experiment. GO-Nanocell (topotecan :CDDP :doxorubicin = $1 \text{ }\mu\text{M} : 0.9 \text{ }\mu\text{M} : 0.3 \text{ }\mu\text{M}$) was added to the cells and incubated for 24h. The cells were visualized by confocal microscopy by using γ H2AX primary antibody (1:100 dilution) and Alexa Flour 594 conjugated secondary antibody (1:500 dilution).^{39,41}

4.4.11 Western blot, flow cytometry, cell viability: Western blot, cell cycle analysis, apoptosis, and cell viability assays were performed by using the method described in ref. 39 and 40. For all of the assays the GO-Nanocell was used having concentration of topotecan, CDDP and doxorubicin of $1 \text{ }\mu\text{M}$, $0.9 \text{ }\mu\text{M}$ and $0.3 \text{ }\mu\text{M}$ respectively. The free drug cocktail used as the control for the cell viability assay was also prepared using the same drug concentrations present in the GO-Nanocell.

4.5 Conclusion

In conclusion, we have engineered a graphene oxide-based self-assembled spherical nanoparticle with lipid coating (GO-Nanocell: GO-NC) which can concurrently comprise DNA damaging drug (cisplatin) with DNA Topoisomerase inhibitors (topotecan and doxorubicin) in a single particle. The spherical shape and 151 nm hydrodynamic diameters of these GO-NCs were determined by DLS, FESEM and AFM studies. Fluorescence confocal microscopy images demonstrated that these GO-NCs internalized into the HeLa cervical cancer cells temporally and homed into sub-cellular lysosomes within 6h. c inhibitors were released from these GO-NCs in improved quantities in a slow and controlled way at acidic pH compared to physiological

condition. These GO-NCs induced DNA damage simultaneously with DNA Topoisomerase inhibition in cancer cells which triggered early and late apoptosis through G2-M phase cell cycle arrest at 24 h and 48h. Finally, these GO-NCs offered remarkably greater efficacy in HeLa cell killing compared to free drug combinations at 48 h. It can be anticipated that; this GO-NCs can serve as a tool to impair multiple targets inside the cancer cells in a synchronized manner for a better therapeutic effect in future cancer therapy.

4.6 Salient Features

- We developed a triple (Topo, Dox and Cisplatin) drug loaded, lipid coated graphene oxide nanoparticle termed as GO-Nanocell.
- PC and cholesterol are major components of the cell membrane, and are thus highly biocompatible. The enveloping of the dual drug conjugated GO nanoparticles with lipids makes it safer for intravenous delivery.
- GO-Nanocells internalized into the HeLa cervical cancer cells temporally and homed into sub-cellular lysosomes, releasing the drugs in a controlled manner.
- The released DNA damaging drug cisplatin and Topoisomerase I and II inhibitors-topotecan and doxorubicin ushered DNA damage along with TOP1 and TOP2 inhibition, which triggered apoptosis in HeLa cells.
- GO-Nanocells offered remarkably greater efficacy in HeLa cell killing compared to free drug combinations at 48 h.

4.7 Appendix

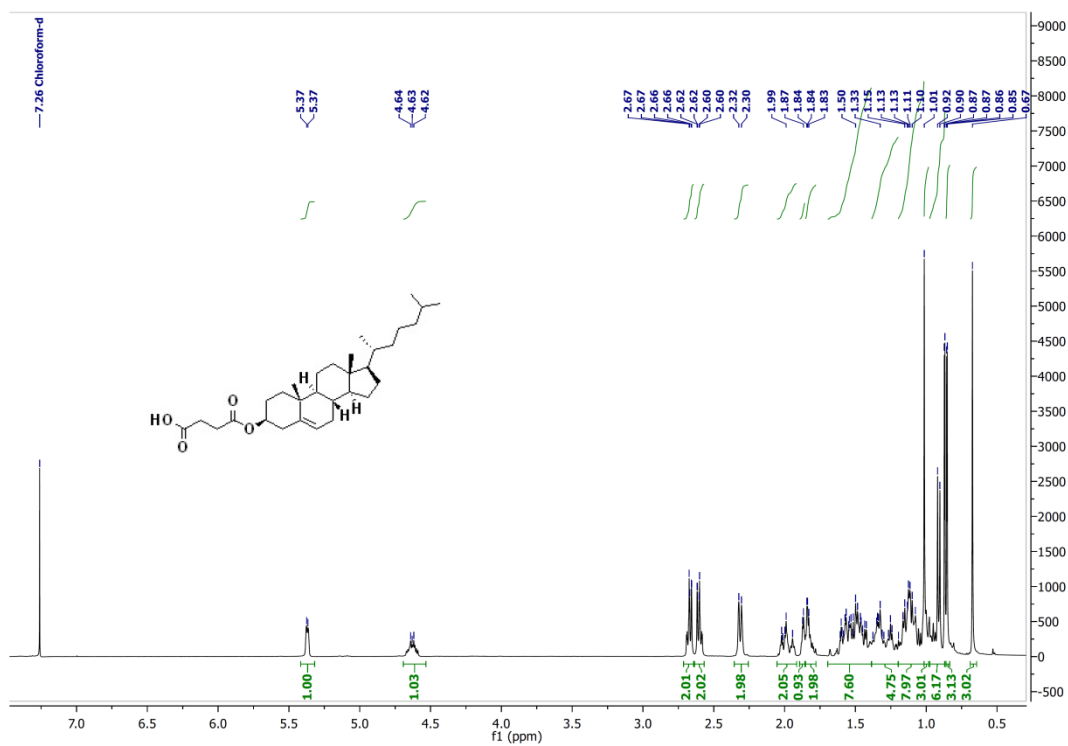


Figure A 4.1: ^1H NMR of Cholesterol-succinic acid.

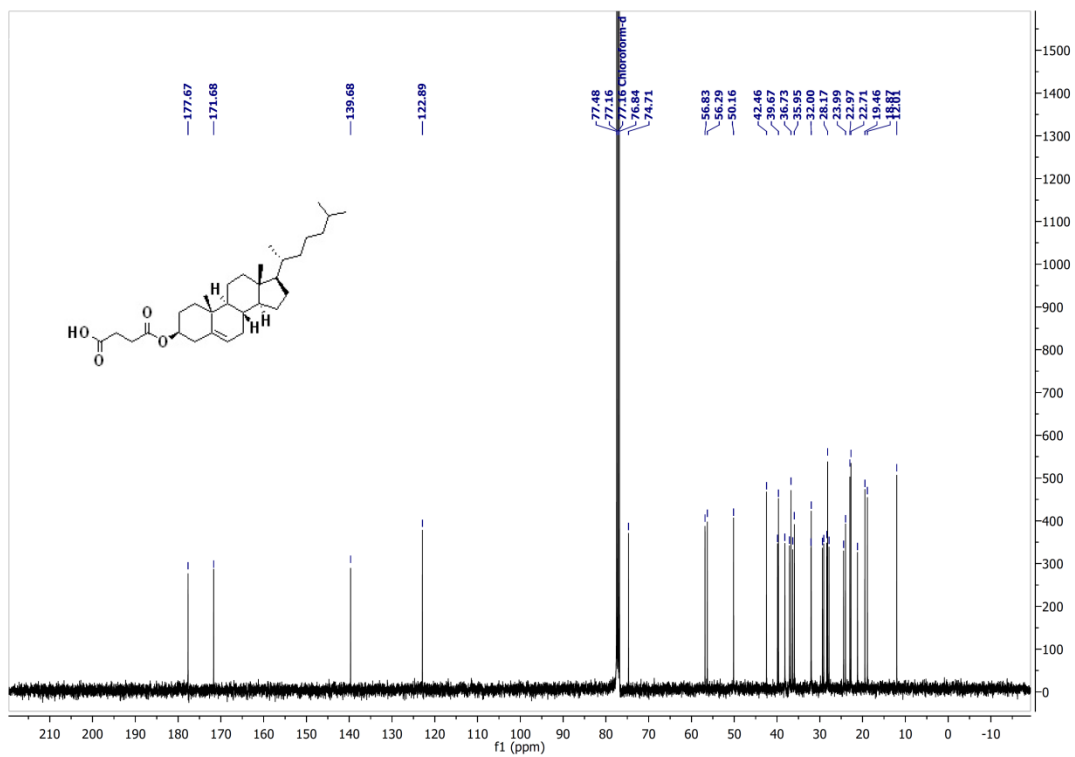


Figure A 4.2: ^{13}C NMR of Cholesterol-succinic acid.

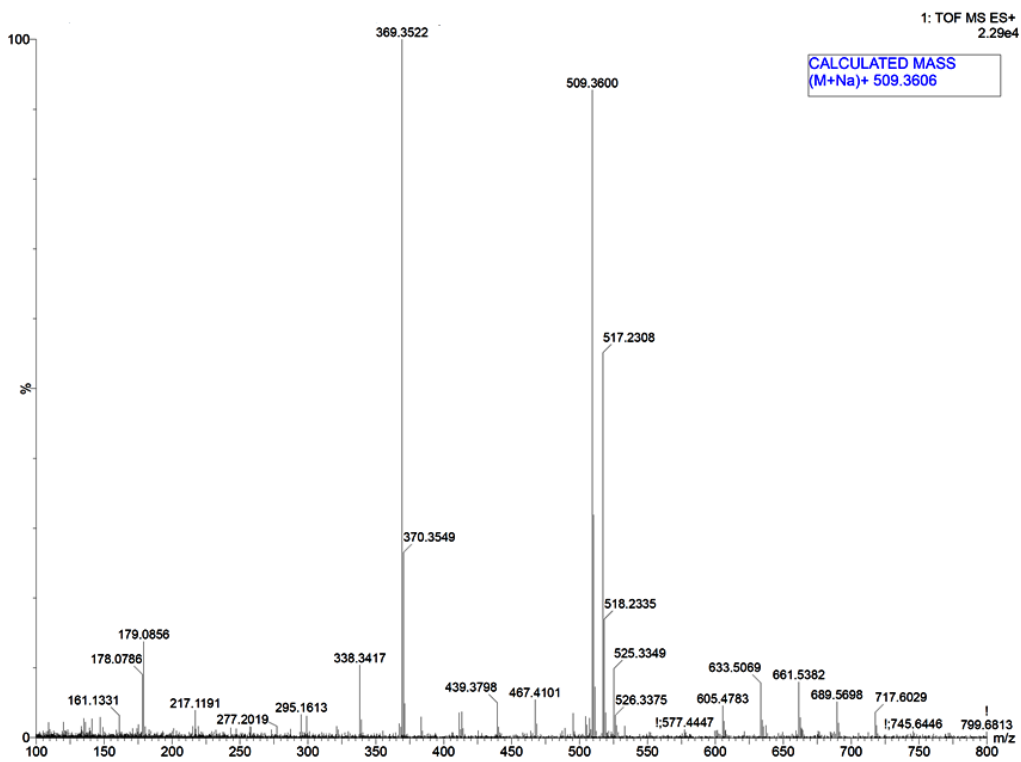


Figure A 4.3: MALDI-TOF of Cholesterol-succinic acid.

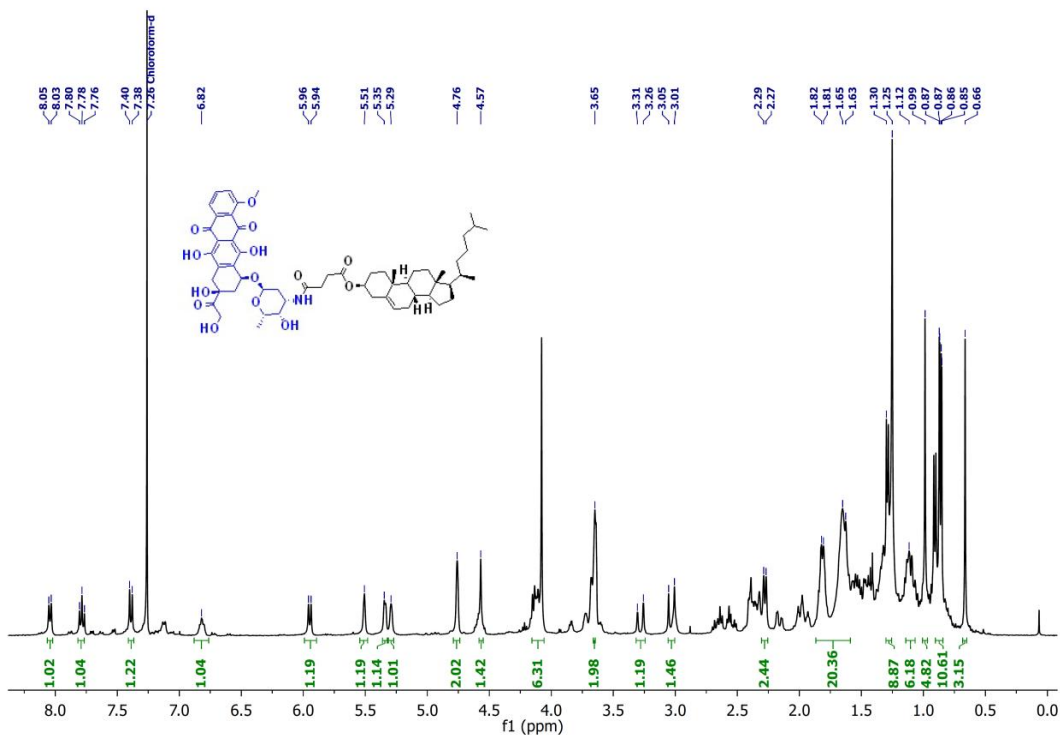


Figure A 4.4: ¹H NMR of Chol-Dox (conjugate 6).

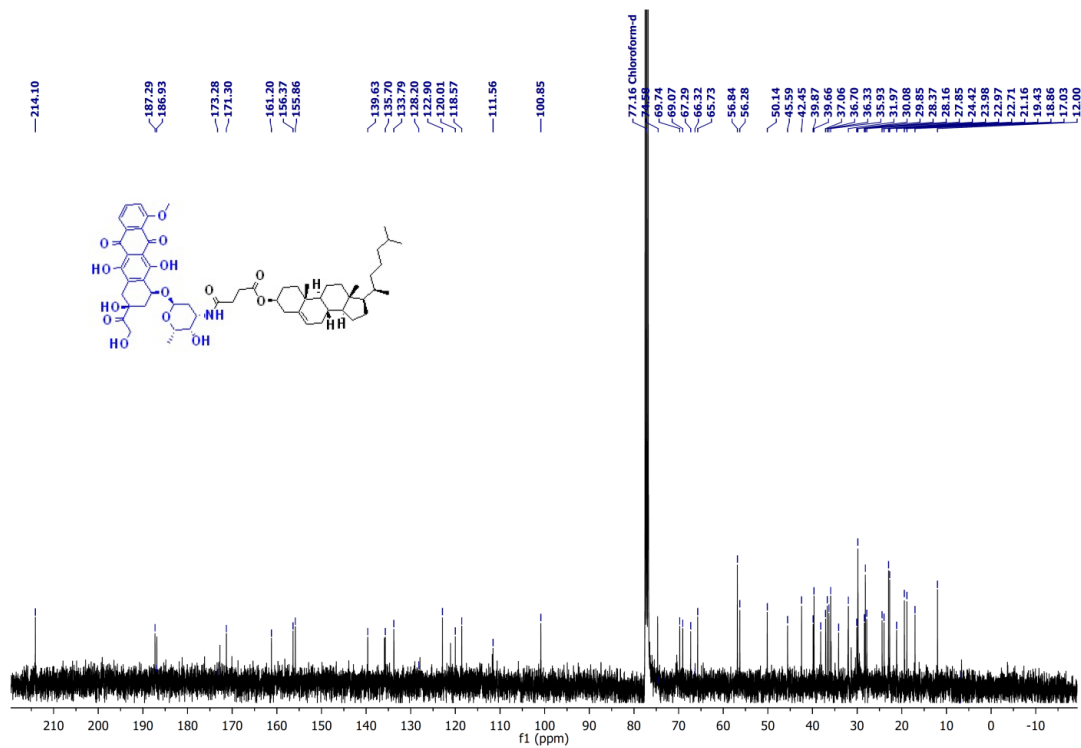


Figure A 4.5: ¹³C NMR of Chol-Dox (conjugate 6).

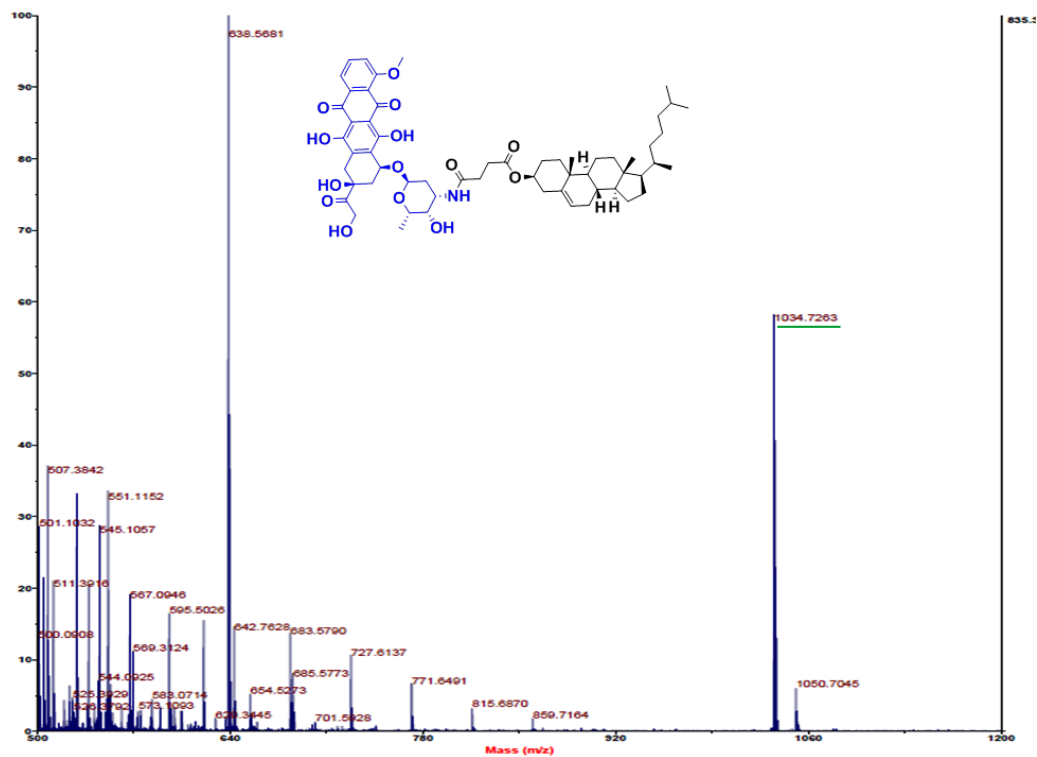


Figure A 4.6: MALDI-TOF of Chol-Dox (conjugate 6).

4.8 References

1. Ferlay, J.; Shin, H. R.; Bray, F.; Forman, D.; Mathers, C.; Parkin, D. M. Estimates of Worldwide Burden of Cancer in 2008: GLOBOCAN 2008. *Int. J. Cancer* **2010**, *127*, 2893–2917.
2. Siegel, R.; Ma, J.; Zou, Z.; Jemal, A. Cancer Statistics, 2014. *CA. Cancer J. Clin.* **2014**, *64*, 9–29.
3. Hoelder, S.; Clarke, P. A.; Workmann, P. Discovery of Small Molecule Cancer Drugs: Successes, Challenges and Opportunities. *Mol. Oncol.* **2012**, *6*, 155-176.
4. Aas, T.; Børresen, A. L.; Geisler, S.; Smith-Sørensen, B.; Johnsen, H.; Varhaug, J. E.; Akslen, L. A.; Lønning, P. E. Specific P53 Mutations are Associated with De Novo Resistance to Doxorubicin in Breast Cancer Patients. *Nat. Med.* **1996**, *2*, 811–814.
5. DeVita, V. T.; Chu, E. A History of Cancer Chemotherapy. *Cancer Res.* **2008**, *68*, 8643–8653.
6. Pearce, A.; Haas, M.; Viney, R.; Pearson, S. A.; Haywood, P.; Brown, C.; Ward, R. Incidence and Severity of Self-Reported Chemotherapy Side Effects in Routine Care: A Prospective Cohort Study. *PLoS One* **2017**, *12*, 1–12.
7. Delgado, J. L.; Hsieh, C. M.; Chan, N. L.; Hiasa, H. Topoisomerases as Anticancer Targets. . *Biochem J.* **2018**, *475*, 373-398.
8. Chen, S. H.; Chan, N.-L.; Hsieh, T. New Mechanistic and Functional Insights into DNA Topoisomerases. *Annu. Rev. Biochem.* **2013**, *82*, 139–170.
9. Corbett, K. D.; Berger, J. M. Structure, Molecular Mechanisms, and Evolutionary Relationships in DNA Topoisomerases. *Annu. Rev. Biophys. Biomol. Struct.* **2004**, *33*, 95–118.
10. Wang, J. C. Cellular Roles of DNA Topoisomerases: A Molecular Perspective. *Nat. Rev. Mol. Cell Biol.* **2002**, *3*, 430–440.

11. Pommier, Y.; Sun, Y.; Huang, S. Y. N.; Nitiss, J. L. Roles of Eukaryotic Topoisomerases in Transcription, Replication and Genomic Stability. *Nat. Rev. Mol. Cell Biol.* **2016**, *17*, 703–721.
12. Vos, S. M.; Tretter, E. M.; Schmidt, B. H.; Berger, J. M. All Tangled up: How Cells Direct, Manage and Exploit Topoisomerase Function. *Nat. Rev. Mol. Cell Biol.* **2011**, *12*, 827–841.
13. Pommier, Y. Drugging Topoisomerases: Lessons and Challenges. *ACS Chem. Biol.* **2013**, *8*, 82–95.
14. Ghilarov, D. A.; Shkundina, I. S. DNA Topoisomerases and Their Functions in a Cell. *Mol. Biol.* **2012**, *46*, 47-57.
15. Pommier, Y. Topoisomerase I Inhibitors: Camptothecins and Beyond. *Nat. Rev. Cancer* **2006**, *6*, 789–802.
16. Nitiss, J. L. Targeting DNA Topoisomerase II in Cancer Chemotherapy. *Nat. Rev. Cancer* **2009**, *9*, 338–350.
17. Movva, S.; Rodriguez, L.; Arias-Pulido, H.; Verschraegen, C. Novel Chemotherapy Approaches for Cervical Cancer. *Cancer* **2009**, *115*, 3166–3180.
18. Patankar, N. A.; Pritchard, J.; Van Grinsven, M.; Osooly, M.; Bally, M. B. Topotecan and Doxorubicin Combination to Treat Recurrent Ovarian Cancer: The Influence of Drug Exposure Time and Delivery Systems to Achieve Optimum Therapeutic Activity. *Clin. Cancer Res.* **2013**, *19*, 865–877.
19. Long, H. J.; Bundy, B. N.; Grendys, E. C.; Benda, J. A.; McMeekin, D. S.; Sorosky, J.; Miller, D. S.; Eaton, L. A.; Fiorica, J. V. Randomized Phase III Trial of Cisplatin with or without Topotecan in Carcinoma of the Uterine Cervix: A Gynecologic Oncology Group Study. *J. Clin. Oncol.* **2005**, *23*, 4626–4633.
20. Moon, J. Y.; Song, I. C.; Ko, Y. B.; Lee, H. J. The Combination of Cisplatin and Topotecan as a Second-Line Treatment for Patients with Advanced/Recurrent Uterine Cervix Cancer. *Medicine* **2018**, *97*, e0340.

21. Robati, M.; Holtz, D.; Dunton, C. J. A Review of Topotecan in Combination Chemotherapy for Advanced Cervical Cancer. *Ther. Clin. Risk Manag.* **2008**, *4*, 213–218.
22. Sengupta, S.; Eavarone, D.; Capila, I.; Zhao, G.; Watson, N.; Kiziltepe, T.; Sasisekharan, R. Temporal Targeting of Tumour Cells and Neovasculature with a Nanoscale Delivery System. *Nature* **2005**, *436*, 568–572.
23. Deng, Z. J.; Morton, S. W.; Ben-Akiva, E.; Dreaden, E. C.; Shopsowitz, K. E.; Hammond, P. T. Layer-by-Layer Nanoparticles for Systemic Codelivery of an Anticancer Drug and SiRNA for Potential Triple-Negative Breast Cancer Treatment. *ACS Nano* **2013**, *7*, 9571–9584.
24. Jiang, T.; Mo, R.; Bellotti, A.; Zhou, J.; Gu, Z. Gel–liposome Mediated Co-delivery of Anticancer Membrane-Associated Proteins and Small-molecule Drugs for Enhanced Therapeutic Efficacy. *Adv. Funct. Mater.* **2014**, *24*, 2295–2304.
25. Wang, Y.; Gao, S.; Ye, W.-H.; Yoon, H. S.; Yang, Y.-Y. Co-Delivery of Drugs and DNA from Cationic Core–shell Nanoparticles Self-Assembled from a Biodegradable Copolymer. *Nat. Mater.* **2006**, *5*, 791–796.
26. Liu, Z.; Tabakman, S. M.; Chen, Z.; Dai, H. Preparation of Carbon Nanotube Bioconjugates for Biomedical Applications. *Nat. Protoc.* **2009**, *4*, 1372–1382.
27. Chaudhuri, P.; Harfouche, R.; Soni, S.; Hentschel, D. M.; Sengupta, S. Shape Effects of Carbon Nanovectors on Angiogenesis. *ACS Nano* **2010**, *4*, 574–582.
28. Sydlik, S. A.; Jhunjhunwala, S.; Webber, M. J.; Anderson, D. G.; Langer, R. In Vivo Compatibility of Graphene Oxide with Differing Oxidation States. *ACS Nano* **2015**, *9*, 3866–3874.
29. Jiang, T.; Sun, W.; Zhu, Q.; Burns, N. A.; Khan, S. A.; Mo, R.; Gu, Z. Furin-Mediated Sequential Delivery of Anticancer Cytokine and Small-Molecule Drug Shuttled by Graphene. *Adv. Mater.* **2015**, *27*, 1021–1028.
30. Chung, C.; Kim, Y. K.; Shin, D.; Ryoo, S. R.; Hong, B. H.; Min, D. H. Biomedical Applications of Graphene and Graphene Oxide. *Acc. Chem. Res.* **2013**, *46*, 2211–2224.

31. Wang, H.; Li, P.; Yu, D.; Zhang, Y.; Wang, Z.; Liu, C.; Qiu, H.; Liu, Z.; Ren, J.; Qu, X. Unraveling the Enzymatic Activity of Oxygenated Carbon Nanotubes and Their Application in the Treatment of Bacterial Infections. *Nano Lett.* **2018**, *18*, 3344–3351.
32. Wang, H.; Liu, C.; Liu, Z.; Ren, J.; Qu, X. Specific Oxygenated Groups Enriched Graphene Quantum Dots as Highly Efficient Enzyme Mimics *Small* **2018**, *14*, 1703710.
33. Lu, C. H.; Yang, H. H.; Zhu, C. L.; Chen, X.; Chen, G. N. A Graphene Platform for Sensing Biomolecules. *Angew. Chem. Int. Ed.* **2009**, *48*, 4785–4787.
34. Shi, S.; Chen, F.; Ehlerding, E. B.; Cai, W. Surface Engineering of Graphene-Based Nanomaterials for Biomedical Applications. *Bioconjugate Chem.* **2014**, *25*, 1609–1619.
35. Song, E.; Han, W.; Li, C.; Cheng, D.; Li, L.; Liu, L.; Zhu, G.; Song, Y.; Tan, W. Hyaluronic Acid-Decorated Graphene Oxide Nanohybrids as Nanocarriers for Targeted and pH-Responsive Anticancer Drug Delivery. *ACS Appl. Mater. Interfaces* **2014**, *6*, 11882–11890.
36. Zhang, L.; Xia, J.; Zhao, Q.; Liu, L.; Zhang, Z. Functional Graphene Oxide as a Nanocarrier for Controlled Loading and Targeted Delivery of Mixed Anticancer Drugs. *Small* **2010**, *6*, 537–544.
37. Mallick, A.; Nandi, A.; Basu, S. Polyethylenimine Coated Graphene Oxide Nanoparticles for Targeting Mitochondria in Cancer Cells. *ACS Appl. Bio Mater.* **2019**, *2*, 14–19.
38. Palvai, S.; More, P.; Mapara, N.; Basu, S. Chimeric Nanoparticle: A Platform for Simultaneous Targeting of Phosphatidylinositol-3-Kinase Signaling and Damaging DNA in Cancer Cells. *ACS Appl. Mater. Interfaces* **2015**, *7*, 18327–18335.
39. Mallick, A.; More, P.; Ghosh, S.; Chippalkatti, R.; Chopade, B. A.; Lahiri, M.; Basu, S. Dual Drug Conjugated Nanoparticle for Simultaneous Targeting of Mitochondria and Nucleus in Cancer Cells. *ACS Appl. Mater. Interfaces* **2015**, *7*, 7584–7598.
40. Nandi, A.; Mallick, A.; More, P.; Sengupta, P.; Ballav, N.; Basu, S. Cisplatin-Induced Self-Assembly of Graphene Oxide Sheets into Spherical Nanoparticles for Damaging Sub-Cellular DNA. *Chem. Commun.* **2017**, *53*, 1409–1412.

41. Ghosh, C.; Nandi, A.; Basu, S. Supramolecular Self-Assembly of Triazine-Based Small Molecule: Targeting Endoplasmic Reticulum in Cancer Cells. *Nanoscale* **2019**, *8*, 1–3.
42. Kelland, L. The Resurgence of Platinum-Based Cancer Chemotherapy. *Nat. Rev. Cancer* **2007**, *7*, 573–584.
43. Silver, D. P.; Richardson, A. L.; Eklund, A. C.; Wang, Z. C.; Szallasi, Z.; Li, Q.; Juul, N.; Leong, C. O.; Calogrias, D.; Buraimoh, A.; Fatima, A.; Gelman, R. S.; Ryan, P. D.; Tung, N. M.; Nicolo, A. D.; Ganesan, S.; Miron, A.; Colin, C.; Sgroi, D. C.; Ellisen, L. W.; Winer, E. P.; Gaber, J. E. Efficacy of Neoadjuvant Cisplatin in Triple-Negative Breast Cancer. *J. Clin. Oncol.* **2010**, *28*, 1145–1153.
44. Yao, X.; Panichpisal, K.; Kurtzman, N.; Nugent, K. Cisplatin Nephrotoxicity: A Review. *Am. J. Med. Sci.* **2007**, *334*, 115–124.
45. Mollman, J. E. Cisplatin Neurotoxicity. *N. Engl. J. Med.* **1990**, *322*, 126–127.
46. Singal, P. K.; Iliskovic, N. Doxorubicin-Induced Cardiomyopathy. *N. Engl. J. Med.* **1998**, *339*, 900–905.
47. Pizzolato, J. F.; Saltz, L. B. The Camptothecins. *Lancet* **2003**, *361*, 2235–2242.
48. Sengupta, P.; Basu, S.; Soni, S.; Pandey, A.; Roy, B.; Oh, M. S.; Chin, K. T.; Paraskar, A. S.; Sarangi, S.; Connor, Y.; Sabbiseti, V. S.; Koppam, J.; Kulkarni, A.; Muto, K.; Amarasiriwardena, C.; Jayawardene, I.; Lupoli, N.; Dinulescu, D. M.; Bonventre, J. V.; Mashelkar, R. A.; Sengupta, S. Cholesterol-Tethered Platinum II-Based Supramolecular Nanoparticle Increases Antitumor Efficacy and Reduces Nephrotoxicity. *Proc. Natl. Acad. Sci.* **2012**, *109*, 11294–11299.
49. Peer, D.; Karp, J. M.; Hong, S.; Farokhzad, O. C.; Margalit, R.; Langer, R. Nanocarriers as an Emerging Platform for Cancer Therapy. *Nat. Nanotechnol.* **2007**, *2*, 751–760.
50. Gilleron, J.; Querbes, W.; Zeigerer, A.; Borodovsky, A.; Marsico, G.; Schubert, U.; Manygoats, K.; Seifert, S.; Andree, C.; Stöter, M.; Epstein-Barash, H.; Zhang, L.; Koteliansky, V.; Fitzgerald, K.; Fava, E.; Bickle, M.; Kalaidzidis, Y.; Akinc, A.; Maier, M.;

Zerial, M. Image-Based Analysis of Lipid Nanoparticle-Mediated siRNA Delivery, Intracellular Trafficking and Endosomal Escape. *Nat. Biotechnol.* **2013**, *31*, 638–646.

51. Kuo, L. J.; Yang, L. X. γ -H2AX- A Novel Biomaker for DNA Double-Strand Breaks. *In Vivo.* **2008**, *22*, 305–310.

52. Curtin, N. J. DNA Repair Dysregulation from Cancer Driver to Therapeutic Target. *Nat. Rev. Cancer* **2012**, *12*, 801–817.

Chapter 5: Conclusion and Future Directions

In this thesis we have developed novel graphene oxide nanoplatforms which can co-load multiple anticancer drugs and have the potential to bring about DNA damage. Chapter 1 gives a brief description of cancer and the various stresses associated with it and how enhancing the stresses can lead to cancer cell death. It also gives an overview of the application of nanotechnology and nanomaterials- specifically grapheneoxide (GO) in cancer treatment; to deliver and target anticancer drugs to damage important cellular organelles. In chapter 2, we demonstrated a remarkable morphological transformation of 2D GO sheets into 3D spherical nanoparticles mediated by cisplatin. The cisplatin assisted self assembled 3D GO-NPs had a size less than 200 nm which makes it favourable for accumulation into tumor tissues through EPR effect. The GO NPs could be further loaded with another aromatic gemotoxic drug like Doxorubicin/Proflavine along with cisplatin. The dual drug loaded GO-NPs internalized into cervical cancer HeLa cells, homed into the acidic lysosomes, and released the drug payloads in a slow and sustained manner. Ultimately, the released drugs lead to DNA damage and induced cell death in cancer cells. In the following chapter, we modified these GO-NPs containing SN38- a Topoisomerase I inhibitor and cisplatin with hydrophilic polymers PEG and PIMA to enhance the the aqueous colloidal stability. In addition, we successfully induced apoptosis in HeLa cells due to Topoisomerase I inhibition and DNA damage. Lastly we coated the GO-NPs with a lipid layer which was conjugated to doxorubicin. Thus we could successfully develop a triple drug loaded lipid coated self-assembled GO-NP (GO-Nanocell) which, simultaneously inhibited Topoisomerase I and II as well as damaged the nuclear DNA resulting in effective cancer cell death.

Taking into consideration all the advancement in the field of GO based nanocarriers for varied application in cancer therapy, it paves the way for its future use in clinics.

This work can be further continued to:

1. Carry out *in vivo* studies of the engineered GO-NPs in mice models to assess the tumor cell killing ability, as well as monitor the biodistribution, as well as determine the cytotoxicity on healthy tissues *in vivo* cytotoxicity of the engineered GO-NPs.
2. Study the plausible mechanism for the cisplatin mediated self assembly of the 2D GO sheets to 3D spherical.

3. Using the same strategy we can develop GO-NPs which can target other organelles, by conjugating targeting moieties on the surface.
4. The triple drug loaded, lipid coated GO-NPs can be further used to inhibit multiple targets inside the cell, eg: we can incorporate a DNA repair inhibitor along with DNA damaging drugs. This will lead to enhanced replication stress in cancer cells.

APPROVAL FROM JOURNALS

Issue 8, 2017 Previous Article Next Article

From the journal:
Chemical Communications

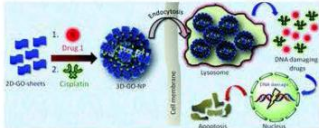
Cisplatin-induced self-assembly of graphene oxide sheets into spherical nanoparticles for damaging sub-cellular DNA

Aditi Nandi^a, Abhik Mallick^a, Piyush More^a, Poulomi Sengupta^b, Nirmalya Reilly^a and Sudipta Basu^{a,b}

Author affiliations

Abstract

This report describes the hitherto unobserved cisplatin induced self-assembly of 2D-graphene oxide sheets into 3D-spherical nano-scale particles. These nanoparticles can encompass dual DNA damaging drugs simultaneously. A combination of confocal microscopy, gel electrophoresis and flow cytometry studies clearly demonstrated that these novel nanoparticles can internalize into cancer cells by endocytosis, localize into lysosomes, and damage DNA, leading to apoptosis. Cell viability assays indicated that these nanoparticles were more cytotoxic towards cancer cells compared to healthy cells.



g/2017/cc/c6cc09006k#

About	Cited by	Related
Society for Photobiology, the European Photochemistry Association, and The Royal Society of Chemistry. For reproduction of material from all other RSC journals and books: Reproduced from Ref. XX with permission from The Royal Society of Chemistry.	If the material has been adapted instead of reproduced from the original RSC publication "Reproduced from" can be substituted with "Adapted from". In all cases the Ref. XX is the XXth reference in the list of references. If you are the author of this article you do not need to formally request permission to reproduce figures, diagrams etc. contained in this article in third party publications or in a thesis or dissertation provided that the correct acknowledgement is given with the reproduced material.	Reproduced material should be attributed as follows: For reproduction of material from NJC: [Original citation] - Reproduced by permission of The Royal Society of Chemistry (RSC) on behalf of the Centre National de la Recherche Scientifique (CNRS) and the RSC For reproduction of material from PCCP: [Original citation] - Reproduced by permission of the PCCP Owner Societies For reproduction of material from PPS: [Original citation] - Reproduced by permission of The Royal Society of Chemistry (RSC) on behalf of the European Society for Photobiology, the European Photochemistry Association, and RSC For reproduction of material from all other RSC journals: [Original citation] - Reproduced by permission of The Royal

Issue 26, 2019 Previous Article Next Article

From the journal:
Journal of Materials Chemistry B


Graphene oxide nanocells for impairing topoisomerase and DNA in cancer cells

Aditi Nandi^a, Chandramouli Ghosh^a, Aman Bajpai^b and Sudipta Basu^{a,b}

Author affiliations

Abstract

DNA topoisomerases and nuclear DNA are important targets for cancer therapy. However, DNA topoisomerase inhibitors and DNA damaging drugs demonstrate a large window of side effects in the clinic. Graphene oxide based biocompatible and biodegradable nano-scale materials have the potential to overcome this complication. However, encompassing different topoisomerase inhibitors along with DNA damaging drugs into 2D-graphene oxide remains a main challenge. To address this, in this manuscript, we have engineered self-assembled spherical 3D-graphene oxide nanoparticles coated with lipid (GO-nanocells) which can concomitantly load and release multiple topoisomerase inhibitors (topotecan and doxorubicin) and DNA damaging drug (cisplatin) in a controlled manner. Fluorescence confocal microscopy confirmed that these GO-nanocells were taken up by HeLa cervical cancer cells and transported into lysosomes temporarily over 6 h. A combination of confocal microscopy, gel electrophoresis, and flow cytometry studies revealed that these GO-nanocells damaged nuclear DNA along with topoisomerase inhibition leading to induction of apoptosis through cell cycle arrest in the G2-M phase. These GO-nanocells killed HeLa cancer cells with remarkably greater efficacy compared to a free drug cocktail at 48 h post-incubation. These self-assembled GO-nanocells can serve as a nanoscale tool to perturb multiple therapeutically important sub-cellular targets simultaneously for improved efficacy in future cancer chemotherapy.



ing/2019/TB/C91800336C#

About	Cited by	Related
For reproduction of material from all other RSC journals and books: Reproduced from Ref. XX with permission from The Royal Society of Chemistry.	If the material has been adapted instead of reproduced from the original RSC publication "Reproduced from" can be substituted with "Adapted from". In all cases the Ref. XX is the XXth reference in the list of references. If you are the author of this article you do not need to formally request permission to reproduce figures, diagrams etc. contained in this article in third party publications or in a thesis or dissertation provided that the correct acknowledgement is given with the reproduced material.	Reproduced material should be attributed as follows: For reproduction of material from NJC: [Original citation] - Reproduced by permission of The Royal Society of Chemistry (RSC) on behalf of the Centre National de la Recherche Scientifique (CNRS) and the RSC For reproduction of material from PCCP: [Original citation] - Reproduced by permission of the PCCP Owner Societies For reproduction of material from PPS: [Original citation] - Reproduced by permission of The Royal Society of Chemistry (RSC) on behalf of the European Society for Photobiology, the European Photochemistry Association, and RSC For reproduction of material from all other RSC journals: [Original citation] - Reproduced by permission of The Royal Society of Chemistry If you are the author of this article you still need to obtain permission to reproduce the whole article in a third party publication with the exception of reproduction of the whole article in a thesis or dissertation.

Polymer conjugated graphene-oxide nanoparticles impair nuclear DNA and Topoisomerase I in cancer†



Aditi Nandi,^a Chandramouli Ghosh^a and Sudipta Basu ^{*b}

Author affiliations

Abstract

Cancer chemotherapy had been dominated by the use of small molecule DNA damaging drugs. Eventually, the emergence of DNA damage repair machinery in cancer cells has led to combination therapy with the DNA topology controlling enzyme, topoisomerase I inhibitor along with DNA impairing agents. However, integrating multiple drugs having diverse water solubility and hence bio-distribution effectively for cancer treatment remains a significant challenge, which can be addressed by using suitable nano-scale materials. Herein, we have chemically conjugated graphene oxide (GO) with biocompatible and hydrophilic polymers [polyethylene glycol (PEG) and ethylene-diamine modified poly-isobutylene-maleic anhydride (PMA-ED)], which can

Polymer conjugated graphene-oxide nanoparticles impair nuclear DNA and Topoisomerase I in cancer

A. Nandi, C. Ghosh and S. Basu, *Nanoscale Adv.*, 2019, **1**, 4965

DOI: 10.1039/C9NA00617F

This article is licensed under a [Creative Commons Attribution 3.0 Unported Licence](#). Material from this article can be used in other publications provided that the correct acknowledgement is given with the reproduced material.

Reproduced material should be attributed as follows:

- For reproduction of material from NJC:
[Original citation] - Published by The Royal Society of Chemistry (RSC) on behalf of the Centre National de la Recherche Scientifique (CNRS) and the RSC.
- For reproduction of material from PCCP:
[Original citation] - Published by the PCCP Owner Societies.
- For reproduction of material from PPS:
[Original citation] - Published by The Royal Society